UNIVERSITA' DEGLI STUDI DI NAPOLI FEDERICO II

SCUOLA POLITECNICA E DELLE SCIENZE DI BASE

DIPARTIMENTO DI INGEGNERIA CHIMICA, DEI MATERIALI E DELLA PRODUZIONE INDUSTRIALE

Dottorato di Ricerca in Ingegneria Chimica (XXVI Ciclo)

CO$_2$ CAPTURE BY TEMPERATURE SWING ADSORPTION IN A SOUND ASSISTED FLUIDIZED BED OF FINE POWDERS

Scientific committee: *Student:*

Prof. Piero Salatino   **Ing. Federica Raganati**

Ing. Riccardo Chirone

Ing. Paola Ammendola

ANNO ACCADEMICO 2013-2014

Abstract

Adsorption using solid sorbents is recognized to be attractive to complement or replace the current absorption technology for CO_2 capture due to its low energy requirement. However, the development of new highly specific CO_2 adsorbent is necessary: a solution is represented by fine materials, whose properties can be tuned at a molecular level by means of functionalization processes to tailor their CO_2 capture performance. Another point to be addressed is the adoption of an adequate reactor configuration, which can, on one hand, fully exploit the potential and properties of these new-concept adsorbent materials by maximizing the contact between the CO_2 molecules and the adsorbent particles, and, on the other hand, improve the heat transfer. In this respect, a fluidized bed could be a good solution, due to larger gas-solid contact efficiency, higher rate of mass and heat transfer and lower pressure drops. In particular, a more suitable reactor configuration is a sound assisted fluidized bed, namely provided with a system for the generation of acoustic vibrations to overcome the high interparticles forces characterizing fine powders. On these bases, the present PhD thesis focuses on the CO_2 capture process by temperature swing adsorption on fine porous materials in a sound assisted fluidized bed.

In order to perform adsorption/desorption tests, a laboratory scale sound assisted fluidized bed experimental rig has been set up. It is equipped with a system for the sound generation and with a continuous analyzer for the CO_2 concentration measurement in the effluent gas stream. For the regeneration tests the reactor is externally heated by an ad-hoc designed heating jacket, provided with a window to allow the fluidization quality to be visually assessed. Both common adsorbent materials, two activated carbons, zeolite HZSM-5 and zeolite 13X, and a highly specific adsorbent material, a metal organic framework HKUST-1, were used.

The experimental results show that the application of the sound can improve the fluidization quality as well as the adsorption efficiency (by maximizing the gas-solid contact) of all the selected adsorbent materials in terms of remarkably higher breakthrough time, adsorption capacity, fraction of bed utilized until breakthrough and adsorption rate. The experimental campaign has been also carried out, at ambient temperature and atmospheric pressure, in order to highlight the effect of some operating variables on the adsorption performances, i.e. sound intensity (120-140dB) and frequency (20-300Hz), CO_2 partial pressure (0.05-0.15atm) and fluidization velocity (0.1-4.5cm/s). In particular, increasing sound intensities yield better adsorption performances, whereas, sound frequency has a not monotone effect on the

fluidization quality and adsorption efficiency. The CO_2 capture capacity increases with CO_2 partial pressure, coherently with the partial pressure being the thermodynamic driving force of the adsorption process. Finally, the dependence of the breakthrough time on the contact time is linear for the tests performed in ordinary conditions, whereas, it is not monotone for the sound assisted tests. At the end of the experimental campaign, all the investigated adsorbent materials have been compared and their different adsorption behaviours explained on the basis of their textural properties. In particular, it has been found that there is a specific pore size range, 8-12 Å, which is the key factor affecting the adsorption capacity of the studied materials under the investigated operating conditions.

Desorption tests have been performed on the materials characterized by the best adsorption performances, the HKUST-1 and one activated carbon at atmospheric pressure. In particular, an extra-situ regeneration strategy (150°C under a vacuum of 50mbar) has been developed to study the stability of HKUST-1 to cyclic adsorption/desorption operations, since HKUST-1 presents problems of thermal stability, limiting the desorption temperature to be used in a temperature swing adsorption process. The results show that HKUST-1 is very stable, keeping its adsorption performances over 10 adsorption/desorption cycles. As regards the activated carbon, two strategy of temperature swing adsorption have been tested in the sound assisted fluidized bed. The first regeneration strategy is an isothermal purge consisting in combining the effect of increasing temperature and decreasing CO_2 partial pressure. The second regeneration strategy, heating and purge, consists in separating the thermal effect from the purging one. The application of the sound makes it possible, from one hand, to remarkably increase the desorption rate and, on the other, to significantly enrich the recovered CO_2 stream. CO_2 recovery and purity have opposing trends: higher desorption times yield a higher CO_2 recovery, but lead to a lower CO_2 purity of the desorbing stream. The desorption rate is positively affected by both desorption temperature (25-150°C) and N_2 purge flow rate (45.2-90.4Nl h^{-1}). The purity of the recovered CO_2 stream is increased by increasing desorption temperatures, whereas, it is not affected by change of the N_2 purge flow rate since dilution does not depend on the purge flow rate but only on the purge volume.

The results obtained show that heating is very effective since 80% of the captured CO_2 can be can be recovered with a 100% purity at a bland desorption temperature of 130°C. It is worth noting that for each desorption temperature the heating and purge strategy always makes it possible to enrich the stream of CO_2 recovered with respect to the standard purge strategy, the CO_2 recovery level being the same. The possibility to use the activated carbon in a cyclic

operation has been also assessed: it is very stable, keeping its adsorption performances over 16 adsorption/desorption cycle.

Finally, considerations about the energy cost and scale-up of the proposed technology for CO_2 capture by temperature swing adsorption have also been reported.

Index

Table index

Figure index

I INTRODUCTION

In the history of civilizations, the 20th century can be regarded as a century of explosive growth in energy consumption and rapid increase in population worldwide along with unprecedented speed of inventions of new technologies and ever-increasing expansion of man-made materials. All these epochal revolutions have created a new world that has become increasingly dependent on combustion of hydrocarbon fuels such as gasoline and diesel fuel. Inventions of electrical power plants and electric home appliances have electrified the world, which is increasingly dependent on electricity largely generated from carbon-based resources such as coal and natural gas [1]. On a global scale, more than 80% of the primary energy supply is satisfied by fossil fuels [1,2], due to their availability, existing reliable technology for energy production, and energy density. However, combustion of fossil fuels produces CO_2 as waste.

Total CO_2 emissions from fossil fuel consumption and flaring of natural gas were 28 $GtCO_2$ per year in 2006 and this value is likely destined to rise because of the increasing worldwide energetic demand. As the dominant form of energy utilized in the world, fossil fuels account for about 75% of current anthropogenic CO_2 emissions [3,4].

In the last decade, significant progress has been made towards a better understanding of the world climate and of the long-term impact of climate change. On February 2, 2007, the Intergovernmental Panel on Climate Change (IPCC) of the United Nations declared that the evidence of a warming trend is "unequivocal" and that human activity has "very likely" been the driving force in that change over the last 50 years. In particular, the observed increase in globally averaged temperatures since the mid-twentieth century is very likely to have occurred due to the increase in anthropogenic greenhouse gas concentrations that leads to the warming of the earth surface and lower atmosphere [5]. Where, the greenhouse effect is the phenomenon in which water vapor, carbon dioxide, methane, and other atmospheric gases absorb outgoing infrared radiation resulting in the raising of the temperature. Without

greenhouse gases, the average temperature on the Earth's surface would be approximately 255K, i.e. well below the freezing point of water, which means that life might not have evolved. Hence, the existence of CO_2 in the atmosphere is vital to living organisms on Earth [6]. Among all the greenhouse gases, CO_2 is blamed to be the main contributor in regard of its amount present in the atmosphere contributing to 60 percent of global warming effects [7], although methane and chlorofluorocarbons have much higher greenhouse effect per mass of gases [8]. IPCC further predicts that, by the year 2100, the atmosphere may contain up to 570ppmv CO_2, causing a rise of mean global temperature of around 1.9°C and an increase in mean sea level of 38m [9]. Also accompanied is species extinction.

I.1   Reducing CO_2 Emissions

When industrialization took off, so did CO_2 emissions (Fig. 1). The globally averaged CO_2 concentration changed only slightly over the period of a thousand years till 20th century, from 280ppmv in 1000 to 285ppmv in 1800, whereas, it increased from this pre-industrial levels to a current level of 392ppmv – a 40% increase [10].
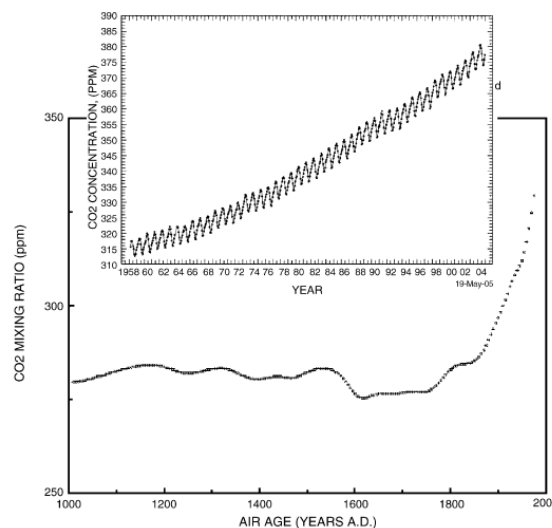
Fig. 1 Atmospheric CO_2 concentrations during 1000–2004 based on the analysis of ice cores for 1000–1997 and actual atmospheric CO_2 analysis during 1958– 2004.

In order to mitigate global warming, it is by now generally accepted that a reduction in emissions of greenhouse gases is necessary [11,12,13]. In particular, in 1997, the Kyoto Protocol was ratified by most of the developed countries setting the stage for an international effort to reduce CO_2 emissions. Many research groups, companies and organizations are working hard to this aim suggesting several possible strategies, such as [14]:

- reducing energy consumption, for example by increasing the efficiency of energy conversion and/or utilization (including enhancing less energy-intensive economic activities);

- switching to less carbon intensive fuels, for example natural gas instead of coal;

- increasing the use of renewable energy sources (e.g., solar energy, wind, and biomass), each of which emits little or no net CO_2;

- sequestering CO_2 by enhancing biological absorption capacity in forests and soils.

Over time, these methods may be effective in reducing CO_2 emissions, but generally they are not applicable to the large number of existing fossil fuel fired power plants. Moreover, in spite of all these efforts, there are many reasons to believe that fossil fuels will continue to dominate the supply of primary energy for several decades to come [15,16]. Hence, yet another way to reduce CO_2 emissions has been suggested: combining the use of fossil fuels with CO_2 capture and storage (CCS). It offers the opportunity to meet increasing demands for fossil fuel energy in the short to medium term, whilst reducing the associated greenhouse gas emissions in line with global targets [17,18]. In an idealized case, this would yield a "carbon neutral" source of heat and power.

I.2 Carbon Capture and Storage (CCS)

The CO_2 emissions from various sources worldwide have been estimated by the International Energy Agency [19]. These are reported in **Tab. 1**. Among all the CO_2 emissions sources, power generation is the single largest one, accounting for 45% of the entire CO_2 emissions.In this respect, one approach that holds great promise for reducing CO_2 emissions into the atmosphere from large fixed industrial sources is carbon capture and storage (CCS). It embodies a group of technologies [5] consisting in the separation of CO_2 from large industrial and energy-related sources, transport to a storage location and long-term isolation from the atmosphere. This approach would lock up (sequester) the CO_2 for thousands of years. However, applying current state-of-the-art flue gas CO_2 capture and separation technologies to existing coal-fired power plants that have an average efficiency of 33% would reduce net plant power output by approximately one-third [20,21]. Therefore, for CCS technologies to be an effective mitigation option, research and development will be critical to achieve wide-scale deployment with acceptable economic and environmental impacts.

Tab. 1 Properties of candidate gas streams that can be inputted to a capture process.

Source	CO$_2$ concentration % vol (dry)	Pressure of gas stream MPa[a]	CO$_2$ partial pressure MPa
CO$_2$ from fuel combustion			
• Power station flue gas:			
Natural gas fired boilers	7 - 10	0.1	0.007 - 0.010
Gas turbines	3 - 4	0.1	0.003 - 0.004
Oil fired boilers	11 - 13	0.1	0.011 - 0.013
Coal fired boilers	12 - 14	0.1	0.012 - 0.014
IGCC[b]: after combustion	12 - 14	0.1	0.012 - 0.014
• Oil refinery and petrochemical plant fired heaters	8	0.1	0.008
CO$_2$ from chemical transformations + fuel combustion			
• Blast furnace gas:			
Before combustion[c]	20	0.2 - 0.3	0.040 - 0.060
After combustion	27	0.1	0.027
• Cement kiln off-gas	14 - 33	0.1	0.014 - 0.033
CO$_2$ from chemical transformations before combustion			
• IGCC: synthesis gas after gasification	8 - 20	2 - 7	0.16 - 1.4

[a]   0.1 MPa = 1 bar.
[b]   IGCC: Integrated gasification combined cycle.
[c]   Blast furnace gas also contains significant amounts of carbon monoxide that could be converted to CO$_2$ using the so-called shift reaction.

The first step, separation and compression (i.e. capture), is currently considerably more costly than transportation and sequestration. Thus, developing new technology to reduce capture costs is the principal research topic at present. In the following the capture techniques will be described, whereas, only a brief summary on the transportation and storage techniques will be presented.

Capture

When burnt with air, fossil fuels release in the atmosphere gases containing CO$_2$, N$_2$, H$_2$O, small amounts of O$_2$ and other elements, as reported in Tab. 2 [4]. Excluding CO$_2$, they don't contribute to the greenhouse effect, so they don't need to be captured. However, N$_2$ represents the biggest part of the entire gas volume, thus making the storage of the whole stream anti-economic as system for the environmental safety.

Tab. 2 Characteristic composition (%vol.) of flue gas deriving from the combustion of fossil fuels.

Elements	Carbon	Natural Gas
Ar	0.8	0.9
O$_2$	3.2	12.3
N$_2$	72	74.5
H$_2$O	10	8.2
CO$_2$	13.8	4.1
SO$_2$	0.1	0

Therefore, the main issue to be solved is to separate CO$_2$ from N$_2$. In this respect, there are basically three technological pathways that can be pursued for CO$_2$ capture: pre-combustion capture, post-combustion capture, oxy-fuel combustion and chemical looping cycle (CLC).

Pre-combustion capture: the N_2 issue can be overcome preparing a C-free fuel (H_2) and separating CO_2 in this stage before the fuel combustion (**Fig. 2**) [22].
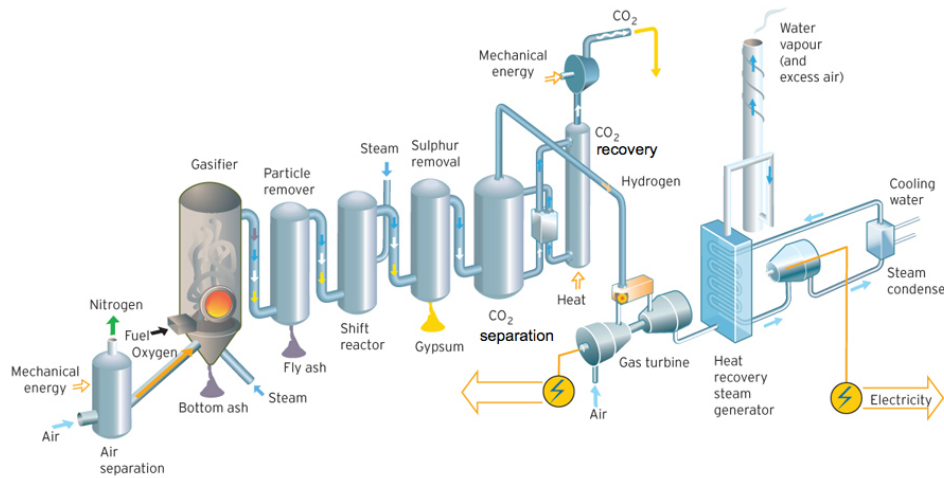
Fig. 2 Pre-Combustion Capture.

This process typically comprises a first stage of reaction producing a mixture of hydrogen and carbon monoxide (syngas) from a primary fuel [21]. The two main routes are to add steam (reaction 1), in which case the process is called 'steam reforming', or oxygen (reaction 2) to the primary fuel, in which case the process is often called 'partial oxidation', when applied to gaseous and liquid fuels, and 'gasification', when applied to a solid fuel, but the principles are the same.

Steam reforming

$$C_xH_y + xH_2O \leftrightarrow xCO + (x + y/2)H_2 \tag{1}$$

Partial oxidation

$$C_xH_y + x/2 O_2 \leftrightarrow xCO + y/2 H_2 \tag{2}$$
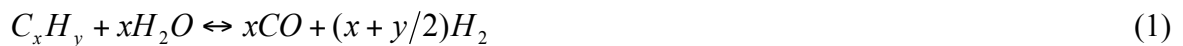
This is followed by the 'shift' reaction to convert CO to CO_2 by the addition of steam.

Water Gas Shift Reaction

$$CO + H_2O \leftrightarrow CO_2 + H_2 \tag{3}$$

Finally, the CO_2 must be removed from the CO_2/H_2 mixture instead of the CO_2/N_2 mixture of a post-combustion process. The concentration of CO_2 in the input to the CO_2/H_2 separation stage can be in the range 15-60% (dry basis) and the total pressure is typically 15-40bar, thus making the CO_2 capture easier if compared to the post-combustion case. The separated CO_2 is then available for storage. However, despite of the easier capture stage, pre-combustion

technique has a remarkable drawback: it can't be applied to pre-existing plants, since the process is entirely different from a standard combustion process.

Post-Combustion: capture of CO_2 from flue gases produced by combustion of fossil fuels and biomass in air is referred to as post-combustion capture. Instead of being directly discharged to the atmosphere, flue gas is passed through an equipment that separates most of the CO_2, which is then fed to a storage reservoir while the remaining flue gas is discharged to the atmosphere (**Fig. 3**) [23].
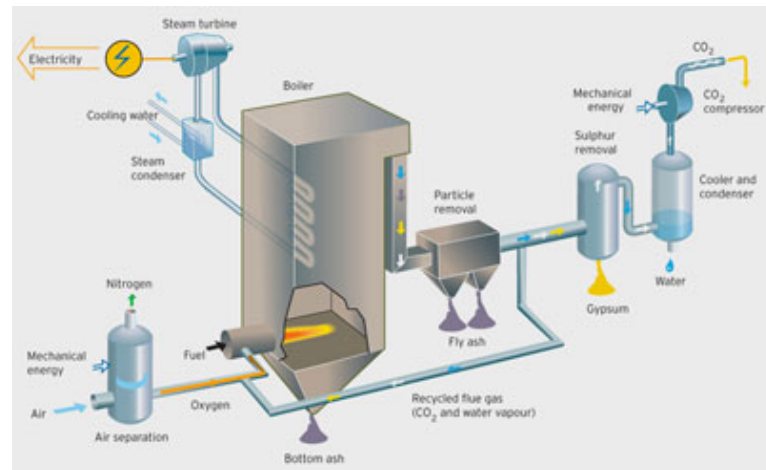
Fig. 3 Post-Combustion Capture.

The main advantage of post-combustion technique, with respect to the other capture options, is that it can be adapted to any existing plants.

Oxy-fuel Combustion: a third option consists in avoiding the introduction of N_2 in the combustion system by using pure oxygen or a mixture of pure oxygen and a CO_2-rich recycled flue gas instead of air (**Fig. 4**) [24,25].
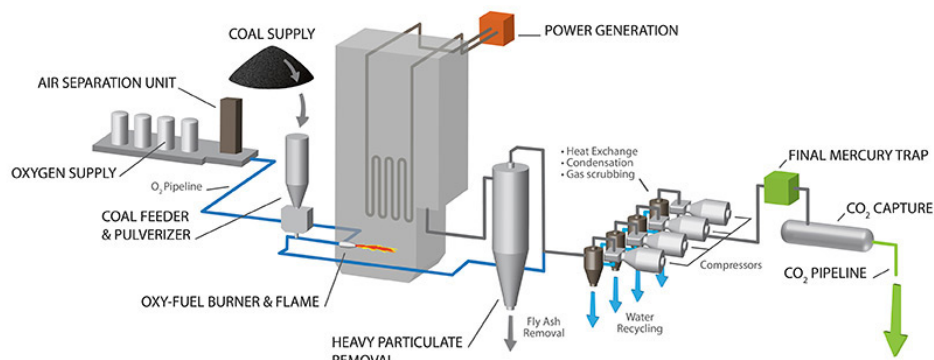
Fig. 4 Oxy-Fuel Combustion.

However, combustion of a fuel with pure oxygen has a combustion temperature of about 3500°C which is far too high for typical power plant materials (the combustion temperature is limited to about 1300-1400°C in a typical gas turbine cycle and to about 1900°C in an oxy-fuel coal-fired boiler using current technology). Hence, the combustion temperature is controlled by the proportion of flue gas (CO_2 and water) recycled back to the combustion chamber, thus making the oxy-fuel combustion applicable to pre-existing boilers, even though an additional air separation unit must be envisaged. The combustion products (or flue gas) consist mainly of carbon dioxide and water vapor together with excess oxygen required to ensure complete combustion of the fuel. The net flue gas, after cooling to condense water vapor, contains from about 80-98% CO_2 depending on the fuel used and the particular oxy-fuel combustion process. Even though the CO_2 capture efficiency is very close to 100%, this capture process has a huge drawback, i.e. the extremely high cost needed for production of pure oxygen.

Chemical Looping Combustion (CLC): the main idea of chemical looping combustion is to split combustion of a hydrocarbon or carbonaceous fuel into separate oxidation and reduction reactions [26,27]. CLC uses a solid oxygen carrier (generally a metal oxide) to transfer the oxygen from the air to the fuel. The advantage with this technique compared to normal combustion is that CO_2 and H_2O are inherently separated from the other components of the flue gas, namely, N_2 and unreacted O_2, and thus no extra energy is needed for CO_2 separation. The CLC system is composed of two reactors, an air and a fuel reactor, as shown in **Fig. 5**.
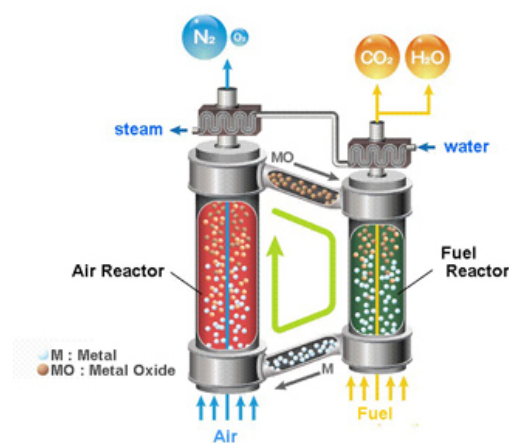
Fig. 5 Chemical Looping Combustion.

The fuel is fed into the fuel reactor where it is oxidized by the lattice oxygen of the oxygen carriers according to:

$$(2n+m)M_yO_x + C_nH_{2m} \rightarrow (2n+m)M_yO_{x-1} + mH_2O + nCO_2 \qquad (4)$$
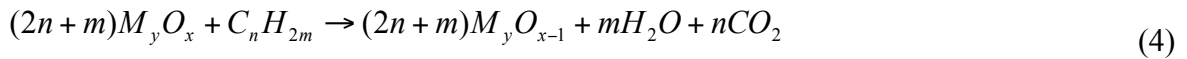
where M_yO_x is the fully oxidized oxygen carrier and M_yO_{x-1} is the oxygen carrier in the reduced form which could be a metal or a metal oxide with lower oxygen content. The exit stream from the fuel reactor contains only CO_2 and water vapor. The pure CO_2 can be readily recovered by condensing water vapor, eliminating the need of an additional energy for CO_2 separation. The water-free CO_2 can be sequestrated or used for other purpose. Once fuel oxidation completed the reduced metal oxide MyOx−1 is transported to the air reactor where it is reoxidized according the reaction:

$$M_yO_{x-1} + 1/2 O_2 \rightarrow M_yO_x + (air : N_2 + unreacted O_2) \qquad (5)$$

Of course, the operating temperatures of the two reactors depend on the nature of the fuel and metal oxide used, but generally they vary in the range 600-1200°C. In particular, the reactoristic configuration which best fits this technique is a Dual Interconnected Fluidized Bed Reactor (DiFB Reactor). In particular, a high-velocity riser and a low velocity bubbling fluidized bed are considered as the air and fuel reactors, respectively. The solid particles leaving the riser are recovered by a cyclone and sent back to the fuel reactor. In the low velocity fluidized bed (fuel reactor), the oxygen is transferred from the carrier to the fuel.

Transportation

While no fully integrated, commercial-scale CCS projects are in operation to date, many of the component technologies for the compression and transportation (e.g., through pre-existing pipelines for instance) of CO_2 are relatively mature. Indeed, transportation of CO_2 from production site to storage site should constitute no major obstacle. Large-scale transportation of CO_2 has already been practiced for decades for use in enhanced oil recovery. Both on-shore and off-shore pipelines are feasible. Whereas, ships offer the most cost-effective option for very long distances.

Storage

The idea behind carbon sequestration is to find large reservoirs for storing CO_2 rather than allowing it to discharge to the atmosphere. Available options for the final handling of the captured CO_2 include underground geological storage, ocean storage and mineral carbonation. Geological storage, which presently seems to be the most plausible alternative, basically means returning the carbon to whence it came. Potential geological storage sites include depleted oil and gas reservoirs, deep unmineable coal beds, deep saline water-saturated reservoir rocks (aquifers). In addition, the captured CO_2 can be an effective solvent to improve oil recovery in Enhanced Oil Recovery (EOR) and used to increase the production of methane from coal beds (ECBM).

I.3 Separation Techniques in Post Combustion Capture

On the basis of what said so far, it emerges that among all the possible CCS technologies, the best option to be applied to existing power plants is the post-combustion strategy. A major difficulty of post-combustion capture is to produce a highly concentrated CO_2 stream matching the purity requirement for transportation and storage while the CO_2 is diluted in the flue gas: between 4% for the natural gas combined cycle (NGCC) and 14% for pulverized coal (PC) [28]. One more explanation for the slow deployment of fully integrated commercial CCS schemes is the considerable cost of the capture phase, which represents approximately two thirds of the total cost for CCS [28]. In conclusion, the energy consumption has to be low while keeping high CO_2 recovery. So, the development of an efficient and cost-effective CO_2 capture technique is considered to be one of the highest priorities in the field of CCS.

An important factor to be taken into account in CO_2 capture is the CO_2 partial pressure of the gas stream to be treated, which is actually a key variable in the selection of the separation method. It can be said that the lower the CO_2 partial pressure of a gas stream, the more stringent the conditions for the separation process. In other words, high CO_2 concentrations are much easier to be captured and purified than lower ones. In this regards, the separation process of a flue gas is not simple, due to the relatively low CO_2 partial pressure (Tab. 2).

In general, there are four types of separation techniques to separate CO_2 from the gas stream: absorption by means of solvents, membranes, cryogenics, adsorption by solid materials and calcium looping cycle [30].

Absorption with solvents

The current leading separation process to perform CO_2 capture from post-combustion flue gases is amine scrubbing. Chemical solvents like mono-ethanolamine (MEA) and di-ethanolamine (DEA) can remove CO_2 from a gas stream by means of a chemical reaction, which can be reversed by heating. Generally, these solvents are characterized by CO_2 recovery rates up to 98% and product purity higher than 99% [32,33,34].

The main attraction of the absorption approach is that it is already commercially available, albeit on a very small scale relative to what would be required by a power station producing hundreds or thousands of megawatts of electricity [35,36]. In particular, MEA scrubbing technology has already started its scale-up, although it is still a technology with high energy penalties, between 4.2 and 4.8 GJ per ton of CO_2 captured [28]. Besides, several other shortcomings affect this technology. First of all, the energy needed for the solvent regeneration is prohibitively expensive, thus detrimentally affecting the efficiency of the entire process. Indeed, if applied to a dilute gas streams (i.e. characterized by low CO_2

concentration), as typical of post-combustion, a large quantity of solvents needs to be used in the capture stage and great amount of energy should be required for their regeneration. Besides, amine solvents have originally been developed to be employed in reducing conditions, therefore, the application to flue gases produced by power plant, namely in oxidizing environment, can lead to their deactivation, unless proper inhibitors are used, thus leading to a further costs increase as well. Also, stable solvent by-products (salts) can accumulate as a result of reaction with acid gas impurities (SO_x and NO_x) during operation. Moreover, amine and water may enter the gas stream, thus releasing amines (as gas and liquid) emissions to air, while possibly also forming other compounds in the atmosphere after emission [37,38]. In sunlight, amines undergo reactions with atmospheric oxidants involving oxidized nitrogen compounds (photo-oxidation) to form compounds such as nitrosamines, nitramines, and amides [39]. Nitrosamines are of particular concern, as they are toxic and carcinogenic to humans at extremely low levels [40].

All things considered, this capture method is clearly energy intensive and it is not cost-effective for reduction of carbon emissions from power plants. In particular, the energy penalty for a coal-fired power station using traditional aqueous MEA for capture has been estimated as 25 to 40% [32].

Membranes

Gas separation membranes allow one component in a gas stream to pass through faster than the others. There are many different types of gas separation membranes, including porous inorganic membranes, palladium membranes, polymeric membranes and zeolites [41,42]. However, in flue gases the low CO_2 partial pressure difference provides a low driving force for gas separation. Therefore, membranes cannot usually achieve high degrees of separation (the maximum percentage of CO_2 removed is lower than for a standard chemical absorption process), so multiple stages and/or recycle of one of the streams is necessary. This leads to increased complexity, energy consumption and costs; in other words, the removal of carbon dioxide using commercially available membranes results in higher energy penalties on the power generation efficiency compared to a standard chemical absorption process. Improvements can be made if more selective membranes become available. The membrane option currently receiving the most attention is a hybrid membrane-absorbent (or solvent) system, thus allowing to combine the best features of membranes and solvent scrubbing. Membrane/solvent systems employ membranes to provide a very high surface area to volume ratio for mass exchange between a gas stream and a solvent resulting in a very compact

system. This results in a membrane contactor system in which the membrane forms a gas permeable barrier between a liquid and a gaseous phase.

Cryogenics

CO_2 can be separated from other gases by cooling and condensation. Cryogenic separation is widely used commercially for streams that already have high CO_2 concentrations (typically >90%) but it is not used for more dilute CO_2 streams [43]. A major disadvantage of this technique is the amount of energy required to provide the refrigeration necessary for the process, particularly for dilute gas streams. So, cryogenics is generally applied to high concentration and/or pressure gas streams, such as in pre-combustion capture processes.

Calcium Looping Cycle

Calcium looping cycle relies on the reversible reaction between calcium oxide and carbon dioxide to form calcium carbonate [44,45]. In particular, a calcium oxide (CaO) sorbent, usually but not exclusively derived from limestone, is repeatedly cycled between two vessels. In one vessel (the carbonator) carbonation of CaO occurs, stripping the flue gas of its CO_2. The $CaCO_3$ formed is then passed to another vessel where calcination occurs (the calciner) and the CaO formed is passed back to the carbonator leaving a pure stream of CO_2 suitable for sequestration Fig. 1.

$$CaO_{(s)} + CO_{2(g)} \leftrightarrow CaCO_{3(s)} \tag{6}$$

Heat from the exothermic carbonation of lime can be used to run a steam cycle, making up for some of the energy losses elsewhere. The carbonation reaction is exothermic and the backward step, known as the calcination reaction, is endothermic. Carbonation is characterized by a rapid initial rate followed by an abrupt transition to a very slow reaction rate, whereas calcination typically proceeds rapidly to completion in minutes over a wide range of conditions [46]. The conditions in the calciner must be a compromise between the increased rate of reaction obtained at higher temperatures and the reduced rate of degradation of sorbent at lower temperatures. The conditions in the carbonator must strike a balance between the increased equilibrium conversion obtained at lower temperatures and the increased rate of reaction at higher temperatures.
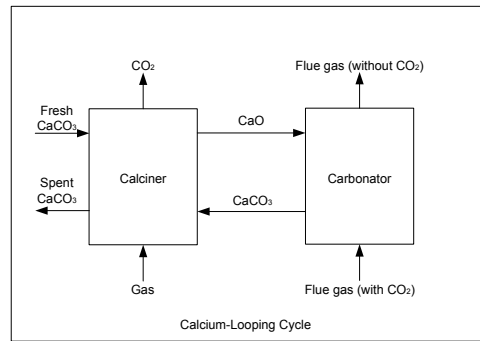
Fig. 6 Schematic description of Calcium Looping Cycle.

The reactoristic configurations which best fits this technique is a Dual Interconnected Fluidized Bed Reactor (DiFB Reactor), constituted by a reactor operated in the range of temperatures 600-700°C, acting as carbonator, and another in the range of temperatures 750-950°C, acting as Calciner, both these two fluidized bed reactors are operated in bubbling conditions. The main drawbacks related to such technology are the sorbent deactivation during the repeated carbonation/calcinations cycles and the sorbent leakage due to comminution phenomena.

Adsorption

Adsorption relies on the thermodynamic properties of a substance to shift from the gas phase to attach itself to a solid material [47]. This attachment can be either physical (van der Waals) or chemical (covalent bonding). Adsorption encompasses the selective removal of CO_2 from a gas stream to the adsorbent, followed by regeneration (desorption), which can be achieved either by reducing pressure (Pressure-Swing Adsorption or PSA), or by increasing temperature (Temperature Swing Adsorption, or TSA) or by passing an electric current through the adsorbent (Electrical Swing Adsorption, or ESA) or process hybrids (PTSA). A key concern for physical adsorbents is balancing a strong affinity for removing an undesired component from a gas mixture with the energy consumption required for their regeneration.

Among all these technological options, adsorption using solid sorbents, together with calcium looping, is one of the most promising alternatives since it appears to offer potential energy savings together with lower capital and operating costs. In particular, the main argument in favor of solid sorbents is that the combination of a lower heat of sorption, a higher CO_2 loading and a lower heat capacity of the solid compared to the aqueous solution of MEA, thus lowering the energy consumption for regeneration [47]. On the contrary, absorption, membranes and cryogenics do not seem to be particularly suitable as capture solution, since, for different reasons, the advantages appear to be greatly outnumbered by the drawbacks, as clearly explained hereafter [31].

I.4 Adsorption Process

Adsorption is a separation process in which certain components of a fluid phase are transferred to the surface of a solid adsorbent (**Fig. 7**). Usually the small particles of adsorbent are held in a fixed bed, and fluid is passed continuously through the bed until the solid is nearly saturated and the desired separation can no longer be achieved.
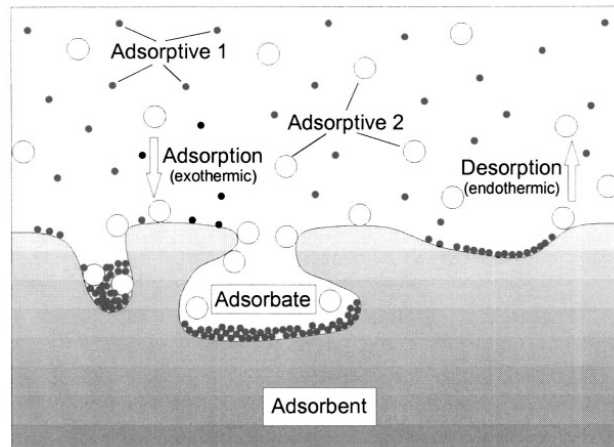
Fig. 7 Adsorption mechanism

In particular, molecules diffuse from the bulk of the fluid to the surface of the solid adsorbent forming a distinct adsorbed phase. Each separation process exploits a difference in a property of the components to be separated. Separation by adsorption depends on one component being more readily adsorbed than another. The selection of a suitable process may also depend on the ease with which the separated components can be recovered. The adsorbent has to be removed at intervals from the process and regenerated, that is, restored to its original condition.

The thermodynamic drive of the process is, as always, to be found in the reduction of the free energy of the process. The adsorption is, obviously, characterized by a decrease of entropy of the adsorbed molecules; in fact, the molecules, previously free to move in the fluid phase, after being adsorbed can only move on the solid surface. Accordingly, the process spontaneity is assured by the liberation of heat involved in the adsorption; in other words, adsorption is an exothermic process.

In particular, adsorption occurs when molecules diffusing in the fluid phase are held for a period of time by forces emanating from an adjacent surface. The surface represents a gross discontinuity in the structure of the solid, and atoms at the surface have a residue of molecular forces that are not satisfied by surrounding atoms such as those in the body of the structure.

These residual or van der Waals forces are common to all surfaces and the only reason why certain solids are designated "adsorbents" is that they can be manufactured in a highly porous form, giving rise to a large internal surface. In comparison the external surface makes only a modest contribution to the total, even when the solid is finely divided [48].

On the basis of the nature of the forces involved in the attraction between the adsorbate molecules and the adsorbent, two kinds of adsorption can be defined: physical and chemical adsorption.

In the former the target molecules are attracted to the surface of pore walls within a high surface-area sorbent by van der Waals forces (shown schematically in **Fig. 8**) and have a low heat of adsorption that is only slightly greater than heat of sublimation of the adsorbate (i.e. low bond energy of the order of 10kcal/mol). Since the forces involved are not strong, this adsorption may be easily reversed. On the contrary, in the latter, additional forces bind absorbed molecules to the solid surface (roughly equal to the heat of reaction, 100kcal/mol), involving the exchange or sharing of electrons, or possibly molecules forming atoms or radicals. In such cases the term chemisorption is used to describe the phenomenon. This is less easily reversed than physical adsorption, and regeneration may be a problem. Moreover, chemisorption is restricted to just one layer of molecules on the surface, although it may be followed by additional layers of physically adsorbed molecules.
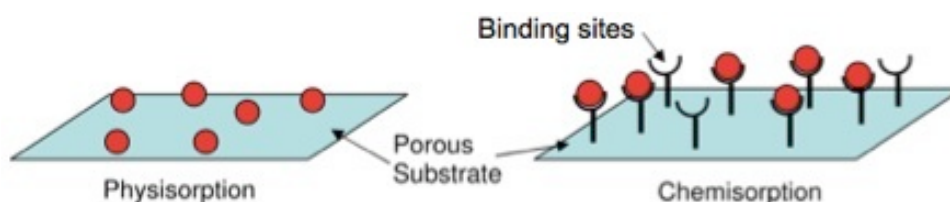
Fig. 8 In physisorption the CO_2 is adsorbed weakly by the substrate itself, in chemisorption, the CO_2 is adsorbed more strongly by specific binding sites.

As said before, when molecules move from a bulk fluid to an adsorbed phase, they lose degrees of freedom and the free energy is reduced by the liberation of heat. For physical adsorption, the amount of heat is similar in magnitude to the heat of condensation. For chemisorption it is greater and of an order of magnitude normally associated with a chemical reaction [51]. If the heat of adsorption cannot be dispersed by cooling, the capacity of the adsorbent will be reduced as its temperature increases.

I.4.1 Thermodynamic Equilibria

Adsorption equilibrium is a dynamic concept achieved when the rate at which molecules adsorb on to a surface is equal to the rate at which they desorb.

The capacity of an adsorbent for a particular adsorbate involves the interaction of three properties: the concentration, C, of the adsorbate in the fluid phase, the concentration of the adsorbate in the solid phase (mass of adsorbed solute per grams of adsorbent), C_s, and the temperature, T, of the system. If one of these properties is kept constant, the other two may be graphed to represent the equilibrium. The commonest practice is to keep the temperature constant and to plot C against C_s to give an adsorption isotherm (**Fig. 9**) [48]. In gas–solid systems, it is often convenient to express C as a pressure of adsorbate.
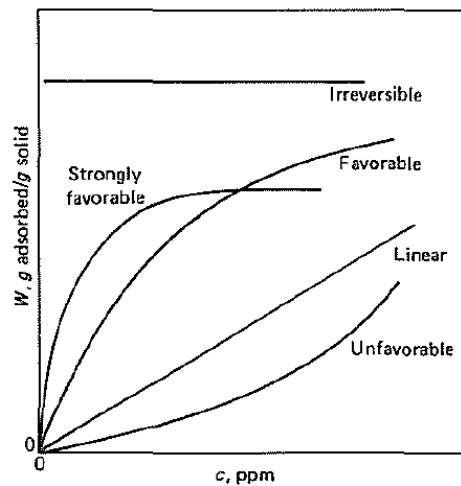
Fig. 9 Typical adsorption isotherms

I.4.1.1 Types of Isotherms

The linear isotherm goes through the origin, and the amount adsorbed is proportional to the concentration in the fluid. Isotherms that are convex upward are called favorable, because a relatively high solid loading can be obtained at low concentration in the fluid. All systems show a decrease in the amount adsorbed with an increase in temperature, and of course adsorbate can be removed by raising the temperature even for the cases labeled "irreversible." However, desorption requires a much higher temperature when the adsorption is strongly favorable or irreversible than when the isotherms are linear. An isotherm that is concave upward is called unfavorable because relatively low solid loadings are obtained and because it leads to quite long mass-transfer zones in the bed.

A general classification of sorption phenomena of gas-solid systems is given by the International Union of Pure and Applied Chemistry (IUPAC) [48]. Sing et al. [48] use roman

numbering from I to VI for their classification (**Fig. 10**). Type I is characterized by a constant sorption maximum and a convex shape. Type II exhibits an inflection point at which the shape changes from convex to concave. A concave isotherm is classified as type III. In some systems, three stages of adsorption may be discerned, giving rise to an isotherm referred to as Type IV. This has two plateaus and, in particular, it consists of two regions that are concave to the gas concentration axis separated by a region that is convex. The concave region that occurs at low gas concentrations is usually associated with the formation of a single layer of adsorbate molecules over the surface. The convex portion corresponds to the build-up of additional layers, whilst the other concave region is the result of condensation of adsorbate in the pores, so called capillary condensation. A concave isotherm with a sorption maximum is referred to as type V. This classification is based on physical adsorption of gases measured in porous or on dense solid materials. In addition to different shapes, it also takes into account different types of hysteresis loops that are caused by capillary condensation in pores.
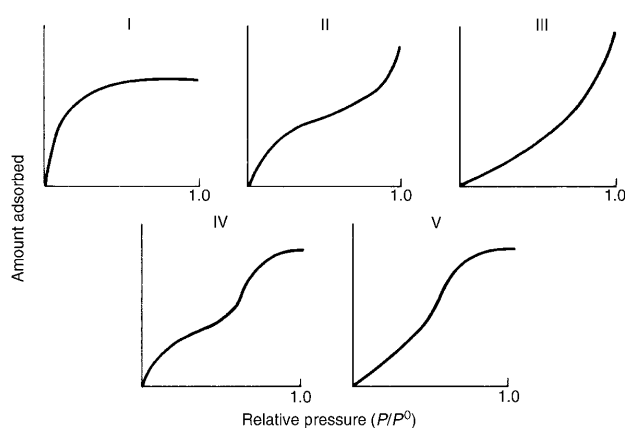
Fig. 10 Types of adsorption isotherms according to IUPAC classification.

It is not possible to predict the shape of an isotherm for a given system, although it has been observed that some shapes are often associated with a particular adsorbent or adsorbate properties. Charcoal, with pores just a few molecules in diameter, almost always gives a Type I isotherm. A non-porous solid is likely to give a Type II isotherm. If the cohesive forces between adsorbate molecules are greater than the adhesive forces between adsorbate and adsorbent, a Type V isotherm is likely to be obtained for a porous adsorbent and a Type III isotherm for a non-porous one. In the activated alumina air-water vapour system at normal temperature, the isotherm is found to be of Type IV.

I.4.1.2 Isotherms Equations

In the case of specific interactions between active sites and solute molecules the most accredited theory is the one proposed by Langmuir (1918) [48]. It is assumed that the process can be modeled by means of a chemical reaction between the adsorbed solute and the active site and no other kinds of interactions solute-solvent-active site exist. In spite of its substantial theoretical assumptions, the Langmuir model is one the most used in the practice, especially when the adsorbate concentration is low. In particular, this model is able to properly describe the case of one layer of molecules adsorbed on the surface of a solid. When this is not the case, other models can be adopted. When the solute concentration is very remarkably low and, in particular, lower than the value needed to realize the whole covering, the process can be described by a linear relation between the solute concentration in the fluid and in the solid phases. On the other hand, when it is possible to assume that the adsorbed solute is disposed over many layers, the interactions between the molecule adsorbed on an intermediate layer and the solute must be taken into account. The model of such a phenomenon has been developed by Bruner, Emmet and Teller (1938) [49] and is usually referred to as BET isotherm.

I.4.1.2.1   Linear Isotherm

At very low concentrations the molecules adsorbed are widely spaced over the adsorbent surface so that one molecule has no influence on another. For these limiting conditions it is reasonable to assume that the concentration in one phase is proportional to the concentration in the other, that is:

$$C_s = K_a C \tag{7}$$

This expression is analogous to Henry's Law for gas–liquid systems even to the extent that the proportionality constant obeys the van't Hoff equation and

$$K_a = K_0 e^{\Delta H / RT} \tag{8}$$

where ΔH is the enthalpy change per mole of adsorbate as it transfers from gaseous to adsorbed phase. At constant temperature, this equation becomes the simplest form of adsorption isotherm.

I.4.1.2.2   Langmuir Isotherm

The assumptions of the Langmuir model are:
- surface is homogeneous, that is adsorption energy is constant over all sites;

- adsorption on surface is localized, that is adsorbed atoms or molecules are adsorbed at definite, localized sites, and do not migrate over the surface;
- each site can accommodate only one molecule or atom;
- there are no interactions between adjacent molecules on the surface.

The Langmuir theory is based on a kinetic principle, that is the rate of adsorption (which is the striking rate at the surface multiplied by a striking coefficient, sometimes called the accommodation coefficient) is equal to the rate of desorption from the surface.

The rate of striking the surface, in mole per unit time and unit area, obtained from the kinetic theory of gas is:

$$R_s = \frac{P}{\sqrt{2\pi MRT}}$$ (9)

where P is the pressure, T the temperature, R the ideal gas constant. Allowing for the sticking coefficient α (which accounts for non perfect sticking), the rate of adsorption in mole adsorbed per unit bare surface area per unit time is:

$$R_a = \frac{\alpha P}{\sqrt{2\pi MRT}}$$. (10)

This is the rate of adsorption on a bare surface. On an occupied surface, when a molecule strikes the portion already occupied with adsorbed species, it will evaporate very quickly, just like a reflection from a mirror. Therefore, the rate of adsorption on an occupied surface is equal to the rate given by (8) multiplied by the fraction of empty sites, that is:

$$R_a = \frac{\alpha P}{\sqrt{2\pi MRT}}(1-\theta)$$ (11)

where θ is the fractional coverage. Here R_a is the number of moles adsorbed per unit area (including covered and uncovered areas) per unit time. The rate of desorption from the surface is equal to the rate, which corresponds to fully covered surface (k_d) multiplied by the fractional coverage, that is:

$$R_d = k_d\theta = k_{d\infty}\exp\left(-\frac{E_d}{RT}\right)\theta$$ (12)

where E_d is the activation energy for desorption, which is equal to the heat of adsorption for physically sorbed species since there is no energy barrier for physical adsorption. The parameter $k_{d\infty}$ is the rate constant for desorption at infinite temperature. Equating the rates of adsorption (11) and desorption (12), we obtain the following famous Langmuir isotherm written in terms of fractional loading:

$$\theta = \frac{bP}{1 + bP} \tag{13}$$

here b is an affinity constant which measures the strength the adsorbate molecules are attracted with on the surface:

$$b(T) = b_\infty \exp\left(\frac{Q}{RT}\right) \tag{14}$$

here Q is the heat of adsorption, R the gas constant and $b\infty$ the pre-exponential factor of the affinity constant:

$$b_\infty = \frac{\alpha}{k_{d\infty}\sqrt{2\pi MRT}} \tag{15}$$

which inversely proportional to the square root of the molecular weight. So, on that basis, the Langmuir equation in terms of concentration is:

$$C_\mu = C_{\mu s}\frac{b(T)P}{1 + b(T)P} \tag{16}$$

where $C_{\mu s}$ is the concentration of the adsorbed phase when the monolayer is complete (i.e. the maximum adsorbed concentration) and C_μ is the concentration of the absorbed phase (**Fig. 11**).
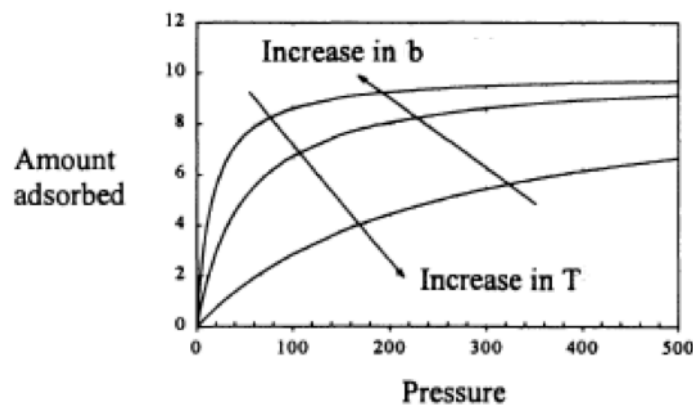
Fig. 11 Behaviour of Langmuir equation

The Langmuir isotherm is derived assuming a uniform surface, not always a valid assumption, but the relation works fairly well for gases that are weakly adsorbed.

I.4.1.2.3   BET Isotherm

In some cases, molecules first adsorb onto the solid surface as a layering process, and when the pressure is sufficiently high multiple layers are formed. Brunauer, Emmett and Teller are the first to develop a theory to account for this multilayer adsorption, and the range of validity of this theory is approximately between 0.05 and 0.35 times the vapor pressure. The BET

theory was first developed for a flat surface (no curvature) and there is no limit in the number of layers, which can be accommodated on the surface. This theory made use of the same assumptions as those used in the Langmuir theory, that is the surface is energetically homogeneous (adsorption energy does not change with the progress of adsorption in the same layer) and there is no interaction among adsorbed molecules. The corresponding equation is:

$$\frac{V}{V_m} = \frac{CP}{(P_0 - P)[1 + (C-1)(P/P_0)]}$$

(17)

Where V_m and C are parameters.

I.4.2 Kinetics

The performance of adsorption processes results, in general, from the combined effects of thermodynamic and rate factors. It is convenient to consider first thermodynamic factors. These determine the process performance in a limit where the system behaves ideally, i.e. without mass transfer and kinetic limitations. There are several resistances that may hinder the movement of a molecule of adsorbate from the bulk fluid outside a particle to an adsorption site on its internal surface. In broad terms, a molecule, under the influence of concentration gradients, diffuses from the bulk phase in the adsorption column to laminar boundary layer surrounding the particle; it then diffuse through this boundary layer to the particle external surface, and, finally, by various possible mechanisms, it diffuses through the pores or the lattice vacancies in the particle until it is held by an adsorption site (**Fig. 12**).
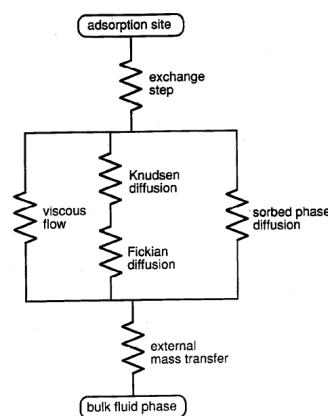
Fig. 12 Mass transport mechanisms for molecule transfer from the surrounding bulk fluid phase to an adsorption site on the adsorbent pore wall.

As regards, the intraparticle transport, several mechanisms has to be taken into account [52]:

i. Pore diffusion in fluid-filled pores. These pores are sufficiently large that the adsorbing molecule escapes the force field of the adsorbent surface. Thus, this process is often referred to as macropore diffusion.

ii. Solid diffusion in the adsorbed phase. This is a diffusion process in pores sufficiently small that the diffusing molecule never escapes the force field of the adsorbent surface. In this case, transport may occur by an activated process involving jumps between adsorption sites. Such a process is often called surface diffusion or micropore or intracrystalline diffusion. The driving force for the process can thus be approximated by the gradient in concentration of the species in its adsorbed state.

iii. Reaction kinetics at phase boundaries. Rates of adsorption and desorption in porous adsorbents are generally controlled by mass transfer within the pore network rather than by the kinetics of sorption at the surface. Exceptions are the cases of chemisorption and affinity-adsorption systems used for biological separations, where the kinetics of bond formation can be exceedingly slow.

I.5   Regeneration Techniques

For adsorption to be used as CO_2 capture technique, an effective and less energy-consumed regeneration of the CO_2 captured adsorbents is definitely needed. The regeneration techniques include: pressure swing adsorption (PSA), vacuum swing adsorption (VSA), temperature swing adsorption (TSA), electric swing adsorption (ESA).

Both PSA and VSA are performed by altering the pressures. More specifically, in PSA, adsorption is typically performed at pressures higher than atmospheric pressure, while desorption is performed at atmospheric pressure. However, in a conventional PSA process, it is the least adsorbing species that can be recovered at high concentrations in the adsorption product [118,119]. However, our interest focuses on the concentration of strongly adsorbed species (CO_2) in the desorption product while maximizing the CO_2 capture efficiency. Moreover, other important shortcomings are that application of conventional pressure swing to combustion flue gas involves compression of a large fraction of inert nitrogen as well, which is expensive, [120] and that the sorbent selectivity for CO_2 drops with increasing pressure, making it more difficult to achieve high purity CO_2 in the desorption gas [119]. To overcome these pitfalls, VSA has been proposed, namely a version of the pressure swing process conducted at ambient pressure with regeneration under vacuum [120,121].

In a conventional TSA regeneration process the temperature of adsorbents is increased by purging the bed with a preheated gas (e.g. steam or N_2) [122]. Direct heating using a carrier gas usually results in the dilution of the desorbed CO_2 by the carrier gas. Also, use of large quantities of heated N_2 for adsorbent bed regeneration would not be suitable for large scale applications. However, the heat for desorption of CO_2 (for regeneration of the solid) can be provided in different ways: besides by directly contacting the solid with hot gas that flows through the bed, the adsorbent can also be heated up by indirect heating via heat exchanger tubes. In this way CO_2 is desorbed without the use of any carrier gas and the desorbed gas can be recovered by thermal expansion thus overcoming the dilution problem (pure CO_2 stream as desorption gas) [28]. In particular, it is worth noting that indirect heating can provide a lot more energy than direct heating because the heating fluid (which is by default water vapour) can be allowed to condense. The heat of condensation releases a lot more energy than a simple cooling down of the gas.

In ESA, heat is generated by Joule effect via electric current passing through the adsorbents (i.e. the increase of temperature is obtained by conducting electricity through a conductive adsorbent). ESA offers several advantages including less heat demanded, fast heating rate, better desorption kinetics and dynamics and independent control of gas and heat flow rates as compared with PSA and TSA [123]. The main disadvantage of ESA compared to thermal swing regeneration is the consumption of electric energy, which is the product of the power plant, whereas, in the case of thermal regeneration, waste heat from the flue gas can be used for sorbent heating. Therefore, the viability of the process implementation depends on the energy spent per amount of CO_2 captured. Moreover, employing ESA in CO_2 capture depends on the availability of adsorbents that combine high CO_2 capacity and selectivity together with electric conductivity. The reference adsorbent employed in ESA is activated carbon, due to its electric conductivity properties. On the contrary, other materials with favorable adsorption properties, like zeolites or MOF, do not conduct electricity and cannot be employed in ESA.

I.6   Adsorbent Materials

As already stated before, adsorption has been recognized to have all the potentialities to become the leader CO_2 capture technology. In this respect, suitable adsorbents for CO_2 removal from flue gas should combine several attributes (Fig. 13), including:
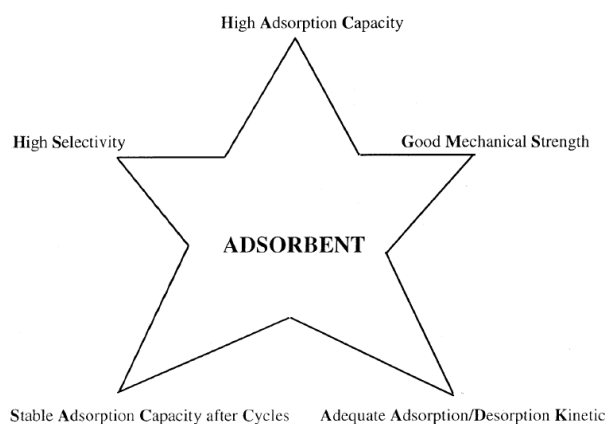
Fig. 13 Properties of the required adsorbent.

- High CO_2 adsorption capacity: CO_2 equilibrium adsorption capacity is one of the main properties used to screen new adsorbents. Knowledge of the equilibrium adsorption isotherms is of prime importance for early evaluation of potential adsorbents [53]. It is well established that from the slope of the adsorption isotherm at low pressure, it is possible to estimate the adsorbate affinity for a given adsorbent. Thus, in terms of CO_2 uptake, the ideal materials should exhibit a CO_2 adsorption isotherm with steep slope (favorable CO_2 adsorption isotherm) corresponding to high uptake at low CO_2 partial pressure. A less steep slope (unfavorable CO_2 adsorption isotherm) is indicative of a lower affinity toward CO_2.

- Fast adsorption/desorption kinetics: adsorption kinetics primarily affects the working adsorption capacity. A suitable CO_2 adsorbent should have a high rate of adsorption, resulting in a working capacity close to equilibrium capacity over a wide range of operating conditions [53];

- High CO_2 selectivity: the adsorbent selectivity toward CO_2 has a direct impact on the degree of purity of the product. This in turn, plays a major role in the economics of the CO_2 adsorption process [54]. Ideally, an adsorbent for flue gas treatment should not adsorb any nitrogen;

- Stability during extensive adsorption–desorption cycling: the lifetime of adsorbents, which determines the frequency of their replacement, is a critical property of equal importance as the CO_2 adsorption capacity, selectivity and kinetics, because of its direct impact on the economics of any commercial scale operation [55];

- Adequate mechanical strength of adsorbent particles [54].

In addition to the above-mentioned characteristics:

- Mild conditions for regeneration: the ease of regeneration of the adsorbent is a key property in the selection of materials for CO_2 separation. More exactly, a key concern is balancing a strong affinity towards CO_2 with the energy consumption required for the regeneration step [56]. Then, depending on the structural and chemical properties of the adsorbent, adsorption–desorption cycling may be achieved via temperature or pressure (or vacuum). In practice, incorporation of functional groups can be used to modify the adsorbent–adsorbate interactions (e.g., Van der Waals, electrostatic, hydrogen bonding or acid–base interactions) and affect the CO_2 uptake and selectivity. Optimum interactions should be neither too weak nor too strong. Too weak bonding results in low CO_2 adsorption capacity at low pressure, but easy regeneration. Conversely, strong bonding induces high adsorption capacity but desorption will be difficult and costly;

- Tolerance to the presence of moisture and other impurities in the feed: in addition to CO_2 and N_2, flue gas contains water vapor and other impurities such as O_2, SO_2 and NO_x. The degree of tolerance and the affinity of the adsorbent to such impurities may affect significantly the strategy to be used, with direct impact on the overall economics of the CO_2 separation process. Moisture is known to adversely affect CO_2 uptake in a variety of physical adsorbents such as zeolites and activated carbon [53]. Consequently, the strategies proposed for CO_2 adsorption from flue gas is likely to include an upstream drying step. It is also generally established that CO_2 adsorbents have high affinity to SO_2 and even some affinity toward NO_x, which may adversely affect the CO_2 adsorption capability of the material. Thus, abatement of SO_2 and NO_x from flue gas prior to CO_2 capture is required in most cases [53];

- Low cost [56].

Typical physisorbents for CO_2 capture include carbon materials, alumino-silicas such as zeolites (13X, 5A), alumino-phosphates (AlPOs) and alumino-silico-phosphates (SAPOs), and more recently metal organic frameworks (MOFs) and carbon nanotubes (CNTs). Whereas, the CO_2 chemical adsorbents are those obtained through incorporation of functional groups into solid supports (i.e. amine-grafted silica, amine functionalized carbons) [57].

I.6.1 Carbons

Because of their wide availability, low cost and high thermal stability, it is largely established that activated carbons have advantages over other CO_2 adsorbents. Among the carbon-based adsorbents reported in the literature, activated carbons (ACs) and carbon nanotubes (CNTs)

are the most investigated materials. CO_2 adsorption on activated carbons has been widely studied experimentally and theoretically [58] and has found commercial applications [48,51]. There is a wide range of activated carbons with a large variety of microporous and mesoporous structures. Activated carbon may be produced from many raw materials such as coal, coke pitch, wood or biomass sources (e.g. saw dust, coconut shells, olive stones), often via two steps: carbonization and activation [59]. Carbon molecular sieves (CMS) are a sub-class of activated carbon with narrow pore size distribution (PSD). They have been commercialized mainly for the separation of air and the production of high purity N_2 [60,61]. However, at low CO_2 partial pressure, activated carbons exhibit lower adsorption capacity and selectivity than zeolites due mainly to their less favorable adsorption isotherms. In spite of the hydrophobic character of carbon-based adsorbents, their CO_2 adsorption ability is adversely affected by the presence of water vapor [62].

As regards the CO_2 vs N_2 selectivity, it weakly dependent on temperature. This behavior of activated carbons was also pointed out by Dreisbach et al. [63] and Kurniwan et al. [64]. They found that CO_2 selectivity over N_2 for Norit type activated carbon is insensitive to the CO_2 pressure change. In terms of regenerability, in light of the low CO_2 adsorption enthalpy (22kJ/mol) [65], it is generally established that activated carbons are easily regenerated allowing their use in pressure swing adsorption (PSA) and temperature swing adsorption (TSA).

However, some activated carbons may contain functional groups that interact strongly with CO_2, thus preventing complete desorption. CO_2 adsorption kinetics on activated carbons is generally comparable to zeolites and depends on the type of diffusion involved, i.e., macropore, micropore or surface diffusion [66-68] and the heterogeneity of the material.

I.6.2 Zeolites and Zeolite-like Materials

Zeolites, which are highly ordered microporous crystalline materials [69], were heavily investigated because they are among the most promising materials for adsorption and separation of CO_2 [70-75]. The great interest of zeolites arises from the fact that a number of their properties, such as pore size and architecture or chemical composition, affect their adsorption performance. For instance, the Si/Al ratio and the nature of extraframework cations can be varied systematically [76,77], playing a major role in controlling the CO_2 adsorptive properties. Exhaustive studies [78-80] reported that the most promising zeolites for CO_2 adsorption are characterized by a low Si/Al ratio, corresponding to high content of

extraframework cations. The presence of aluminum atoms in these silicate-based molecular sieves introduces negative framework charges that are compensated with exchangeable cations within the pores. There are often alkali cations such as sodium or lithium that generate strong electrostatic interactions with carbon dioxide. The number and nature of extraframework cations affect the CO_2 adsorption properties of zeolites. Maurin et al. [80] investigated experimentally and theoretically, the CO_2 adsorption capacity and enthalpy for several faujasite-type zeolites in sodium form, with different Si/Al ratios, namely, dealuminated NaY (DAY, Si/Al=∞), NaY (Si/Al=2.4) and low silica NaX (NaLSX, Si/Al=1). At low pressure for both adsorption and desorption, 13X (or NaX with Si/Al=1.25) and NaY were claimed to be the most suitable adsorbents with favorable CO_2 adsorption isotherms. Purely siliceous NaY [80], silicalite, ITQ3 and ITQ7 [71] exhibited at least 12 times lower adsorption capacity than NaY and NaLSX at 0.1 bar and room temperature. The adsorption capacity at 0.1 bar followed the sequence Cs<Rb≈K<Li≈Na for X zeolites, in a more recent contribution [81]. In terms of CO_2 adsorption kinetics, zeolites are ranked among the fastest adsorbents, reaching equilibrium capacity within minutes [82]. Moreover, a large number of studies were devoted to NaX faujasite using different recycling configurations, including temperature swing and pressure swing adsorption [76,77,28]. Although the CO_2 adsorption enthalpy on X and Y zeolites was found to be dependent on the nature of extraframework cations, within the range of 30–50kJ/mol, it is low enough to allow reversible CO_2 adsorption. Zeolites generally operate without any loss in performance, provided that the feed stream is strictly dry. Although low silica materials exhibit high adsorption capacity and selectivity at low pressure with favorable isotherms, they are very sensitive to the presence of water, which strongly inhibits the adsorption of CO_2 [83].

I.6.3 MOFs and Zeolite-like MOFs

Although an emerging class of porous materials, metal organic frameworks (MOFs) have attracted a growing interest, motivating extensive studies, both theoretically and experimentally. In particular, their high surface area (e.g. MOF-177 was reported to have a record surface area of about 4500m^2/g of material [84]) and the diversity of their metallic centers and organic functionalities direct the potential applications of these materials towards gas adsorption and separation. The structure of MOFs is obtained by the assembly of metallic centers and organic linkers through strong covalent bonds [85]. Depending on the metal and organic ligand selected, networks with various pore shape, size, volume and chemistry can be

synthesized and thus adapted to the specific needs of the adsorption process considered [85,86,87]. In particular, the pore sizes can be adjusted from several angstroms to a few nanometers by varying the sizes of the organic linkers [86,88-90]. Moreover, the properties and functions of the pores can be easily tuned for specific applications by post-synthetic modification of the parent MOFs [88,91-94]. The integrity of these pores and channels can be retained after careful removal of the guest species. The remaining voids within the 3D structures then can adsorb other guest molecules [88,95,96].

Considerable efforts have been expended on the synthesis of MOF materials in the last several years [88,89,97]. MOFs are synthesized generally by hydrothermal or solvothermal methods. Some novel electrochemical approach has also been reported recently [98]. The state of the art is in the choice of metal centers and design and synthesis of organic ligands.

Contributions in the synthesis of novel MOFs and their CO_2 adsorption properties were reported by Millward and Yaghi [99]. Their early work was followed by an extensive effort to develop new types of MOFs for the separation and storage of CO_2 [100-107]. In terms of kinetics, MOFs are as fast CO_2 adsorbents as zeolites according to some computational studies [101-112].

Generally, self-diffusivities or intracrystalline diffusivities for gas adsorbed in MOFs are larger than in zeolites because of larger pores and open structures in MOF materials [113-116] Liu et al. [117] reported that the main resistance for CO_2 adsorption in HKUST-1 (or CuBTC, BTC standing for benzene tricarboxylate) and Ni/DOBDC (DOBDC, standing for 2,5-dioxido-1,4-benzenedicarboxylate) is macropore diffusion. So the CO_2 adsorption rate is generally much faster than CO_2 adsorption in NaX and 5A zeolites where micropore diffusion is the rate control mechanism. Due to the favorable properties mentioned above, MOFs stand out from other porous materials for gas storage and separation applications. However, it is generally recognized that by far the most critical issue for the stability of these materials is their hydrothermal stability. The behavior of MOFs and their subfamilies in hydrated conditions varies widely, from materials that irreversibly degrade even under mild conditions to materials that are highly stable in boiling water.

I.7 Issues of CO₂ Capture by Adsorption

In light of what said so far, it occurs that, adsorption using solid sorbents is recognized to be attractive to complement or replace the current absorption technology due to its low energy requirement. It is also clear that the regeneration energy, followed by the capital cost of

capture-specific equipment, are the two variables contributing most significantly to the cost of CO_2 capture [57]. One significant contributor to the regeneration energy is the maximum separation efficiency which can be achieved by a given capture material. Enhancing this efficiency will have the greatest potential for lowering the overall cost of capture systems in near-term, with improvements in the capture capacity of new materials representing one of the foremost challenges [57].

Since the adsorption efficiency of a given material is the result of a complex combination of physical and chemical characteristics, the development of CO_2 specific adsorbents is necessary. The need, in other words, exists to design new materials whose physical and chemical properties can be tuned at the molecular level [57]. In this respect, nanomaterials are very versatile and simple to adjust according to the application at hand. Indeed, solely owing to their special size and shape, ultra-fine particles are particularly suitable to be easily tailored and/or functionalized on the surface with different ligands to induce significant changes in their physical and chemical properties [124]. Just for instance, one viable route for enhancing the adsorption efficiency can be the increasing of the affinity of the adsorbent surface to CO_2. In practice, chemical modification of the adsorbent material by the incorporation of functional groups with a great chemical affinity towards CO_2 (i.e. basic functionalities) can be used to modify the adsorbent–adsorbate interactions [125,126] (e.g., Van der Waals, electrostatic, hydrogen bonding or acid–base interactions) and positively affect the CO_2 uptake and selectivity. In particular, optimum interactions should be neither too weak (i.e. easy regeneration, but low CO_2 adsorption capacity at low pressure) nor too strong (i.e. high adsorption capacity, but difficult and costly desorption) [57].

It is evident that the materials development issue goes hand in hand with a process one. Indeed, as much as fulfilling an adsorbent material may be, each adsorbent strengths/weaknesses must be considered in the context of a practical adsorption process for effective CO_2 separation. Therefore, the question of how the most promising materials will perform in an actual separation process must be addressed. Ultimately, winning adsorbents will be those that effectively work within a practical and efficient CO_2 separation process [57].

I.7.1 Reactor Configurations

Although certain attributes of solid sorbents prove to be promising, they still must be integrated into a viable process, which includes the implementation of equipment that can

take full advantage of the sorbent properties and maximize the separation efficiency. If a solid-based CO_2 capture technology is to be commercialized in the near future, processes and equipment that are already commercially available for other applications must be evaluated and employed to the greatest extent possible [127].

The major constraints for CO_2 capture for operating conventional power plants are as follows:

   i.   Large volumetric flow rate per power plant. Typical flue gas flow rate of an operating 500MWpower plant is in excess of 3.4×10^4 m^3/min [128]. The final reactor design needs to result in a reasonable number of modules and reactor size.

   ii. Low available pressure drop for reactor design. The flue gas pressure at the tail end of a power plant is close to atmospheric. With proper integration it was estimated that the available pressure drop for CO_2 capture reactor is approximately 0.21bar [128]. Any increase in pressure drop requirement will incur substantial fan cost to increase flue gas pressure.

   iii. Low CO_2 partial pressure for adsorption. Although the CO_2 generation in a fossil fuel-fired conventional power plant is confined in the flue gas, the CO_2 concentration in the flue gas is only about 10-15%.

Common adsorption operations are generally performed in fixed-bed reactors. However, this technology does not appear suitable to fully exploit all the potential of an ad-hoc adsorbent material manufactured in the form of fine powder. Indeed, for fine materials to be used in fixed bed operations, a previous pelletization step should be needed to overcome the prohibitively high pressure drops related to fine particles beds. Therefore, serious benefits over fixed-bed adsorption methods are likely expected if a reliable and proper processing technology is developed to directly use these free-flowing fine powders. Moreover, for exothermic reactions (such as CO_2 adsorption) and endothermic reactions (such as CO_2 regeneration), fixed beds are generally not recommended [128]. Temperature swing in fixed bed reactors, serving as both the adsorber and the regenerator, is inherently inefficient because the beds have to be alternately cooled and heated to the correct reactor temperature for the proper reactions to occur. Poor local heat dissipation for the exothermic adsorption reactions and poor heat transfer to the solid sorbents for the endothermic regeneration reactions also will produce local "hot" and "cold" spots, respectively, preventing efficient conversions (i.e. reduction of CO_2 uptake during adsorption and slow-down of desorption kinetics during regeneration). In other words, a fixed bed operation will intrinsically involve temperature excursion inside the reactor. In particular, as already discussed in the paragraph about the regeneration techniques, a major problem linked to TSA is the large volume of gas

required due to the low heat capacity of the heating gas. It can be easily expected that this drawback would be magnified in the case of a fixed bed reactor due to the intrinsically poor heat transfer coefficients.

All these things considered, a viable alternative to fixed bed reactors is represented by fluidized bed reactors. Indeed, gas fluidization is generally considered to be one of the best available techniques to handle and process large quantities of powders. Indeed, this technology offers several advantages over fixed bed operation. In particular, fluidized beds are characterized by a very efficient gas-solid contact and intense solid mixing, thus increasing the efficiency of the reactor operation in terms of extremely high mass and heat transfer coefficients. This high heat transfer rate means an easier temperature control during both adsorption and regeneration step, namely the thermal equilibrium between the particles and the fluidizing gas can be attained very quickly. In particular, during adsorption, the heat generated due to the exothermicity of the process would be easily handled: due to a very efficient heat dissipation, the temperature of particles can be controlled within a very narrow temperature range around the desired CO_2 adsorption temperature, thus obtaining a particle temperature uniformity which cannot be easily accomplished by any other reactor designs. Moreover, fluidized bed reactors would be an effective solution also in the unfortunate case of particularly large exothermic heat of adsorption causing the solid sorbent particles to be heated up beyond the desired CO_2 adsorption temperature. Indeed, the solution would be to embed heat transfer surfaces inside the fluidized bed adsorber to remove the heat generated during CO_2 capture, thus keeping the solid sorbents at the desired capture temperature (embedding heat transfer surface in fluidized beds is already practiced commercially in fluidized bed combustion of coal, for example [128]). Likewise, as regards the desorption step, in a fluidized bed reactor the bed of adsorbent material would be very quickly and uniformly heated up by the purge gas (in the case of direct heating) or by the introduction of immersed heat exchanger tubes (in the case of indirect heating), thus avoiding the presence of low temperature zones inside the reactor, which would decrease the desorption kinetics. As regards the shortcomings, a major problem generally linked to the fluidized bed technology is the attrition phenomenon. Indeed, the attrition in a fluidized bed tends to be higher than in a fixed bed, but the extent of attrition greatly depends on the operating velocity and the strength of the sorbents. Because of the small sizes of the solid sorbents employed, the operating velocity tends to be low and thus it can be expected that the attrition rate may not be excessive.

I.7.2 Sound-Assisted Fluidization

On the basis of their primary particle size and material density, fine powders fall under the Geldart group C (<30 μm) classification, which means that fluidization is expected to be particularly difficult (i.e. characterized by plug formation, channeling and agglomeration) because of cohesive forces (such as van der Waals, electrostatic and moisture induced surface tension forces) existing between particles and becoming more and more prominent as the particle size decreases [129]. However, despite their Geldart classification, there are growing experimental evidences that nanoparticles can be smoothly fluidized for an extended window of gas velocities, thus implying that primary particle size and density cannot be taken as representative parameters for predicting their fluidization behaviour [130]. Indeed, because of the above-mentioned inter-particle forces, fine particles are always found to be in the form of large-sized porous aggregates [131,132], rather than as individual particles, when packed together in a gaseous medium. Therefore, gas fluidization of fine particles actually occurs in the form of aggregates, whose properties (size/density) highly affect the fluidization nature. Even though, on one hand, the agglomeration makes possible the fluidization of such materials, on the other hand, it limits their potential because of the undesired decrease in specific surface area. Accordingly, the formation of aggregates should be reduced to keep as small as possible the aggregate size in order to properly exploit the potential of fine powders. In other words, the achievement of a smooth fluidization regime is closely related to an efficient break-up of the large aggregates yielded by cohesive forces. To this aim and to overcome these inter-particle forces and achieve a smooth fluidization regime, externally assisted fluidization can be used, thus involving the application of additional forces generated, for example, by acoustic, electric, magnetic fields or mechanical vibrations to enhance the dynamics of the powder in the fluidized bed. Among all these available techniques, sound assisted fluidization has been indicated as one of the best technological option to smoothly fluidize fine and ultra-fine powders [133].

This technique holds several advantages. First of all it is not intrusive, since neither additional equipment nor materials must be inserted in the bed. Besides, the powders to be employed do not need to have any peculiar property. Moreover, it is widely reported in literature [136] that the application of acoustic field is capable of reducing the elutriation of fine particles from fluidized bed, preventing problems related to downstream carryover of fine particles such as clogging of valves. In Last but not least, this technique is extremely economic and user-friendly, since the extra needed equipment (signal generator, audio amplifier loudspeaker and oscilloscope) is very easily available in commerce.

I.8 Aim of the PhD Thesis

On the basis of the data collected from the bibliographic study, it emerges that adsorption using solid sorbents has the potential to become one of the leading CO_2 capture techniques by complementing or replacing the current absorption technology due to its low energy requirement. To date, great attention is focused on the development of highly specific adsorbent materials, namely materials with great affinity towards CO_2 molecules. Sure enough, the scientific community is moving in this direction, putting the emphasis on the manufacture of designed nanomaterials in which a molecular level of control can be achieved as a means of tailoring their CO_2 capture performance. Beside the material issue, another crucial aspect is represented by the regeneration of the sorbent: for adsorption to be used as CO_2 capture technique, an effective and less energy-consumed regeneration of the CO_2 captured adsorbents is definitely needed. In this respect, it emerges from the literature study, that temperature swing adsorption is one of the best technological alternatives, presenting several advantages over the other technological options:

- Pressure swing adsorption applied to combustion flue gas would involve compression of a large fraction of inert nitrogen, which is highly expensive. Moreover, the sorbent selectivity for CO_2 drops down with increasing pressure, making it more difficult to achieve high purity CO_2 in the desorption gas.

- The main disadvantage of electric swing adsorption is, instead, the consumption of electric energy, which is the product of the power plant, whereas, with the thermal regeneration, waste heat from the flue gas can be used for sorbent heating. Moreover, employing ESA in CO_2 capture is limited by the availability of adsorbents that must combine high CO_2 capacity and selectivity together with electric conductivity (for instance, materials with favorable adsorption properties, like zeolites or MOF, do not conduct electricity and cannot be employed in ESA).

Therefore, on the basis of these concerns, a major point to be addressed is the development of an adequate reactor configuration, which can fully exploit the potential and properties of these new-concept adsorbent materials by maximizing the contact between the CO_2 molecules and the adsorbent particles. Temperature swing in fixed bed reactors, serving as both the adsorber and the regenerator, is naturally inefficient because the beds have to be alternately cooled and heated to the correct reactor temperature for the proper reactions to occur. More specifically, fixed beds are recommended neither for exothermic reactions (CO_2 adsorption) nor for endothermic reactions (CO_2 regeneration), because poor local heat dissipation for the

exothermic adsorption reactions and poor heat transfer to the solid sorbents for the endothermic regeneration reactions will produce local "hot" and "cold" spots, respectively, preventing efficient conversions. In light of these considerations, a fluidized bed could be a viable alternative to the fixed bed configuration. Indeed, in fluidized beds the rate of mass and heat transfer between particles and gas per unit bed volume is extremely high due to the large interfacial particle-gas surface area. However, due to their intrinsic cohesive character, fine particles cannot be fluidized in ordinary condition, namely the use of assistance methods is required to achieve a smooth fluidization regime. Several externally assisted fluidization techniques are proposed in literature, all of that involving the application of additional forces generated, for example, by acoustic, electric, magnetic fields or mechanical vibrations to enhance the dynamics of the powder in the fluidized bed. Since the application of acoustic vibrations does not require any material modification, it is rather cheap and can be easily implemented from the technical point of view using simple sound generator devices, it is foreseen that sound assisted fluidization might be also competitive at the industrial level.

Therefore, the objective of the present PhD thesis is the to study a CO_2 capture process by temperature swing adsorption on fine porous materials in a sound-assisted fluidized bed reactor. To this aim several steps are needed:

- Design and setup of a suitable fluidized bed reactor to perform an experimental campaign, which will be:

  - made of Pyrex in order to work both at high and low temperature to carry out adsorption and desorption tests, as well, and in order to be optically accessible;

  - provided with equipment for the generation of the acoustic field;

  - provided with a system for the analysis of CO_2;

- Selection and characterization of CO_2 adsorbent materials with different chemico-physical properties;

- Realization of a systematic experimental campaign to in-depth examine the main operating variables influencing the CO_2 adsorption process;

- Study of a possible regeneration strategy in order to perform a cyclic process, with assessment of the stability of the sorbents to several adsorption/desorption cycles and the investigation of effect of the main operating variables affecting the desorption process.

More specifically, the activity carried out during the first year consisted in an in-depth study and bibliographic investigation. This made it possible to point out the main characteristics of the CO_2 capture by physical adsorption highlighting its problems and prospects. Moreover, a

lab-scale sound assisted fluidized bed reactor was designed to perform adsorption/desorption experiments and different adsorbent materials were selected. In particular, following the information retrieved from literature, common adsorbent materials, such as activated carbons and zeolites, were chosen, to firstly assess the capability of the sound assisted fluidization in actually promoting the CO_2 adsorption process, whereas a highly specific adsorbent material, a metal organic framework, was selected, to apply the sound assisted fluidization technology also to cutting-edge materials.

The second year was devoted to the realization and set-up of the sound assisted fluidized bed apparatus. Then, all the selected adsorbent materials were characterized from a chemico-physical point of view by determining particles size distribution, pore size distribution and specific surface area, by SEM, XRD, Fourier Transform Infrared (FTIR) analysis, and by CO_2 Temperature Programmed Desorption (TPD) experiments. Once realized the experimental apparatus, ordinary and sound assisted fluidization tests were carried out to characterize the fluid-dynamic behaviour of all the sorbents. After this preliminary characterization, adsorption tests were carried out. In particular, the effect of different operating variables on the adsorption efficiency was studied:

- the characteristic parameters of the acoustic field (sound intensity and frequency);
- fluidization velocity;
- CO_2 partial pressure.

During the same year, a parallel research activity was carried out at the Department of Electronics and Electromagnetism - Faculty of Physics - University of Seville in order to further assess the capability of the sound in promoting the capture of CO_2. In particular, during this stay, it was investigated the application of sound assisted fluidization technique on the capture of CO_2 at Ca-looping conditions. The aim of this research activity was to apply the same technology, i.e. the sound assisted fluidization, and to assess its effectiveness also to a different CO_2 capture process, which is characterized by remarkably higher operating temperatures.

During the last year the research activity consisted in performing regeneration tests of the spent sorbents by TSA. According to several works reported in literature, the main drawback of TSA is the dilution of the desorbed CO_2 by the carrier gas. Indeed in common TSA, the column is heated by a hot gas (air, nitrogen...) for the desorption step. Due to the low heat capacity of gases, a large volume of gas is required to significantly heat the bed, thus leading to the desorption of the adsorbate diluted in the heating gas. As a possible way to avoid this problem, the heat for regeneration of the solid can be provided by indirect heating, instead of

directly contacting the solid with hot gas that flows through the bed, thus remarkably reducing the volume of purge gas and limiting the dilution effect. Therefore, the standard regeneration strategy consisted in fluxing N_2 at a fixed desorption temperature (isothermal purge): the temperature inside the reactor was firstly increased to the desired desorption temperature by external heating (i.e. without fluxing any purge gas) and then the CO_2 partial pressure reduced by fluxing pure N_2 through the already hot bed (purge). The possibility to perform adsorption/desorption cycles in the sound assisted fluidized bed apparatus was evaluated, thus also studying the sorbents stability to cyclic operation. Then, the effect of desorption temperature and purge flow rate was evaluated. A second regeneration method was tested in order to improve the desorption step, namely find a possible technique to enrich the recovered CO_2 stream with respect to the standard regeneration strategy. The idea lying at the basis of this regeneration strategy was to discriminate the contribution to the CO_2 recovery given by heating from that given by purge (in the standard regeneration strategy the thermal effect cannot be distinguished by that given by purge). Indeed during the external heating the CO_2 could be desorbed without the use of any carrier gas and the desorbed gas could be recovered by thermal expansion, thus completely eliminating the dilution problem (pure CO_2 stream as desorption gas). More precisely, differently from the standard regeneration strategy, during the heating step the column was not isolated and the CO_2 was contextually recovered, then, only when no more CO_2 was desorbed (i.e. the thermodynamic equilibrium corresponding to the chosen desorption temperature was reached and the CO_2 still adsorbed to the sorbent surface could not be recovered) N_2 was fluxed inside the column and the remaining CO_2 was recovered.

Finally, considerations about the energy cost and scale-up of the proposed capture process have been also realized.

I.9 Summary

In Chapter II the description of the adsorbent materials, the different techniques used to characterize the materials as well as the designed and realized experimental apparatus for the adsorption/desorption tests and the test procedures employed in this study are described in details.

Chapter III reports the experimental results. In particular, the results from the chemico-physical and fluid-dynamic characterization of all the materials are firstly presented. Then, the results of the adsorption tests for each sorbent, the effect on the adsorption efficiency of the

main operating variables (sound parameters, fluidization velocity and CO_2 partial pressure) and the comparison among their adsorption performances are reported. Following the results of regeneration and cyclic tests are presented. Finally, the results obtained from the parallel research activity on the capture of CO_2 at Ca-looping conditions, carried out at the Department of Electronics and Electromagnetism - Faculty of Physics - University of Seville, is reported.

Chapter IV summarizes the main conclusions achieved during the activity carried out in this PhD thesis.

II EXPERIMENTAL SECTION

II.1 Materials

Considering that the research activity will be initially devoted to the verification of the sound assisted fluidization in actually promoting the CO_2 adsorption process, common adsorbent materials have been firstly used. On the basis of the data collected in the literature, it emerges that typical physisorbents for CO_2 capture include activated carbons and zeolites.

Two kinds of activated carbons and zeolites were used, because of their availability, and with different chemico-physical properties to investigate their effect on the adsorption performances. The activated carbons are: an activated carbon DARCO FGD (Norit) and an activated charcoal powder (Sigma Aldrich). They are characterized by a similar surface area but a different pore size distribution. As regards the zeolites, considering that a great number of properties (pore size and architecture, chemical composition, etc.), affect their adsorption performance [78-80], the choice has been made taking into account the Si/Al ratio and the nature of the extraframework cations. In particular, two opposite zeolites have been selected: a Zeolite H-ZSM-5 (Zeolite Int.), i.e. an acid high Si/Al ratio zeolite, and a Molecular sieves-13X powder (Sigma Aldrich), i.e. a basic low Si/Al ratio zeolite. With reference to the effect of the extraframework cation, a limited number of tests has been performed on a zeolite Y in the ammonium (NH_4-Y) and sodium form (Na-Y). In particular, these zeolites have been provided by the DICMaPI of the Federico II University of Naples. Hereafter all the materials will be addressed according to the nomenclature reported in **Tab. 3**. After the validation of the technology with the use of common adsorbents the attention has been focused on the application of the sound assisted fluidization to a new-concept adsorbent material: HKUST-1 (or MOF-199). In particular, this specific MOF has been selected because it presents several advantages over other MOFs: elevated surface area, larger than that typical of common activated carbons; water stability; simple synthesis procedure (i.e. anhydrous conditions not

required); the precursors are easily available and not expensive. Unlike all the other materials used, this one is not commercially available. It was synthetized in the laboratories of the Istituto di Ricerche sulla Combustione of Naples.

<p align="center">**Tab. 3 Nomenclature used for the sorbent materials**</p>

Materials	Nomenclature
Activated Carbon (Norit)	AC Norit
Activated Carbon (Sigma Aldrich)	AC Sigma
Zeolite H-ZSM-5	H-ZSM-5
Zeolite 13X	13X
Molecular sieve HKUST-1	HKUST-1

This material is water-stable and contains Cu^{2+} dimers as the metallic units linked to oxygen atoms from benzene tricarboxylate (BTC) [134,135]. In particular, it was prepared by mixing 10g of copper nitrate hemipentahydrate and 5g of 1,3,5 benzenetricarboxylic acid (BTC) in 850mL of N,N dimethylformamide (DMF) followed by stirring and sonication for 5min. Ethanol (850mL) was then added to the mixture, which was then stirred and sonicated for 5 more min. Finally, deionized water (850mL) was added to the mixture and then stirring and sonication for 30min. All crystals were dissolved at this point. The mixture was then heated at 85°C in an oil bath. The mixture was kept in the oil bath for 21h under stirring. After cooling, the crystals were filtered, washed and immersed in dichloromethane. The crystals were collected after filtration and washing with dichloromethane. Drying was then performed by heating the crystals at 170°C for 28h.

II.2 Materials and their Physico-chemical Characterization

All the materials have been characterized using the experimental techniques reported below.

- ▪ *Particles size distribution* obtained by using a laser granulometer (Master-sizer 2000 Malvern Instruments), after the dispersion of the powders in water under mechanical agitation of the suspension and with or without the application of ultrasound (US). This apparatus is based on the diffraction properties of the considered material introduced in a solvent (water in this case). Two LASER sources, the first He/Ne with 633 nm wavelength (red) and the second diode laser with 450 nm wavelength (blue), are aligned with a 3D photodiode revelator. Two low angle lateral and one back scattering detectors are also present in the analysis cell. This system allows detection of particles in the range 0.02-2000 μm.

- *Pore size distribution and superficial area measurements* have been performed according to the BET (Brunauer Emmet Teller) method using N_2 at 77K with a QUANTACHROM 1-C analyzer. Before each measurement the samples were subjected for 12h to a degassing treatment under vacuum at 150°C.

- *Morphological characterization by SEM analysis* have been carried out with a Philips XL30 SEM equipped with an EDAX instrument for micro-analysis in order to highlight the powders typical structures.

- *Thermogravimetric analysis* have been performed in order to characterize the thermal stability of the materials and to obtain some preliminary information on the adsorption performance with a Perkin-Elmer TGA-7 thermobalance coupled with a Perkin-Elmer spectrum GX FT-IR for the analysis of the released gases. In the former case, the sample of adsorbent material was heated both in inert environment (N_2, 30ml min^{-1}) and in air (30ml min^{-1}) from 30°C up to 750°C at a rate of 10°C min^{-1}. In the latter, the sample was heated at 10°Cmin^{-1} up to 120°C in N_2 flow in order to remove possible moisture. Then, the sample was cooled down to ambient temperature and, after the stabilization of the weight, 10%vol. CO_2 has been introduced.

- *XRD characterization* was also performed on the materials in order to control their crystalline composition. The analysis was carried out using a Philips PW1710 diffractometer operating between 5°2θ and 60°2θ with a Cu Kα radiation.

- *Fourier Transform Infrared (FTIR) analysis*. The spectra were recorded on a Nicolet iS10 spectrometer using the attenuated total reflectance (ATR) method by using a germanium crystal. The spectra were acquired on the powdered samples without KBr addition.

- *CO_2 Temperature programmed desorption (TPD)* experiments were carried out with a Micromeritics AutoChem 2920 II equipped with a TCD detector. In particular, the sample (100mg) was pretreated in helium up to 150/250°C at 10°C min^{-1}. The material was kept one hour at this temperature. Then the sample was cooled to ambient temperature. After that the material was subjected for 1 hour to an adsorption step with a 15%vol. CO_2/N_2 mixture. Then the flow was switched again to helium and the sample was heated up to 250°C at 10°C min^{-1} and kept for 1 hour at this temperature. Beside the CO_2 TPD, also blank tests were performed. The sample was pretreated in He for 1h (the material was heated up to 150°C at 10°C min^{-1}) and then cooled to ambient temperature (no CO_2 adsorption was carried out). After that the sample was heated up to 250°C at 10°C min^{-1} and kept for 1 hour at this temperature.

II.3 Experimental Apparatus

The first aim of this PhD thesis was the design and set-up of a laboratory scale sound assisted fluidized bed experimental apparatus to perform adsorption/desorption tests. A view of the reactor is shown in **Fig. 14a** and the scheme of the plant is schematized in **Fig. 14b.**

The fluidized bed consists of a Pyrex column of 40mm ID and 1500mm high, equipped with a porous gas distributor plate located at 300mm from the bottom of the column. The section of the column below the gas distributor acts as wind-box: it is filled with Pyrex rings in order to maximize the uniformity of the gas flow rate entering the fluidized bed. Indeed, this solution provides a good dispersion of the fluidizing gas and limits fluidization troubles due to the formation of preferential channels, namely the feed of the fluidizing gas through a limited number of points.
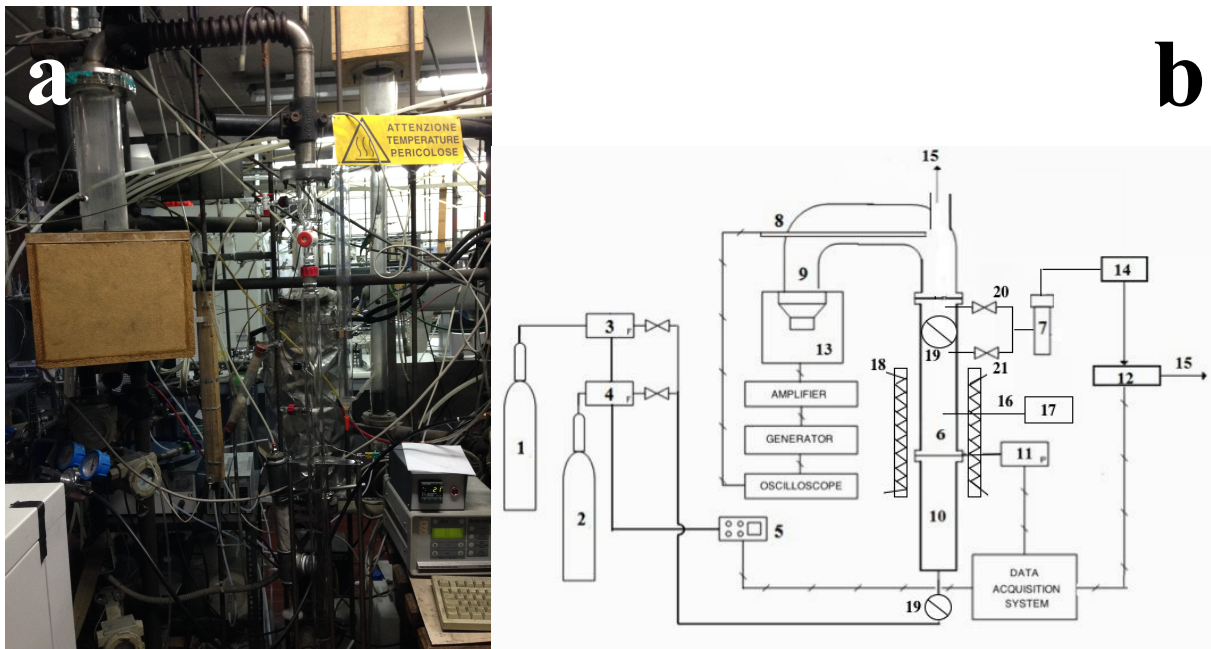
Fig. 14 Experimental apparatus (a) picture and (b) scheme: (1) N$_2$ cylinder; (2) CO$_2$ cylinder (3) N$_2$ flow meter; (4) CO$_2$ flow meter; (5) controller; (6) 40 mm ID fluidization column; (7) filter; (8) microphone; (9) sound guide; (10) wind-box; (11) pressure transducer; (12) CO$_2$ analyzer; (13) loudspeaker; (14) pump; (15) stack; (16) thermocouple; (17) temperature controller; (18) heating jacket; (19) two-way valve; (20) upper gas sampling probe; (21) lower gas sampling probe.

The column is provided with a pressure probe located at 5mm above the gas distributor to measure the pressure drops across the bed of sorbent particles. This solution makes it possible to eliminate the contribution to the pressure drop given by the gas distributor plate. In particular, a Hartmann & Braun pressure transducer has been used.

A temperature probe is located at 400mm from the top of the column. In particular, the temperature inside the reactor is monitored at the center of the bed (60mm from the gas distributor) by means of a type K thermocouple (Chromel-Alumel) with a diameter of 1mm. This thermocouple is connected to a temperature controller in order to monitor it during the experimental tests and keep it at the desired value.

Gas feed is prepared using separate N_2 (99.995%) and CO_2 (99.995%) cylinders. The flowrates have been set and controlled by two mass flow controllers (Brooks 8550S for CO_2 and Bronkhorst for N_2).

The acoustic field is introduced inside the column through a sound wave guide located at the top of the freeboard. The sound wave guide has been properly designed [136] to prevent the elutriated powders from dirtying the loudspeaker. The sound-generation system is made of a digital signal generator to obtain an electric sine wave of specified frequency whose signal is amplified by means of a power audio amplifier rated up to 40W. The signal is then sent to a 8W woofer loudspeaker placed downstream the sound wave guide. This experimental set-up was also designed according to the Helmholtz resonator, i.e. one of the most used engineering noise control methods, in order to reduce the sound insulation even for high intensity acoustic fields. More specifically, by using this device sound is reflected back to the system, thus reducing the required sound insulation.

The analysis system consists of a continuous analyzer, which is the best solution since the adsorption/desorption process is intrinsically a transient process. The analyzer is provided with an infrared (AO2020, URAS 14) and a paramagnetic detector (AO2020, MAGNOS 106) for the measure of the CO_2 and O_2 concentration, respectively. Since the top of the column needs to be open to the atmosphere for the acoustic system to properly work, only a fraction of the outlet gas stream is taken and sent to the analysis. In particular, the gas sampling is performed by means of a pump (SCC-S sample gas feed unit from ABB), which can sucks at the desired flow rate from two different sampling probes, located at 50 and 400mm from the top of the column. Since the analysis system is realized by means of very sensitive devices, a ceramic filter, able to capture all the elutriated fine particles, has been placed downstream the outlet of the column and before the inlet to the pump, thus preventing any damage to both the pump and the analyzer. The remaining part of the outlet gas flow rate is sent to the stack.

The experimental apparatus is interfaced to a PC via Ethernet as regards the analysis of gas, and via a National Instrument data acquisition card as regards the acquisition of pressure drops. A program realized in LabView, provides the simultaneous reading and acquisition of the gas concentrations and values of pressure drops across the bed.

As regards the regeneration tests, to heat the column to the desired desorption temperature, a heating jacket (Tyco Thermal Controls GmbH) is wrapped around its external surface. In particular, it has been ad-hoc designed: it is 50cm high with an isothermal height of 35cm and it is also provided with a window, which allows the fluidization quality to be visually assessed also during the desorption step. According to the type of regeneration strategies to be applied, a system consisting in two two-way valves, located at the top (50mm below the upper sampling probe) and at the bottom of the column, makes it possible to isolate the fluidized bed reactor by sealing both the inlet and outlet.

II.4 Preliminary Fluid-dynamic Characterization

All the adsorbent materials have been previously characterized to assess their fluidization quality both in ordinary and sound assisted conditions. All the tests have been performed at ambient temperature and pressure using N_2 as fluidizing gas in order to prevent any intensification of the powder cohesiveness due to air moisture. Each tests consists in recording the values of the pressure drops across the bed and of the height of the bed, for each selected value of the superficial gas velocity, in order to construct the corresponding fluidization and expansion curves. The adopted sound intensities (SPLs) and frequencies are reported in **Tab. 4**. For all the tests a proper amount of sorbent material has been loaded in the fluidization column in order to obtain a bed height of about 15cm. **Tab. 4** also reports the amount of sorbent (m) loaded in each case. The experimental procedure involves different steps. The gas flow rate is rapidly increased up to its established maximum value and then gradually reduced in steps. For each reduction in the gas flow rate, the material is given a sufficient long time interval (3min) to reach steady state conditions. During this time the pressure drop across the bed and the superficial gas velocity of are monitored. After this time interval, the height of the bed, which is necessary to the evaluation of the bed expansion, is measured and its value inserted in the panel of the program. Once the value of zero gas flow rate is reached, the same procedure is repeated, but in the opposite direction, i.e. the superficial gas velocity is gradually increased until reaching again the initial maximum value of gas flow rate. The experimental procedure followed for the sound assisted tests is substantially the same as that used in the absence of sound. The only difference is that, after making all the preliminary actions, the desired acoustic field is switched on and the system is given a time of about 10min to be stabilized under its effect. From these data it is possible to obtain, the corresponding fluidization curves, plotting the dimensionless pressure drops (the

$\Delta P/\Delta P_0$, ΔP_0 being the static weight of the bed) as a function of the superficial gas velocity, and the relative expansion curves, plotting the dimensionless bed expansion ratio (H/H_0, H_0 being the initial bed eight after loading in the fluidization column) versus the superficial gas velocity. Then, the minimum fluidization velocity, u_{mf}, has been calculated from the pressure drop curves by means of a graphic procedure. Finally, the bed expansion data have been elaborated in order to estimate the size of the fluidizing aggregates according to the method reported in [133].

Tab. 4 Operating conditions of the fluidization tests.

	SPL, dB	Frequency, Hz	m, g
AC Norit	120, 125, 135, 140	20, 50, 80, 120, 300	110
AC Sigma	125, 130, 135, 140	30, 50, 80, 150	30
H-ZSM-5	140	80	85
13X	125, 130, 135, 140	10, 30, 50, 80, 120, 150	88
HKUST-1	125, 130, 140	20, 50, 80, 120, 300	50

II.5 Adsorption Tests

All adsorption tests have been carried out at ambient temperature and pressure. For all the sorbent materials, except from HKUST-1, each test has been carried out with a fresh batch. In particular, each batch has been treated prior to each adsorption test by heating the powder up to 140°C, in order to remove any trace of moisture. As regards HKUST-1, all the tests have been performed using the same sample. Therefore, at the end of each adsorption tests the sample has been regenerated by heating the powder up to 150°C under vacuum conditions (50mbar) in order to remove any trace of CO_2 and moisture.

In a typical experiment, the sorbent is loaded in the column in order to obtain a bed height of 15cm. Then, in a pre-conditioning step of about 10min, N_2 is fluxed in the column in order to stabilize a fluidization regime at fixed operating conditions in terms of superficial gas velocity and sound parameters. This is followed by the adsorption step in which a CO_2/N_2 gas mixture at a fixed CO_2 concentration is fed through the column.

The CO_2 concentration in the column effluent gas is continuously monitored as a function of time (breakthrough curve) until the gas composition approaches the inlet gas composition value, i.e., until bed saturation is reached.

CO_2 concentration profiles (breakthrough curves) have been obtained as a function of time t, which has been counted from the time the gas mixture takes to flow from the fluidized bed to the analyzer. This transit time has been previously measured for each gas flow rate by flowing the gas mixture through the empty bed.

Each adsorption test has been performed both in ordinary and sound assisted fluidization conditions. In particular, the effect of sound parameters (SPL and frequency), fluidization velocity and CO_2 partial pressure on adsorption efficiency has been investigated. **Tab. 5** reports all the operating conditions and the amount of sorbent selected for the adsorption experiments carried out in this work. The comparison among the adsorption performances of all the adsorbent materials has been made keeping constant all the operating conditions and in light of the their chemico-physical characteristics.

Tab. 5 Operating conditions of the adsorption tests.

	Fluidization velocity, cm/s	CO_2 inlet concentration, %vol. in N_2	SPL, dB	Frequency, Hz	m, g
AC Norit	0.1, 0.25, 0.5, 0.75, 1, 1.5, 2	5, 10, 15	120, 125, 135, 140	20, 50, 80, 120, 300	110
AC Sigma	1, 1.5, 2	5, 10, 15	140	80	30
H-ZSM-5	1.5, 2, 5	5, 10, 15	140	80	85
13X	1.5, 3, 4.5	5, 10, 15	140	80	88
HKUST-1	1, 1.5, 2	5, 10, 15	125, 130, 140	20, 50, 80, 120, 300	50

II.6 Desorption Tests and Cyclic Operation

Desorption tests have been performed on the materials characterized by the best adsorption performaces, the MOF (HKUST-1) and one activated carbon (AC Norit) at atmospheric pressure. In particular, since HKUST-1 presents problems of thermal stability, thus constituting an upper limit for the desorption temperature to be used in a TSA process, a preliminary TPD study has been performed to find a proper regeneration strategy. In particular, an extra-situ regeneration strategy has been realized, combining the increase of temperature (150°C) with a slight vacuum (50mbar). Cyclic adsorption/desorption tests have been performed according to this regeneration strategy, thus obtaining information about

HKUST-1 stability to cyclic operations and not on the desorption performances. In particular ten adsorption/desorption cycles have been performed.

As regards AC Norit, which does not show significant limits on the choice of the desorption temperature, regeneration tests have been performed to recover the CO_2 from the spent sorbent by means of TSA in the sound assisted experimental apparatus. As for the adsorption step, the desorption performances have been studied varying the operating conditions. More specifically, for regeneration two methods have been tested: isothermal purge and heating and purge. For both the strategies the previous adsorption step has been performed with an inlet CO_2 concentration of 10%vol. in N_2 and an inlet gas flow rate of 67.8Nl h^{-1} (corresponding to a superficial gas velocity of 1.5cm/s, i.e. higher than the minimum fluidization velocity of the material) under sound assisted conditions of 140dB-80Hz, representing the optimal values of sound parameters to maximize the fluidization quality and, then, the gas-solids contact efficiency, which, in turn, positively affects the CO_2 adsorption performance of fine solid materials. All the desorption operating conditions are reported in **Tab. 6**.

Isothermal purge: the desorption is realized by fluxing N_2 through the heated bed of sorbent, namely the captured CO_2 is recovered by the contribution of two contemporary effects, increasing temperature and decreasing CO_2 partial pressure. Just after the adsorption step, the column is heated up to the desired desorption temperature (**Tab. 6**) by means of the heating jacket. During this heating step (lasting about 1h to reach thermal equilibrium), the column is isolated, namely the acoustic field is switched off, the inlet to the column is closed and the top of the column is also sealed by a two-way valve so that all the desorbed CO_2 remains confined inside the column. When the bed reaches the desired temperature, the acoustic field is switched on, the inlet to the column is open (N_2 is flowed) and the column exit is unsealed (purge step) so that both the already desorbed CO_2 and that still adsorbed inside the pores of the sorbent left the column diluted in the N_2 stream. The temperature of the column is maintained constant during the purge. In order to define the optimal operating conditions for CO_2 recovery the effect on the desorption efficiency of the desorption temperature and the purge flow rate has been evaluated for this regeneration method.

Heating and purge: the recovery of the captured CO_2 is realized in two steps so that the effect of the increasing temperature (heating) and reducing CO_2 partial pressure can be isolated, namely it has been possible to discriminate the amount of CO_2 desorbed by heating from that recovered by purge. Just after the adsorption step, the column is heated up to the desired desorption temperature (**Tab. 6**) by means of the heating jacket. During this heating step, the inlet to column is closed and the acoustic field is switched off so that the desorbed CO_2 can

leave the column only due to a thermic effect (i.e. the system continuously shifts to new adsorption equilibria as the temperature increases). More precisely, during the Heating step the outlet of the column is left open so that the pump can suck from the lower probe at a constant flow rate (40Nl h^{-1}) both all the CO_2 continuously desorbed from the bed and air from the atmosphere. So, the CO_2 desorbed reaches the analyzer through the probe diluted in air. When the analyzer stops detecting CO_2 in the outlet stream (i.e. the desired regeneration temperature and the corresponding adsorption equilibrium has been reached, so no more CO_2 is desorbed from the bed), the inlet to column is opened and nitrogen is flowed at a flow rate of 67.8Nl h^{-1} (purge step). The temperature of the column was maintained constant during the purge.

Besides these two strategies, a not isothermal regeneration procedure has also been used to better highlight the differences between ordinary and sound assisted desorption tests. Indeed, the beneficial effect given by sound application is expected to be emphasized during a not isothermal desorption phase: the poor fluidization quality (i.e. channeling) characterizing the ordinary tests necessarily implies worse heat and mass transfer coefficients with respect to sound assisted tests (characterized by good gas-solid mixing), thus hampering the desorption process.

Not isothermal purge: after the adsorption step (performed under ordinary or sound assisted conditions) the heating of the column (20°C min^{-1}) up to the desired desorption temperature of 70°C is started and, at the same time, the feed is switched from 10%vol. CO_2 in N_2 to pure N_2 (i.e. heating happens contextually to purge) under ordinary or sound assisted conditions (140dB-80Hz). The outlet desorption stream leaves the column and reaches the analyzer through the upper probe.

Tab. 6 Operating conditions of the desorption tests.

N$_2$ purge flow rate, Nl h^{-1}	Desorption temperature, °C	SPL, dB	Frequency, Hz	m, g
45.2, 67.8, 90.4	25, 40, 70, 100, 130, 150	140dB	80Hz	110

Finally, the possibility to perform adsorption/desorption (the procedure for the adsorption test is fully described in the previous paragraph) cycles in the sound assisted fluidized bed apparatus was evaluated, thus assessing the sorbent stability to cyclic operation. A cycle is a sequence of adsorption-desorption steps. More precisely for the cycles tests the standard regeneration strategy has bee used (isothermal Purge). The cyclic tests have been performed

at 140dB and 80Hz and with an inlet gas flow rate of 67.8Nl h^{-1} (10%vol. CO_2 in N_2 and pure N_2 during adsorption and desorption, respectively) both in the adsorption and desorption phase. The regeneration of the sorbent has been realized with a desorption temperature of 70°C. The adsorption-desorption sequence is repeated for 16 consecutive cycles on the same sample in order to test its stability under repeated adsorption/desorption cycles.

III RESULTS

III.1 Materials characterization

III.1.1 Activated Carbon Norit

Fig. 15**a** and **Tab. 7** report the cumulative size distributions and the Sauter mean diameter of the powder. The application of ultrasound (US) involves the break-up of aggregates (2μm without US) into smaller ones (0.39μm with US). According to the Sauter mean diameter, the powder belongs to Group C of Geldart classification.
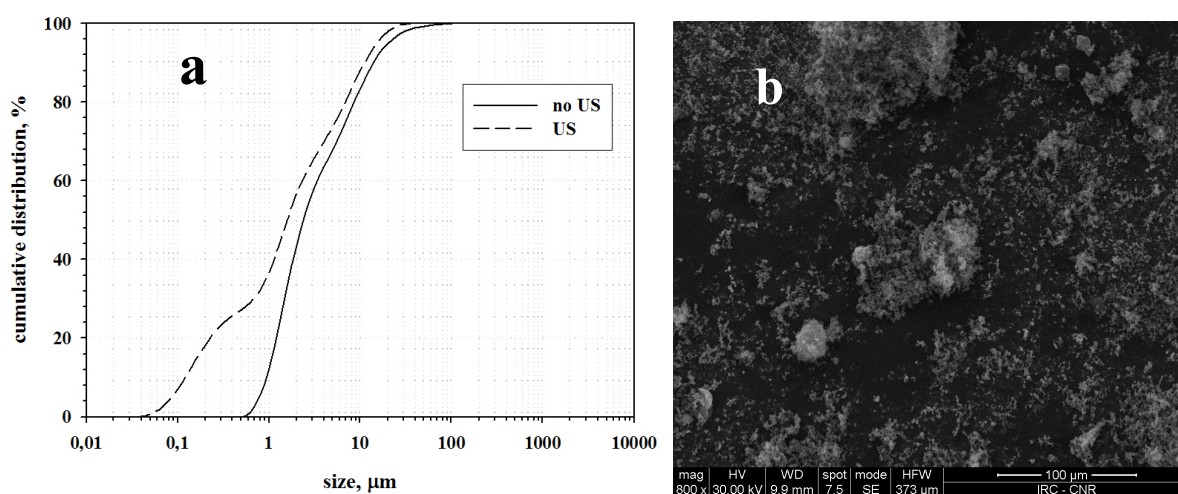
Fig. 15 Granulometric distribution (a) and SEM image (b) of the AC Norit.

Tab. 7 Properties of AC Norit.

D_{SAUTER}, μm with/without US	BET surface area, m^2/g	Bulk density, kg/m^3	Pore volume cm^3/g
0.39/2	1060	510	1.34

The analysis of the SEM images, reported in Fig. 15b, confirms that the powder appears in the form of aggregates as large as tens of microns.

As clearly shown in Fig. 16**a**, the activated carbon is characterized by a significantly broad pore size distribution. Indeed, besides the pores in the mesoporosity (2nm < d < 50nm) it also has micropores (d < 2nm). In particular, the microporous region is bimodal with more than a half of the micropores characterized by a dimension lower than 0.9nm. As reported in **Tab. 7**, the powders is characterized by a relatively large surface area and pore volume.
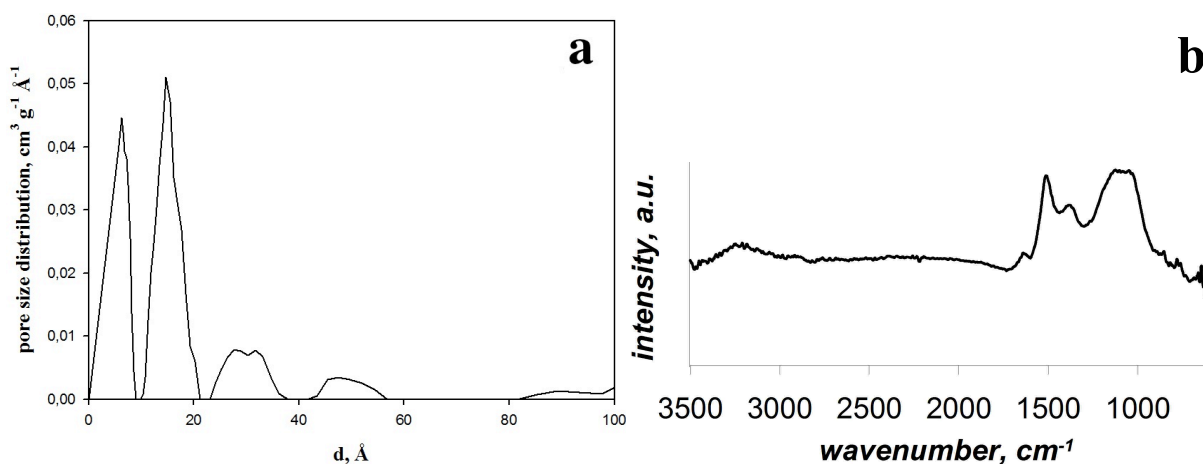
Fig. 16 Pore size distribution (a) and FT-IR spectra (b) of ACNorit.

Fig. 16**b** reports the FT-IR analysis. The spectra are characterized by a broad shape thus confirming of the presence of a complex carbon network. In particular, it exhibits bands at 1650-1750cm^{-1} (C=O stretching vibrations from carbonyl and carboxylic groups), 1500-1600cm^{-1} (skeletal vibration of the sp^2 graphitic domains). An enhanced broad band in the 1300-1100cm^{-1} region ascribable to the overlapping of C-OH and C-O stretching vibrations is also visible.

The thermal stability of the sample was characterized by thermogravimetric analysis. The curve in inert environment (Fig. 17**a**) exhibits a high weight loss at 300-350°C corresponding to the collapse of the structure (namely carbocarboxylate groups, the organic linkers of the structure) accompanied by the release of CO_2. It emerges that AC Norit is stable up to 400°C (in Fig. 17**a**). Indeed, for temperatures higher than 400°C the sample starts thermally decomposing. As regards the thermogravimetric analysis in air (in Fig. 17**a**), the plot presents a deep weight loss between 400 and 600°C corresponding to the bulk oxidation of the graphitic core. The non-sharpness of the weight drop testifies the occurrence of the progressive decomposition of oxygenated functionalities (carbonylic/carboxylic). It is noteworthy that a high amount of unburned material (~ 20% in weight, possibly metal residuals) is detected.

In order to have some preliminary information about the adsorption performance a TG adsorption test has been performed. In Fig. 17**b** the temperature profile and the percentage weight loss of the sample, obtained from this thermogravimetric analysis, are reported. The relative IR spectra have shown that only water is emitted up to 120°C. The amount of CO_2 adsorbed until saturation is 0.17mmol/g.
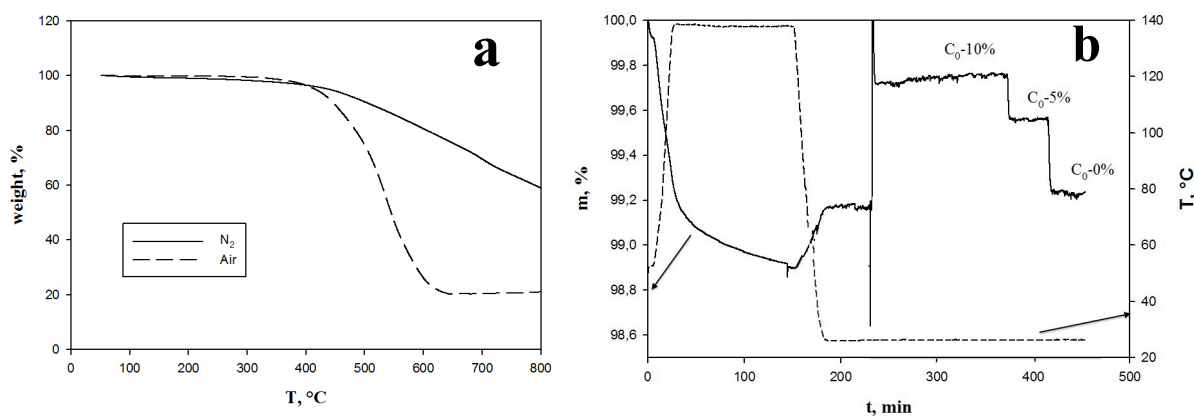
Fig. 17 Thermogravimetric analysis of AC Norit in N_2 and in air (a) and in CO_2/N_2 mixture (b).

After the adsorption step has taken place (i.e. after the stabilization of the weight) the CO_2 concentration has been decreased to 5%vol. As expected, being the CO_2 partial pressure the driving force of the adsorption process, the sample desorbs part of the CO_2 adsorbed in the previous step, which has occurred in a CO_2 richer ambient. Finally, the CO_2 concentration has been set to zero. The sample entirely desorbs the CO_2 previously adsorbed, as confirmed by the sample weight returning to the initial value. This evidence confirms that the CO_2 is physisorbed on the activated carbon, namely no chemisorption has occurred.

III.1.2   Activated Carbon Sigma Aldrich

Fig. 18**a** and **Tab. 8** report the cumulative size distribution and the Sauter mean diameter of the powder. The application of ultrasound (US) has only a slight effect, the dimension of the powder passing from 18.8μm to 15.4μm. According to the Sauter mean diameter, the powder belongs to Group C of Geldart classification.
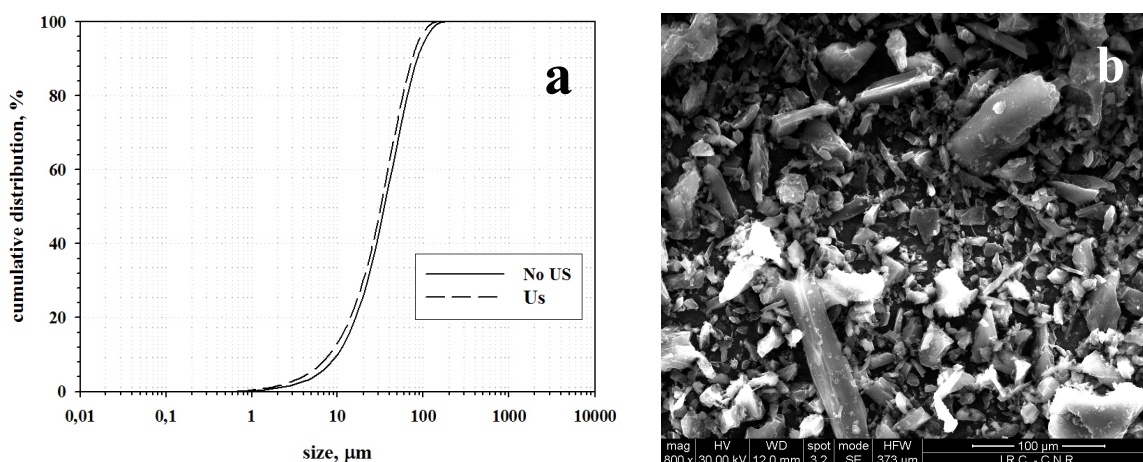
Fig. 18 Granulometric distribution of AC Sigma.

The analysis of the SEM image, reported in Fig. 18b, powder appears in the form of irregular particles, some of which are needle-shaped. Indeed the application of ultrasound has only a slight effect, that is to unfix the smaller particles from the larger ones.

Tab. 8 Properties of AC Sigma.

D_{SAUTER}, μm with/without US	BET surface area, m^2/g	Bulk density, kg/m^3	Pore volume cm^3/g
15.4/18.8	1038	318	1.14

As for the BET surface area and total pore volume the values obtained are slightly lower than that obtained for the AC Norit.

The activated carbon Sigma is characterized by a broad pore size distribution (micropores and mesopores) and by a total pore volume similar to that of AC Norit (**Tab. 7**), even though the pore size distribution is quite different. In particular, as regards the microporous region, a great amount of micropores is characterized by a dimension lower than 1.2nm. As reported in **Tab. 7**, the powders is also characterized by a relatively large surface area.

The FT-IR spectrum of activated carbon Sigma, reported in Fig. 19 is very similar to that of AC Norit (Fig. 16**b**). Indeed, it also exhibits bands at 1650-1750cm^{-1} (C=O stretching vibrations from carbonyl and carboxylic groups), 1500-1600cm^{-1} (skeletal vibration of the sp^2 graphitic domains). An enhanced broad band in the 1300-1100cm^{-1} region ascribable to the overlapping of C-OH and C-O stretching vibrations is also visible. Differently from AC Norit, a broad band in at 3000-3500cm^{-1} indicates the presence of O-H functionalities.

51
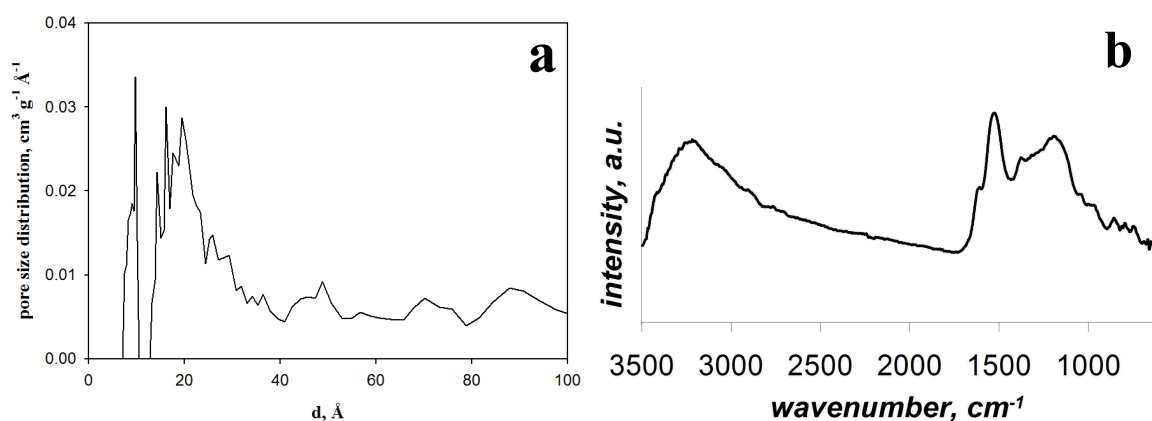
Fig. 19 Pore size distribution (a) and FT-IR spectra (b) of AC Sigma.

Also the thermal stability of this activated carbon is similar to that of AC Norit. From the thermogravimetric analysis in inert environment (N_2) it emerges that AC Norit is stable up to 400°C (Fig. 20). As regards the thermogravimetric analysis in air (Fig. 20), plot presents a deep weight loss between 400 and 600°C corresponding to the bulk oxidation of the graphitic core, the non-sharpness of the weight drop showing the occurrence of the progressive decomposition of oxygenated functionalities (carbonylic/carboxylic).
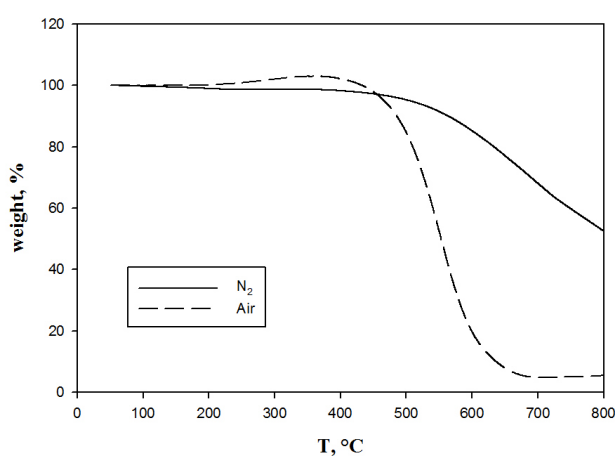
Fig. 20 Thermogravimetric analysis of AC Sigma in inert environment (N_2) and air.

In conclusion, the two activated carbons are characterized by very similar chemical functionalities and thermal stability, whereas, they show some differences in the pore size distribution and BET surface area.

III.1.3 Zeolite H-ZSM-5

Zeolite H-ZSM-5 is the hydrogen form of ZSM-5 zeolite. In particular, it can be classified as a hig-silica zeolite, having a Si/Al=140. Considering that whenever an Al^{3+} cation replaces a

Si^{4+} cation, an additional positive charge is required to keep the material charge-neutral, with proton (H^+) as the cation, the material becomes acidic (i.e. the acidity is proportional to the Al content).

Fig. 21**a** and **Tab. 9** report the cumulative size distribution and the Sauter mean diameter of the powder. The application of ultrasound (US) involves the break-up of large aggregates (21.8μm without US) into smaller ones (1.62μm without US). According to the Sauter mean diameters, the powder belongs to Group C of Geldart classification.
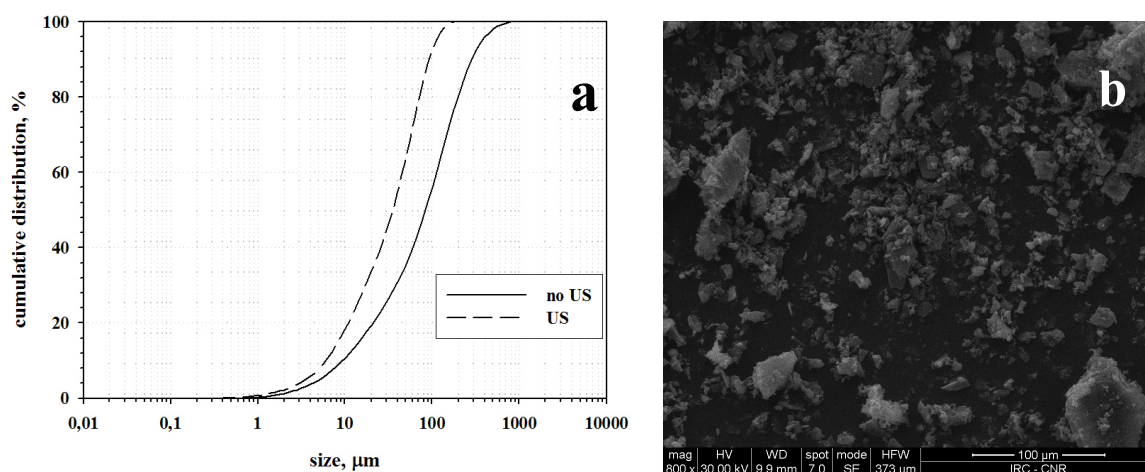
Fig. 21 Granulometric distribution of H-ZSM-5.

Tab. 9 Properties of H-ZSM-5.

D_{SAUTER}, μm with/without US	BET surface area, m^2/g	Bulk density, kg/m^3	Pore volume cm^3/g
12.6/21.8	400	450	0.41

The analysis of the SEM image, reported in Fig. 21**b**, confirms that the powder appears in the form of aggregates as large as tens of microns.

As clearly shown in Fig. 22, the zeolite used in this experimental campaign is basically microporous (d < 2nm). In particular almost all the pores has a dimension lower than 0.6nm (in particular, it has a mean pore size 0.55nm) and, as reported in **Tab. 9**, it is characterized by a pore volume remarkably lower than that of the two activated carbons and by a surface area of about $400m^2/g$.
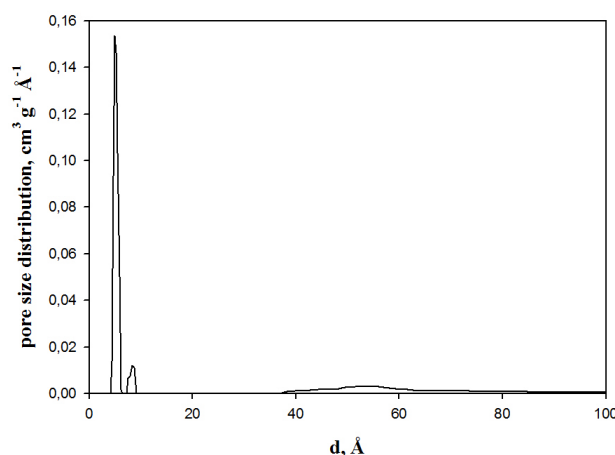
Fig. 22 Pore size distribution of H-ZSM-5.

III.1.4 Zeolite 13X

Molecular sieve 13X is the sodium form of the type X crystal. In particular, it can be classified as a low-silica (or equivalently aluminium-rich) zeolite, having a Si/Al=1.25. As a consequence it contains almost the maximum number of cation exchange sites balancing the framework aluminum, and thus the highest cation contents and exchange capacities. These compositional characteristics combined give type X zeolites the most highly heterogeneous surface known among porous materials, due to exposed cationic charges nested in an aluminosilicate framework, which results in high field gradients. The presence of Na^+ cations gives 13X a basic functionality.

Fig. 23 and **Tab. 10** report the cumulative size distribution and the Sauter mean diameter of the powder. Differently from what observed for the other materials, in this case the application of ultrasound has a negligible effect, the dimension of the powder passing from 3.2 to 3.1μm. According to the Sauter mean diameter, the powder belongs to Group C of Geldart classification.
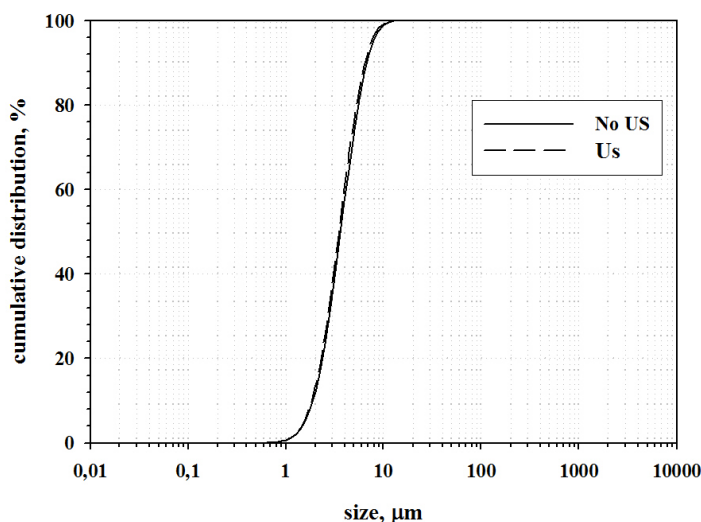
Fig. 23 Granulometric distribution of 13X.

Tab. 10 Properties of 13X.

D_{SAUTER}, μm with/without US	BET surface area, m^2/g	Bulk density, kg/m^3	Pore volume cm^3/g
3.1/3.2	960	467	0.41

The analysis of the SEM images, reported in Fig. 24, confirms the powder appears in the form of aggregates. However, the size obtained from the granulometric analysis is the dimension of the primary particles.
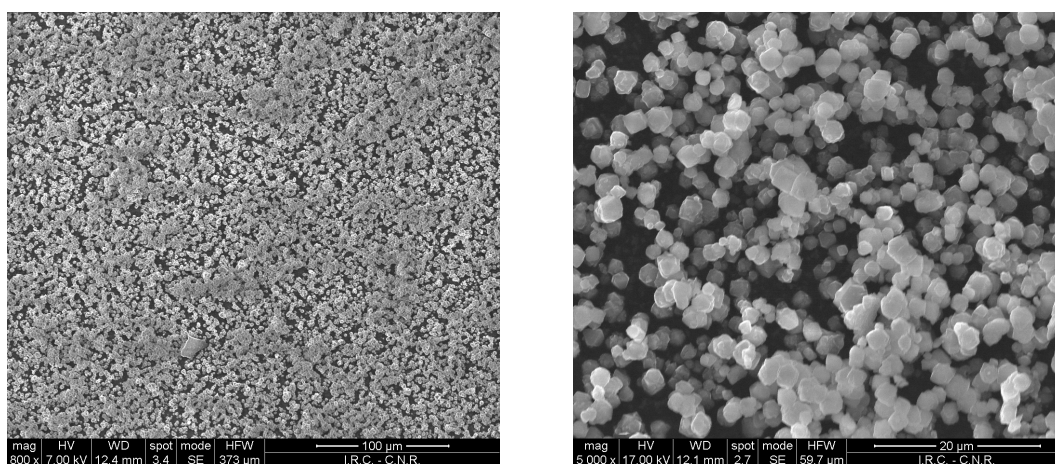
Fig. 24 SEM images of 13X.

As clearly shown in Fig. 25 13X is basically microporous (d < 2nm) and it is characterized by the same pore volume as the H-ZSM-5 (**Tab. 10**). In particular, it exhibits pores in the range 0.6-0.9nm. As reported in **Tab. 10**, the powders is characterized by a surface area larger than that of H-ZSM-5 but lower than both the activated carbons.
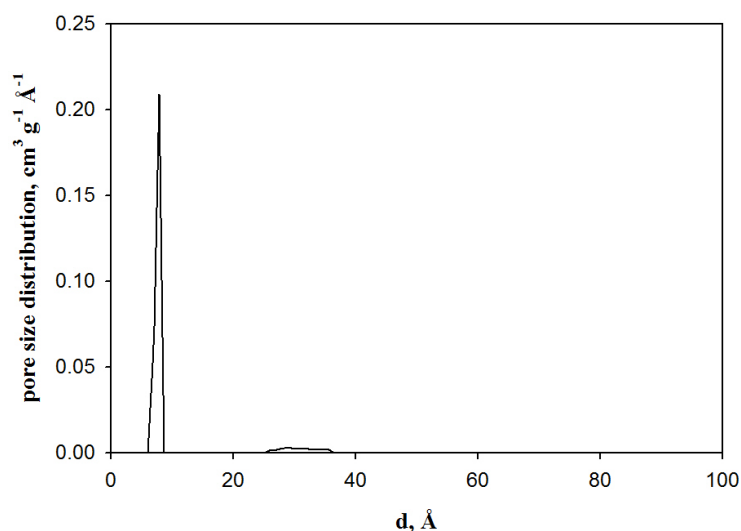
Fig. 25 Pore size distribution of 13X.

III.1.5 HKUST-1

Fig. 26**a** and **Tab. 11** report the cumulative size distributions and the Sauter mean diameter of the powder. The application of ultrasound (US) has only aslight effect reducing the Sauter mean diameter from 5.6μmto 4.3μm. According to the Sauter mean diameter 4.3μm, the powder belongs to Group C of Geldart classification.
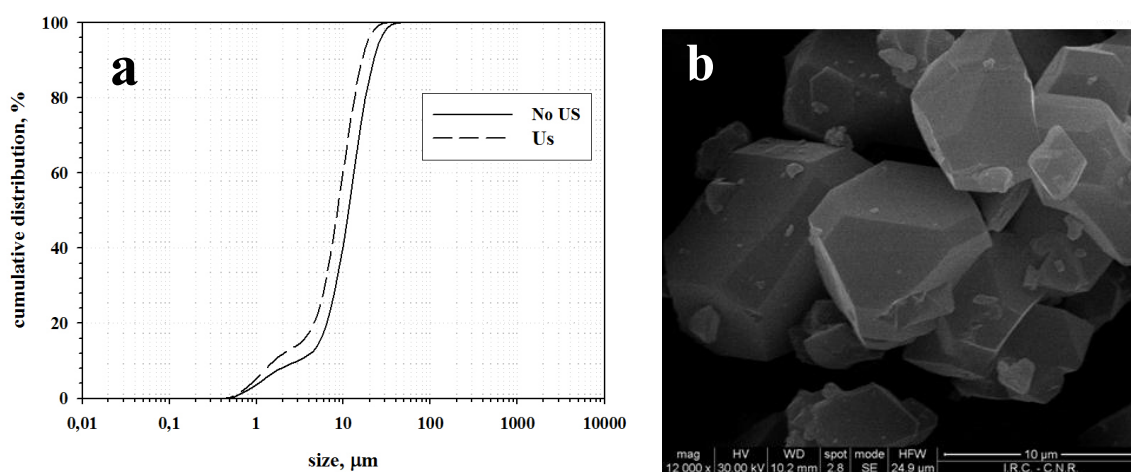
Fig. 26 Granulometric distribution (a) and SEM image (B) of HKUST-1.

Tab. 11 Properties of HKUST-1.

D_{SAUTER}, μm with/without US	BET surface area, m^2/g	Bulk density, kg/m^3	Pore volume cm^3/g
4.3/5.6	680	265	0.66

The analysis of the SEM images, reported in Fig. 26**b**, clearly shows that the powder is formed by irregular particles. In particular, the morphology and shape of the crystals can be observed. As reported in **Tab. 11**, HKUST-1 is characterized by a surface area lower than that of the activated carbons and 13X. Moreover, the BET surface area obtained for HKUST-1 is lower than that reported in literature (up to values of $1780 m^2/g$ [84]). Most likely this discrepancy is due to the fact that, differently from what reported in literature [84], HKUST-1 was prepared in large amount for this experimental campaign, thus leading to a lower control on its chemico-physical characteristics.

A diffraction experiment was run on standard glass slide for the background correction. The XRD spectra obtained (Fig. 27a) are those of the HKUST-1 [84], thus confirming its typical crystallographic structure.
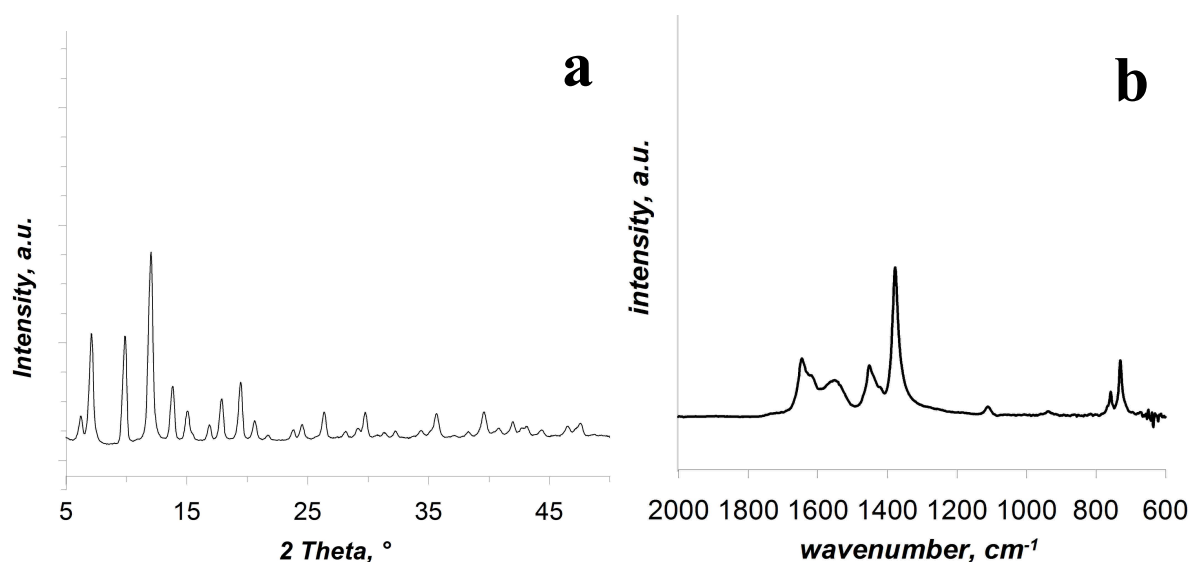
Fig. 27 a) X-ray diffraction (XRD) pattern of HKUST-1; b) FT-IR spectra of HKUST-1.

The FT-IR spectra of the HKUST-1 (Fig. 27b) are plotted in the $600-3500$ cm^{-1} wavenumber region. Spectra are baseline corrected and shifted for clarity. The spectrum of HKUST-1 is consistent to those reported in literature [84]. The bands at 1645 and 1590 cm^{-1} and at 1450 and 1370 cm^{-1} correspond to the asymmetric and symmetric stretching vibrations of the carboxylate groups in benzene tricarboxylate (BTC), respectively.

Similarly to what observed for the two zeolites, also HKUST-1 is a microporous material, with all the pores lower than 2nm (Fig. 28a). In particular, it exhibits a total pore volume intermediate between the activated carbons and the zeolites (**Tab. 11**).

As regards the thermal stability of HKUST-1, the thermogravimetric curve in inert environment (Fig. 28b) exhibits that HKUST-1 structure collapses at 350°C. However, the decomposition of the material starts around 200°C.
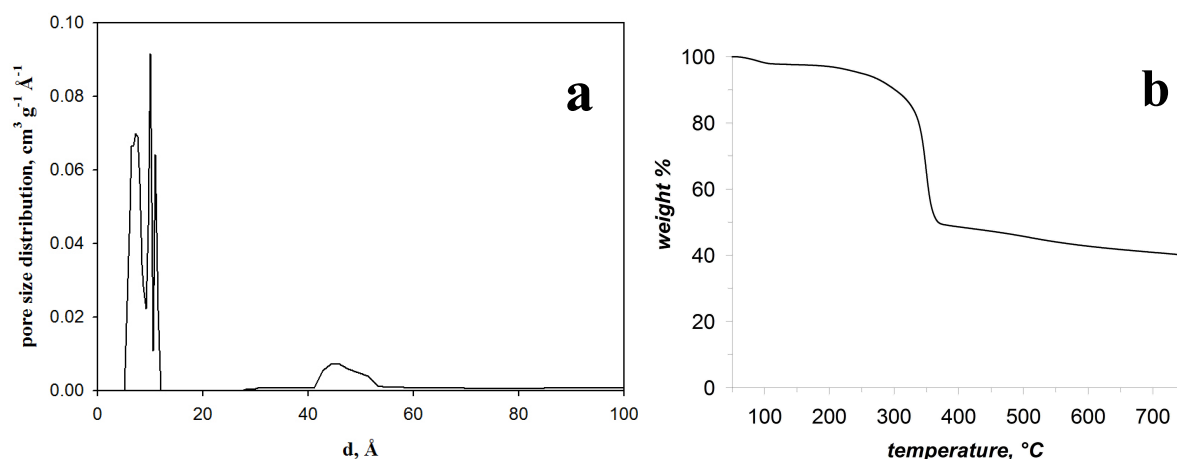
Fig. 28 Pore size distribution (a) and thermogravimetric analysis in N$_2$ (b) of HKUST-1.

III.2 Fluid-dynamic Characterization

In the following paragraphs the results of the ordinary and sound assisted fluidization tests for all the adsorbent materials are reported.

III.2.1   Activated Carbon Norit

Fig. 29 reports the dimensionless pressure drops ($\Delta P/\Delta P_0$) and bed expansion curves (H/H_0) obtained in ordinary and sound assisted conditions (140dB-80Hz), respectively. For uniform fluidization, the pressure drops are equal to the material weight per unit area (i.e. $\Delta P/\Delta P_0 = 1$), thus meaning that the whole bed is fluidized. Without the application of any acoustic field the fluidization quality is particularly poor (channeling), as clearly confirmed by the fact that asymptotic value reached by the pressure drops is lower than 1. On the contrary, pressure drops and expansion curves obtained with the assistance of sound are far more regular, both qualitatively and quantitatively. Therefore, the application of the sound is required to achieve a proper fluidization regime, which is closely related to an efficient break-up of the large aggregates yielded by cohesive forces into smaller structures easily to be fluidized [131,133].
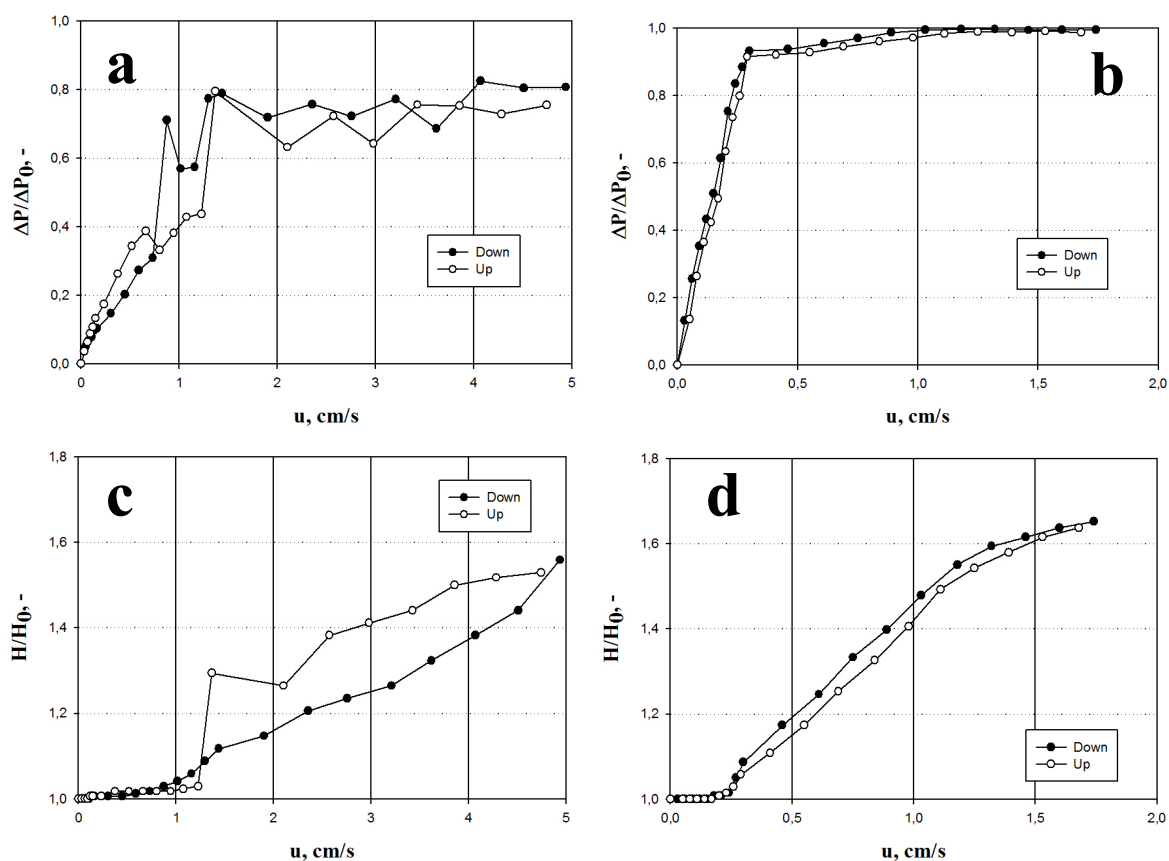
Fig. 29 AC Norit pressure drops (a) and expansion curves (c) under ordinary fluidization conditions; pressure drops (b) and expansion curves (d) under sound assisted fluidization conditions (140dB-80Hz).

In particular, an in-depth study has been carried out in order to evaluate the most effective acoustic conditions, namely whether it is possible or not to find optimal values of SPL and frequency. The results on the effect of SPL and frequency on the fluidization quality are reported in **Fig. 30**, in terms of pressure drops and expansion curves. As regards the role played by the SPL, it is clear from **Fig. 30**a and c that sound intensities higher than or equal to 125dB are enough to obtain a good fluidization quality. In other words, 125dB is a kind of threshold value for this activated carbon. Indeed, all the tests performed at higher SPL (125, 135 and 140dB) are characterized by quite similar pressure drops and expansion curves, which means that any additional increase of sound intensity does not succeed in further enhancing the fluidization quality. On the contrary, the test performed at 120dB is remarkably worse in terms of both pressure drops and expansion ratio.
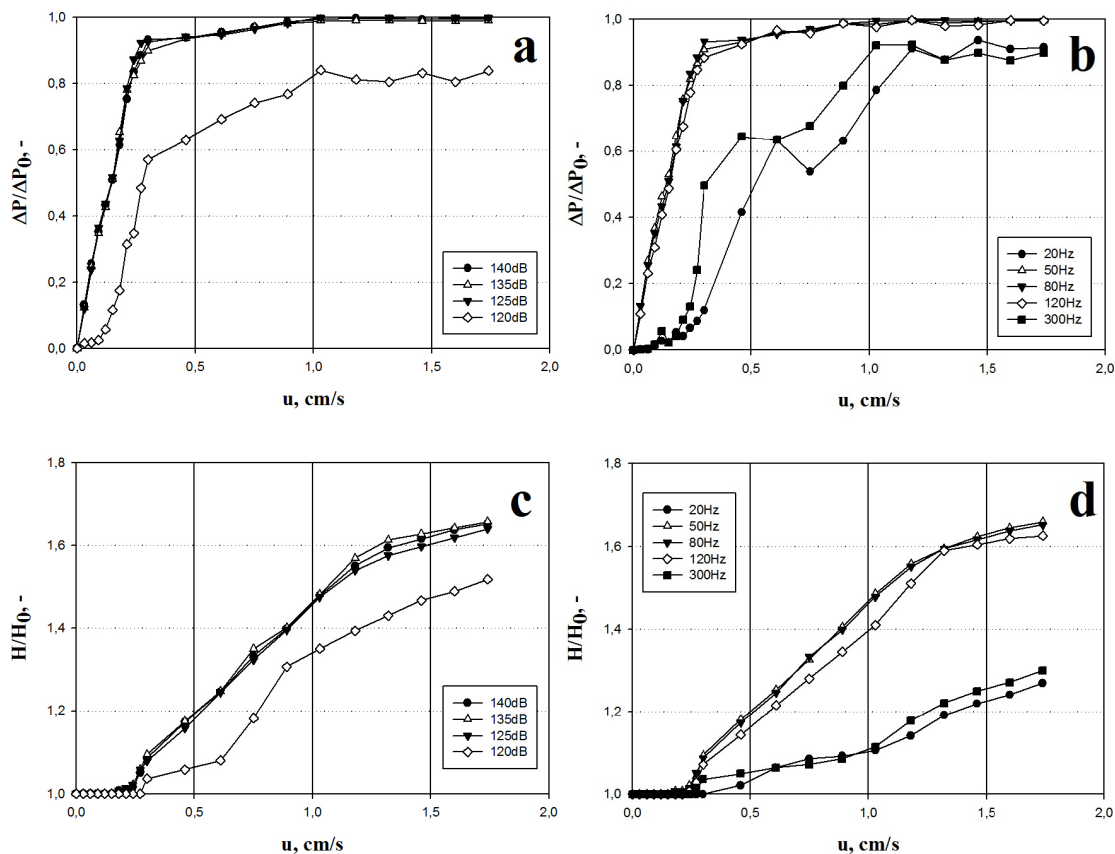
Fig. 30 Norit activated carbon: effect of SPL on pressure drops (a) and bed expansion (c) curves at fixed frequency (80Hz); Effect of frequency on pressure drops (b) and bed expansion (d) curves at fixed SPL (140dB).

As regards the sound frequency, the results reported in **Fig. 30**b and d show that it has a not monotone effect on the fluidization quality. Actually, it is possible to find an optimum range of frequency (50-120Hz) giving the best fluidization quality. Either too low or too high frequencies, which fall out of this range (20, 300Hz), correspond to worse fluidization qualities.

All these remarks regarding the effects of SPL and frequency can be even more clearly inferred from **Fig. 31**, which reports the minimum fluidization velocity, u_{mf}, (evaluated from the pressure drops curves by means of a graphical method) as function of SPL and frequency. Firstly, all the sound assisted tests are characterized by lower u_{mf} with respect to the test performed in ordinary conditions, thus confirming the ability of the sound in enhancing the fluidization quality. As for the SPL, u_{mf} is sharply decreased passing from 120 to 125dB and then it holds steady, the further increase of SPL nonetheless. Provided the SPL is higher than 120dB, a reasonably good fluidization quality can be attained. As for the frequency, the curve

is characterized by a minimum value (in the range 50-120Hz), corresponding to the best sound frequencies.
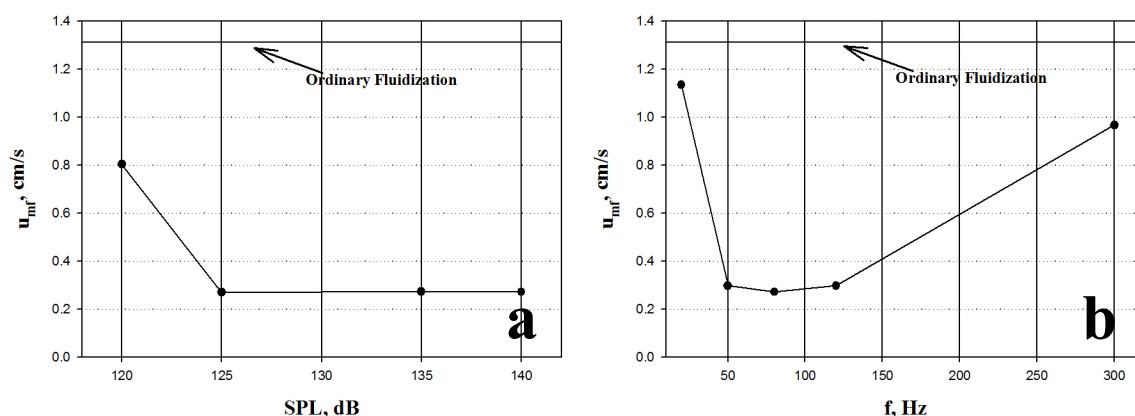
Fig. 31 Activated carbon: effect of SPL (at fixed f = 80Hz) and frequency (at fixed SPL=140dB) on u_{mf}.

As regards the SPL, the observed behaviour is do to the fact that an increase of the sound intensity implies an intensification of the energy introduced in the bed, namely the external force yielded by the acoustic field on the aggregates is enhanced. Therefore, large aggregates are likely expected to break into smaller ones, thus determining a consequent and reasonable decrease of u_{mf}. On the other hand, the explanation of the not monotone effect of sound frequency on the fluidization quality, which has already been found for other ultra-fine powders in a previous experimental campaign [131,133], is most likely that for too high frequencies the acoustic field is not able to properly propagate inside the bed and, in turn, to promote the break-up of aggregates; while for too low frequencies the relative motion between smaller and larger sub-aggregates, which leads to the break-up of the large aggregates originally present in the bed, is practically absent. Whereas, between these values there is a range of optimal frequencies able to promote a maximum aggregates break-up, leading to a decrease of u_{mf}.

As a further validation of all these observations, the fluidizing aggregate size has been evaluated by working out the bed expansion data [133]. The application of the sound allows to remarkably reduce the aggregate size, thus confirming the capability of the acoustic field to improve the break-up mechanism of larger aggregates yielded by the strong interparticle forces existing between particles due to the cohesiveness. Indeed, the calculated aggregate size is 310μm in the ordinary test, varying in the range 80-100μm in the sound assisted tests.

III.2.2 Activated Carbon Sigma Aldrich

Fig. 32 shows the dimensionless pressure drops and bed expansion curves for the ordinary and sound assisted tests (140dB-80Hz), respectively. In ordinary conditions, namely without the application of any acoustic field, the fluidization quality is particularly poor (channeling). The application of the sound, on the contrary, makes it possible to obtain far more regular pressure drops and expansion curves, both qualitatively and quantitatively. In other word, the application of the sound is necessary to achieve a proper fluidization regime, which is closely related to an efficient break-up of the large aggregates yielded by cohesive forces into smaller structures easily to be fluidized [131,133].
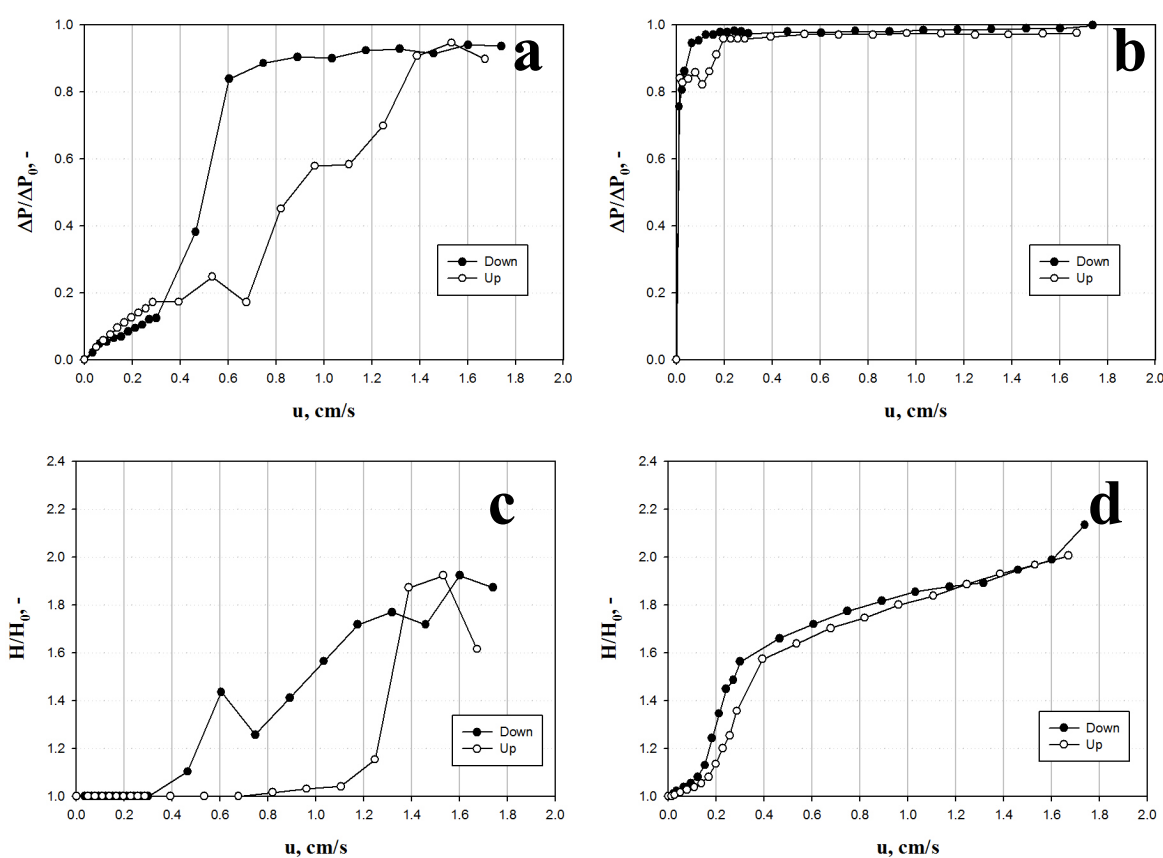
Fig. 32 AC Sigma pressure drops (a) and expansion curves (c) under ordinary fluidization conditions; pressure drops (b) and expansion curves (d) under sound assisted fluidization conditions (140dB-80Hz).

An in-depth study has been carried out in order to evaluate the most effective acoustic conditions, namely whether it is possible or not to find optimal values of SPL and frequency. **Fig. 33** and **Fig. 34** report the fluidization curves of all the tests performed as affected by SPL and frequency, respectively. In order to make it clear the effect of the sound parameters on the fluidization quality the trend on u_{mf} as function of SPL and frequency has been obtained (**Fig. 35**).
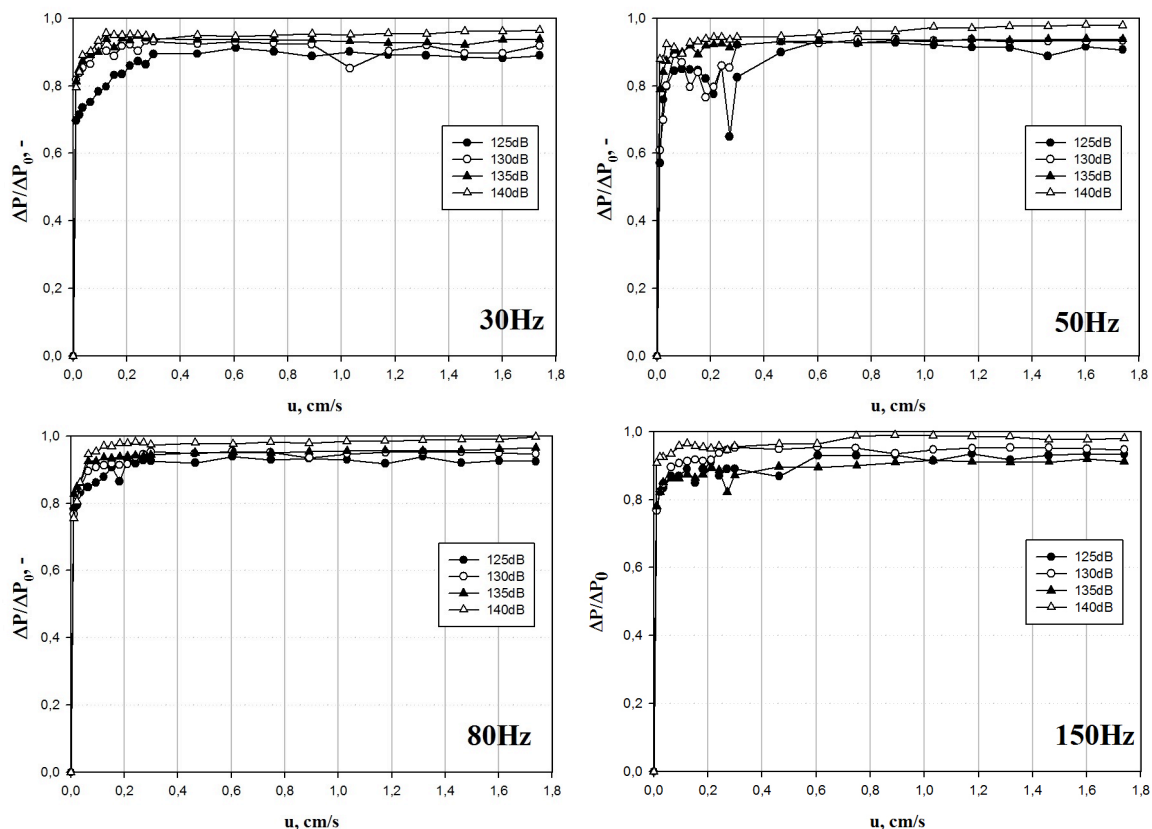
Fig. 33 AC Sigma: Effect of SPL on pressure drops for the tests performed at different sound frequencies.

As regards the role played by the SPL, it is clear from **Fig. 33** that even at the lowest sound intensity (125dB) a good fluidization quality can be achieved, even though a slight improvement can be observed with the increase of SPL whatever the frequency. However, as clearly shown in **Fig. 35** at fixed frequency, an increase of SPL results in a slight decrease of u_{mf}. In light of these results about the effect of SPL it emerges that all the investigated sound intensities are capable of promoting an efficient break-up of the initial aggregates in fluidizable aggregates, even though there is a slight beneficial effect with the increase of SPL, du to the intensification of the energy introduced in the bed and consequently a more efficient break-up of large aggregates into smaller ones.

As regards the sound frequency, the results reported in **Fig. 34** and **Fig. 35** show that for the largest SPLs (140 and 135dB) it has a negligible effect. On the contrary at the lowest SPLs (125 and 135dB) frequencies higher than 50Hz make it possible to decrease the u_{mf}, thus obtaining a better fluidization quality.
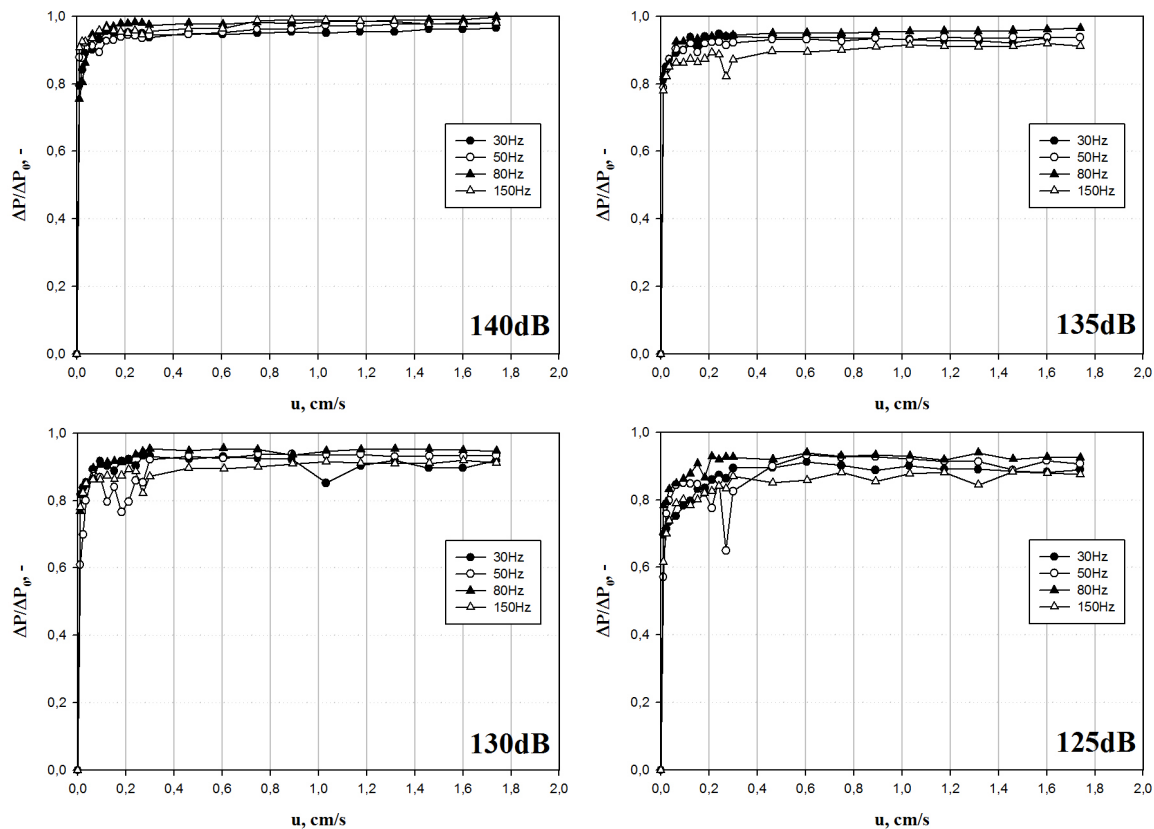
Fig. 34 AC Sigma: Effect of sound frequency on pressure drops for the tests performed at different SPLs.
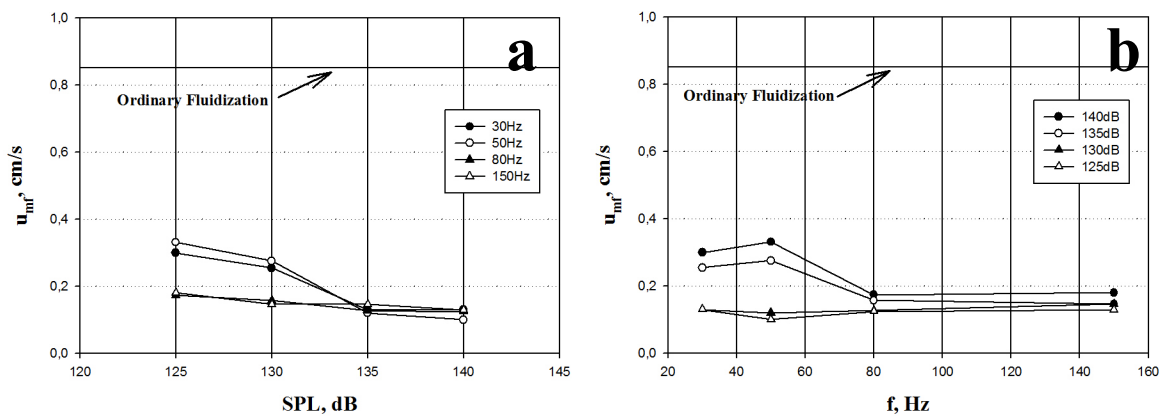
Fig. 35 AC Sigma: Effect of (a) SPL and (b) frequency on u_{mf}.

III.2.3   Zeolite H-ZSM-5

Fig. 36 reports the dimensionless pressure drops and bed expansion ratio obtained in ordinary and sound assisted conditions (140dB-80Hz).

64
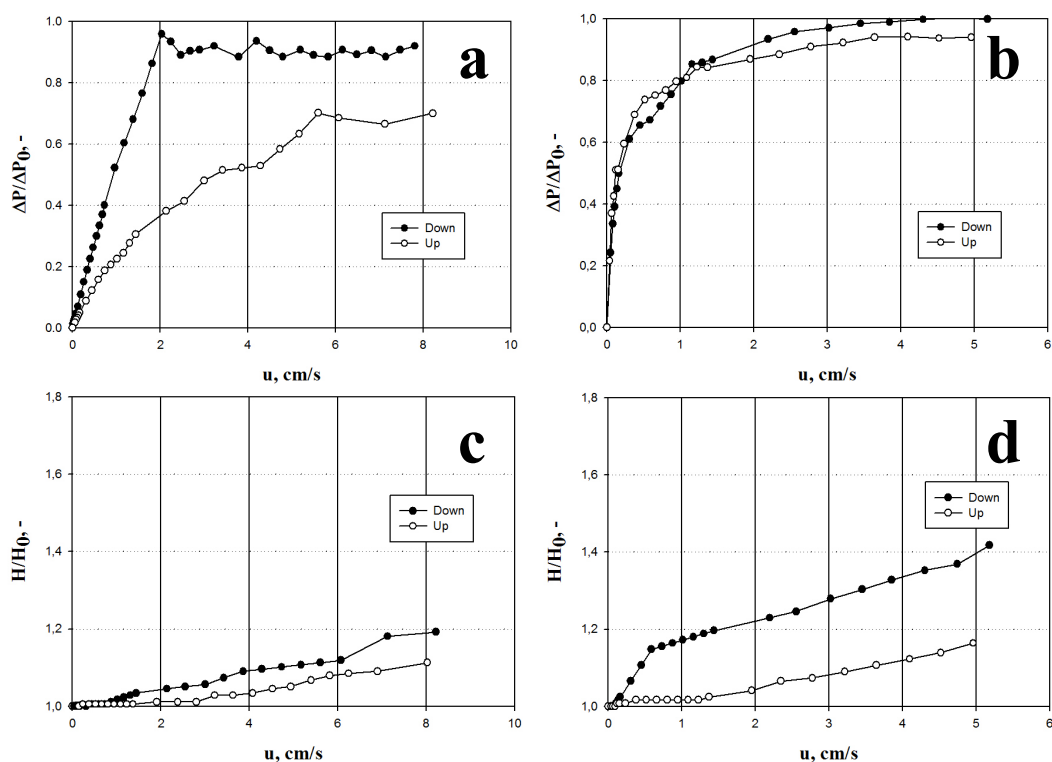
Fig. 36 H-ZSM-5 pressure drops (a) and expansion curves (c) under ordinary fluidization conditions; pressure drops (b) and expansion curves (d) under sound assisted fluidization conditions (140dB-80Hz).

Differently from what observed for the activated carbons, also in ordinary conditions the zeolite fluidization quality is quite acceptable. In particular, the analysis of the curves suggests that the application of the sound results in a more regular behaviour in terms of both pressure drops and bed expansion ratio. Also in this case, the size of fluidizing aggregates has been evaluated: 280 and 660μm with and without the application of the sound, respectively. This trend is confirmed by the minimum fluidization values: 1 and 4cm/s for ordinary and sound assisted tests, respectively.

III.2.4   Zeolite 13X

In **Fig. 37**a and c the dimensionless pressure drops and bed expansion curves obtained in ordinary conditions are reported. The analysis of the curves suggests that also in these conditions (i.e. without the application of any acoustic field) the powder can be fluidized, even though with some instability as clearly confirmed by the fluctuations of the pressure drops around the asymptotic value (this behaviour is due to channels crossing the bed). Therefore, the application of the sound is required to achieve a stable fluidization regime and higher bed expansion, as clearly confirmed by the curves reported in **Fig. 37b** and d.
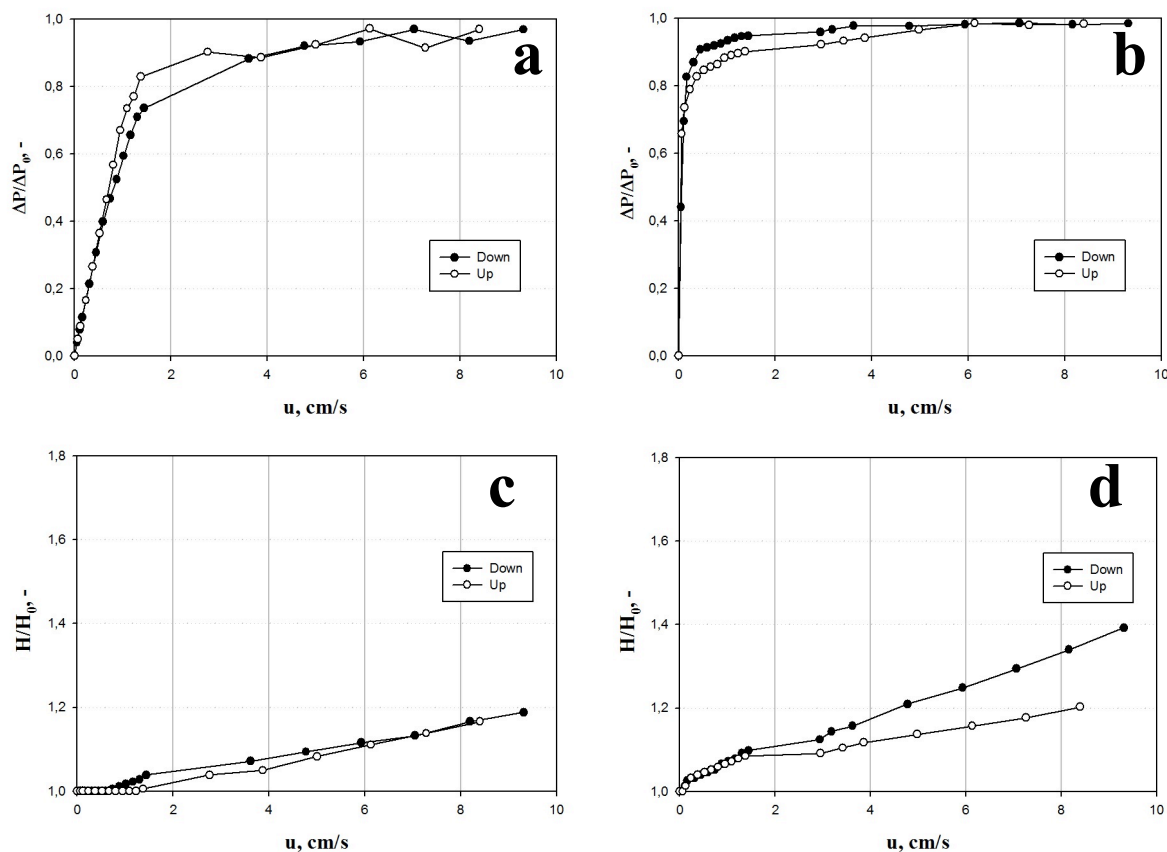
Fig. 37 13X pressure drops (a) and expansion curves (c) under ordinary fluidization conditions; pressure drops (b) and expansion curves (d) under sound assisted fluidization conditions (140dB-80Hz).

Fig. 38 and **Fig. 39** report the fluidization curves of all the tests performed as affected by SPL and frequency, respectively. In order to make it clear the effect of the sound parameters on the fluidization quality the trend on u_{mf} as function of SPL and frequency has been obtained (**Fig. 40**).

As regards the role played by the SPL, it is clear from **Fig. 38** that sound intensities higher than or equal to 125dB are enough to obtain a good fluidization quality. However, as clearly shown in **Fig. 40** at fixed frequency, an increase of SPL results in a decrease of u_{mf}. As already discussed for the two activated carbons, this behaviour is due to the fact that that all the investigated sound intensities are capable of promoting an efficient break-up of the initial aggregates in fluidizable aggregates. The slight beneficial effect observed with the increase of SPL is due to an intensification of the external force yielded by the acoustic field on the aggregates, which causes the large aggregates are to break into smaller ones.
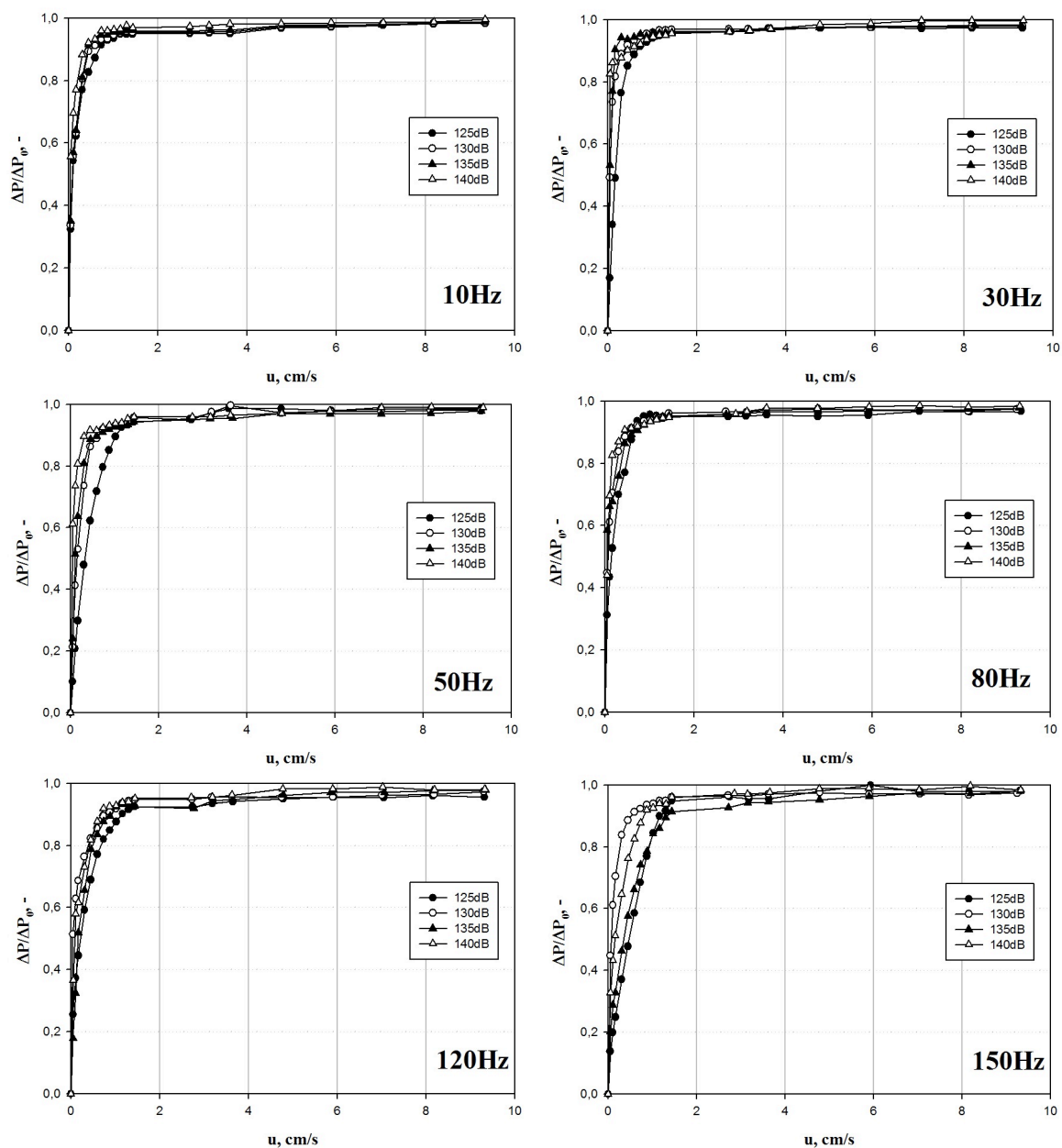
Fig. 38 13X: Effect of SPL on pressure drops for the tests performed at different sound frequencies.

As regards the sound frequency, the results reported in **Fig. 39** and **Fig. 40** show that it has a not monotone effect on the fluidization quality. Actually, it is possible to find an optimum range of frequency (10-80Hz) giving the best fluidization quality.
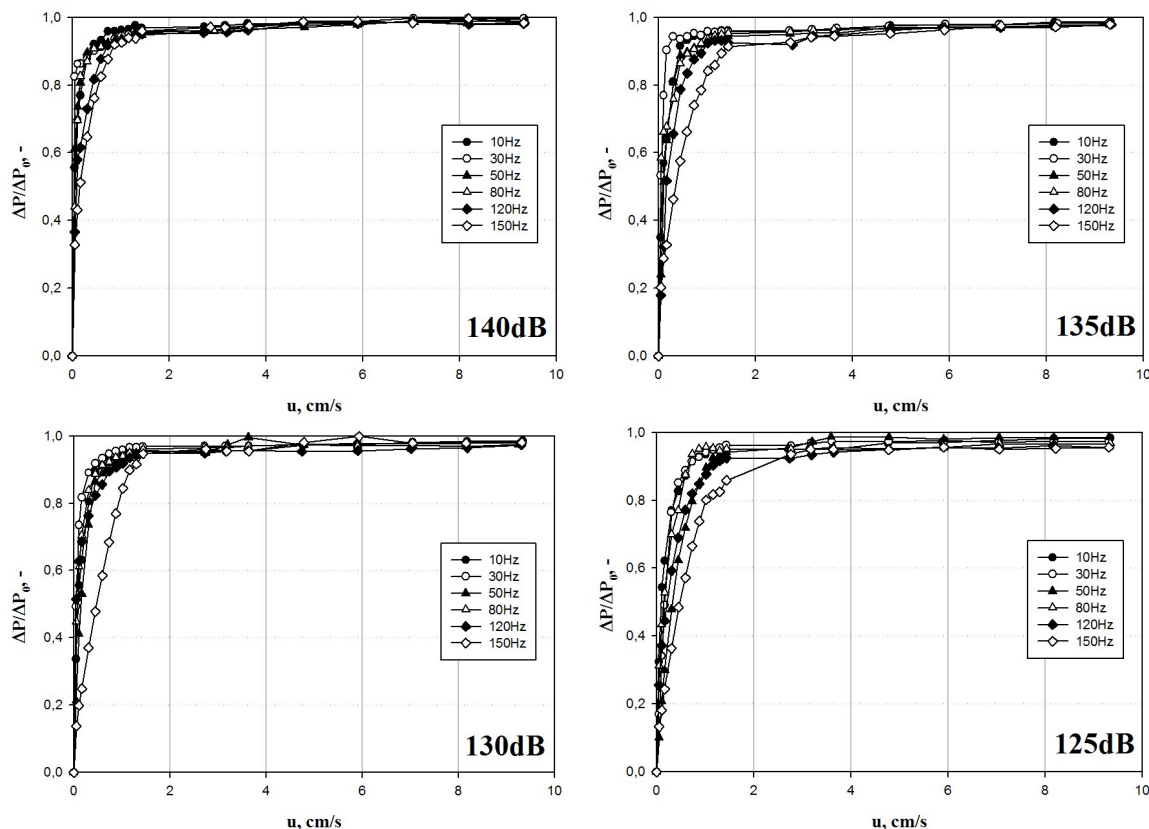
Fig. 39 13X: Effect of sound frequency on pressure drops for the tests performed at different SPLs.
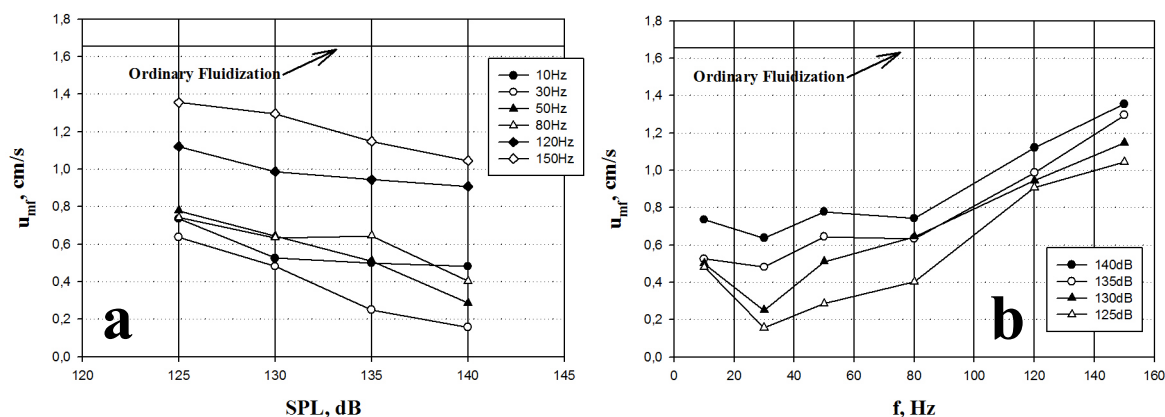
Fig. 40 13X: Effect of (a) SPL and (b) frequency on u_{mf}.

III.2.5 HKUST-1

In **Fig. 41**a the dimensionless pressure drops obtained in ordinary conditions are reported. The bed expansion curves are not presented because the powder adhered to the column wall making it impossible to read the bed height. In these conditions the material cannot be fluidized (channeling occurs inside the bed) as clearly confirmed by the pressure drops curve, which does not reach an asymptotic value. Therefore, the application of the sound is required to achieve a proper fluidization regime, which is closely related to an efficient break-up of the

large aggregates yielded by cohesive forces into smaller structures easily to be fluidized. This is clearly confirmed by the fluidization curves obtained in sound assisted conditions (**Fig. 41b**).
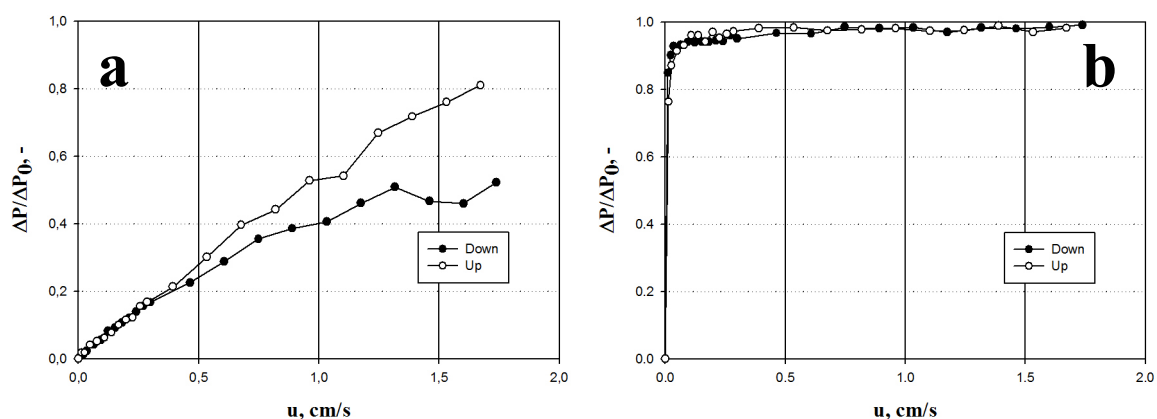
Fig. 41 HKUST-1 pressure drops and expansion curves for (a) ordinary and (b) sound assisted, 140dB-80Hz, tests.

Fig. 42 reports the effect of SPL and frequency on the fluidization quality. In the first place, the analysis of these curves confirms that under the application of the acoustic field, the material can be properly fluidized. Indeed, regular pressure drop have been obtained. Then, as regards the role played by the SPL, it is clear from **Fig. 42**a that for sound intensities lower than 140dB the fluidization quality is remarkably worse. Indeed, both at 130dB and 125dB the fluidization curve is lower than in the tests performed at 140dB, thus meaning that a fraction of the bed is not properly fluidized. **Fig. 43**a reports the trend of u_{mf} as a function of SPL. Coherently to what observed from the fluidization curves, increasing SPLs result in lower values of u_{mf}.
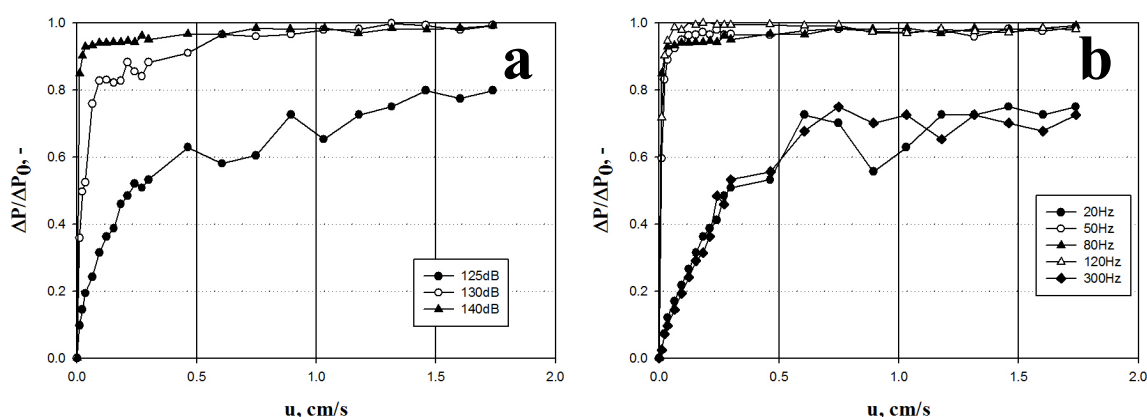
Fig. 42 HKUST-1: Effect of SPL on pressure drops (a) at fixed frequency (80Hz); Effect of frequency on pressure drops (b) at fixed SPL (140dB).

As regards the sound frequency, the results reported in **Fig. 42**b and **Fig. 43**b show that it has a not monotone effect on the fluidization quality. More specifically, the frequencies falling in the range 50-120Hz represent in the optimum range for this material. The evaluation of the

fluidizing aggregates diameter was not carried out, since the impossibility of evaluating the expansion curves.
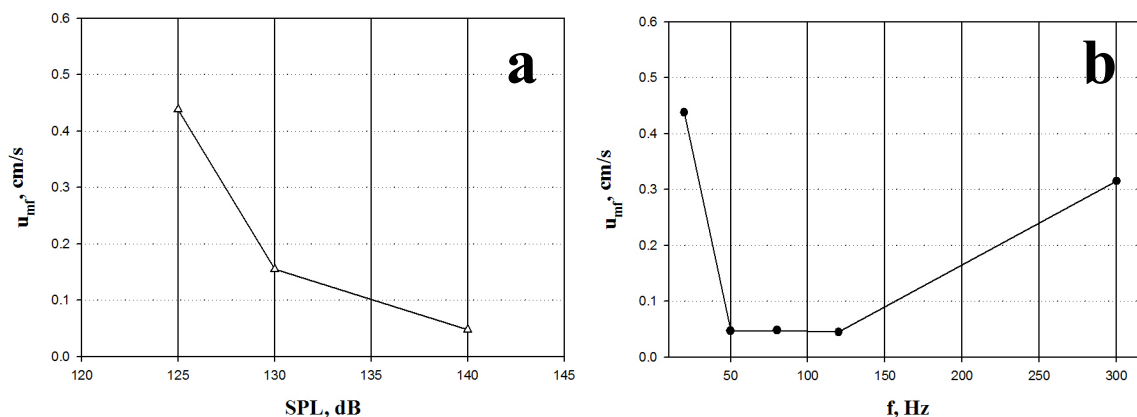
Fig. 43 HKUST-1: Effect of (a) SPL and (b) frequency on u$_{mf}$.

III.3 Adsorption Tests

III.3.1 Activated Carbon Norit

III.3.1.1 Effect of the Sound Application

Fig. 44a reports the typical breakthrough curves (i.e. C/C$_0$ versus time, C and C$_0$ being the CO$_2$ concentration in the effluent and feed stream, respectively) obtained in ordinary and one of the sound assisted tests. These curves have been worked out to calculate: i) the moles of CO$_2$ adsorbed per unit mass of adsorbent, n_{ads}, calculated by integrating the breakthrough curves according to the following mass balance:

$$n_{ads} = \frac{P}{RT} \int_0^{t_{eq}} \left(Q_{CO_2}^{in} - Q_{CO_2}^{out} \right) dt \qquad (18)$$

ii) the breakthrough time, t$_b$, or break point, which is the time it takes for CO$_2$ to be detected at the adsorption column outlet (5% of the inlet concentration); iii) the fraction of bed utilized at breakpoint (W), namely the ratio between the CO$_2$ adsorbed until the break point and that adsorbed until saturation; iv) the rate of the adsorption process, which has been evaluated as the difference between the time it takes for CO$_2$ to reach the 95% of the inlet concentration at the adsorption column outlet, t$_{95}$, and t$_b$. In order to highlight the most significant portion of the curve, namely the section before and soon after t$_b$, the same graph has been also reported in logarithmic scale (**Fig. 44b**).
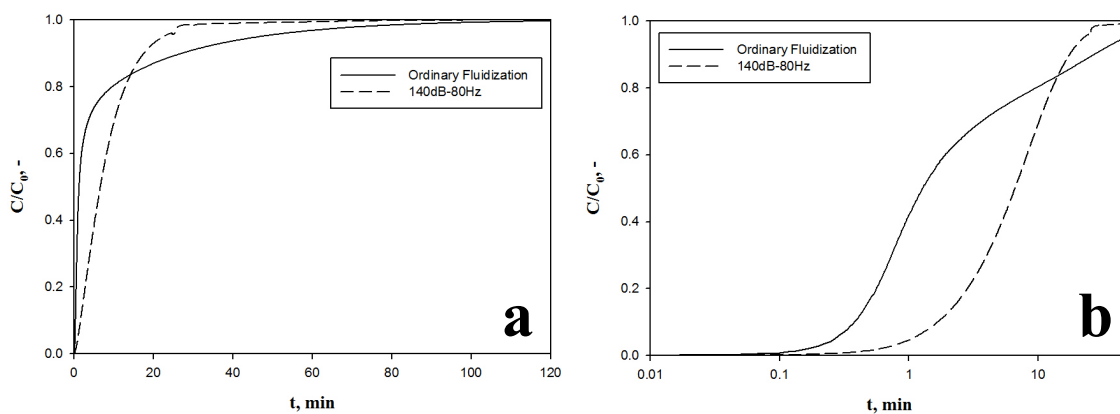
Fig. 44 AC Norit breakthrough curves obtained in ordinary and sound assisted conditions, in (a) linear and (b) logarithmic scale. u=1.5cm/s; C_0=10%vol.

Tab. 12 reports all the parameters of n_{ads}, t_b, W and t_{95}-t_b obtained in the tests performed at three different CO_2 inlet concentrations and fluidization velocities. The superficial gas velocities used in these tests are high enough to provide a good fluidization quality (see paragraph III.2.1) at all the different sound parameters, since they are all larger than the corresponding u_{mf}. The analysis of the curves (**Fig. 44**) and the results reported in **Tab. 12** show that the application of the sound clearly affects both the adsorption rate and the global adsorption capacity. Indeed, the total amount of CO_2 adsorbed until saturation, reported in **Tab. 12**, is strongly improved by the application of the sound: the percentage increase with respect to the tests in ordinary conditions moves from 13% for the test performed at 140dB-80Hz, 2cm/s and 10%vol. of CO_2 in the inlet stream up to 23% for the test performed at 140dB-80Hz, 1.5cm/s and 10%vol. CO_2.

The sound greatly increases the breakthrough time, which in all the sound assisted tests is more than five times the value obtained in ordinary conditions (see **Tab. 12**). Consequently, the application of the sound also results for all the tests (i.e. for all the CO_2 inlet concentration and for all the SPL investigated) in a great enhancement of the fraction of bed utilized at break point (W), which moves from values always lower than 4%, in the tests performed in ordinary conditions, up to values of about 15%, in all the sound assisted tests. The beneficial effect shown by the sound is due to the enhancement of the fluidization quality with respect to the tests performed in ordinary conditions, namely without the aid of any external force. In particular, the fluidization of cohesive powders is based on a break-up and re-aggregation mechanism, which is greatly enhanced by the application of acoustic fields [131,133]; so, the improved fluidization quality arising from the application of the sound is likely to be the main reason of the observed enhancement of the adsorption efficiency. In other words, the continuous aggregates break-up and re-aggregation mechanism makes the surface of the activated carbon more readily available for the adsorption process.

The application of the sound also greatly enhances the breakthrough time and the kinetics of the entire process. Indeed, under the application of acoustic fields the CO_2 concentration profile goes to saturation in remarkably shorter times with respect to the tests performed in ordinary conditions, and also the values of t_{95}-t_b are notably decreases in the sound assisted tests. In order to point out the differences existing between the ordinary and sound assisted tests, the rate of CO_2 concentration increase, r_{CO_2}, has been evaluated and plotted as a function of time (**Fig. 45**). Soon after $t=t_b$, r_{CO_2} abruptly rises up for the tests performed in ordinary conditions.

Tab. 12 Results of the adsorption tests obtained for AC Norit.

Superficial gas velocity	Sound Parameters	CO_2 inlet concentration											
		5%				10%				15%			
		t_b s	n_{ads} mmol/g	W %	t_{95}-t_b min	t_b s	n_{ads} mmol/g	W %	t_{95}-t_b min	t_b s	n_{ads} mmol/g	W %	t_{95}-t_b min
2cm/s	Ordinary	15	0.22	3.6	44	8	0.30	2.7	36	7	0.37	2.7	24
	140dB-80Hz	65	0.26	15	13	51	0.34	12	15	43	0.46	15	12
1.5cm/s	Ordinary	19	0.23	3	63	12	0.31	2.7	47	10	0.38	2.8	50
	140dB-80Hz	80	0.27	11	30	63	0.37	15	22	58	0.44	14	19
1cm/s	Ordinary	27	0.23	2.8	78	20	0.31	3	71	15	0.38	2.7	57
	140dB-80Hz	185	0.28	16	31	165	0.38	20	31	155	0.47	23	31

The explanation of this evidence is likely to be found in the fluidization quality being extremely poor and unstable in ordinary conditions; indeed, unable to overcome the cohesiveness of the fine powder, most of the fluid menages to flow across the bed only by finding channels of minimum resistance. Spreading across the bed, these channels allow for a bypass of an appreciable volume of gas, thus hampering the quality of fluid-solid contact, which is the main factor ruling any adsorption process.
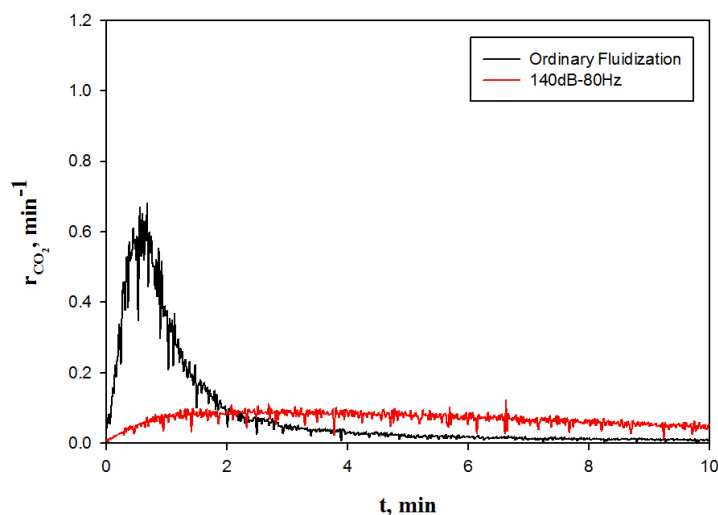
Fig. 45 AC Norit adsorption rate for ordinary and sound assisted tests. u=1.5cm/s; C_0=10%vol.

Therefore, it is most likely that adsorption mainly takes place on those aggregates placed at the wall of the gas channels, whereas most of the adsorption surface is nearly precluded to the fluid. Soon after the extremely quick saturation of the adsorption sites on those easily available aggregates, CO_2 is logically found to appear in the effluent gas. Therefore, the rather steep slope (i.e. high r_{CO_2}) of the CO_2 concentration profile is due to the above-mentioned majority of fluid bypassing the bed without truly taking part to the adsorption process. After this sharp rise, a likewise abrupt decrease of slope can be observed in the breakthrough curve, which very slowly goes to saturation. The explanation of this behaviour is twofold: the channels being subjected to perturbations, which bring fresh aggregates into contact with CO_2, and the smaller portion of fluid actually permeating the bed. In other words, while most of the inflow CO_2 bypasses the bed, only a small fraction takes part to the adsorption, which is actually very slow, as clearly confirmed by the extremely slow breakthrough curve tail, which practically accounts for the whole adsorption process. In particular, the extremely slowness of the breakthrough tail is probably due to action of two different aspects: the slow adsorption kinetics yielded by the poor fluidization quality and the fact that, despite a fixed flow of CO_2 is fed to the bed, only a limited fraction takes part to adsorption while the majority flows through the bed unaltered (i.e. the CO_2 flow actually undergoing adsorption is smaller than the nominal one, because of the bypassing gas), thus reasonably slowing down the process. On the contrary, the sound assisted tests are characterized by more regular breakthrough curves. Indeed, as clearly shown in **Fig. 45**, no abrupt change of slope is present. Moreover, the application of acoustic fields allows not only to enhance the adsorption capacity of the activated carbon (i.e. the total amount of CO_2 adsorbed until saturation) but also to speed up the adsorption process (namely the time for CO_2 to approach the saturation value is remarkably decreased) due to fastest adsorption kinetics. This is likely due to the enhancement of the fluidization quality (which brings better gas-solid contact and mass transfer coefficients) yielded by the application of the acoustic field. In particular, the application of the sound greatly enhances the break-up mechanism of fluidizing aggregates [131,133], thus continuously renewing the surface exposed to the fluid.

In order to verify these considerations a further test has been carried out. This test has been started in ordinary condition, and only at a time t=t*, corresponding to the above-mentioned change of slope typical of ordinary adsorption test, the sound has been switched on (**Fig. 46**).
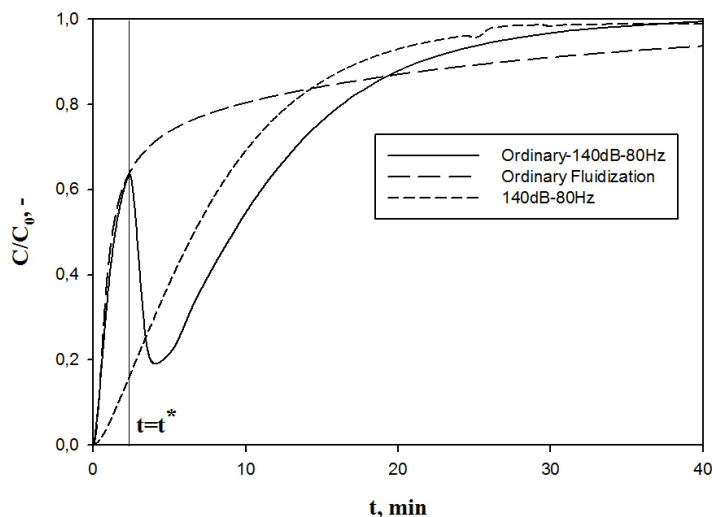
Fig. 46 AC Norit breakthrough curve obtained switching on the sound at t=t*. u=1.5cm/s; C_0=10%vol.

The analysis of the curve obtained clearly shows that for $t<t^*$ the CO_2 concentration profile is reasonably the same as that obtained in ordinary conditions (i.e. the bypassing gas makes the CO_2 concentration abruptly rise). At $t=t^*$ the CO_2 concentration suddenly drops down before rising up again, but following now the typical trend of the sound assisted test. This behaviour confirms the ability of the sound to better exploit the adsorption capacity of the activated carbon. Indeed, as soon as the sound has been switched on, that specific surface, precluded to the fluid in ordinary conditions, suddenly becomes available causing CO_2 concentration to drop down because of the renewed activated carbon adsorption capacity.

III.3.1.1.1 Effect of SPL

The effect of SPL on CO_2 adsorption efficiency has been evaluated by carrying out tests at fixed frequency (80Hz) and different sound intensity (from 120 up to 140dB). The comparison among all the tests performed in terms of breakthrough curves, moles of CO_2 adsorbed, t_b and W are reported in **Fig. 47**. The data obtained in ordinary conditions have also been reported for comparison. The analysis of these results is rather clear: the SPL effect on CO_2 adsorption process reflects what observed in the fluidization tests. Indeed, the adsorption process undergoes a significant enhancement only when SPLs higher or equal to 125dB are applied, which is perfectly consistent with the obtained activated carbon fluid-dynamic behaviour.
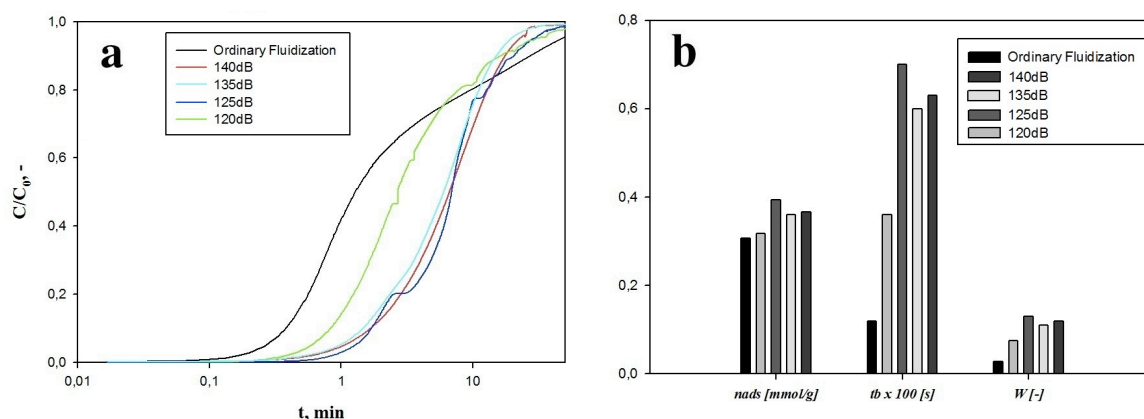
Fig. 47 AC Norit: effect of SPL on CO$_2$ adsorption. a) Breakthrough curves; b) CO$_2$ adsorption efficiency, in terms of n$_{ads}$, t$_b$ and W. u=1.5cm/s; C$_0$=10%vol; f=80Hz.

In particular, the best performances are obtained when the fluidization quality is maximum, namely when the gas-solid contact efficiency is maximized. Indeed, 125dB is a sort of threshold intensity beyond which any further increase of SPL is ineffective, and sure enough all the tests performed at higher SPL are very similar in terms of breakthrough curves shape, moles of CO$_2$ adsorbed, t$_b$ and W. Whereas, the behaviour observed at 120dB is intermediate. These results are an additional proof of the tight link existing between the adsorption efficiency and the fluid-dynamics of the system.

III.3.1.1.2 Effect of Sound Frequency

In order to point out the effect of sound frequency on CO$_2$ adsorption efficiency, tests have been performed at fixed SPL (140dB) and varying the sound frequency (from 20 to 300Hz). The comparison among all the tests performed in terms of breakthrough curves shape, moles of CO$_2$ adsorbed, t$_b$ and W is reported in **Fig. 48**.

As well as for the SPL, also the results obtained in these tests are in perfect agreement with those obtained from the fluidization tests. Indeed, the best results in terms of CO$_2$ adsorption efficiency can be achieved when sound frequencies falling in the same optimum range (50-120Hz) are applied. In particular, the best performances are obtained when the fluidization quality is maximum, namely when the efficiency of the gas-solid contact is the highest. Indeed, the tests performed at intermediate frequencies (50, 80 and 120Hz) are characterized by very similar behaviours (breakthrough curves, n$_{ads}$, t$_b$ and W). Whereas, the adsorption tests carried out at 20 and 300Hz are remarkably worse.
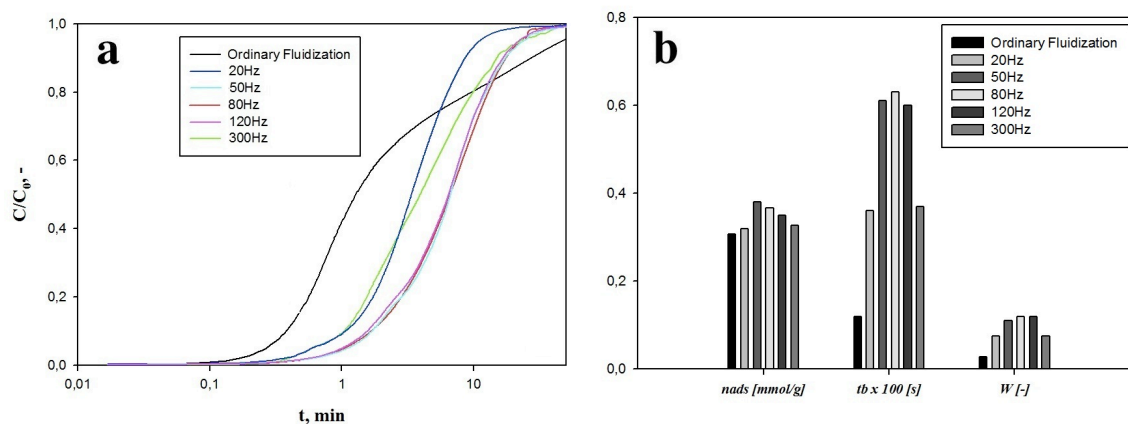
Fig. 48 AC Norit: effect of sound frequency on CO$_2$ adsorption. a) Breakthrough curves; b) CO$_2$ adsorption efficiency, in terms of n$_{ads}$, t$_b$ and W. u=1.5cm/s; C$_0$=10%vol; SPL=140dB.

III.3.1.2   Effect of CO$_2$ Partial Pressure

Fig. 49 reports the breakthrough curves obtained in ordinary and sound assisted conditions for the tests performed at a fixed fluidization velocity (2cm/s) and at three different inlet CO$_2$ concentration (5, 10 and 15%vol. in N$_2$).
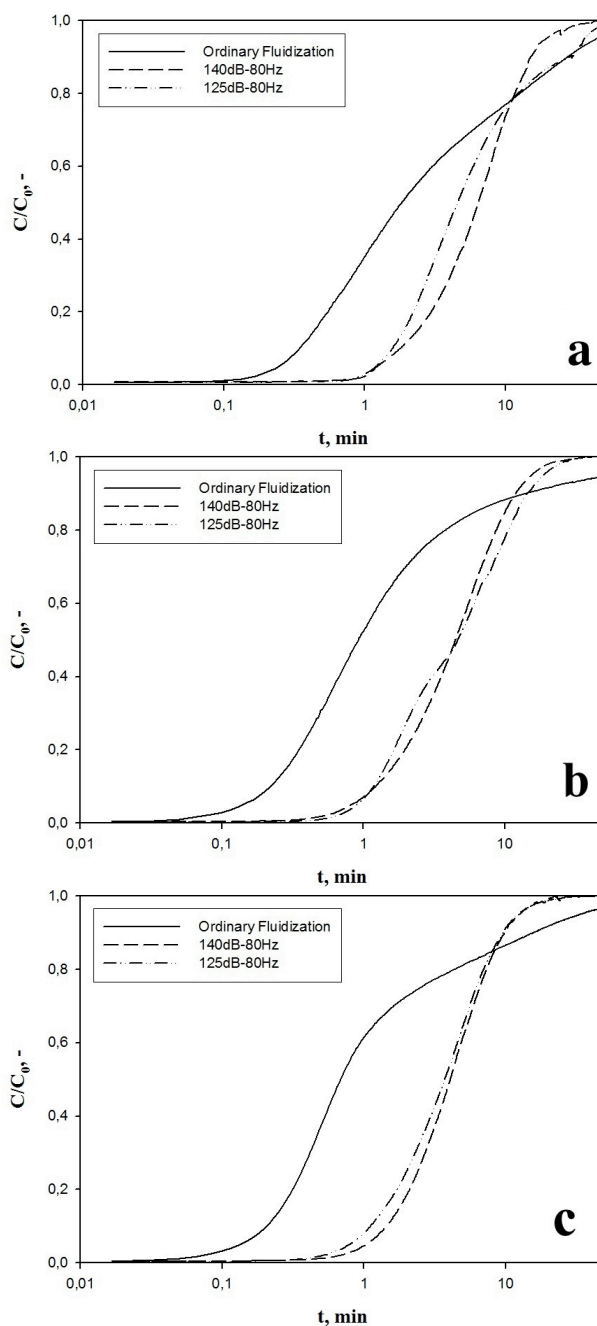
Fig. 49 AC Norit breakthrough curves in ordinary and sound assisted conditions. u=2cm/s; a) C_0=5%vol; b) 10%vol.; c) 15%vol.

The analysis of the results reported in

Tab. 12, shows, as expected, that the CO_2 capture capacity of the adsorbent at a fixed temperature increases with CO_2 partial pressure. This trend is absolutely consistent from a thermodynamic point of view since the CO_2 partial pressure represents the driving force of the adsorption process. The adsorption process becomes faster with the increase of the CO_2 inlet concentration, as confirmed by the decrease of t_{95}-t_b. In this case the increase of the CO_2 inlet concentration corresponds to a decrease of t_b as the result of the combined effect of two phenomena: on the one hand, from a thermodynamic point of view, the increase of P_{CO_2} implies an increase of the adsorption capacity of the sorbent, thus involving a consequent

increase of t_b; but on the other the increase of P_{CO_2} makes the adsorption process faster, thus implying a quicker saturation of the sorbent and consequently a decrease of t_b. Therefore all these things considered, the latter aspect prevails on the first. As regards W, the abovementioned aspects counterbalance each other, thus keeping it constant.

The experimental results have been elaborated and fitted by the Langmuir [48] equation:

$$n_{ads} = n_{ads}^s \frac{bP_{CO_2}}{1+bP_{CO_2}}$$

(19)

where n_{ads} are the moles of CO_2 adsorbed per unit mass of activated carbon, n_{ads}^s the moles adsorbed until saturation, b the affinity coefficient between the adsorbent and adsorbed phases and P_{CO_2} the CO_2 partial pressure in the gaseous phase. **Fig. 50** reports the adsorption isotherms calculated in ordinary and sound assisted tests. Analysis of the curves highlights the beneficial effect played by the application of the acoustic field on adsorption performances.
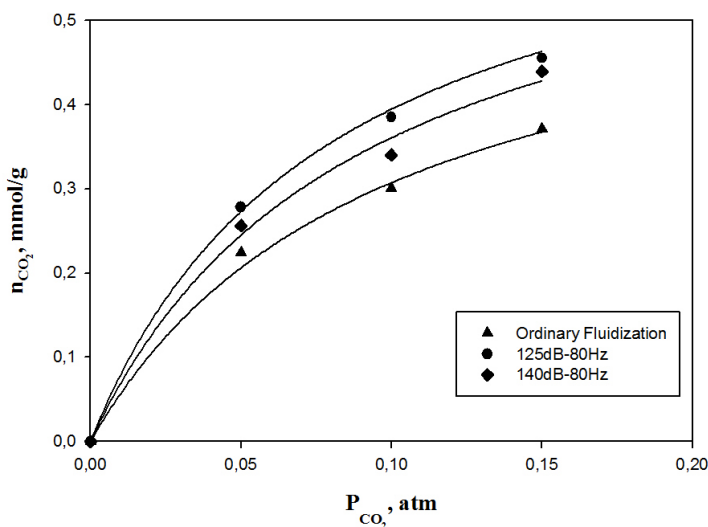
Fig. 50 AC Norit adsorption isotherms in ordinary and sound assisted test, u=2cm/s.

Under sound assisted fluidization the adsorption isotherms move to more favorable adsorption conditions. Further, this evidence has been confirmed by the values obtained for the fitting parameters of the Langmuir equation; the isotherms obtained in sound assisted conditions are characterized by higher values not only of n_{ads}^s but also of b, which, being an affinity coefficient between the two phases, is expected to be the same. Therefore, the observed increase of b confirms how the application of the sound intrinsically affects the adsorption process making the activated carbon more affine to CO_2, due to improved availability of its surface to CO_2 molecules.

III.3.1.3   Effect of Fluidization Velocity

In order to point out the effect of the fluidization velocity on the adsorption process tests have been performed at three different gas velocities (1, 1.5 and 2cm/s) for each CO_2 inlet concentration (5, 10 and 15%vol.). It is possible to define a contact time as the ratio between the mass of adsorbent and the CO_2 volumetric flow. From the data reported in **Tab. 12** it emerges that an increase of the contact time (t_c), i.e. a decrease of superficial gas velocity, results, as one might expect, in an increase of t_b. As regards t_{95}-t_b, it decreases with the increase of the fluidization velocity (i.e. a decrease of the contact time) because the adsorption process becomes faster. As regards n_{ads}, under sound assisted conditions a decrease of t_c results in an increase of the moles of CO_2 adsorbed. This is probably due to the fact that at the highest fluidization velocities (i.e. the lowest contact times) the time it takes the fluid to flow the height of the bed is too low with respect to the time it takes for the adsorption to be completed. In other words, it is most likely that the timescale of the adsorption process is higher than the contact time corresponding to that fluidization velocity, i.e. the residence time is low and some CO_2 may have passed through the bed unreacted, even when adsorption sites are available. Under ordinary fluidization conditions n_{ads} are not affected by any change of t_c (i.e. fluidization velocity). This evidence is probably due to the fact that without the application of any acoustic field the fluidization quality is particularly poor for all the investigated fluidization velocities (i.e. the limit to the full exploitation of AC Norit surface is the not effective gas-solid contact, therefore any change of t_c is negligible in terms of CO_2 uptake). As regards W, it generally increases with an increase of t_c for the sound assisted test, whereas it is basically not affected by t_c in the tests performed under ordinary fluidization conditions. However, it must be noted that the trend of W with t_c is the complex result of several contributions. As a matter of fact, t_b has been found to monotonically increase with t_c, nonetheless, the dependence between W and t_b is not trivial. Even though W is linearly proportional to n_{ads} at t_b, the increase of t_b with the increase of t_c (namely decrease of inlet gas flow rate) would necessarily implies an increase of n_{ads} at t_b and consequently an increase of W, only in the case of constant inlet gas flow rate. Since different t_c mean different inlet gas flow rate the trend of n_{ads} at t_b and W with t_c cannot be predicted a priori. W is also dependent on n_{ads} (which is the denominator of the formula to calculate W) and, as stated above, the increase of t_c results in an increase of n_{ads} under sound assisted fluidization conditions. Finally, it should be noted that the increase of t_c should be disadvantageous for W because it implies a decrease of the adsorption kinetics (as confirmed by the increase of t_{95}-t_b).

In particular, the dependence of the breakthrough time on the contact time has been pointed out. The curves obtained are shown in **Fig. 51**, **Fig. 52** and **Fig. 53**, for CO_2 inlet concentration od 5,10 and 15%vol., respectively, and the results are reported in **Tab. 12**.
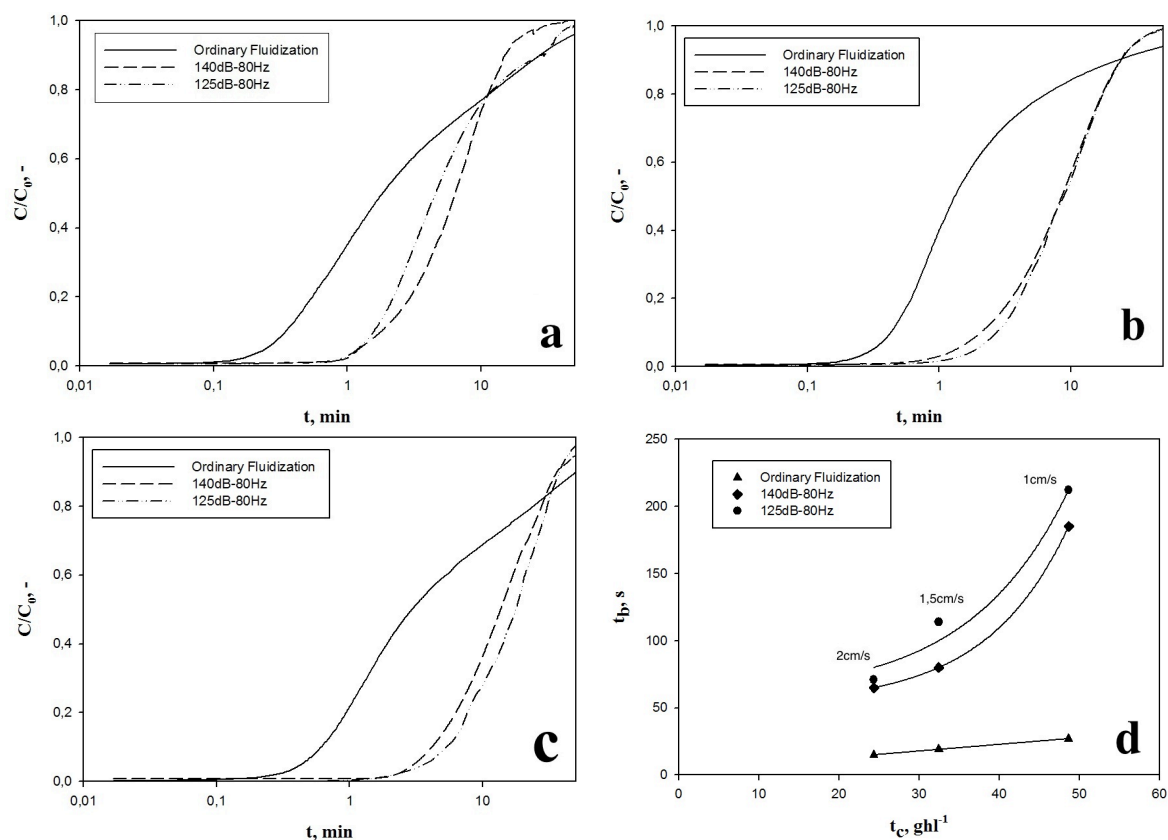
Fig. 51 AC Norit breakthrough curves in ordinary and sound assisted conditions. C_0=5%vol; a) u=2cm/s; b) u=1.5cm/s; c) u=1cm/s. d) Breakthrough time as function of contact time.

As a matter of fact, the fluidization velocity is expected to affect the breakthrough time because the mere increase of the fluidization velocity results in decrease of the contact time. However, as clearly shown in **Fig. 51**d, **Fig. 52**d and **Fig. 53**d the dependence of the breakthrough time on the contact time, i.e. the fluidization velocity, is linear, as one could expect, only for the tests performed in ordinary conditions. Whereas, the breakthrough time is found to exponentially increase with the contact time, namely decreasing the fluidization velocity from 2 to 1cm/s, for the sound assisted tests. This evidence is likely due to the role played by fluidization velocity in sound assisted tests. Indeed, in ordinary conditions the system is quite insensible to changes of fluidization velocity, being the fluidization quality always very poor. Therefore, the observed linear increase of the breakthrough time with the decrease of the fluidization velocity is only due the CO_2 taking more time to flow through the bed. On the other side, in sound assisted tests, changes of the fluidization velocity greatly affect the fluid-dynamics of the system. In particular, the decrease of the fluidization velocity results in a more homogeneous fluidization regime, which is characterized by a lower by-pass

80

of gas through the bed with respect to the tests performed at higher fluidization velocity. This evidence is confirmed by the bed expansion curves reported in **Fig. 29**b, which shows a quiet sharp change of slope at superficial gas velocities higher than 1cm/s, thus confirming the occurrence of bubbles (i.e. bypass of gas).
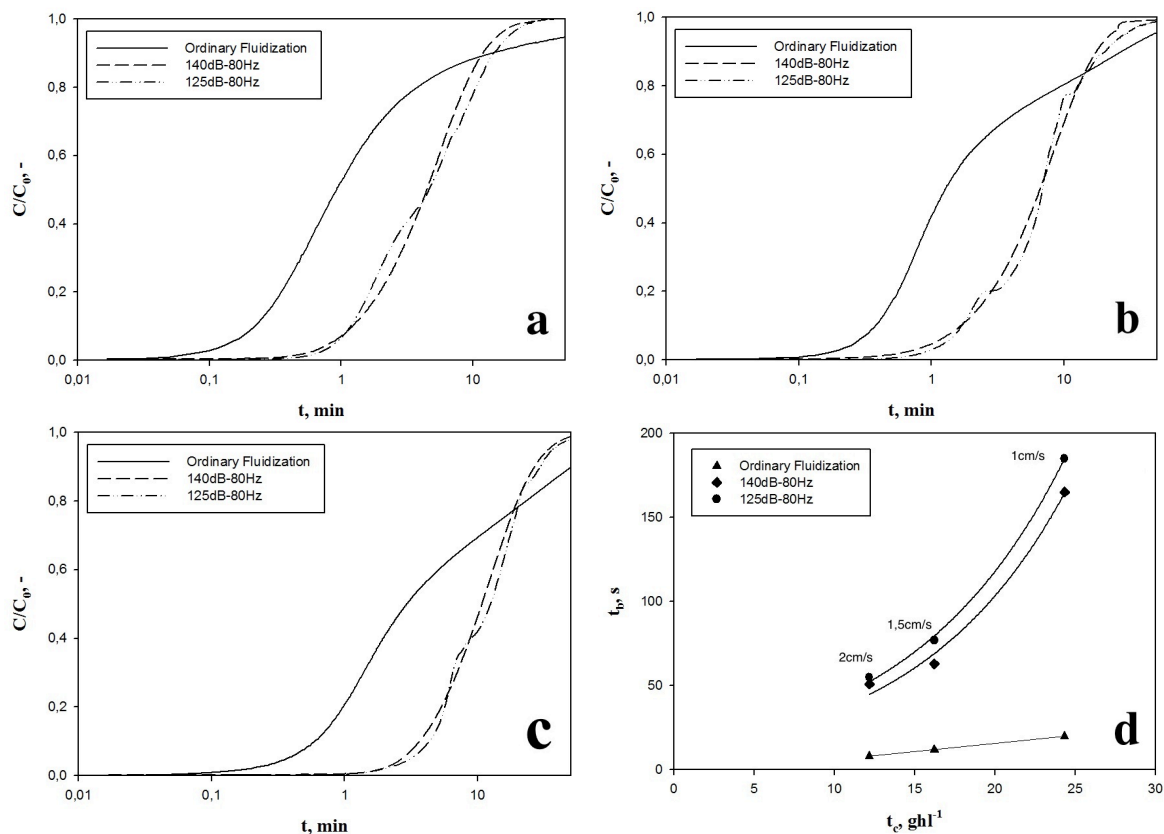
Fig. 52 AC Norit breakthrough curves in ordinary and sound assisted conditions. C_0=10%vol; a) u=2cm/s; b) u=1,5cm/s; c) u=1.5cm/s. d) Breakthrough time as function of contact time.

As a consequence, the breakthrough time is more than tripled passing from 2 to 1cm/s. Moreover, the fluidization velocity slightly affects the adsorption capacity of the activated carbon and the fraction of bed utilized until breakpoint, as clearly shown in **Tab. 12**. All the results presented so far have been performed at velocities higher than the minimum fluidization velocities (0.2cm/s). Then, further tests have been performed at lower superficial gas velocities (0.75, 0.5 and 0.25 and 0.1cm/s) and at 10%vol. of CO_2 in the inlet stream, in order to investigate the behaviour of the breakthrough time (**Fig. 54**).

The analysis of **Fig. 54** suggests, as reasonably expected, that in ordinary conditions the breakthrough time keeps linearly increasing for fluidization velocities lower than 1cm/s. However, the most remarkable observation is that the trend obtained for the sound assisted tests is not monotone. In particular, after the above-mentioned exponential increase obtained decreasing the fluidization velocity from 2 to 1cm/s, two more sections can be identified, corresponding to different windows of fluidization quality. In particular, a further increase of

the contact time, obtained decreasing the gas velocity from 1cm/s down to 0.25cm/s, results in an exponential decrease of the breakthrough time; whereas, a linear increase of the breakthrough time is obtained by finally decreasing the fluidization velocity down to 0.1cm/s. It is worth noting that in this last section the breakthrough times obtained in the sound assisted tests are basically the same obtained in the tests performed in ordinary conditions.
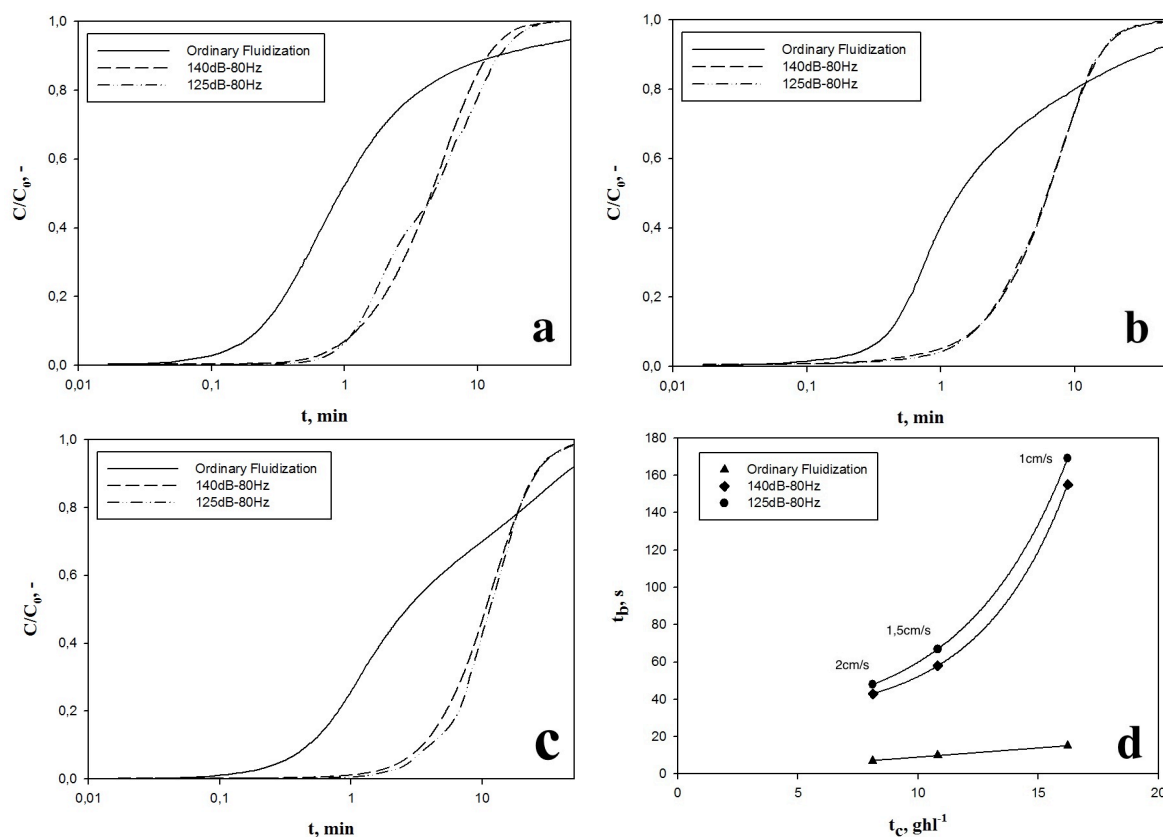
Fig. 53 AC Norit breakthrough curves in ordinary and sound assisted conditions. C_0=15%vol; a) u=2cm/s; b) u=1.5cm/s; c) u=1cm/s. d) Breakthrough time as function of contact time.

The first exponential decreasing trend of the breakthrough time is due to the worsening of the fluidization quality as a result of the further decrease of the fluidization velocity. On the other hand, the last section of the curve, namely the linear increase of t_b, is due to the fact that the bed is not actually fluidized in the tests performed at the lowest velocities (0.25 and 0.1cm/s), being the minimum fluidization velocity 0.2cm/s. In other words, the fluidization quality is very poor and qualitatively very similar to that of the tests performed in ordinary conditions. That is the reason why the breakthrough times trend is quantitatively and qualitatively the same as the tests performed without the assistance of any acoustic field.
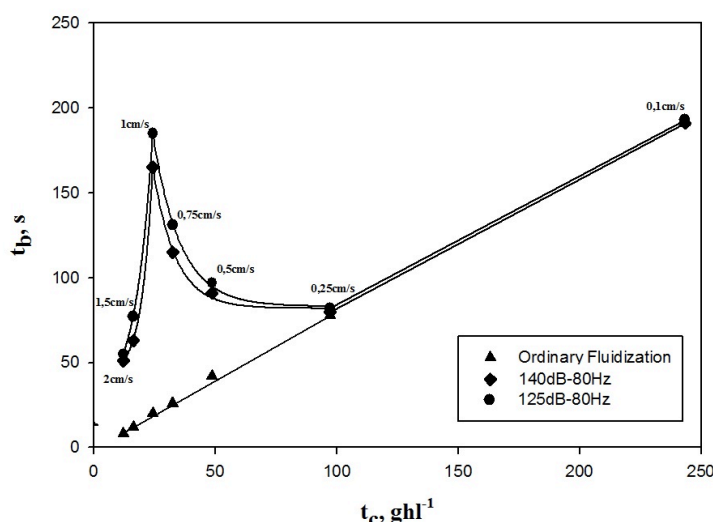
Fig. 54 AC Norit breakthrough times as functions of contact time for ordinary and sound assisted tests, C_0=10%vol. in N_2.

III.3.1.4   Fluidized Bed vs Fixed Bed

Two additional adsorption tests (u=1.5cm/s and C_0=10%vol.) have been carried out in fixed bed (the fixed bed conditions have been ensured by reversing the flow inside the column, i.e. the gas flow has been fluxed from the top of the column) in order to actually prove the unsuitability of this configuration to carry out CO_2 adsorption on fine powders. In particular, the first additional test has been performed on the activated carbon fine particles, and the second one on the pelletized activated carbon (180-400mm).

The curves obtained are shown in **Fig. 55**a, which also reports as comparison the curves obtained in ordinary and sound assisted fluidization tests (140dB-80Hz) under the same operating conditions. **Fig. 55**b summarizes the corresponding adsorption performances. As expected, the fixed bed operation with the fine particles strongly worsen the adsorption process, in terms of breakthrough time (6s), W (2%) and CO_2 adsorption capacity (0.18mmol/g), which is less than a half of that obtained under sound assisted fluidization conditions. Indeed, after t=t_b the breakthrough curve sharply rises and goes to saturation. This behaviour, as expected, is due to the strong cohesiveness of the materials making the gas pass through the bed only through channels, namely without actually permeating it. The pelletized activated carbon can adsorb 0.21mmol/g of CO_2 under fixed bed conditions. In other words, the use of sound assisted fluidized bed technology improves the gas-solid contact efficiency, thus enhancing the capture capacity by 76% with respect to the test performed under fixed conditions even on pelletized sorbent. This is probably due to diffusive resistances inside the pellets, which limit the exploiting of the entire available surface of the material.
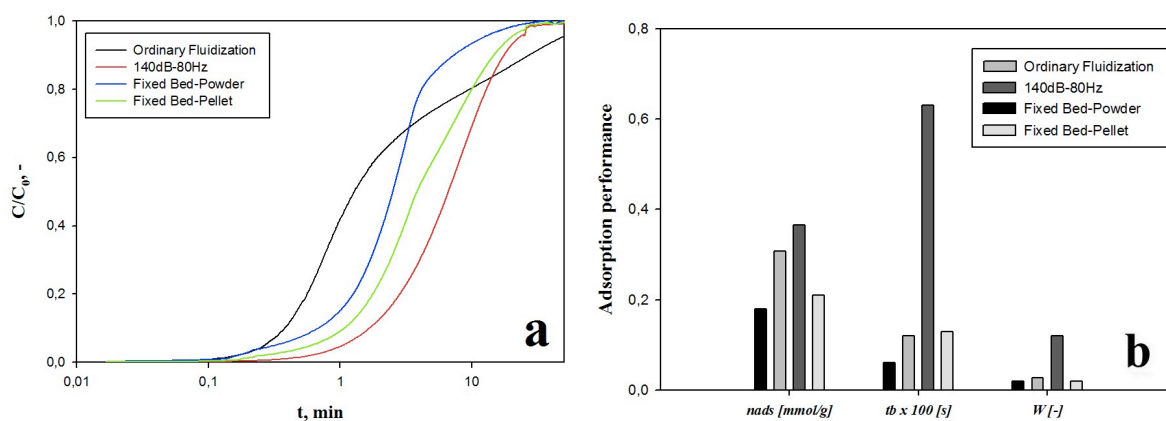
Fig. 55 a) Breakthrough curves in ordinary fluidization, sound assisted fluidization and fixed bed conditions with powder and pellets; b) CO_2 adsorption efficiency, in terms of n_{ads}, t_b and W. u=1.5cm/s; C_0=10%.

In order to assess the feasibility of the sound assisted fluidization and to make a comparison among different technologies for the CO_2 capture by adsorption, the results obtained have been elaborated in order to identify the operating conditions of the bed which could allow reaching a 90% capture in a realistic application.

In particular, three parameters have been evaluated to identify the best operating conditions: t^*, n^* and W^*, namely the time at which the process must be stopped in order to achieve 90% of CO_2 capture (in other words, once this time is reached the adsorption process must be stopped and the bed regenerated), the moles correspondingly captured in this time and the fraction of bed used, respectively. As clearly reported in **Tab. 13**, the application of the acoustic fields of proper intensity and frequency allows to better exploit the capture capacity of the bed. Indeed, for for the same capture efficiency (90%), the application of an acoustic field makes it possible to remarkably increase the amount of CO_2 captured and the fraction of bed used. Indeed, in a hypothetical realistic process when the adsorption process is stopped and the bed switched to regeneration a lower amount of bed would be exploited under all the other cases (fixed bed, ordinary and worse sound assisted fluidized bed conditions).

Tab. 13 Results of the adsorption tests when 90% of CO_2 capture is reached. C_0=10%; u=1.5cm/s.

	t^*	n^*	W^*
	min	mmol/g	%
Ordinary Fluidization	0.7	0.03	8.2
Fixed bed - powder	0.9	0.03	19
Fixed bed - pellet	1.3	0.05	25
140dB-80Hz	3.1	0.12	32

Finally, the increase of temperature due to the exothermicity of the process is the same as that obtained in fluidization conditions (2-3K). Considering that the moles of CO_2 adsorbed are

remarkably lower, the advantage of fluidized bed over fixed bed due to the higher heat transfer capacity is evident. In other words, the obtained temperature increase, normalized to the moles of CO_2 adsorbed, is almost a half of that obtained under fixed bed conditions, being n_{ads} in fixed bed conditions a half of that obtained in fluidized bed conditions. This result is consistent with the data reported by other authors in fixed bed conditions [137]. The lower increase of temperature under fluidized conditions is due to the high heat transfer capacity typical of fluidized beds.

On the basis of all these results, it can be inferred that sound assisted fluidization of fine solid sorbents is a valid alternative technology to the fixed bed one, which require also an additional previous step of pelletization.

III.3.2   Activated Carbon Sigma Aldrich

III.3.2.1   Effect of the Sound Application

Fig. 56a and **b** show the comparison between the breakthrough curves obtained in ordinary and sound assisted fluidization conditions for the tests performed at 1.5cm/s and 15%vol. of CO_2 in linear and logarithmic scale concentration, respectively.
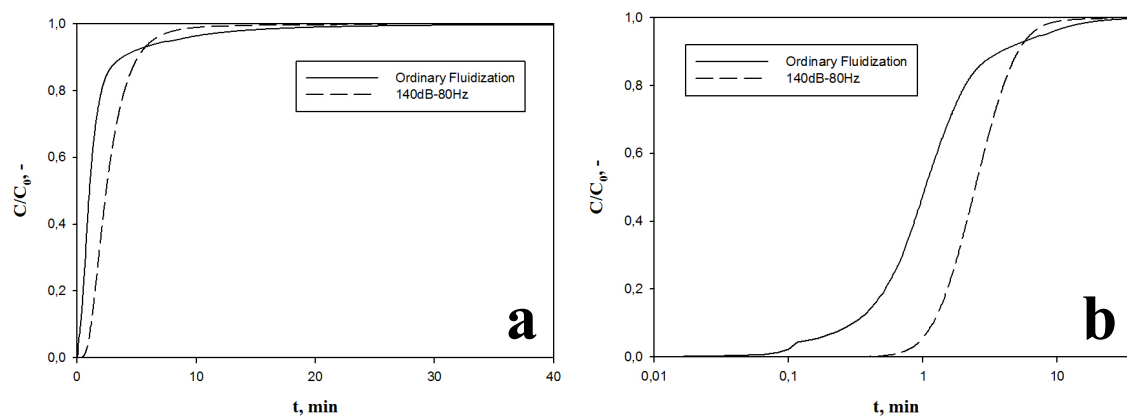
Fig. 56 AC Sigma breakthrough curves obtained in ordinary and sound assisted conditions in linear (a) and logarithmic (b) scale. C_0=15%vol.; u=1.5cm/s

The analysis of the curves suggests that the application of the sound greatly enhances the breakthrough time, which, as reported in **Tab. 14**, in sound assisted conditions is about five times the value obtained in ordinary conditions.

Tab. 14 Results of the adsorption tests obtained for AC Sigma.

Superficial gas velocity	Sound Parameters	CO_2 inlet concentration											
		5%				10%				15%			
		t_b s	n_{ads} mmol/g	W %	t_{95}-t_b min	t_b s	n_{ads} mmol/g	W %	t_{95}-t_b min	t_b s	n_{ads} mmol/g	W %	t_{95}-t_b min
2cm/s	Ordinary	23	0.24	18	6	14	0.38	13	5	11	0.49	11	5
	140dB-80Hz	63	0.31	38	5	54	0.48	39	4	42	0.64	33	4
1.5cm/s	Ordinary	31	0.21	21	7	24	0.38	17	7	12	0.49	9	8
	140dB-80Hz	91	0.32	42	6	68	0.50	37	5	59	0.69	33	5
1cm/s	Ordinary	44	0.23	20	14	14	0.38	13	5	28	0.52	14	10
	140dB-80Hz	174	0.35	52	8	143	0.51	51	7	126	0.71	47	7

The application of the sound affects also the global adsorption capacity. Indeed, the total amount of CO_2 adsorbed until saturation, n_{ads}, is increased of 28% with respect to the test performed in ordinary conditions (**Tab. 14**). W is also greatly enhanced by sound. Finally, the application of the sound improves the kinetics of the entire process, as confirmed by the values of t_{95}-t_b.

III.3.2.2   Effect of CO_2 Partial Pressure

Fig. 57a, b and c reports the breakthrough curves obtained sound assisted conditions (140dB-80Hz) for three different CO_2 inlet concentration at 1.5cm/s.

As regards the influence of CO_2 partial pressure, the analysis of the results reported in **Tab. 14**, shows, as expected, that the CO_2 capture capacity of the adsorbent increases with CO_2 partial pressure. This trend is absolutely consistent from a thermodynamic point of view since the CO_2 partial pressure represents the driving force of the adsorption process. Similarly to what observed for the AC Norit, the increase of the CO_2 inlet concentration results in a decrease of t_b and t_{95}-t_b.

The experimental results have been elaborated and fitted by the Langmuir equation (18) in order to obtain the adsorption isotherm, reported in **Fig. 57**d.
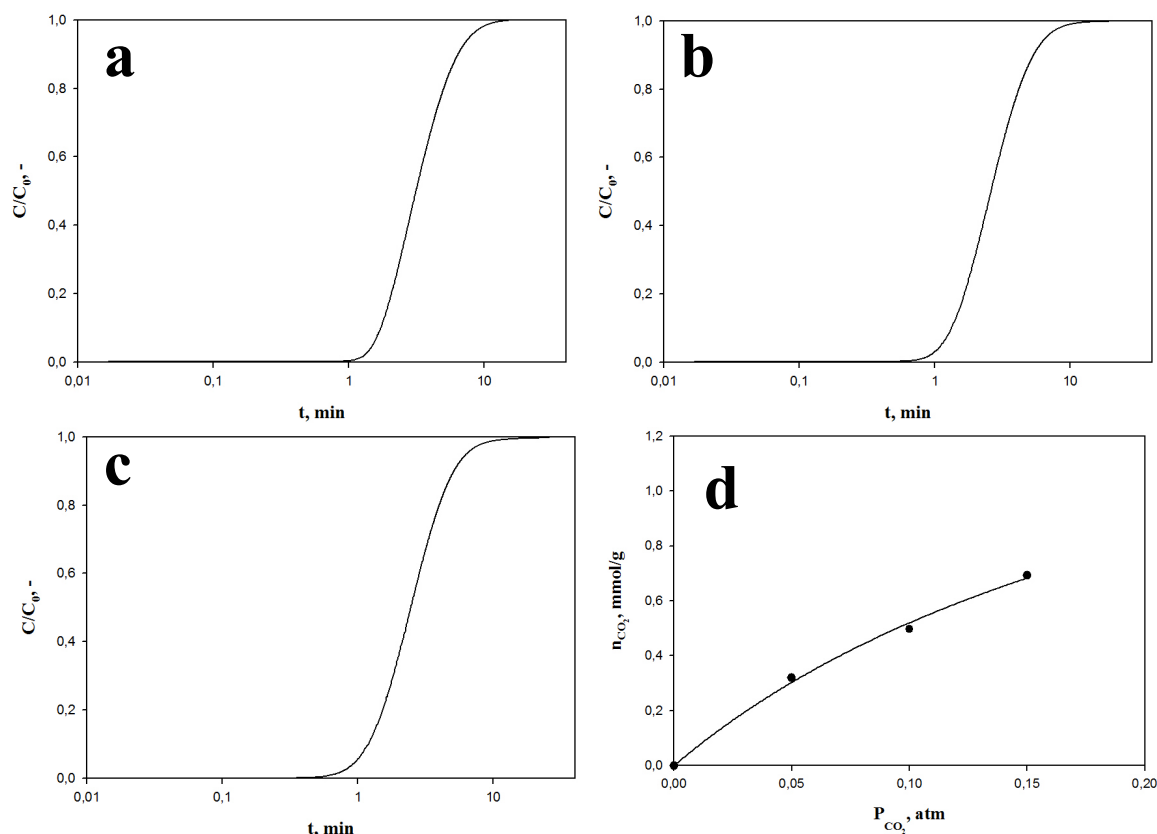
Fig. 57 AC Sigma breakthrough curves obtained in sound assisted conditions (140dB-80Hz) with (a) C_0=5%vol; (b) C_0=5%vol. and (c) C_0=5%vol. d) Adsorption isotherm. u=1.5cm/s.

III.3.2.3   Effect of Fluidization Velocity

In order to point out the effect of the fluidization velocity on the adsorption process tests have been performed at three different gas velocities (1, 1.5 and 2cm/s) for each CO_2 inlet concentration (5, 10 and 15%vol.). The data reported in **Tab. 14** show that an increase of the contact time, namely a decrease of fluidization velocity, results in an increase of t_b. As regards the kinetics, an increase of the fluidization velocity results in a faster adsorption process, as clearly confirmed by the decreasing trend obtained for t_{95}-t_b. As regards n_{ads}, a decrease of t_c results in a slight increase of the moles of CO_2 adsorbed under sound assisted conditions. This is probably due to the fact that for the highest fluidization velocities the timescale of the adsorption process is slightly higher than the contact time corresponding to that fluidization velocity. On the contrary the CO_2 uptake is not affected by changes of fluidization velocity under ordinary fluidization conditions because the fluidization quality is always very poor for all the investigated fluidization velocities (i.e. the any change of t_c do not affect the availability of AC Sigma surface). As regards W, it generally increases with an increase of t_c under sound assisted conditions, whereas the trend is not always monotone under ordinary fluidization conditions.
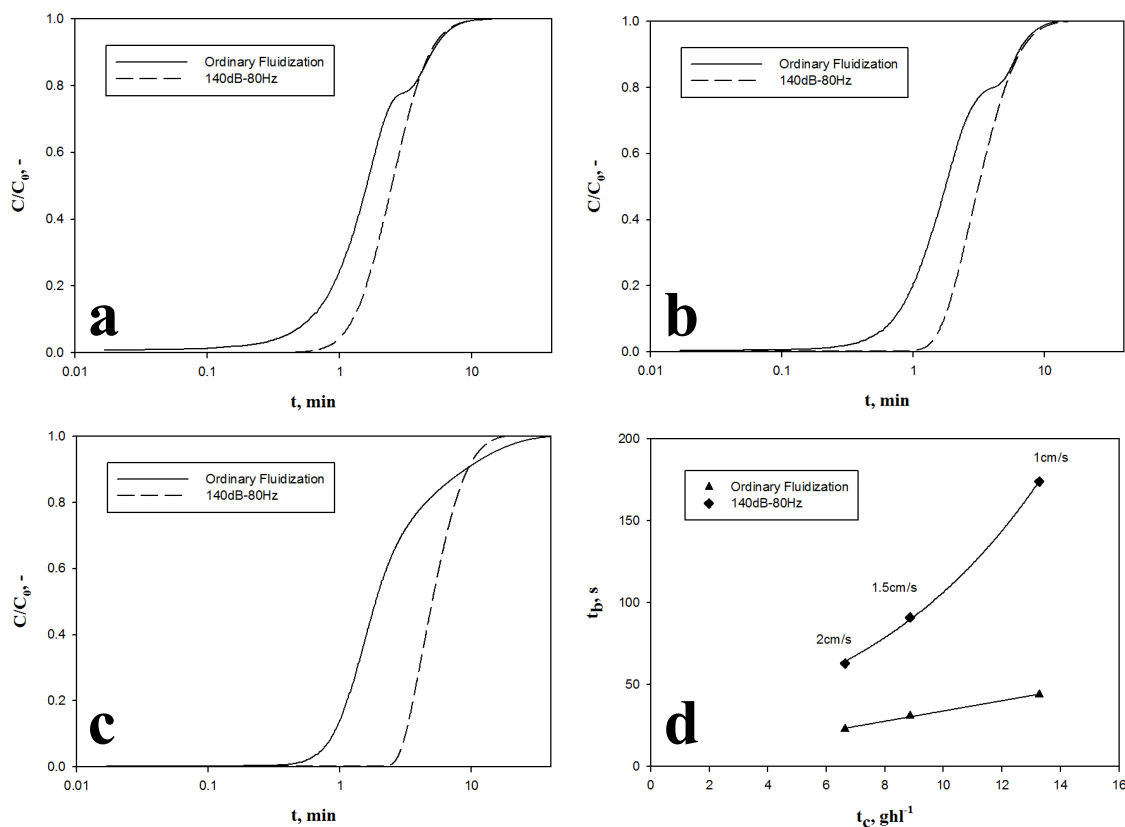
Fig. 58 AC Sigma breakthrough curves in ordinary and sound assisted conditions. C_0=5%vol; a) u=2cm/s; b) u=1.5cm/s; c) u=1cm/s. d) Breakthrough time as function of contact time.

Several aspects influence the trend of W. As defined W is linearly proportional to n_{ads} at t_b and, as stated above, t_b has been found to be an increasing monotonic function of t_c. However, this increase of t_b with t_c, does not necessarily lead to an increase of n_{ads} at t_b, and consequently an increase of W, since at different t_c correspond different inlet gas flow rates. Under sound assisted fluidization conditions the increase of t_c also results, as said before, in a slight increase of n_{ads}, which is the denominator of the formula to calculate W (i.e. W is inversely proportional to n_{ads}). Finally, the increase of t_c implies a decrease of the adsorption kinetics (as confirmed by the increase of t_{95}-t_b), thus negatively affecting W.

As for the AC Norit, the dependence of the breakthrough time on the contact time has been pointed out. The curves obtained are shown in **Fig. 58**d, **Fig. 59**d and **Fig. 60**d, and the results are reported in **Tab. 14**. As observed for AC Norit, for the sound assisted tests the breakthrough time is found to exponentially increase with t_c, namely decreasing the fluidization velocity from 2 to 1cm/s, whereas the trend is linear in ordinary conditions.

Fig. 59 AC Sigma breakthrough curves in ordinary and sound assisted conditions. C_0=10%vol; a) u=2cm/s; b) u=1.5cm/s; c) u=1cm/s. d) Breakthrough time as function of contact time.

This evidence is due to the fact that, the decrease of the fluidization velocity results in a more homogeneous fluidization regime, which is characterized by a lower by-pass of gas through the bed with respect to the tests performed at higher fluidization velocity. This evidence is confirmed by the bed expansion curves reported in **Fig. 32**, which shows a change of slope at a superficial gas velocities higher than 0.3cm/s, thus confirming the occurrence of bubbles (i.e. bypass of gas) for increasing values of fluidization velocity.

Fig. 60 AC Sigma breakthrough curves in ordinary and sound assisted conditions. C_0=15%vol; a) u=2cm/s; b) u=1.5cm/s; c) u=1cm/s. d) Breakthrough time as function of contact time.

III.3.3 Zeolite H-ZSM-5

III.3.3.1 Effect of the Sound Application and Fluidization Velocity

Fig. 61a and b the comparison between the breakthrough curves obtained in ordinary and sound assisted fluidization conditions in linear and logarithmic scale concentration, respectively. show the comparison between the breakthrough curves obtained in ordinary and sound assisted fluidization conditions, at a superficial gas velocity of 2 and 5cm/s, respectively. The analysis of the curves suggests that for this material the application of the acoustic field does not affect the shape of the breakthrough curves and, consequently, the global adsorption capacity, namely the CO_2 adsorbed until saturation.
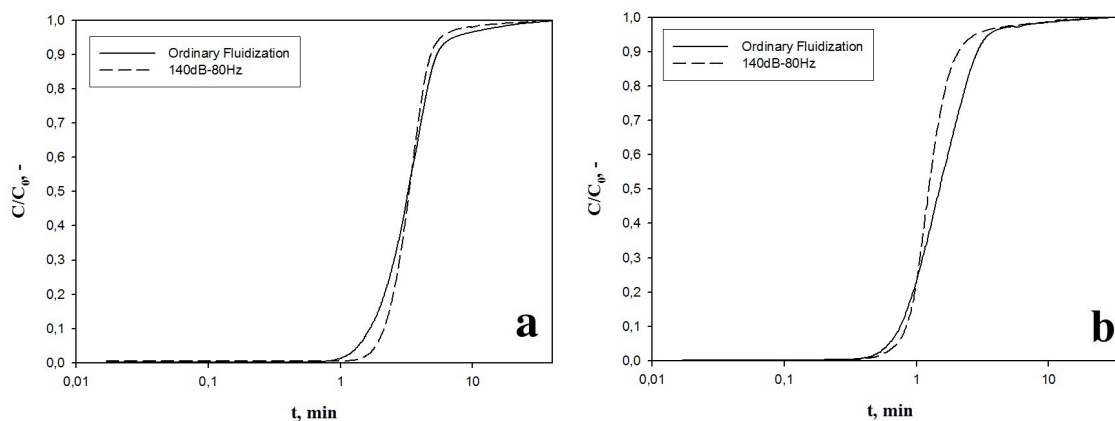
Fig. 61 Breakthrough curve as obtained in fluidized bed tests carried out with H-ZSM-5 in ordinary conditions and under the effect of an acoustic field (140dB-80Hz). C_0=10%vol.; a) u=2/s; b) u=5cm/s.

Analysis of data reported in **Fig. 61** and **Tab. 15**, shows that in all the operating conditions the amount of CO_2 adsorbed, n_{ads}, is about 0.3mmol/g.

Tab. 15 Results of the adsorption tests obtained for H-ZSM-5. C_0=10%

Fluidization velocity	2cm/s				5cm/s			
	t_b s	n_{ads} mmol/g	W %	t_{95}-t_b	t_b s	n_{ads} mmol/g	W %	t_{95}-t_b
Ordinary Fluidization	90	0.29	39	22	39	0.30	39	3
140dB-80Hz	119	0.29	52	4	45	0.29	47	2

There is a positive effect of the application of sound on the breakthrough times, the kinetics of the process (t_{95}-t_b) and consequently the fraction of bed utilized until break point (W). As regards the effect of the fluidization velocity a higher superficial gas velocity corresponds to lower breakthrough times due to the decrease of the contact time between the gaseous and solid phases; in other words, the CO_2 concentration front takes less time to reach the outlet of the bed, as confirmed by the linear dependence observed between the breakthrough times and the contact times.

Similarly to what observed for AC Norit an increase of the fluidization velocity results, even though in a slighter way, in a decrease of W and t_{95}-t_b (i.e. improvement of the kinetics).

III.3.3.2   Effect of CO_2 Partial Pressure

Fig. 62a, b, c and d reports the breakthrough curves obtained sound assisted conditions (140dB-80Hz) for three different CO_2 inlet concentration at 1.5cm/s.

As regards the influence of CO_2 partial pressure, the analysis of the results reported in **Tab. 16**, shows, as expected, that the CO_2 capture capacity of the adsorbent increases with CO_2 partial pressure. This trend is absolutely consistent from a thermodynamic point of view since the CO_2 partial pressure represents the driving force of the adsorption process.

Similarly to what observed for the two activated carbons, the increase of the CO_2 inlet concentration results in a decrease of tb and t_{95}-t_b. Whereas, a decrease of W can be observed. The relative adsorption isotherm, obtained fitting the he experimental results by Langmuir equation (18), is reported in **Fig. 62**d.
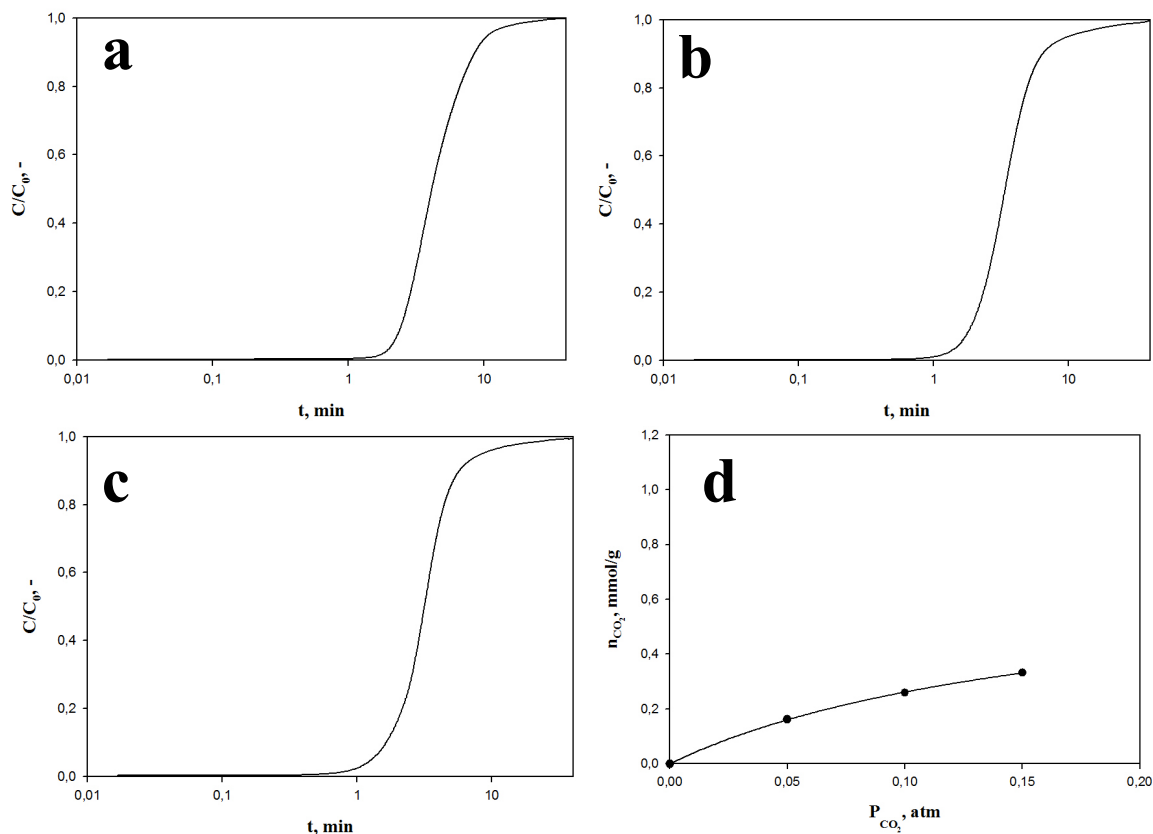
Fig. 62 H-ZSM-5 breakthrough curves obtained in sound assisted conditions (140dB-80Hz) with (a) C_0=5%vol.; (b) C_0=10%vol. and (c) C_0=15%vol. d) Adsorption isotherm. u=1.5cm/s.

Tab. 16 Results of the adsorption tests obtained for H-ZSM-5. u=1.5cm/s

	CO₂ inlet concentration											
	5%				10%				15%			
Sound Parameters	t_b s	n_{ads} mmol/ g	W %	t_{95}-t_b min	t_b s	n_{ads} mmol/g	W %	t_{95}-t_b min	t_b s	n_{ads} mmol/g	W %	t_{95}-t_b min
140dB-80Hz	80	0.16	42	9	96	0.26	36	8	130	0.33	33	7

III.3.4   Zeolite 13X

III.3.4.1   Effect of the Sound Application

Fig. 63a and **b** show the comparison between the breakthrough curves obtained in ordinary and sound assisted fluidization conditions for the tests performed at 1.5cm/s and 15%vol. of CO_2 in linear and logarithmic scale concentration, respectively.
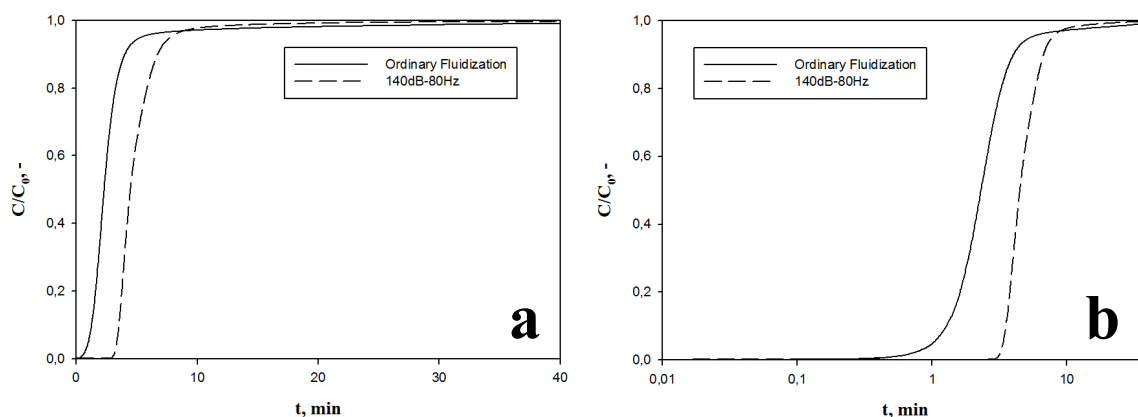
Fig. 63 13X breakthrough curves obtained in ordinary and sound assisted conditions in linear (a) and logarithmic (b) scale. C_0=15%vol.; u=1.5cm/s

The analysis of the curves suggests that the application of the sound greatly enhances the breakthrough time, which, as reported in **Tab. 17**, in sound assisted conditions is more than three times the value obtained in ordinary conditions.

Tab. 17 Results of the adsorption tests obtained for 13X.

Superficial gas velocity	Sound Parameters	CO₂ inlet concentration											
		5%				10%				15%			
		t_b s	n_{ads} mmol/g	W %	t_{95}-t_b min	t_b s	n_{ads} mmol/g	W %	t_{95}-t_b min	t_b s	n_{ads} mmol/g	W %	t_{95}-t_b min
1.5cm/s	Ordinary	81	0.09	40	5	64	0.18	31	6	64	0.27	31	4
	140dB-80Hz	281	0.22	63	7	221	0.37	55	8	201	0.41	64	4
3cm/s	Ordinary	83	0.19	41	5	69	0.33	37	7	59	0.34	43	3
	140dB-80Hz	115	0.23	46	6	88	0.35	44	4	78	0.37	53	3
4.5cm/s	Ordinary	81	0.20	50	5	55	0.32	45	4	40	0.32	47	2
	140dB-80Hz	80	0.23	47	4	65	0.34	49	3	54	0.35	59	3

The application of the sound affects also the global adsorption capacity. Indeed, the total amount of CO_2 adsorbed until saturation, n_{ads}, is increased of 51% with respect to the test performed in ordinary conditions (**Tab. 17**). W is also greatly enhanced by sound. Finally, the application of the sound improves the kinetics of the entire process as confirmed by the values of t_{95}-t_b.

III.3.4.2   Effect of CO_2 Partial Pressure

Fig. 64a, b, c and d reports the breakthrough curves obtained sound assisted conditions (140dB-80Hz) for three different CO_2 inlet concentration at 1.5cm/s.

As regards the influence of CO_2 partial pressure, the analysis of the results reported in **Tab. 17**, shows, as expected, that the CO_2 capture capacity of the adsorbent increases with CO_2 partial

pressure. This trend is absolutely consistent from a thermodynamic point of view since the CO_2 partial pressure represents the driving force of the adsorption process. Also in this case, the increase of the CO_2 inlet concentration results in a decrease of t_b.

The relative adsorption isotherm, obtained fitting the experimental results by Langmuir equation (18), is reported in **Fig. 64**d.
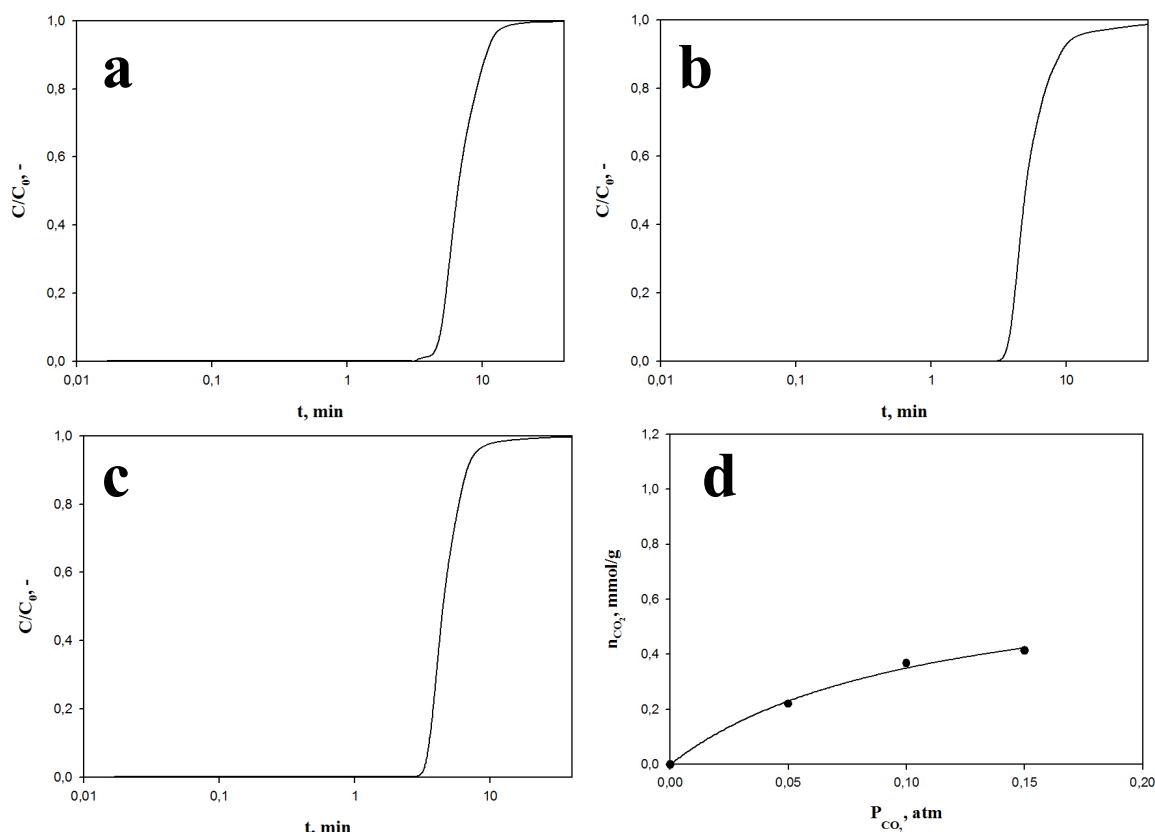
Fig. 64 13X breakthrough curves obtained in sound assisted conditions (140dB-80Hz) with (a) C_0=5%vol.; (b) C_0=10%vol. and (c) C_0=15%vol. d) Adsorption isotherm. u=1.5cm/s.

III.3.4.3   Effect of Fluidization Velocity

In order to point out the effect of the fluidization velocity on the adsorption process tests have been performed at three different gas velocities (1.5, 3 and 4.5cm/s) for each CO_2 inlet concentration (5, 10 and 15%vol.). All the trends observed for the two activated carbons are confirmed. Indeed, the data reported in **Tab. 17** show that an increase of t_c, namely a decrease of fluidization velocity, results in an increase of t_b and t_{95}-t_b, and a slight increase of n_{ads} under sound assisted conditions. As regards W, it has a not monotone trend in under sound assisted conditions, whereas it generally decreases with a decrease of the fluidization velocity under ordinary fluidization conditions.
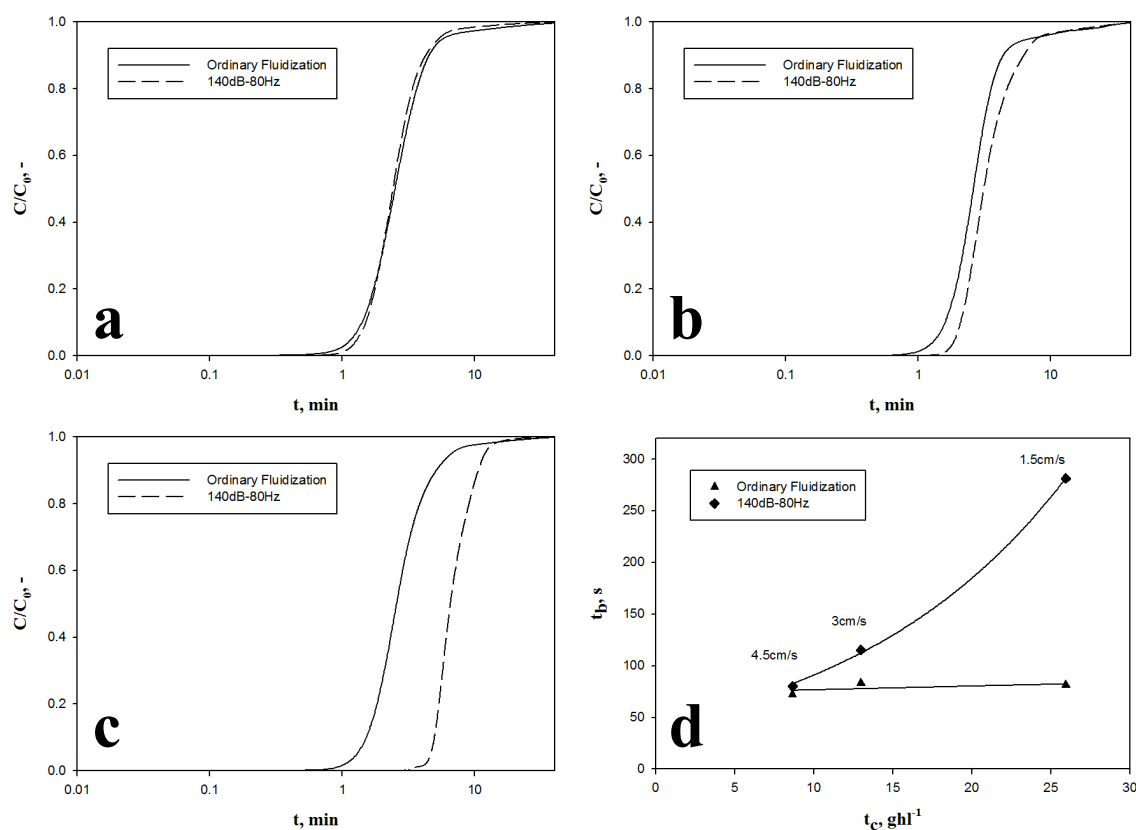
Fig. 65 13X breakthrough curves in ordinary and sound assisted conditions. C_0=5%vol; a) u=4.5cm/s; b) u=3cm/s; c) u=1.5cm/s. d) Breakthrough time as function of contact time.

Like already stated for the two activated carbons, the trend of W with t_c is not at all trivial and, consequently it cannot be predicted a priori. As defined, W is linearly proportional to n_{ads} at t_b and inversely proportional to n_{ads}. Even though an increase of t_c means, as stated above, an increase of t_b, this does not necessarily lead to an increase of n_{ads} at t_b and consequently of W. The increase of t_c results under sound assisted fluidization conditions, as said before, in a slight increase of n_{ads}, which is the denominator of the formula to calculate W, and in an increase of t_{95}-t_b (i.e. slowdown of the adsorption kinetics), thus negatively affecting W.

In particular, the dependence of breakthrough on the contact time has been pointed out. The curves obtained are shown in **Fig. 65**, **Fig. 66** and **Fig. 67**, and the results are reported in **Tab. 17**. As observed for AC Norit, for the sound assisted tests the breakthrough time is found to exponentially increase with t_c, namely decreasing the fluidization velocity from 2 to 1cm/s, whereas the trend is linear in ordinary conditions.
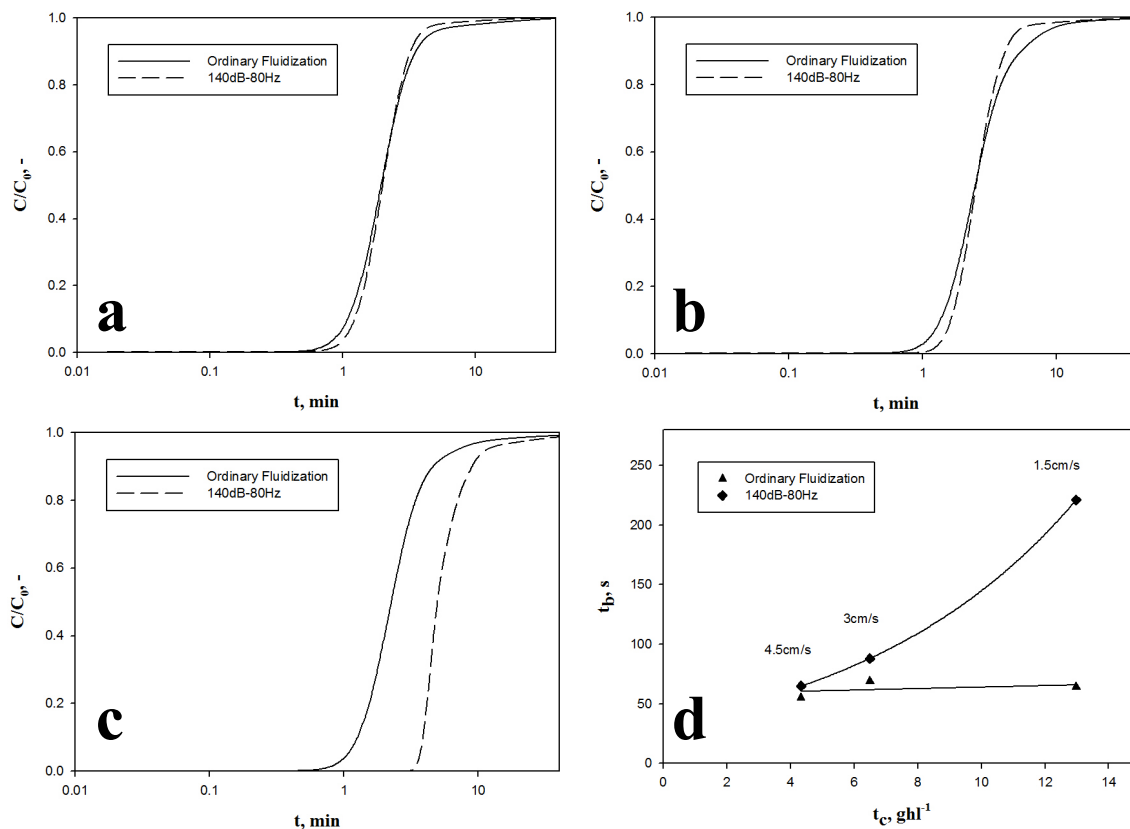
Fig. 66 13X breakthrough curves in ordinary and sound assisted conditions. C0=10%vol; a) u=4.5cm/s; b) u=3cm/s; c) u=1.5cm/s. d) Breakthrough time as function of contact time.

This evidence is due to the fact that, the decrease of the fluidization velocity results in a more homogeneous fluidization regime, which is characterized by a lower by-pass of gas through the bed with respect to the tests performed at higher fluidization velocity. This evidence is confirmed by the bed expansion curves reported in **Fig. 32**, which shows a change of slope at a superficial gas velocities higher than 0.3cm/s, thus confirming the occurrence of bubbles (i.e. bypass of gas) for increasing values of fluidization velocity.
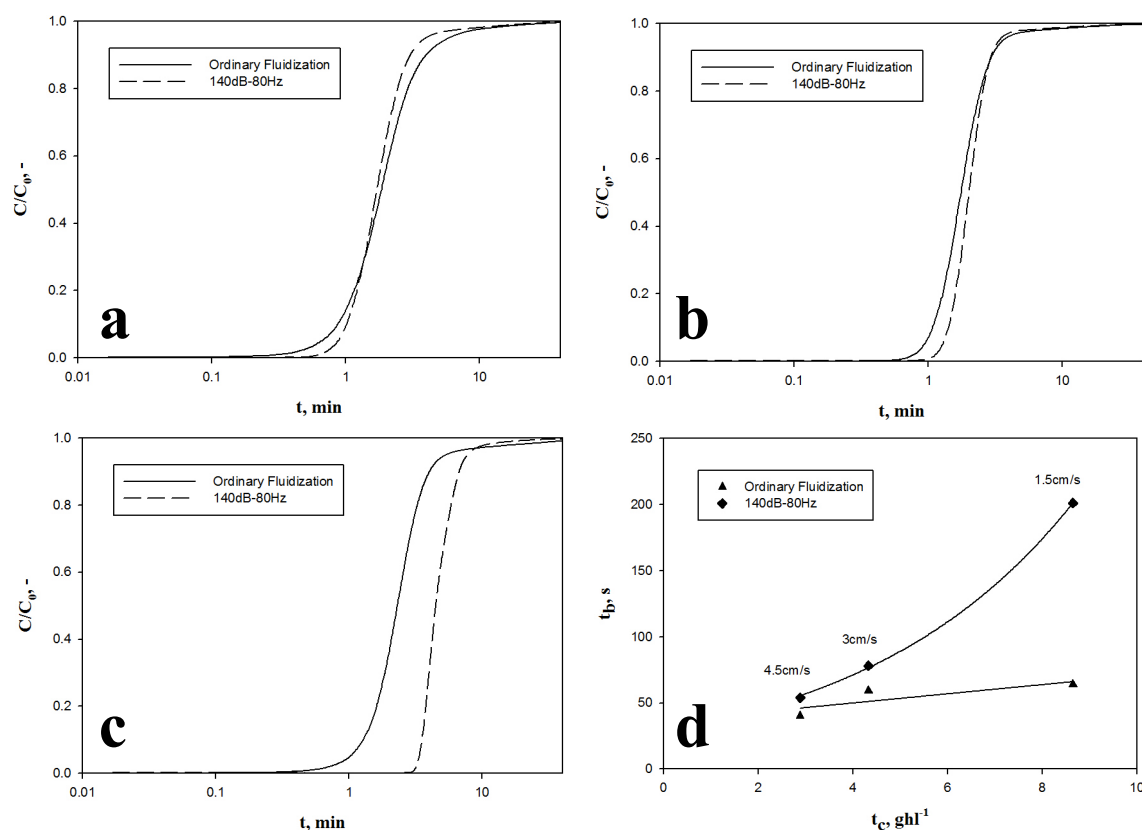
Fig. 67 13X breakthrough curves in ordinary and sound assisted conditions. C_0=15%vol; a) u=4.5cm/s; b) u=3cm/s; c) u=1.5cm/s. d) Breakthrough time as function of contact time.

III.3.5   HKUST-1

III.3.5.1   Effect of the Sound Application

Fig. 68a and **b** show the comparison between the breakthrough curves obtained in ordinary and sound assisted fluidization conditions (140dB-80Hz) for the tests performed at 1.5cm/s and 15%vol. of CO_2 in linear and logarithmic scale concentration, respectively. The analysis of the curves suggests that the application of the sound greatly enhances the breakthrough time, which, as reported in **Tab. 18**, in sound assisted tests is more than five times the value obtained in ordinary conditions.
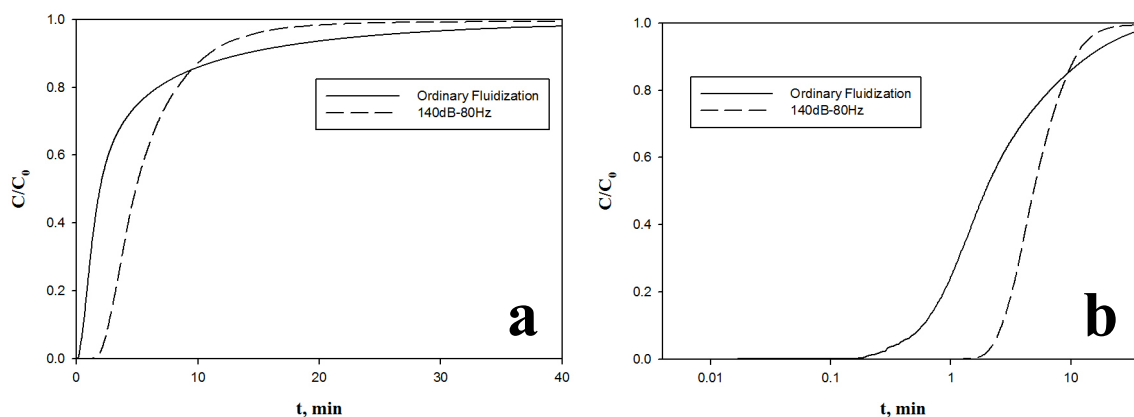
Fig. 68 HKUST-1 breakthrough curves obtained in ordinary and sound assisted conditions in linear (a) and logarithmic (b) scale. C_0=15%vol.; u=1.5cm/s

The application of the sound affects also the global adsorption capacity. Indeed, the total amount of CO_2 adsorbed until saturation, n_{ads}, is increased up to values of 53% with respect to the tests performed in ordinary conditions (**Tab. 18**). W is also greatly enhanced by sound, moving from values lower than 6%, in the tests performed in ordinary conditions, up to 33%, in the sound assisted tests.

Tab. 18 Results of the adsorption tests obtained for HKUST-1.

Sound Parameters	CO_2 inlet concentration											
	5%				10%				15%			
	t_b	n_{ads}	W	t_{95}-t_b	t_b	n_{ads}	W	t_{95}-t_b	t_b	n_{ads}	W	t_{95}-t_b
	s	mmol/g	%	min	s	mmol/g	%	min	s	mmol/g	%	min
Ordinary Fluidization	23	0.32	6	30	27	0.53	7	23	26	0.78	8	19
140dB-80Hz	186	0.51	29	22	165	0.92	30	10	141	1.14	29	12

Finally, the application of the sound greatly improves the kinetics of the entire process. Indeed, the application of acoustic fields allows to speed up the adsorption process: under sound assisted conditions the time for CO_2 to approach the saturation value is remarkably decreased, being both the values of n_{ads} and average rate of CO_2 adsorption higher than those obtained in ordinary conditions. This is also confirmed by the values of t_{95}-t_b.

As for the AC Norit also in this case, the effectiveness of the sound in enhancing the adsorption process has been confirmed by switching on the sound during a test started in ordinary conditions (**Fig. 69**).
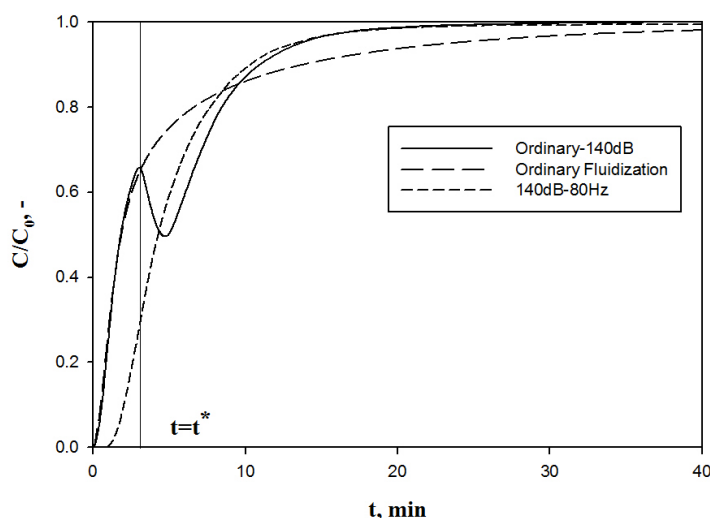
Fig. 69 HKUST-1 breakthrough curve obtained switching on the sound at t=t*. u=1.5cm/s; C_0=15%vol.

The analysis of the curve obtained clearly shows that for $t<t^*$ the CO_2 concentration profile is reasonably the same as that obtained in ordinary conditions (i.e. the bypassing gas makes the CO_2 concentration abruptly rise). At $t=t^*$ the CO_2 concentration suddenly drops down before rising up again, but following now the typical trend of the sound assisted test. This behaviour confirms the ability of the sound to better exploit the adsorption capacity of the material. Indeed, as soon as the sound has been switched on, that specific surface, precluded to the fluid in ordinary conditions, suddenly becomes available causing CO_2 concentration to drop down because of the renewed HKUST-1 adsorption capacity.

III.3.5.1.1 Effect of SPL

The effect of SPL on CO_2 adsorption efficiency has been evaluated by carrying out tests at fixed frequency (120Hz) and different sound intensity (125, 130 and 140dB). The comparison among the tests performed in terms of breakthrough curves are reported in **Fig. 70**. The data obtained in ordinary conditions have also been reported for comparison.

The analysis of these results is rather clear: the SPL effect on CO_2 adsorption process reflects what observed in the fluidization tests. Indeed, for sound intensities lower than 140dB the adsorption process is remarkably worse. A sound intensities lower than 140dB are not enough to obtain a proper fluidization quality. It is most likely that the part of the bed which is not properly fluidized does not really take part to the adsorption process, thus worsening the adsorption effectiveness in terms of n_{ads}, t_b, W. These results are an additional proof of the tight link existing between the adsorption efficiency and the fluid-dynamics of the system, namely with the gas-solid contact efficiency.
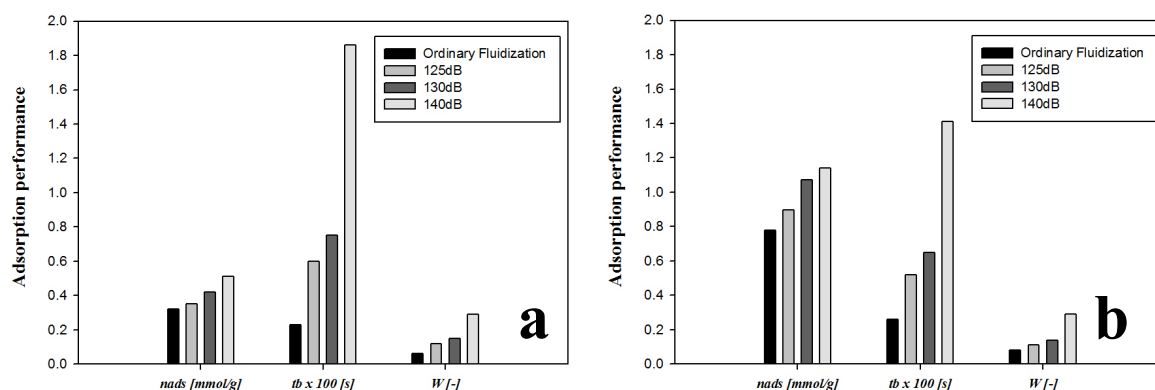
Fig. 70 HKUST-1: effect of SPL on CO$_2$ adsorption performance. a) C$_0$=5%; b) C$_0$=15%. f=80Hz.

III.3.5.1.2 Effect of Sound Frequency

In order to point out the effect of sound frequency on CO$_2$ adsorption efficiency, tests have been performed at fixed SPL (140dB) and different sound frequency (from 20 to 300Hz). The comparison among the tests performed in terms of breakthrough curves are reported **Fig. 71**. The data obtained in ordinary conditions have also been reported for comparison.

As well as for the SPL, also the results obtained in these tests are in perfect agreement with those obtained from the fluidization tests. As inferred from the fluidization tests, the effect of the sound frequency in the investigated range is not monotone. More specifically, the frequencies falling in the range 50-120Hz represent in the optimum range for this material also in terms of adsorption efficiency.
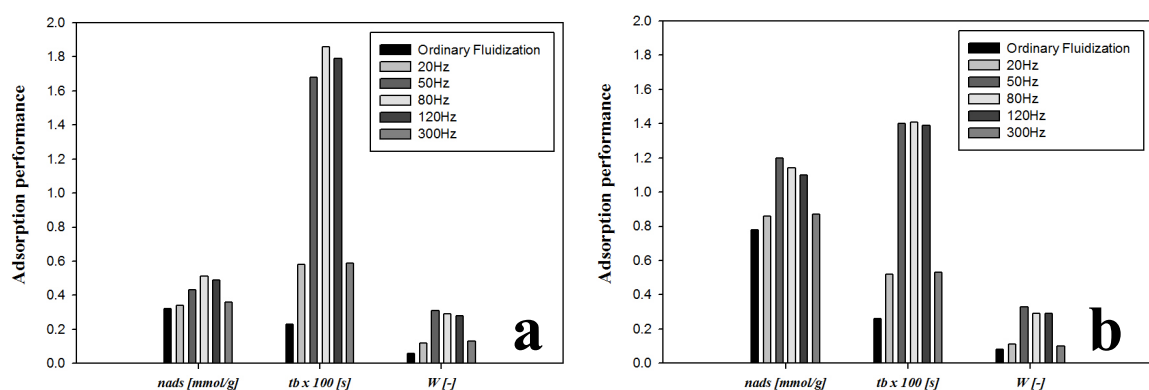
Fig. 71 HKUST-1: effect of sound frequency on CO$_2$ adsorption performance. a) C$_0$=5%; b) C$_0$=15%. SPL=140dB.

III.3.5.2 Effect of CO$_2$ Partial Pressure

Fig. 72a, b, c and d reports the breakthrough curves obtained sound assisted conditions (140dB-120Hz) for three different CO$_2$ inlet concentration at 1.5cm/s.

As regards the influence of CO_2 partial pressure, the analysis of the results reported in **Tab. 18**, shows, as expected, that the CO_2 capture capacity of the adsorbent increases with CO_2 partial pressure. This trend is absolutely consistent from a thermodynamic point of view since the CO_2 partial pressure represents the driving force of the adsorption process.

Similarly to what observed for the two activated carbons, the increase of the CO_2 inlet concentration results in a decrease of t_b. Whereas, W is kept constant.

The relative adsorption isotherm, obtained fitting the he experimental results by Langmuir equation (18), is reported in **Fig. 72**d.
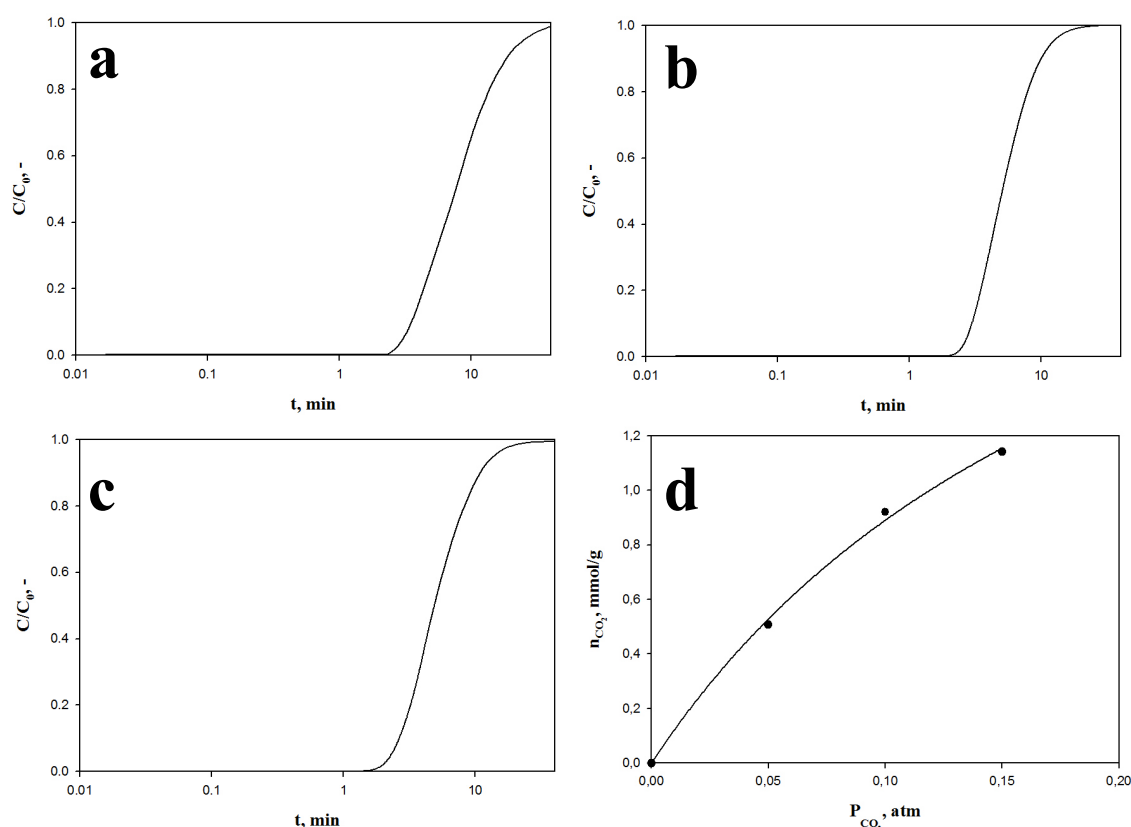
Fig. 72 HKUST-1 breakthrough curves obtained in sound assisted conditions (140dB-80Hz) with (a) C_0=5%vol.; (b) C_0=10%vol. and (c) C_0=15%vol. d) Adsorption isotherm. u=1.5cm/s.

III.3.6   Comparison Among the Different Adsorbent Materials

On the basis of the results obtained all the adsorbent materials have been compared (**Fig. 73** and **Tab. 19**) in terms of n_{ads}, t_b, t_{95}-t_b, W and moles of CO_2 adsorbed at t_b (n_{ads} at t_b). HKUST-1 is by far the adsorbent characterized by the highest CO_2 adsorption capacity, as clearly confirmed by the most favorable adsorption isotherm (**Fig. 73**d), whereas, the activated carbons and the zeolites follow, respectively. As regards the activated carbons, the Sigma Aldrich one is characterized by the best adsorption performances. Indeed, in all the

investigated conditions, it adsorbs a higher amount of CO_2 (as also confirmed by the more favorable adsorption isotherm) in considerably less time.

Tab. 19 Comparison of the experimental results obtained for all the adsorbent materials in the adsorption tests performed under sound assisted conditions (140dB-80Hz). u=1.5cm/s.

Materials	*CO_2 inlet concentration*														
	5%					**10%**					**15%**				
	n_{ads} mmol/g	t_b s	t_{95}-t_b min	W %	n_{ads} at t_b mmol/g	n_{ads} mmol/g	t_b s	t_{95}-t_b min	W %	n_{ads} at t_b mmol/g	n_{ads} mmol/g	t_b s	t_{95}-t_b min	W %	n_{ads} at t_b mmol/g
AC Norit	0.28	114	29	15	0.042	0.37	63	22	15	0.056	0.44	58	19	14	0.062
AC Sigma	0.32	334	6	42	0.135	0.50	249	6	37	0.182	0.69	216	5	33	0.230
H-ZSM-5	0.16	168	9	41	0.068	0.26	124	8	36	0.093	0.33	104	7	33	0.110
13X	0.22	351	7	63	0.139	0.37	276	8	55	0.202	0.41	251	4	64	0.265
HKUST-1	0.51	414	22	29	0.148	0.92	365	10	30	0.272	1.14	312	12	29	0.334

Considering that different mass of adsorbent has been used for the different materials, t_b are normalized to AC Norit.

Moreover, it also gives the highest t_b, W and kinetics. In particular, its kinetics is comparable to that obtained for zeolite 13X. Since the activated carbons are characterized by very similar FT-IR spectra (Fig. 16b and Fig. 19), the observed different adsorption performances cannot be referred to different chemical functionalities. Besides, not even the different BET surface area (**Tab. 20**) can account for these differences, since the AC Sigma BET surface is slightly lower than that of AC Norit. So their different behaviour is mainly due to the different pore size distribution.
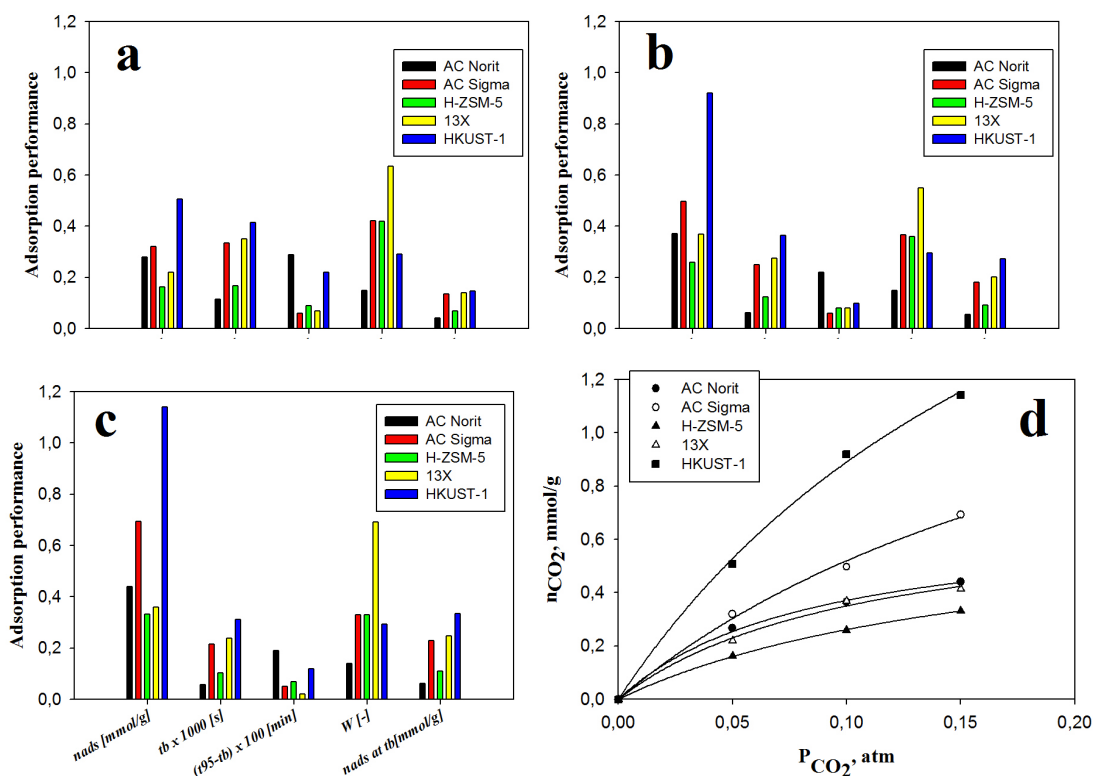
Fig. 73 Comparison of all the adsorbent materials in sound assisted conditions (140dB-80Hz). a) C_0=5%; b) C_0=10%; c) C_0=15%; d) Adsorption isotherms. u=1.5cm/s.

Moreover, from the analysis of the TG curves obtained in air, it emerges that a high amount of unburned material (~ 20% in weight, possibly metal residuals) is detected in the case of AC Norit, thus meaning that it is characterized by a remarkable amount of inorganic matter. It is possible that this inorganic matter can be responsible of a different pore distribution with respect to the AC Sigma (i.e. some of the pores can be occluded).

The results obtained for both the zeolites used in this work, agree with several works reported in literature, which rank zeolites among the fastest adsorbents, reaching equilibrium capacity within minutes [82]. They are both characterized by faster adsorption kinetics with respect to AC Norit, whereas, their kinetics are comparable to that of AC Sigma. In particular, the 13X is the zeolite giving the best adsorption capacity, t_b, W and n_{ads} at t_b. This difference could be due the different structure and nature of the extraframework cation of the two zeolites. Indeed, the Si/Al ratio and the number/nature of extraframework cations play a major role in controlling the CO_2 adsorptive properties [76,77]. In particular, the most promising zeolites for CO_2 adsorption are those having a low Si/Al ratio, corresponding to high content of extraframework cations, because the presence of aluminum atoms in the structure introduces negative framework charges that are compensated with exchangeable cations within the pores. In the case of zeolite 13X (Si/Al=1.25) these cations are Na^+, which are capable of generating strong electrostatic interactions with carbon dioxide. In other words 13X has a basic functionality, which can interact with the acid CO_2 molecules. On the contrary, the H-ZSM-5 is characterized by a prevalence of Si atoms with respect to Al ones (Si/Al=140) and the extraframework cations are H^+, which give the zeolite an acid character, thus reducing the affinity towards CO_2 molecules with respect to zeolite 13X. However, the different behaviour shown by the two zeolites could also be to their different pore size distribution. In order to assess which one between the nature of extraframework cations and the pore size distribution is the main parameter influencing the adsorption process under the investigated operating conditions, a limited number of tests has been performed on a zeolite Y. In particular, this zeolite has been exchanged in the ammonium (NH_4-Y) and sodium form (Na-Y) in order to analyze the effect of the extraframework cation, the pore size distribution being the same. The results obtained, reported in **Fig. 74**, show that the two zeolites are characterized by very similar adsorption performances (0.18 and 0.19mmol/g for NH_4-Y and Na-Y, respectively), thus meaning that the adsorption process is predominantly affected by the pore size distribution rather than by the chemical nature of the extraframework cation under the investigated operating conditions.

From the comparison between the activated carbons and the zeolites it emerges that the AC Sigma is characterized by adsorption performances comparable to that of 13X, in terms of t_b, whereas it has a higher adsorption capacity (n_{ads}) and kinetics and a lower W. So, AC Sigma is competitive with respect to 13X, despite the basic character of the zeolite.
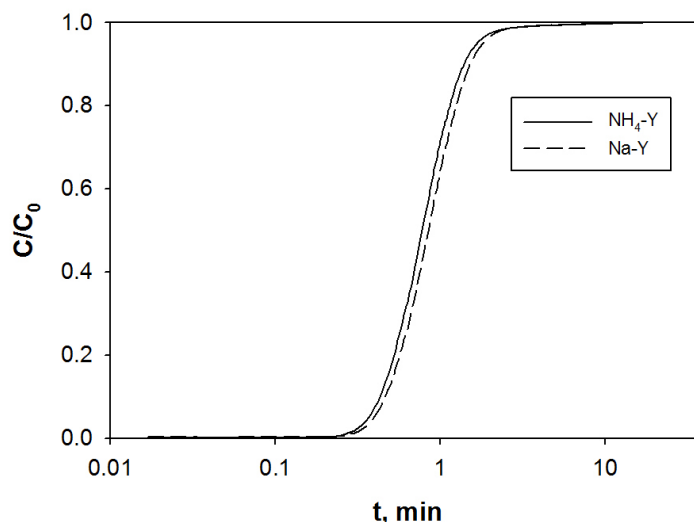
Fig. 74 Comparison between the breakthrough curves obtained for NH$_4$-Y and Na-Y. C$_0$=10%; u=1.5cm/s.

Summing up, HKUST-1 is adsorbent characterized by the best CO_2 adsorption capacity. As regards the kinetics, HKUST-1 is slower than both the zeolites and activated Sigma Aldrich (lower t_{95}-t_b). Moreover, it also has worse performances in terms of W. However, in the scenario of a real adsorption process the interest is focused on the CO_2 adsorbed until t_b, because when the concentration reaches the break point, the flow is stopped or diverted to a fresh adsorbent bed (so that the used bed can be regenerated). From this point of view, HKUST-1 is still the sorbent giving the best performances. The larger adsorption capacity compensates the lower W (namely slower adsorption kinetics) and indeed the moles adsorbed at t_b are higher with respect to all the other adsorbent.

On the basis of the above-mentioned considerations, it emerges that their different adsorption performances can be explained referring to their different pore size distribution. However, none of the textural properties, BET surface area and the total pore volume, can be considered as key adsorption parameters. Sure enough, AC Norit is characterized by the best textural properties (**Tab. 20**). On the contrary, HKUST-1 has a BET surface area lower than AC Sigma and comparable to that of 13X and AC Norit (**Tab. 20**).

Likewise, its total pore volume is remarkably lower than that of both the two activated carbons. However, despite these average characteristics, HKUST-1 shows the best CO_2 uptake. This means that although the total pore volume is the highest in the activated carbons, not all the pores are effective for an optimum adsorption capacity. As a matter of fact, **Fig. 75a**

and b show that the amount of CO_2 adsorbed is practically independent of the total volume of pores and BET surface area, respectively. Since no correlation can be found with the total pore volume one has to assume that there should be a specific pore size which is the key factor defining the total adsorption capacity on the studied materials.
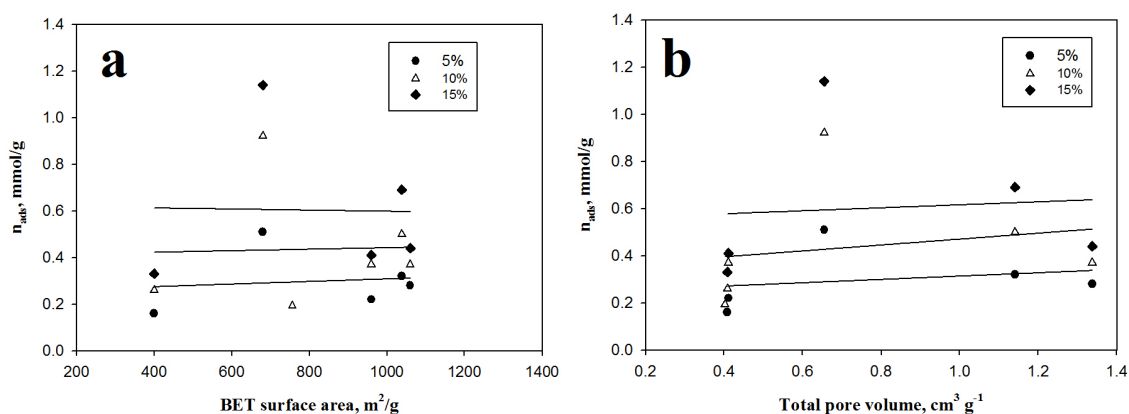
Fig. 75 Correlation between the amount of CO_2 adsorbed (n_{ads}) and: (a) BET surface area; (b) total pore volume.

In this sense, **Fig. 76**a and b show the comparison among the pore size distributions of all the adsorbents and the relationship between the adsorbed amount of CO_2 and the total volume of micropores falling in the range 8.3-12Å (**Tab. 21**). In this case, an increasing correlation can be clearly observed, thus confirming the importance of a specific porosity for CO_2 adsorption under the investigated operating conditions, i.e. at low CO_2 partial pressure. In light of all these considerations, the excellent performance observed for HKUST-1 under all the investigated operating conditions can be explained. This sample, with an average BET surface area ($680m^2/g$) as well as total pore volume ($0.66cm^3/g$) with respect to the activated carbons and zeolites, exhibits the maximum volume of that specific micropores ($0.15cm^3/g$) already suggested as primarily responsible for the observed uptake. In summary, the total amount of CO_2 adsorbed increases with increasing volume of specific micropores.

Tab. 20 Comparison among the textural properties of all the adsorbent materials.

Materials	Total pore Volume cm^3/g	BET surface are, m^2/g
AC Norit	1.34	1060
AC Sigma	1134	589
13X	0.41	751
H-ZSM-5	0.41	400
HKUST-1	0.66	734
Na-Y/NH$_4$-Y	0.40	756

This result is in agreement with literature works reporting that adsorbent materials characterized by a high volume of narrow micro-pores (< 1 nm) exhibited high CO_2 adsorption capacity [138-142], even though they refer to CO_2 partial pressure as high as 1atm, i.e. larger than that typical of a post-combustion flue-gas (CO_2 1−15%vol. and atmospheric pressure). On the other side, performances of solid sorbents under typical flue gas conditions have been poorly investigated. In particular, in micropores (<20Å [49]) adsorption is governed by CO_2-surface interactions, with wall-wall interactions also playing a significant role. More specifically, adsorbate-adsorbent interaction energy is substantially enhanced when the adsorption takes place in very narrow pores because of the overlapping of the potential fields from the neighboring walls [140,141]. In other words, due to this extra strong pore wall-wall interaction, CO_2 that is close to the pore walls has enhanced interaction with the surfaces, thus leading to the complete filling of the narrow micropores. Under these circumstances, the adsorption mechanism consists of volume-filling rather than surface coverage typical of meso-macroporous materials and the CO_2 molecules occupying these narrow micropores are bound as significantly condensed phase (i.e in a liquid-like state). In particular, Sevilla et al. [140] reported that this enhancement of the adsorption energy is negligible for micropore widths larger than around three/four times the molecular diameter of CO_2 molecules (3.3Å). Therefore, in agreement with the results obtained, the size limit for volume-filling can be reasonably established at about 12Å for CO_2. On the contrary, other pores present in the adsorbent materials, such as either larger micropores (>12Å) and mesopores (>20Å) or too small micropres (<8.3Å), are most likely not relevant for CO_2 capture under post-combustion operating conditions (i.e $P_{CO2} \leq$ 1atm). This is because they are unable to adsorb significant CO_2 amounts at the very low relative pressures existing under such conditions: micropores with dimension lower than 8.3Å are probably too small for these low CO_2 partial pressures, whereas in larger pores (>20Å) CO_2 is considerably less densely adsorbed, being the influence of the surface-surface interactions weaker. This is the reason for the lack of correlation between the CO_2 adsorption capacity of sorbents and their overall textural properties such as total pore volume or BET surface area.
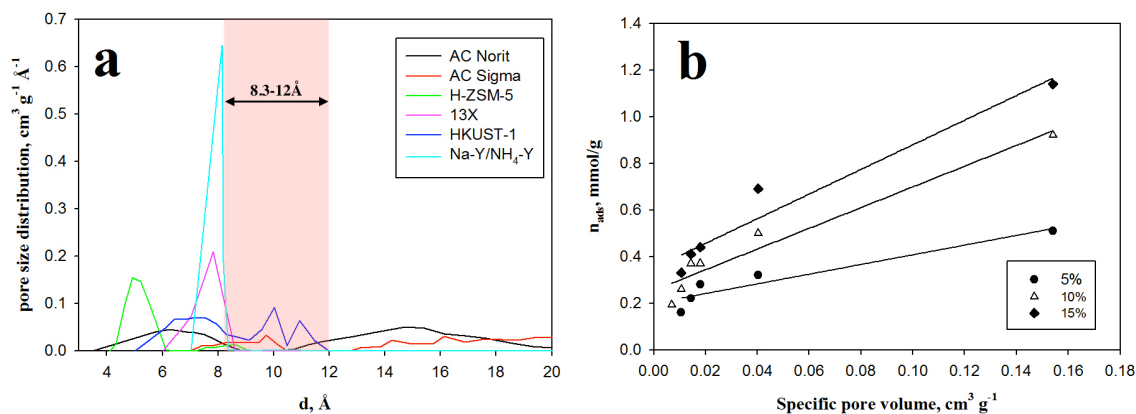
Fig. 76 Comparison among the pore size distribution of all the adsorbent materials (a) and correlation between the amount of CO$_2$ adsorbed (n$_{ads}$) and the volume of specif micropores (8.3-12 Å) (b).

Tab. 21 Volume of specific micropores of all the adsorbent materials

Materials	Volume of micropores in the range 8.3-12 Å, cm^3/g
AC Norit	1.79 10^{-2}
AC Sigma	4.03 10^{-2}
13X	1.43 10^{-2}
H-ZSM-5	1.06 10^{-2}
HKUST-1	1.54 10^{-1}
Na-Y/NH$_4$-Y	6.92 10^{-3}

III.4 Desorption Tests

III.4.1 HKUST-1 Regeneration Strategy

An accurate study has also been carried out in order to select an efficient regeneration strategy for HKUST-1. From the thermogravimetric analysis (Fig. 28) it is clear that 350°C is a thermal limit of the material, even though the decomposition of the material starts around 200°C. So, two temperatures, 250 and 150°C have been investigated as possible regeneration temperatures. However, before testing the material in the fluidization column, a CO$_2$ TPD analysis has been performed to have more detailed information about possible damages to the HKUST-1 structure. **Fig. 77** reports the CO$_2$ TPD profiles obtained at 250°C (a) and 150°C (b).
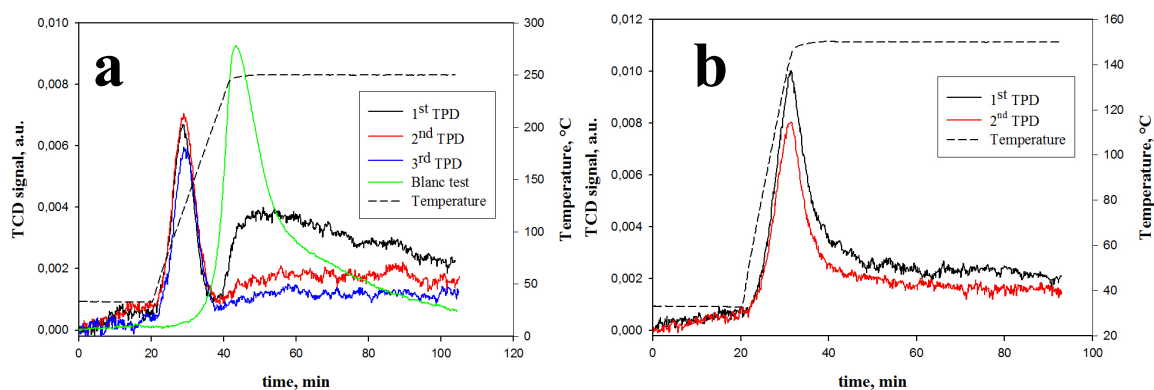
Fig. 77 CO$_2$ TPD profiles of HKUST-1 at 250°C (a) and 150°C (b).

As regards the CO$_2$ TPD tests performed at 250°C (**Fig. 77a**), the first TPD profile is characterized by two peaks, the former at around 130°C and the latter around 250°C. The same sample subjected to two more TPDs showed a different behavior. In particular, the second peak tends to disappear while the first peak has a decreasing trend, thus meaning that the sample is not stable. In order to assess the nature of this instability, namely whether this instability is related to the fact that a temperature of 250°C is not enough to properly regenerate the material (so the CO$_2$ desorbed tends to decrease with respect to the first TPD) or enough to decompose the material, a blank test has been performed without any previous CO$_2$ adsorption step. The TPD profile obtained for the blank test was also reported in **Fig. 77a**. For temperatures lower than 210°C the sample does not desorb anything, whereas a peak is present at 250°C, thus confirming that HKUST-1 starts decomposing around 250°C, according to the thermogravimetric analysis in inert atmosphere. As next step, a lower temperature (150°C) was investigated. To this aim both pretreatment and TPD were performed at 150°C. Both the TPD profiles obtained present only a peak at 130°C, which, in particular, decreases in the second TPD (**Fig. 77b**). The lowering of the CO$_2$ adsorption capacity cannot be attributed to the sample decomposition, since the blank test has demonstrated that it starts at 210°C. It can be concluded that the treatment at 150°C is too mild to properly regenerate the material by completely desorbing the CO$_2$ trapped into the pores.

On the basis of all these considerations, it clearly emerges that the sole thermal treatment is not effective to properly regenerate HKUST-1. Therefore, a mixed regeneration strategy has been adopted: bland temperature and vacuum have been combined by heating up the sample to 150°C under a vacuum of 50mbar. This treatment has not been performed in the fluidized bed apparatus but extra-situ. In order to verify the repeatability of the adsorption tests and the effectiveness of this regeneration strategy the two tests performed at 140dB-80Hz (with 5 and 15% CO$_2$ inlet concentration) have been carried out once again after 10 adsorption/desorption

cycles and the obtained results have been compared to those relative to the first adsorption test under the same operating conditions (**Fig. 70**). The adsorption effectiveness can be properly reproduced as confirmed by the overlap of the repeated test breakthrough curve with the original one (**Fig. 78**) and by all the adsorption parameters (**Tab. 22**).

Tab. 22 Experimental results obtained for fresh and regenerated HKUST-1. SPL=140dB, f=80Hz

	CO$_2$ inlet concentration							
	5%				**15%**			
	t_b	n_{ads}	**W**	t_{95}-t_b	t_b	n_{ads}	**W**	t_{95}-t_b
	s	**mmol/g**	**%**	**min**	**s**	**mmol/g**	**%**	**min**
Fresh	146	0.48	24	22	141	1.14	29	12
Regenerated after 10 cycles	141	0.45	25	20	150	1.11	31	10
Regenerated without vacuum					41	0.94	17	10

As a further confirmation the same test has been repeated but regenerating the sample without vacuum, namely only heating the powder up to 150°C. In this case the powder cannot be entirely regenerated. Indeed, the adsorption effectiveness is remarkably worsened (**Fig. 78** and **Tab. 22**).

All these remarks regarding the effectiveness of the regeneration process (bland temperature and vacuum) and the repeatability of the adsorption tests have been confirmed by characterizing the sample after it has been subjected to several adsorption-desorption cycles.
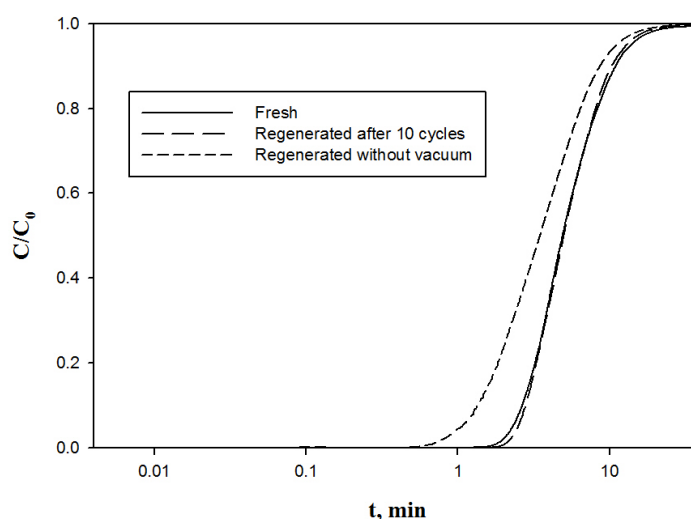
Fig. 78 HKUST-1: effect of the regeneration strategy. SPL=140dB, f=80Hz; C$_0$=15%; u=1.5cm/s.

The comparison of chemico-physical characteristics between the freshly prepared and regenerated HKUST-1 after 10 cycles is reported in **Fig. 79** and **Tab. 23**. The FT-IR and XRD analyses showed that the sample keeps its chemical and crystallographic structure even after several adsorption-desorption treatments. This is also confirmed by the SEM image, which shows that the crystal is not affected by the treatments. Finally, the TG plot confirms structure is the same as the fresh sample, indeed the same collapse of the HKUST-1 structure can be

observed at 350°C. The particle size distribution is also substantially unvaried as well as the BET surface area and pore size distribution.
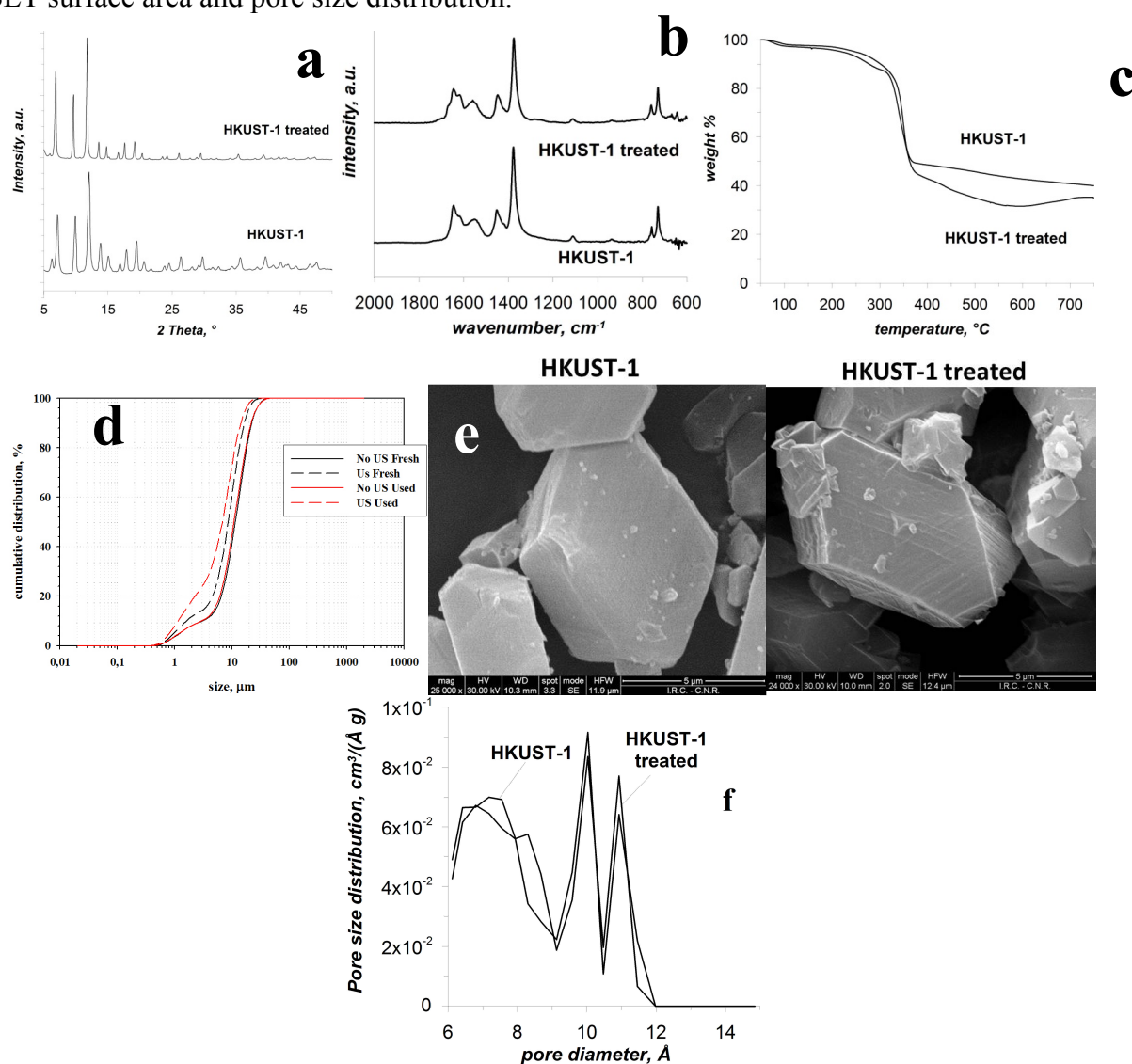
Fig. 79 Freshly prepared HKUST-1 and regenerated after 10 cycles (a) XRD patterns, (b) FT-IR spectra, (c) thermogravimetric analysis in N$_2$, (d) particle size distribution, (e) SEM analysis, (f) pore size distribution.

Tab. 23 Properties of freshly prepared and regenerated after 10 cycles HKUST-1.

HKUST-1	D$_{SAUTER}$, µm with/without US	BET surface area, m^2/g	Bulk density, kg/m^3
Fresh	4.3/5.6	734	265
Regenerated after 10 cycles	3.2/5.5	662	265

Fig. 80 reports the pore size distribution of HKUST-1 after being subjected to TPD analyses. It is clear that the material subjected to TPD at 250°C is characterized by a dramatic decrease of all the porosity and in particular of the microporosity falling in the range 8-12Å, i.e. that effective for the adsorption process. This loss of porosity, which is due to the degradation process that HKUST-1 undergoes at 250°C, negatively affects the adsorption capacity as

110

observed from the TPD analysis. On the contrary, after the TDP at 150°C, the material keeps its original porous structure (especially that in the effective range 8-12Å) and adsorption capacity, being the material stable after the regeneration strategy at 150°C (under vacuum).
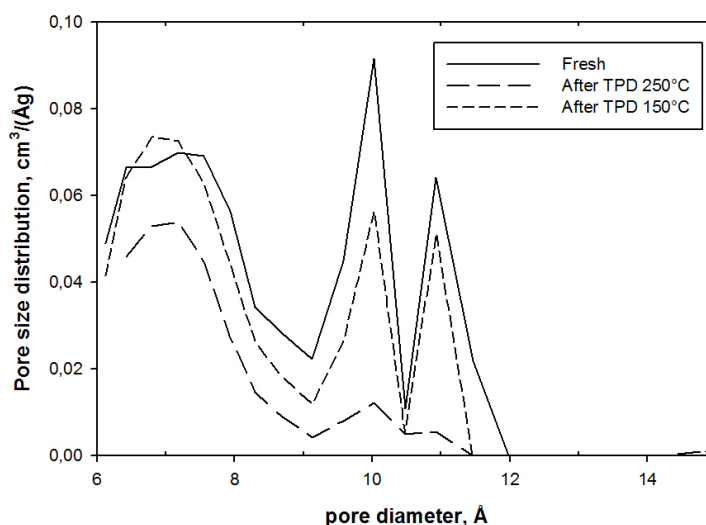
Fig. 80 Pore size distribution of freshly prepared HKUST-1 and after TPD at 250 and 150°C.

III.4.2 TSA on Activated Carbon Norit

III.4.2.1 Effect of the Sound application

The effect of sound application on the desorption performances has been highlighted by performing desorption tests according to the isothermal purge strategy. Both the ordinary and sound assisted desorption tests have been performed after an ordinary adsorption step so that the comparison between the desorption tests could be made the adsorbed CO_2 being the same. **Fig. 81** reports the comparison between the desorption curves obtained under ordinary and sound assisted conditions. The desorption curve has the general form of a peak followed by a tail. In particular, the concentration pattern reaches a maximum in CO_2 outlet concentration for relatively low desorption times (about 2min), indicating that most of the adsorbed CO_2 is quickly removed from the samples. After this fast stage, the curves show a relatively longer tail indicating that the residual CO_2 desorption takes place slowly as a result of driving force reduction. The sample can be completely regenerated, i.e. the amount of CO_2 desorbed is the same as the amount adsorbed in the previous adsorption step, under both ordinary and sound assisted fluidization conditions. However, the desorption profiles are quite different. It is clear that the application of the sound makes it possible to obtain a more regular desorption profile, whereas, the desorption curve is particularly unstable under ordinary fluidization conditions. This is most likely due to the formation of gas preferential channels inside the bed, thus

inevitably hindering the regular desorption of CO_2 from the bed of particles. The actual temperature profile inside the bed has also been reported in **Fig. 81**. As one could anticipate, the heating rate is faster under sound assisted conditions due to better gas-solid contact efficiency, and consequently higher heat transfer coefficients, with respect to the test performed under ordinary fluidization conditions.
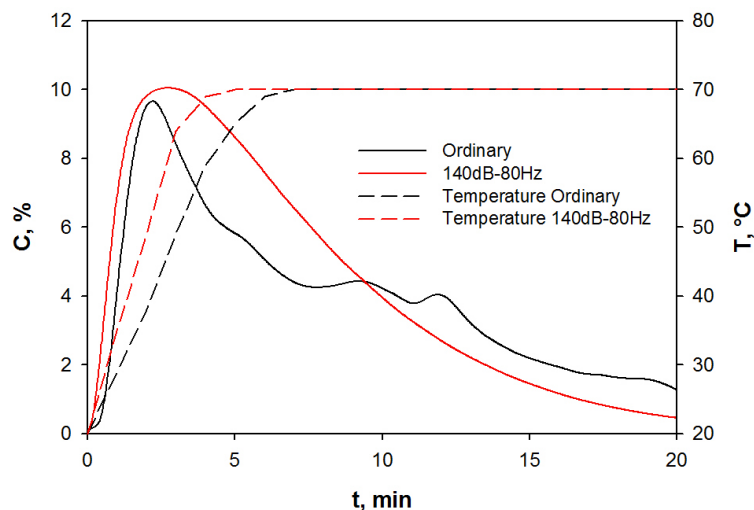
Fig. 81 CO_2 outlet concentration profiles during not isothermal desorption tests under ordinary and sound assisted conditions. The sorbent temperature profile is also reported. N_2 purge flow rate=67.8Nl h^{-1}; heating=20°C min^{-1} up to T_{des}=70°C. Adsorption step: ordinary fluidization; inlet flow rate=67.8Nl h^{-1}; C_0=10%vol.

CO_2 desorption curves have then been elaborated in order to analyze the desorption efficiency. In particular, the main parameters characterizing the CO_2 desorption process are the CO_2 recovery, the time required for the desorption process at a fixed regeneration level (t_d) and CO_2 mean concentration in the desorbing flow (C_m), especially the latter being the key aspect to be considered for CO_2 storage purposes.

In particular, the CO_2 mean concentration in the desorbing flow up to the time t_i can be expressed as:

$$C_m = \frac{V_i^{CO_2}}{V_d^{CO_2}+V_d^{N_2}} = \frac{\int_0^{t_d} Q_{CO_2}^{out}(t)dt}{(\int_0^{t_d} Q_{CO_2}^{out}(t)dt)+(Q_{N_2}^p \cdot t_d)} \tag{20}$$

where $V_d^{CO_2}$ and $V_d^{N_2}$ represent the total volume of CO_2 desorbed and the N_2 purge gas volume fed to the column up to time t_d, respectively, $Q_{CO_2}^{out}(t)$ and $Q_{N_2}^p$, the CO_2 outlet flow rate (which is function of the time t) and the N_2 purge gas flow rate fed to the column.

Due to the shape of desorbing profiles (**Fig. 81**), a higher desorption time (t_d) is expected to give a more effective regeneration, namely a higher CO_2 recovery, but it leads to a lower CO_2 mean concentration (C_m) in the desorbing flow. This is clearly shown in **Fig. 82**: the CO_2 recovery is an increasing function of t_d, whereas, on the contrary, C_m is a decreasing function

of t_d. More specifically, higher recovery levels require higher time for desorption, but, at the same time, the desorption rate decreases with time due to a lower driving force, and, consequently, a larger purge volume is required to remove the residual adsorbed CO_2, thus determining a dilution effect.
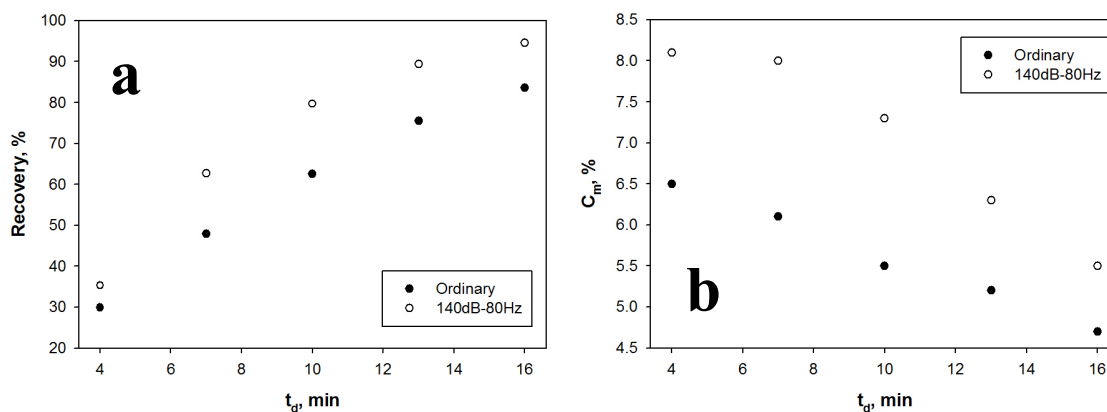
Fig. 82 CO_2 recovery level (a) and CO_2 mean concentration of the desorbing stream (b) as functions of the desorption time. N_2 purge flow rate=67.8Nl h^{-1}; heating=20°C min^{-1} up to T_{des}=70°C. Adsorption step: ordinary fluidization; inlet flow rate=67.8Nl h^{-1}; C_0=10%vol.

A direct comparison between the ordinary and sound assisted desorption tests has been made, the CO_2 recovery level being the same.
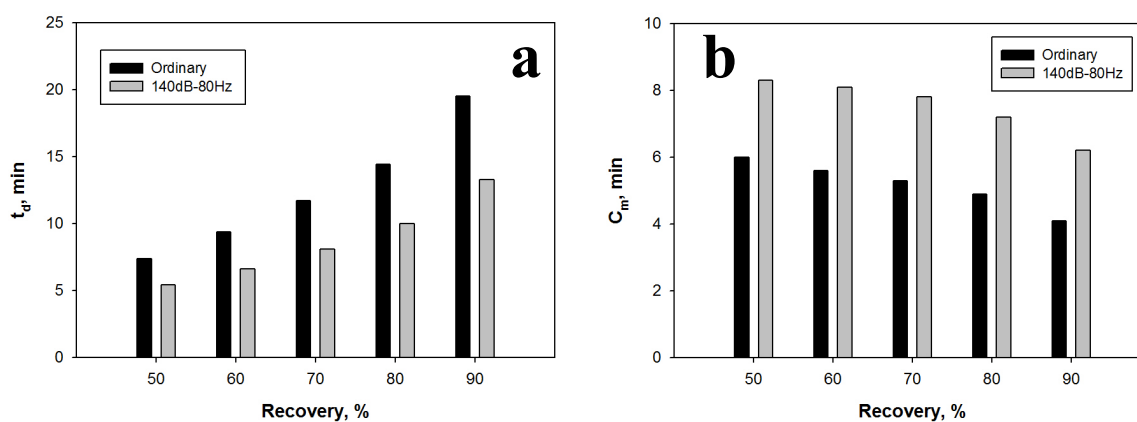
Fig. 83 Comparison between the ordinary and sound assisted (140dB-80Hz) desorption tests in terms of desorption time (a) and CO_2 mean concentration of the desorbing stream (b), at different recovery levels. N_2 purge flow rate=67.8Nl h^{-1}; heating=20°C min^{-1} up to T_{des}=70°C. Adsorption step: ordinary fluidization; inlet flow rate=67.8Nl h^{-1}; C_0=10%vol.

In particular, five different desorption times, t_i, have been considered, each corresponding to a different CO_2 recovery percentage (R = i) of the total adsorbed amount and CO_2 mean concentration, C_i (e.g. t_{90} corresponding to a 90% of total CO_2 recovered by desorption, and C_{90} being the related CO_2 mean concentration in the desorbing flow). The values and trends of t_i and C_i are reported in **Fig. 83**a and b, respectively. It is clear that the application of the sound makes it possible, from one hand, to remarkably increase the desorption rate (shorter desorption time needed to obtain the same CO_2 recovery, **Fig. 83a**) and, on the other, to

significantly enrich the recovered CO_2 stream (up to 32% more concentrated streams, the recovery being the same).

Considering that in a real CO_2 capture process the efficiency of the regeneration would obviously be affected by the previous adsorption step, a not isothermal desorption test has been performed after a sound assisted adsorption phase. The obtained desorption profile and the relative values and trends of t_i and C_i are reported in **Fig. 84** and **Fig. 85**, respectively.
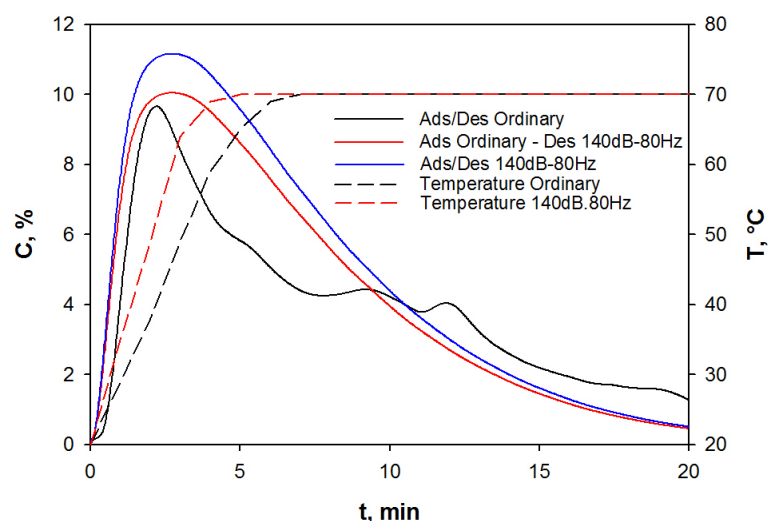
Fig. 84 CO_2 outlet concentration profiles during not isothermal desorption tests under ordinary and sound assisted conditions. The sorbent temperature profile is also reported. N_2 purge flow rate=67.8Nl h^{-1}; heating = 20°C min^{-1} up to T_{des}=70°C. Adsorption step: ordinary fluidization/140dB.80Hz; inlet flow rate=67.8Nl h^{-1}; C_0=10%vol.

It is clear that the application of the sound in both the phases (adsorption and desorption) makes it possible to further increase the enrichment of the desorbing stream (up to 12% more concentrated stream than that obtainable from the same sound assisted desorption test performed after ordinary adsorption), since the amount of the capture CO_2 is increased. As regards t_d, it is worth noting that for a fixed recovery level, the amount of CO_2 to be desorbed after the sound assisted adsorption is larger than after the ordinary adsorption (since the total amount of adsorbed CO_2 is larger). Nonetheless, the desorption time is slightly decreased.
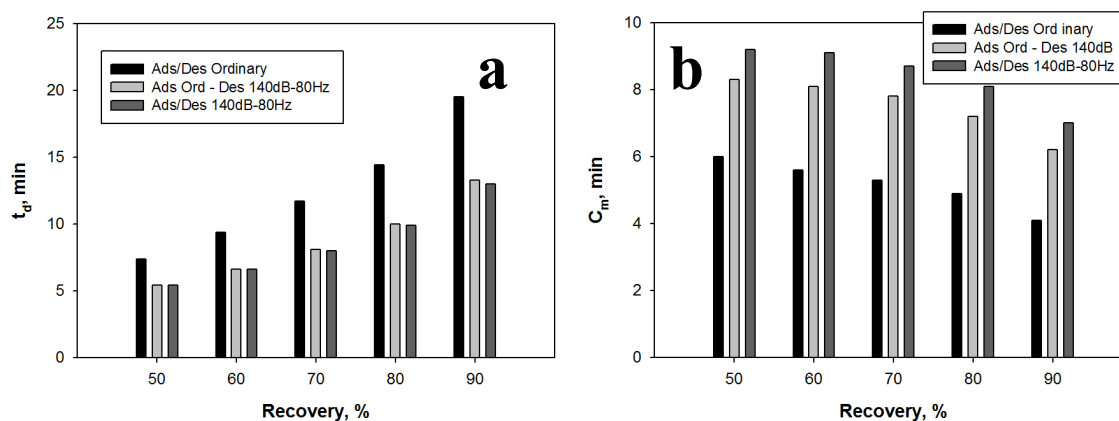
Fig. 85 Comparison between the ordinary and sound assisted (140dB-80Hz) desorption tests in terms of desorption time (a) and CO_2 mean concentration of the desorbing stream (b), at different recovery levels. N_2 purge flow rate=67.8Nl h^{-1}; heating=20°C min^{-1} up to T_{des}=70°C. Adsorption step: ordinary fluidization/140dB.80Hz; inlet flow rate=67.8Nl h^{-1}; C_0=10%vol.

Finally, three consecutive desorption tests have been performed on the same sample of AC Norit under both ordinary and sound assisted fluidization conditions (for the sound assisted case the acoustic field has been applied in both adsorption and desorption phase). The obtained desorption profiles are reported in **Fig. 86**.
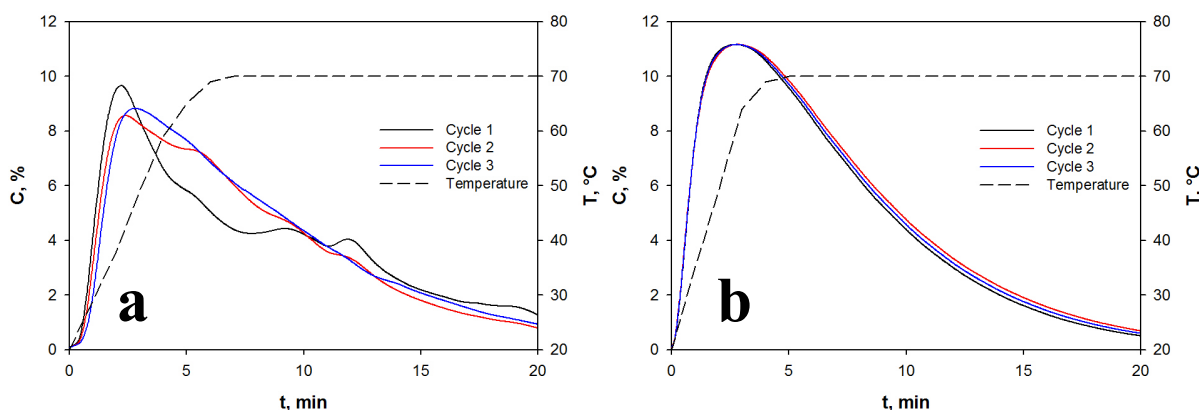
Fig. 86 Comparison between three consecutive desorption profiles obtained from the same AC Norit sample under both ordinary (a) and sound assisted, 140dB-80Hz, (b) fluidization conditions. N_2 purge flow rate=67.8Nl h^{-1}; heating=20°C min^{-1} up to T_{des}=70°C. Adsorption step: ordinary fluidization (a)/140dB.80Hz (b); inlet flow rate=67.8Nl h^{-1}; C_0=10%vol.

The regeneration process is very stable under sound assisted fluidization conditions, as clearly confirmed by the perfect overlapping of the three desorption profiles (**Fig. 86**b). On the contrary, the desorption curves are not replicable under ordinary fluidization conditions since when and where the formation of channels takes place inside the bed is random and, consequently, not predictable.

III.4.2.2   Isothermal Purge Desorption Tests

According to the experimental plan reported in **Tab. 6**, several CO_2 recovery tests from the spent activated carbon were carried out in order to study the effect of operating conditions for CO_2 capture by means of TSA. In particular, the effects of desorption temperature (T_{des}) and N_2 flow rate on AC Norit regeneration and CO_2 recovery were investigated. **Fig. 87** and **Fig. 88** report the CO_2 desorption profiles as affected by desorption temperature and N_2 purge flow rate, respectively.

For each desorption temperature (even at ambient temperature) the adsorbed CO_2 can be totally desorbed (recovery=100%), thus confirming that it is only weakly bonded on the AC

Norit surface, in agreement to literature indicating the CO_2 adsorption on activated carbon as a physisorption [62]. Moreover, the concentration pattern reaches a maximum in CO_2 outlet concentration, which, except for the desorption run at ambient temperature, is remarkably higher (at least doubled and up to almost 6 times) than the inlet value of 10% vol., for relatively low desorption times (about 2 min).

As regards the effect of the regeneration temperature, as clearly shown in **Fig. 87**, the desorption curves become narrower and higher as the temperature increases, thus denoting a faster desorption process. This evidence can be ascribed to an enhancement of the regeneration kinetics, which is due to a decrease in CO_2 adsorption capacity (i.e. enhancing the desorption) coupled to an increase in both N_2 and CO_2 molecular diffusivities. Similarly to what observed for T_{des}, the results also show a positive effect on desorption rate induced by an increase of $Q_{N_2}^p$, as confirmed by narrower desorption peaks corresponding to larger N_2 purge flow rates (**Fig. 88**). More specifically, the time needed to obtain a desired CO_2 recovery percentage monotonically decreases with both desorption temperature and N_2 purge flow rate, as clearly observed in the inset of **Fig. 87** and **Fig. 88**. The values of t_i and C_i determined for each N_2 purge flow rate and desorption temperature are listed in **Tab. 24**.
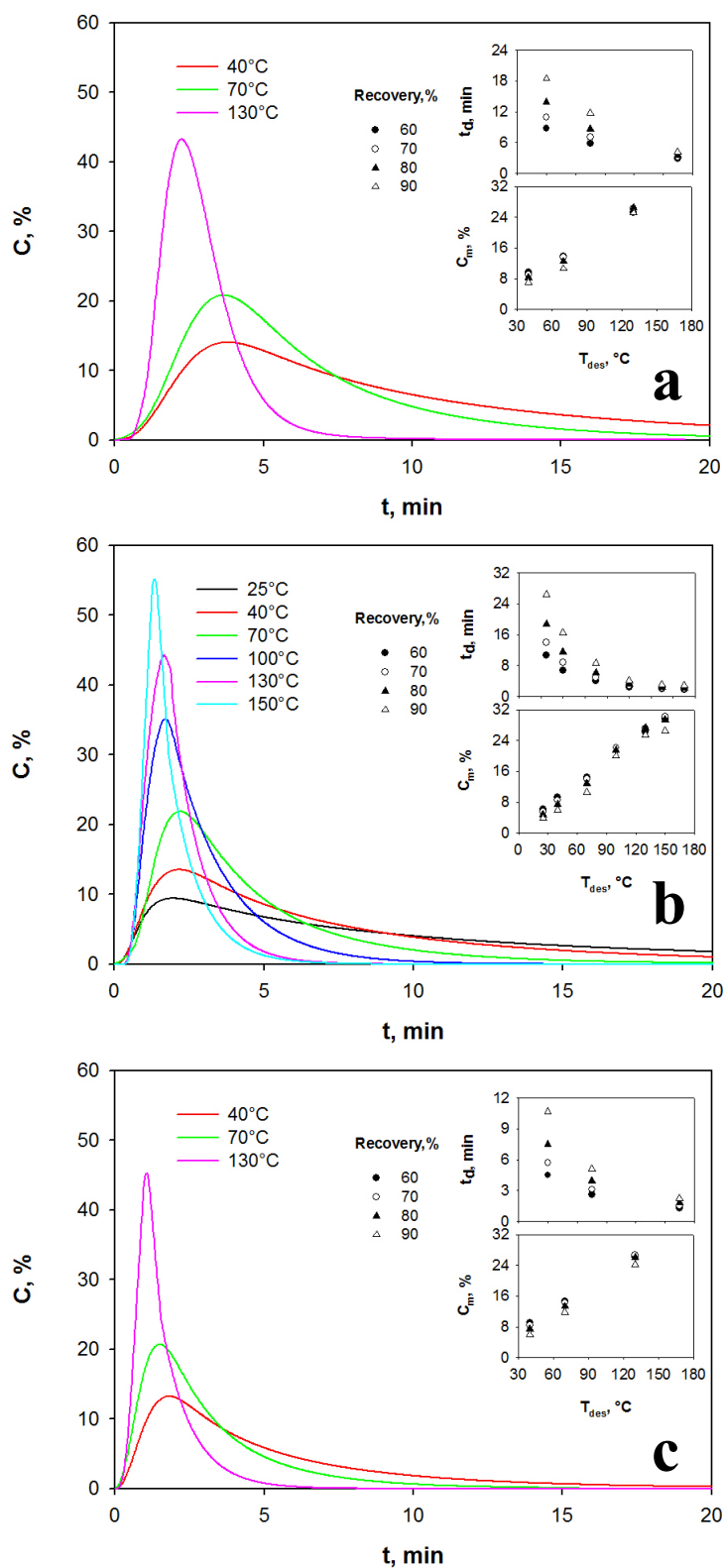
Fig. 87 CO$_2$ outlet concentration profiles during desorption as a function of the desorption temperature. N$_2$ purge flow rate = (a) 45.2Nl h^{-1}, (b) 67.8Nl h^{-1} and (c) 90.4Nl h^{-1}. SPL=140dB; Sound frequency=80Hz. In the inset, t$_d$ and C$_m$ vs T$_{des}$. Adsorption step: SPL=140dB; Sound frequency=80Hz; inlet flow rate=67.8Nl h^{-1}; C$_0$=10%vol.

117

Furthermore, from **Tab. 24** (plotted in the inset of **Fig. 87** and **Fig. 88**), it is clear that, for each N_2 purge flow rate, the CO_2 mean concentration in the desorbing flow increases with increasing temperatures but it decreases with higher CO_2 recovery levels. Differently, for each temperature and for each CO_2 recovery level, the purge gas flow rate has no influence on the maximum CO_2 concentration, which is mainly due to the desorption temperature. Moreover, C_i slightly varies with $Q_{N_2}^p$ and not monotonically (inset of **Fig. 88**). Indeed, from Equation 20, $V_i^{CO_2}$ is not dependent on the N_2 purge flow rate, since for a fixed CO_2 recovery level, the volume of CO_2 desorbed is constant (i.e. it is the same fraction of the total volume of CO_2 adsorbed); on the contrary, $V_i^{N_2}$ is affected by $Q_{N_2}^p$, since it is given by $V_i^{N_2} = Q_{N_2}^p \cdot t_i$, however, the dependence is not obvious. Indeed, when $Q_{N_2}^p$ increases, the time, t_i, required to reach the stated CO_2 recovery level decreases accordingly, thus resulting in a not monotone trend of $V_i^{N_2}$ and consequently of C_i.

In conclusion, from the data reported in **Tab. 24**, it is clear that desorption temperatures lower than 70°C are always not favorable, because, for all the investigated $Q_{N_2}^p$, the desorbing gas flow is more diluted than the gas stream treated during the adsorption step (i.e. $C_i < 10\%$vol.). At 70°C, a 90% recovery level would yield a desorbing gas as concentrated as the inlet gas stream, whereas the mean CO_2 concentration could be increased to about 15% for a solid regeneration level of 60%. However, this compromise would eventually lead to a 40% decrease in the activated carbon CO_2 adsorption capacity after the regeneration. A desorption temperature of 150°C appears to be the best operating condition to obtain higher values of C_i: at 100°C and 130°C not even lowering the recovery level to 60% would yield an equally concentrated stream. Finally, it is worth to note that the time needed to obtain a 90% regeneration level at 150°C is almost the same that the time required to obtain a 70% regeneration level at 100°C (t_{90} at 150°C ≈ t_{70} at 100°C), whereas, t_{80} at 150°C is almost the same that t_{70} at 130°C. In order to maximize C_i for storage purpose, a desorption degree of 80–90% obtained at 150°C and for desorption flow gas rate lower than 90Nl h^{-1} can be considered as the optimal operating conditions among those investigated, being a proper compromise between the amount of CO_2 recovered and its concentration in the desorbed gas (26-29%vol.).
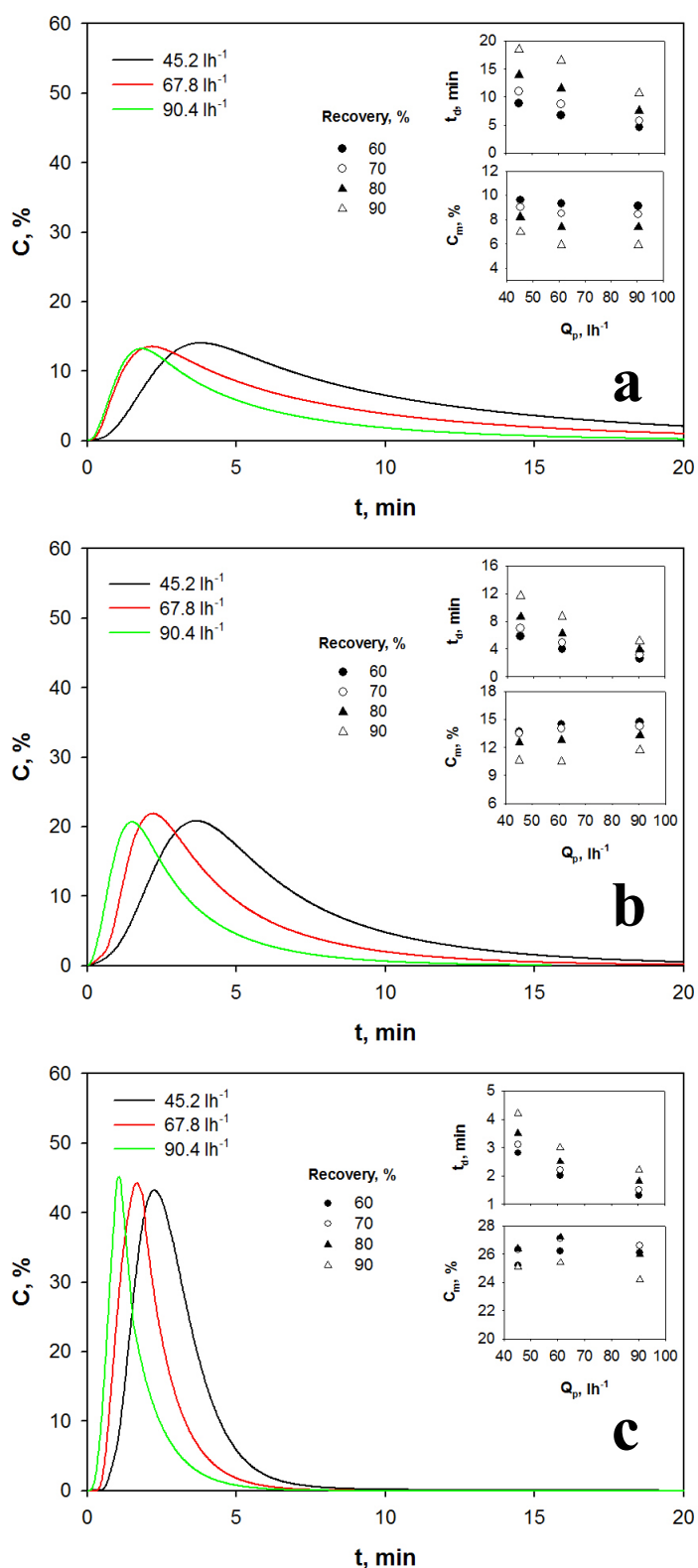
Fig. 88 CO$_2$ outlet concentration profiles during desorption as a function of N$_2$ purge flow rate. Desorption temperature= (a) 40°C, (b) 70°C and (c) 130°C. SPL=140dB; Sound frequency=80Hz. In the inset, t$_d$ and C$_m$ vs Q$_p$. Adsorption step: SPL=140dB; Sound frequency = 80Hz; inlet flow rate=67.8Nl h^{-1}; C$_0$=10%vol.

119

Tab. 24 Results obtained from the AC Norit isothermal purge desorption tests.

$Q^p_{N_2}$, Nl h^{-1}	T_{des}, °C	t_{60}	t_{70}	t_{80}	t_{90}	C_{60}	C_{70}	C_{80}	C_{90}
	40	8.8	10.9	13.9	18.5	9.6	9.0	8.2	7.0
45.2	70	5.8	7.0	8.6	11.7	13.7	13.5	12.5	10.6
	130	2.8	3.1	3.5	4.2	25.2	26.3	26.4	25.1
	25	10.7	14.0	18.8	26.4	6.1	5.5	4.7	3.8
	40	6.7	8.7	11.5	16.5	9.3	8.5	7.4	5.9
	70	4.0	4.9	6.2	8.7	14.5	14.0	12.8	10.5
67.8	100	2.4	2.8	3.3	4.1	22.0	22.1	21.5	19.9
	130	2.0	2.2	2.5	3.0	26.2	27.1	27.2	25.4
	150	1.65	1.9	2.2	2.9	29.5	30.1	29.4	26.4
	40	4.5	5.7	7.5	10.7	9.1	8.4	7.4	5.9
90.4	70	2.6	3.1	3.9	5.1	14.7	14.3	13.3	11.7
	150	1.3	1.5	1.8	2.2	26.1	26.6	26.0	24.2

III.4.2.3   Separate Heating and Purge Desorption Tests

As already discussed in the previous paragraph the main parameters characterizing the efficiency of the desorption process are the purity of the recovered CO_2 stream and the percentage of CO_2 recovered with respect to that captured during the previous adsorption step. Since these two parameters have opposing trends, it is necessary to find the most convenient compromise between the two of them.

In light of these considerations, a second regeneration method has been conceived in order to improve the performances in the desorption step, namely find a possible way to enrich the recovered CO_2 stream with respect to the standard regeneration strategy (desorption by purge at a fixed temperature). So, the second regeneration strategy is based on the idea of separating the contribution to the CO_2 recovery given by Heating, which could be capable of yielding a pure CO_2 stream, from that given by purge, which necessarily causes a dilution effect. More precisely, differently from the standard regeneration strategy described in the previous paragraph, during the heating step the column is not isolated, so a first CO_2 recovery happens contextually to the heating of the activated carbon bed (i.e. CO_2 is recovered only due to a thermal effect). Then, when no more CO_2 is desorbed (i.e. the thermodynamic equilibrium corresponding to the chosen desorption temperature is reached and the CO_2 still adsorbed to the sorbent surface cannot be recovered at that temperature) N_2 is fluxed inside the column and the remaining CO_2 is recovered, thus enhancing the recovery obtainable by the only heating step.

According to the procedure described in details in the Experimental section, during the heating step the CO_2 is recovered by sucking at constant flow rate and it is diluted in air. So,

knowing the suction flow rate and the CO_2 concentration, the recovered carbon dioxide has been calculated by integration. The results obtained are reported in **Tab. 25**.

Tab. 25 CO_2 recovery during the heating and purge steps.

T_{des}, °C	Recovery by Heating, %	Recovery by Purge, %	Total, %
40	17.73	82.07	99.8
70	48.02	51.18	99.2
100	66.94	32.46	99.4
130	79.53	19.77	99.3
150	81.73	17.67	99.4

It is clear that increasing desorption temperature the amount of CO_2 desorbed is increased. This behaviour is due to the fact that at higher temperatures the thermodynamic equilibrium shifts towards conditions more and more unfavorable for adsorption, so more CO_2 is desorbed and less is still adsorbed within the AC Norit pores. **Fig. 89**a reports the trend of the CO_2 recovery obtainable with the sole heating step as function of the desorption temperature. Clearly, the recovery monotonically increases with the temperature, passing from a value of about 18% at 40°C up to a value of about 82% at 150°C. So, heating is very efficient for desorbing carbon dioxide since a large part of the adsorbed carbon dioxide can be recovered (80% at 130°C).
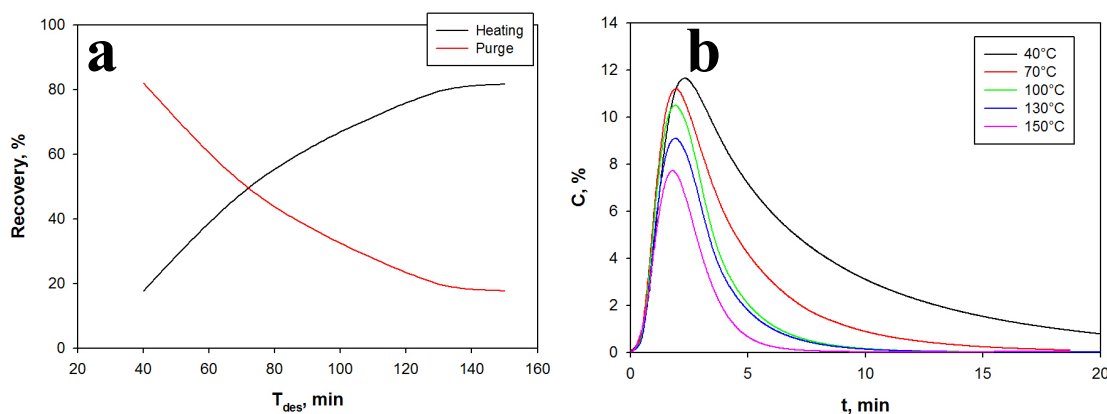
Fig. 89 a) CO_2 recovery during Heating and Purge as function of desorption temperature; b) CO_2 outlet concentration profiles during the purge step. Purge step: N_2 purge flow rate=67.8Nl h[-1]; SPL=140dB; Sound frequency=80Hz. Adsorption step: SPL=140dB; Sound frequency=80Hz; inlet flow rate=67.8Nl h[-1]; C_0=10%vol.

However, it is clear that it is impossible to get back all the carbon dioxide whatever the temperature of the regeneration. Indeed, to recover the remainder it is necessary to lower the partial pressure of CO_2 and this is possible using N_2 as purge gas (purge step). **Fig. 89**b reports the outlet CO_2 concentration profiles obtained during the purge step at the different desorption

temperatures. The trend obtained is coherent with the results obtained from the heating step: clearly, as T_{des} is increased the desorption peak becomes lower, since less CO_2, still adsorbed on the AC Norit surface, remains to be desorbed. In other words the trend obtained for the CO_2 recovery by purge is complementary to that obtained for the CO_2 recovery by heating (**Fig. 89**a), namely monotonically decreasing with T_{des}. The closure of the mass balance, reported in **Tab. 25**, has been obtained calculating the CO_2 recovery by purge by integration of the desorption peaks.
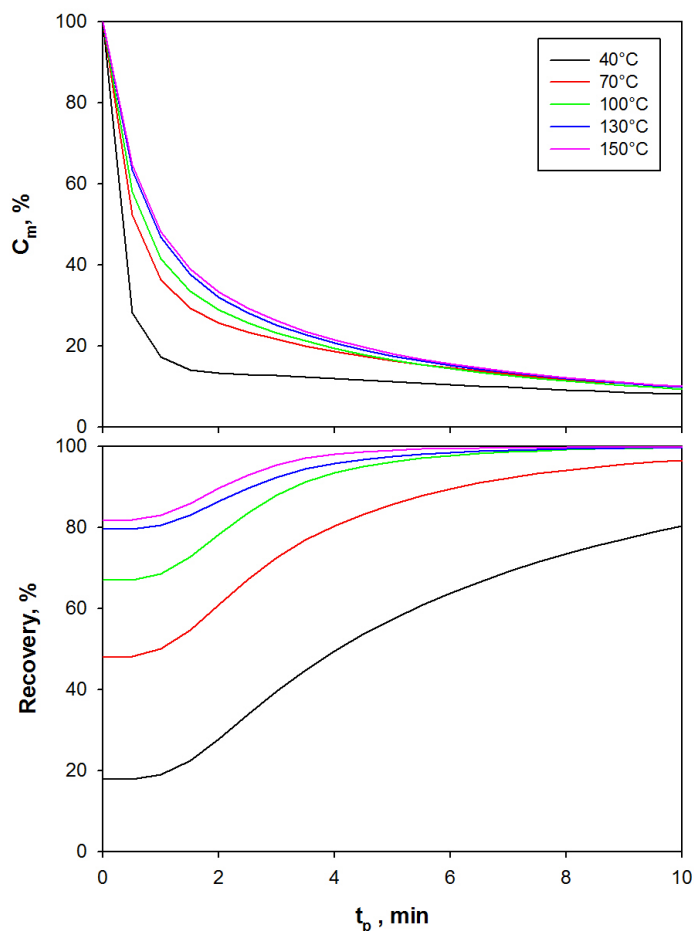
Fig. 90 a) CO_2 mean concentration (C_m) and recovery as function of purge time at different desorption temperatures. Purge step: N_2 purge flow rate=67.8Nl h^{-1}; SPL=140dB; Sound frequency=80Hz. Adsorption step: SPL=140dB; Sound frequency=80Hz; inlet flow rate=67.8Nl h^{-1}; C_0=10%vol.

As already stated above, the purity of the CO_2 recovered during the heating step is unfortunately affected by the experimental procedure used for these tests, which envisaged the suction of air from the atmosphere beside the CO_2 desorbed from the bed. In other words, limitations due to the experimental apparatus end up diluting a stream that would be 100% pure CO_2. In other words, eliminating the contribution given by the air from the suction the stream recovered by heating is CO_2 100%vol. A remarkable result is that 80% of the captured

carbon dioxide can be recovered at a temperature of 130°C (which is a quiet mild desorption temperature) as a 100%vol. CO_2 stream. Moreover, as already shown in the previous paragraph, the dilution does not depend on the purge flow rate but only on the purge volume. So, the only way to limit the dilution effect is to make the purge time very short. Now, it is interesting to define a mean CO_2 concentration of the recovered stream (C_m), which takes into account the two separate steps of heating and purge. **Fig. 90**a and b report the trend obtained for C_m and the corresponding CO_2 recovery as a function of the purge time (t_p). For each curve the initial state is the end of the heating step. The CO_2 purity decreases immediately with the introduction of the purge gas, whereas the CO_2 recovery is accordingly increased. The observed decrease trend of C_m is obviously slower when the regeneration temperature is higher. Indeed, in this case, there is less CO_2 to desorb still remaining inside the bed, namely the majority of the whole CO_2 captured has already been desorbed during the heating step.

For each fixed value of CO_2 recovery it is possible, by elaborating the curves reported in **Fig. 90**, to obtain the value of CO_2 purity (C_m), thus obtaining a trend of C_m as a function of CO_2 recovery. **Fig. 91** shows the comparison between the two regeneration strategies at the different desorption temperatures. It is clear that for each desorption temperature the heating and purge strategy always makes it possible to enrich the stream of CO_2 recovered with respect to the isothermal purge strategy, the CO_2 recovery level being the same. However, at the lowest desorption temperatures (40 and 70°C) the difference between the two methods is not so remarkable since only a minor fraction of the total CO_2 captured is recovered due to heating (i.e. the majority of the CO_2 is still recovered by purge, thus making the two methods more or less equivalent). On the contrary, already at 100°C the difference starts becoming appreciable. Temperatures higher than 100°C are enough to obtain 100%vol. CO_2 purity with recovery levels higher than 50% and the maximum recovery still corresponding to a pure CO_2 stream increases with desorption temperatures. Obviously, even at the highest desorption temperatures, the trends of C_m corresponding to the two different regeneration strategies tend to converge with increasing the CO_2 recovery level. Indeed, even though for temperatures higher then 100°C more than 70% of the CO_2 is recovered as a pure stream after the heating step, with increasing CO_2 recovery levels the purge time becomes large enough to cause a remarkable dilution effect.
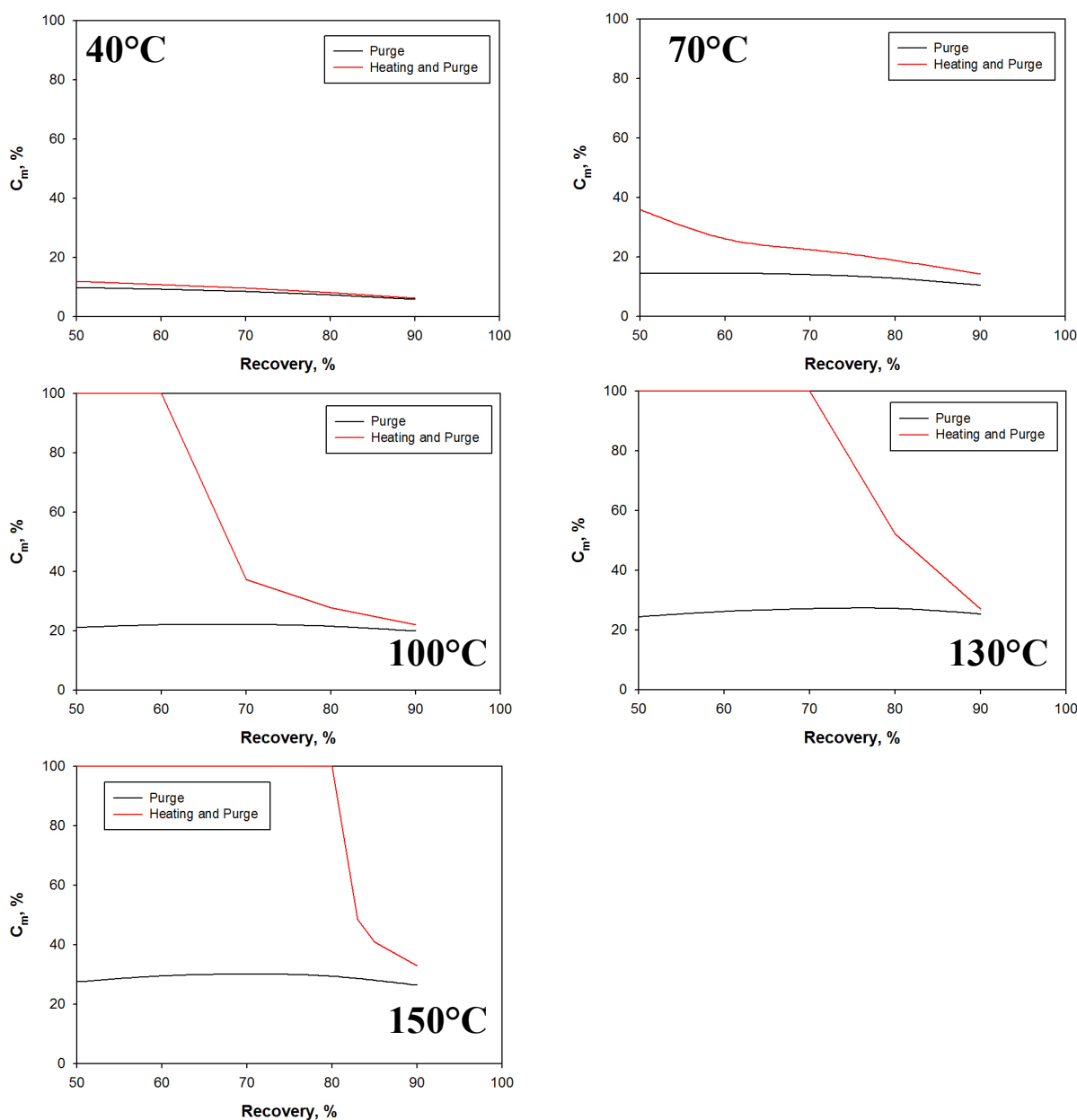
Fig. 91 a) CO$_2$ mean concentration as function of recovery obtained with the isothermal purge and heating and purge strategies at different T$_{des}$. Purge step: N$_2$ purge flow rate=67.8Nl h^{-1}; SPL=140dB; Sound frequency=80Hz. Adsorption step: SPL=140dB; Sound frequency=80Hz; inlet flow rate=67.8Nl h^{-1}; C$_0$=10%vol.

III.4.3   Cyclic Adsorption/Desorption Tests

TSA cyclic tests have been performed in order to verify the possibility of AC Norit reuse, to determine its CO$_2$ adsorption capacity within consecutive cycles of adsorption–desorption. In particular, the desorption stage has been carried out according to the isothermal purge strategy described in the Experimental section. **Fig. 92**a reports the CO$_2$ breakthrough curves and **Fig.**

124

92c the regeneration profiles obtained for all the consecutive adsorption/desorption cycles. These curves have been worked out to evaluate: n_{ads}, t_b, t_{95}-t_b and W.
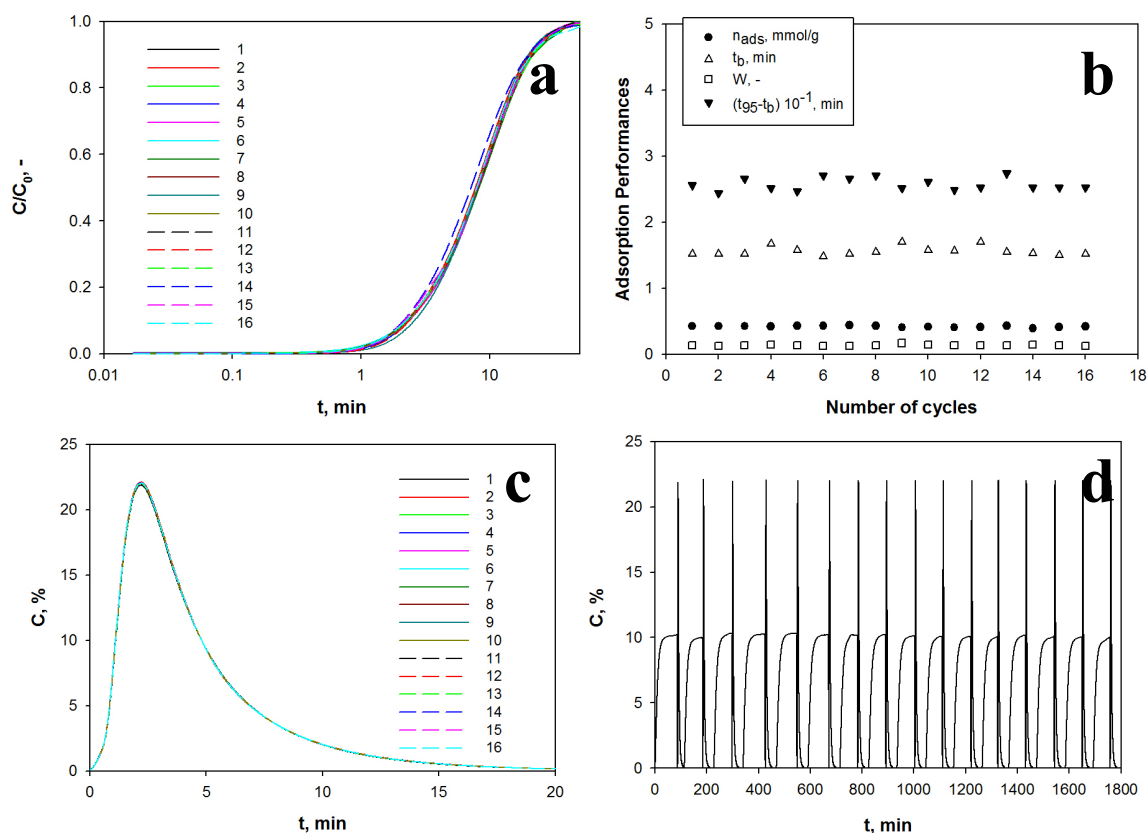
Fig. 92 Results of 16 adsorption/desorption cycles under sound assisted fluidization conditions. a) CO_2 outlet concentration profiles during consecutive adsorption tests; b) CO_2 adsorption performances vs the number of cycles; c) CO_2 outlet concentration profiles during consecutive desorption tests; d) sequence of 16 CO_2 adsorption/desorption cycles. Adsorption step: SPL=140dB; Sound frequency=80Hz; inlet flow rate=67.8Nl h^{-1}; C_0=10% vol. Desorption step: SPL=140dB; Sound frequency=80Hz; T_{des}=70°C; N_2 purge flow rate=67.8Nl h^{-1}.

The overlap of the adsorption/desorption profiles indicates that the activated carbon is very stable to cycles. Moreover, **Fig. 92**b reports all the parameters evaluated to define the CO_2 adsorption performances of the activated carbon over 16 consecutive adsorption–desorption cycles. Results clearly indicate that all the parameters are practically constant upon the number of cycles, thus implying that the material can be completely regenerated (i.e. adsorption is reversible) due to the establishment of relatively weak interactions between CO_2 molecule and the sorbent surface active sites, as widely confirmed by the related literature which commonly classifies activated carbons as physisorbents [62]. Most importantly, this feature is extremely desirable for potential industrial scale applications, especially if compared to other technologies based on solid sorbents (e.g. Calcium looping), which suffer from a rapid degradation of CO_2 capture capability during multiple capture/regeneration

125

cycles (caused for example by pore blocking or adsorbent sintering), thus requiring a continuous make-up of fresh sorbent.

III.5 Energy Cost Estimation

An estimation of the electricity consumption of CO_2 capture from a typical flue gas by a fixed bed adsorption process and subsequent sorbent regeneration is reported to be around $2MJ/kg_{CO2}$ [143]. In particular, this value was obtained under adsorption operating conditions which are very similar to those used in our work and regeneration operating conditions typical of activated carbons [144]. On the basis of this literature value and the data reported in **Fig. 55** (comparison among fixed bed, ordinary fluidized bed and sound assisted fluidized bed) an energy cost estimation can be evaluated for the sound assisted fluidized bed technology.

The sound generation system used in the experimental set-up implies an additional consumption of electrical energy under the application of acoustic fields. On the other hand, the increase of adsorption rate would yield a saving of energy during the adsorption phase, as the time needed for capturing a given amount of CO_2 would be reduced. Moreover, the application of the sound also increases the kinetics of the sorbent regeneration, as shown in the previous paragraphs, thus being energy saving also during the regeneration phase, as already assessed in a recent study.

On the basis of the experimental results obtained on lab-scale we can estimate the additional energy consumption related to the application of sound. When subjected to an acoustic field of 140dB-80Hz it can be evaluated that the reactor absorbs a power of around 2W (this energy requirements is the same in large scale applications). Considering for example the test performed at 1.5cm/s and 10%vol. of CO_2 inlet concentration on AC Norit, by taking into account the duration of the sound assisted test necessary to achieve a 90% capture (3.1min), corresponding to 0.12mmol/g of CO_2 captured, it gives an electricity consumption of $0.64MJ/kg_{CO2}$ ($178kWh/ton_{CO2}$).

However, this is not an effective additional cost with respect to the same test performed in ordinary fluidized bed or fixed bed conditions.

Indeed, making a comparison with the same amount of CO_2 adsorbed, the time needed to capture the same amount of CO_2 (0.12mmol/g) under ordinary fluidized bed and fixed bed (with pelletized sorbent) conditions is 12 and 5.4min, respectively. Considering that all the tests were performed at the same operating conditions, the energy required to pump the inlet gas flow during the first 3.1min is equivalent for all the tests.

Thus, the total energy consumption in all cases differs only by the energy required to sustain the process in ordinary fluidized bed and fixed bed tests for the additional time (about 9 and 2min, respectively) as compared to the energy necessary for generating the acoustic field during the sound assisted test (3.1min). In light of these considerations and assuming as reference the abovementioned literature data on the fixed bed conditions, the total electricity consumption for CO_2 adsorption and sorbent regeneration in a sound assisted fluidized bed can be estimated as high as 1.78MJ/kg_{CO2}. So, this value is lower than that corresponding to the use of fixed bed, and, most importantly, it is remarkably lower than that typically obtained in an amine based absorption process for post combustion CO_2 capture (up to 4.8MJ/ kg_{CO2} [28,145]).

III.6 Large Scale Application of Sound Assisted Fluidization

As carefully reviewed in a recent work [146], sono-processing has been proven as a useful technique way not only to improve the fluidization quality and gas-solid mixing but also to intensify heat/mass transfer controlled reactions in numerous processes carried out at high superficial gas velocity (1–10m/s). However, the superficial gas velocity of a sound assisted fluidized bed to be used in an actual industrial process strictly depends on the dimension of the particles. In particular, for fine particles (i.e. <100μm) to be used it is necessary to work with superficial gas velocities in the order of the cm/s. In this case one of the main problems regarding the scale-up of sound assisted fluidization arises from sound intensity attenuation across the bed height. In particular, for such fine materials and for low frequency sound waves (around 100Hz), it can be estimated that the SPL is reduced by 10dB for each 10cm of bed [146]. So, it would not be possible to use bed higher than 40-50cm. Accordingly, the only way to scale-up the process is represented by increasing the reactor diameter.

However, this diameter increase would lead to another cause of sound intensity attenuation, namely the divergence of the acoustic wave. At a large distance r from the source, the wave can be no longer considered as a plane wave and the total energy of the wave front is spread out over a spherical surface area $4\pi r^2$. Therefore, the intensity of the expanding spherical wave would be decreased proportionally to $1/r^2$. A feasible technique to avoid spherical spreading loss is to use an array of loudspeakers, which may produce a plane wave if conveniently placed. Theoretical calculations as well as already existing practical implementations for the physical reproduction of plane-wave acoustic fields by continuous planar and linear secondary source arrangements can be found in the specialized literature

[147,148]. Moreover, the use of an array of loudspeakers would also provide a greater reliability for continuous operation, since replacement of one of the loudspeakers can be easily carried out without the interruption of the sound assisted process.

III.7 CO$_2$ Capture by Ca-looping in a Sound Assisted Fluidized Bed

In this section the result of a study on the capture performance of a fluidized bed of CaO at Ca-looping conditions as affected by acoustic vibrations are reported. This research activity has been carried out at the Department of Electronics and Electromagnetism - Faculty of Physics - University of Seville. The aim of this research activity was to verify the capability of sound assisted fluidization to be to a different CO$_2$ capture process, which is characterized by remarkably higher operating temperatures.

Carbonation of CaO particles occurs in two phases [149]. A first fast carbonation stage is characterized by the sorption of CO$_2$ on the free surface of the particles. After that a thin layer of CaCO$_3$ (between 30 and 50nm thick [149]) covers the free surface of the sorbent particles and CO$_2$ sorption turns to be controlled by a much slower phase characterized by the diffusion of CO$_2$ through the solid CaCO$_3$ layer. It must be taken into account that carbonation of CaO during the fast phase proceeds under mass/heat transfer control. Thus, the rate of CO$_2$ capture in the fast phase by a fluidized bed is not just controlled by the kinetics of the chemical reaction itself, but also by the transport of CO$_2$ and heat to the particles surface. In this regard, carbonation can be hindered by poor and heterogeneous gas/solids contact and mass/heat transfer [150].

Acoustic vibrations are useful to promote gas/solids mixing uniformity in fluidized beds by forcing particle vibrations, which reduces aggregation and disrupts gas channels thus homogenizing fluidization and increasing the gas/solids contact efficiency [131]. On the other hand, sound waves induce a number of phenomena taking place at the gas/solids interface, such as acoustic streaming, which contribute to enhance mass/heat transfer rates in gas/solids reactors [151]. The fundamental principle is that attenuation of acoustic energy flux makes momentum flux available to force streaming motions around the solids. Accordingly, it is seen that the imposition of acoustic vibrations on a steady gas flow yields remarkable improvements in the efficiency of industrial processes such as fuel combustion, pyrometallurgical, and pollutant removal processes involving gas-solid reactions at high temperatures [151]. Altogether, the improvement of gas/solids contact efficiency in a heterogeneous fluidized bed and the enhancement of mass/heat transfer at the gas/solids

interface, would serve to enhance fast capture of CO_2 in a fluidized bed carbonator at Ca-looping conditions.

Natural limestones are considered as the most suitable candidates to be employed in the Ca-looping process due to their low price, wide availability and easy handling [152]. The capture capacity of calcined limestones in the fast phase decreases with increasing the number of calcination/carbonation cycles, which is attributed to the decrease of the sorbent reactive surface area as a result of material sintering during calcination at high temperatures [150,152]. Most natural limestones exhibit a residual fast capture capacity that remains constant after a large number of cycles, which is just about 0.06 (grams of CO_2 sorbed/grams of CaO) [153]. Such a small value can be compensated by high solid circulation rates to obtain sustained capture efficiencies in pilot plants [154]. Nevertheless, enhancing the fast capture capacity and regenerability of Ca-based sorbents would represent a substantial benefit on the CaL process performance as long as it would allow for a reduction of the solid circulation rates and energy requirements in the calciner [152].

III.7.1 Experimental Section

III.7.1.1 Materials

CaO from Sigma Aldrich has been used as CO_2 sorbent. **Fig. 93**a reports the particle size distributions and the Sauter mean diameter of the powder obtained by means of laser based diffractometry using a Mastersizer 2000, Malvern Instruments. According to the Sauter mean diameter, reported in **Tab. 26**, the powder belongs to Group C of Geldart classification.
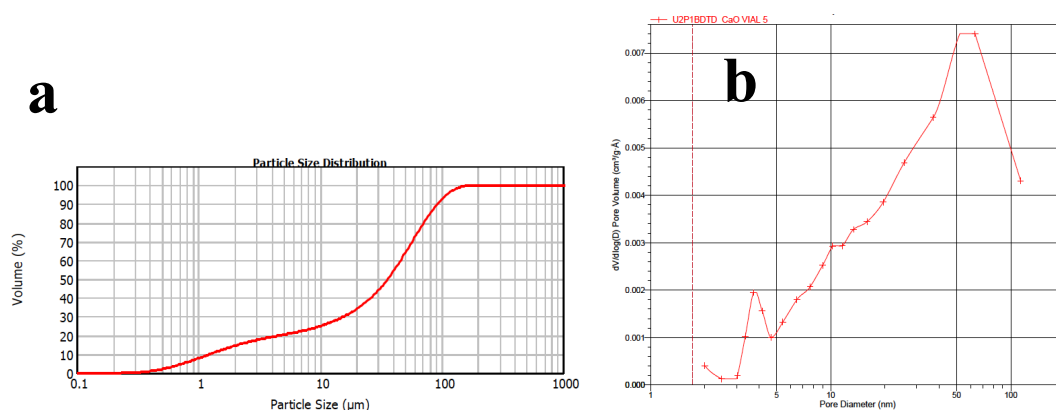
Fig. 93 a) Particle size distribution of CaO samples suspended in isopropanol (stirred and ultrasonicated); b) Pore size distribution of CaO.

Tab. 26 Properties of CaO.

Materials	D_{SAUTER}, μm with US	BET surface area, m^2/g
CaO	4.27	2.79

Fig. 93b reports the pore size distribution and **Tab. 26** the BET surface area. CaO is basically mesoporous (2nm < d < 100nm) and it is characterized by a very low surface area.

III.7.1.2   Experimental Apparatus

The experimental setup used in these experiments is schematized in **Fig. 94**. The material (100g), corresponding to a bed height of 5cm, is placed in a 50mm i.d. quartz reactor where it rests over a porous quartz plate that serves as gas distributor.
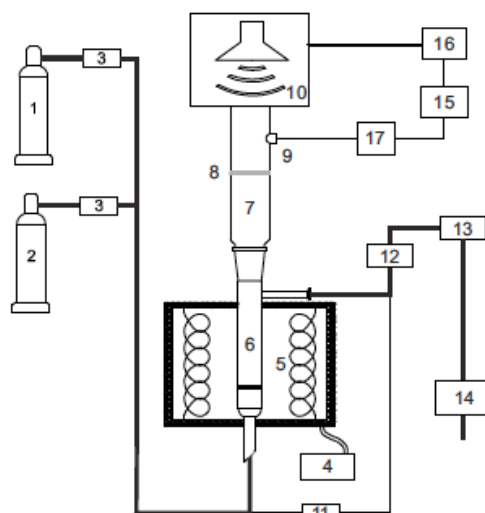
Fig. 94 Sketch of the experimental setup. 1: Compressed gas used for carbonation (15% CO$_2$/85% N$_2$ vol/vol). 2: Compressed gas used for calcination (dry air). 3: Mass flow controllers. 4: Temperature controller. 5: Furnace. 6: Quartz reactor. 7: Sound wave guide. 8: Elastic membrane. 9: Microphone. 10: Loudspeaker. 11: Differential pressure transducer. 12: Particulate filter. 13: Mass flow meter. 14: Gas analyzer. 15: Signal amplifier. 16: Signal generator. 17: Oscilloscope.

The sound generation system consists of a digital signal generator that produces an electric sine wave of fixed frequency, which is amplified by a power audio amplifier. The amplified signal excites a 8W woofer loudspeaker, which can be placed far from the high temperature zone thanks to the ability of sound waves to propagate through the gas without significant losses. The acoustic vibration is driven to the reactor by means of a PVC wave guide. The Sound Pressure Level is sampled by a l/4" condenser microphone. An elastic membrane in the sound wave guide serves to prevent gas leakages and to protect the loudspeaker from elutriated particles. Measurements of the differential gas pressure ΔP between a point just above the gas distributor plate and atmospheric pressure were also performed at ambient

temperature by using a 40mm i.d. polycarbonate cell to which acoustic vibrations could be also applied. The CO_2 concentration in the inlet and outlet gas streams has been measured by a Servomex 4900 infrared gas analyzer.

III.7.1.3   Preliminary Fluid-dynamic Characterization

The CaO has been previously characterized to assess its fluidization quality both in ordinary and sound assisted conditions, at atmospheric temperature and pressure. All the adopted sound parameters are reported in **Tab. 27**. For each test, pressure drop curves have been obtained.

Tab. 27 Operating conditions of the fluidization tests.

	SPL, dB	Frequency, Hz
CaO	130, 140, 150	100, 130, 160

III.7.1.4   Ca-looping Tests

All the operating conditions of the Ca-looping tests are reported in **Tab. 28**. For each test a fresh batch of CaO has been used. The inlet gas flow is fixed to 2000cm^3/min (which is about five times the u_{mf}) and can be switched to dry air (used for calcination) or to a mixture of 15%vol. of CO_2 in N_2 (used for carbonation) by means of mass flow controllers. The material is firstly subjected to a calcination step (T=900°C) for 15min during which $Ca(OH)_2$ and $CaCO_3$, present as impurities, decompose to CaO. A carbonation step (T=650°C) then proceeds, followed by subsequent calcination up to complete decarbonation. The CO_2 concentration in the column effluent gas is continuously monitored as a function of time during both carbonation and calcination steps.

Tab. 28 Operating conditions of the Ca-looping tests.

	SPL, dB	Frequency, Hz	CO_2 inlet concentration in N_2, %vol.
CaO	130, 140, 150	100, 130, 160	15

A preliminary study on the cyclic operation has been performed both in ordinary and sound assisted conditions (140dB-130Hz). In particular, a typical test consists of two carbonation/calcination cycles, performed on the same batch, namely without unloading the reactor.

III.7.2   Fluid-dynamic Characterization

Fig. 95 shows the dimensionless pressure drop vs. gas velocity for fresh CaO, which exhibits in ordinary conditions a rather heterogeneous behavior. Once the gas velocity is sufficiently high to fluidize the bed, ΔP is stabilized around a value notably smaller than the static weight of the bed (ΔP_0) and displays strong oscillations due to the visible development of transient channels through which the gas finds a bypass indicating very poor gas-solids contact efficiency.
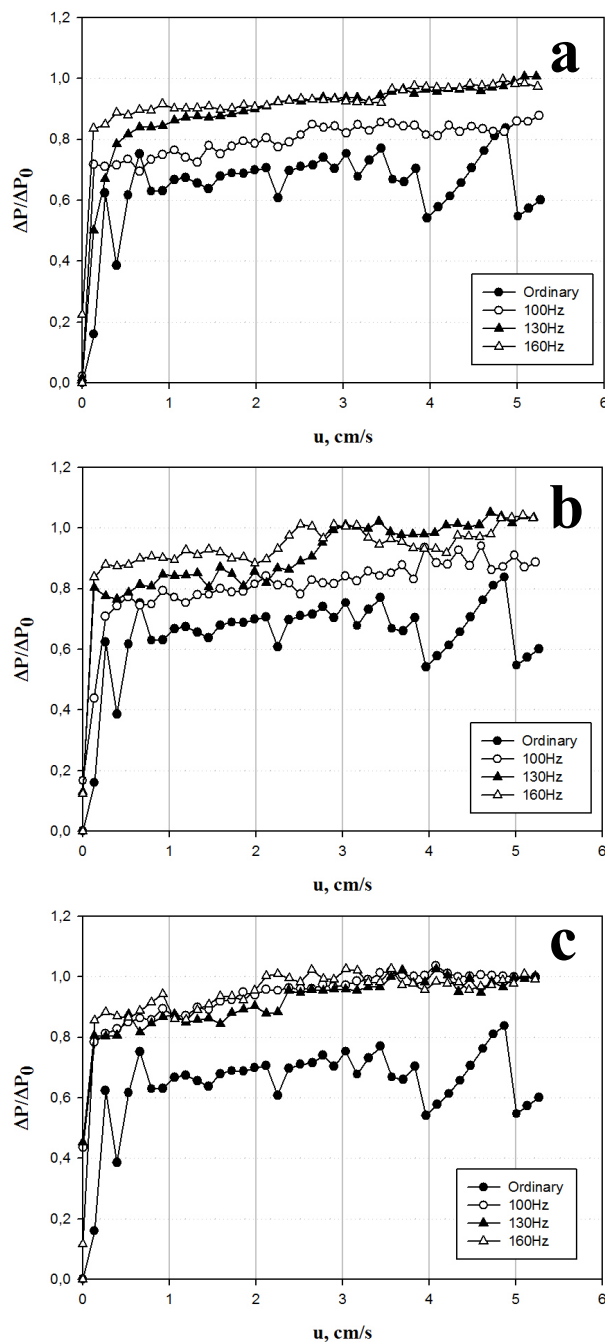
Fig. 95 Fluidization curves under ordinary and sound assisted conditions as affected by acoustic vibrations of different intensities, 130dB (a), 140dB (b) and 150dB (c), and frequencies (indicated).

On the other hand, **Fig. 95** demonstrates that acoustic vibrations serve to smooth the fluctuations of $\Delta P/\Delta P_0$, which reaches a plateau that approaches the unity. In particular, as regards the sound frequency, the improvement of the fluidization quality is far more remarkable passing from 100 to 130Hz, whereas a further increase to 160Hz causes a less evident effect. As regards the SPL, an increase of the sound intensity results in an improvement of the fluidization uniformity. Visually, it is observed that gas channels are destabilized, the bed is expanded and gas-solids mixing uniformity is improved. For example, applying sound of intensity ~150dB and frequency f = 130Hz, it is $\Delta P/\Delta P_0 \sim 1$ for gas velocities u > 2.5 cm/s, indicating fluidization uniformity.

III.7.3   Ca-looping Tests

CO_2 breakthrough curves as affected by acoustic vibrations are plotted in **Fig. 96**a, the curve obtained in ordinary conditions is also reported as comparison. In order to evaluate the efficiency of the Ca-loping process two parameters have been evaluated: t_5 and t_{10}, which are the time it takes for CO_2 outlet concentration to reach the 5 and 10% of the inlet concentration, respectively. All the results are reported in **Tab. 29**. As can be observed, the sound causes a significant drop of the CO_2 concentration measured in the effluent gas during the first minutes of carbonation (fast phase). This is also confirmed by the remarkable increase of t_5 observed for the sound assisted tests with respect to the ordinary one (**Tab. 29**). Moreover, as expected, there is a clear correlation between the enhancement of CO_2 capture in the fast phase, which is ruled by the gas-solids mass/heat transfer, and the improvement of fluidization uniformity (as seen in **Fig. 95**). The main effect is observed when the sound intensity is increased, while the effect of frequency is less relevant. Note also that the CO_2 breakthrough curves tend to converge at $t \simeq 50$min when $\%CO_2 \simeq 10\%$ (as clearly shown by the values obtained for t_{10}, reported in **Tab. 29**, which are substantially the same for all the tests). This suggests that from this point, CO_2 sorption becomes ruled by the slow diffusive phase for which the gas-solids mixing efficiency is not a determinant factor. As regards the effect of the sound parameters, the results obtained confirm the tight link existing between the fluidization quality and the effectiveness of the capture process. Indeed, as regards the frequency, a remarkable enhancement of the capture process can be observed passing from 100 to 130Hz, whereas a further increase of the sound frequency is substantially negligible. All these remarks are confirmed by the values of t_5 (**Tab. 29**). As regards the sound intensity, the results obtained confirm the beneficial effect deriving from an increase of SPL, which has

been observed in the fluidization tests. Indeed the test performed at 150dB is better then the test preformed at 140dB (being the frequency the same, 100Hz).
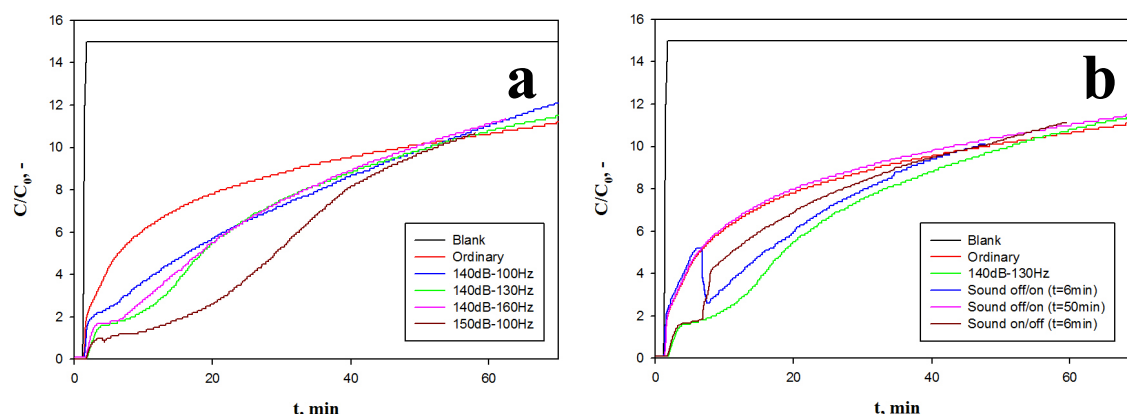
Fig. 96 a) CO_2 concentration in the effluent gas of the fludized bed (u=2.1cm/s) measured during carbonation as affected by acoustic vibrations. Results from blank tests (empty cell) are also shown. b) CO_2 breakthrough curves obtained by turning on/off the acoustic vibration.

In order to further confirm the capability of the sound in promoting the CO_2 capture an ad-hoc test has been performed. In particular, CO_2 breakthrough curves have been obtained by turning on/off the acoustic vibration during carbonation (**Fig. 96**b). Turning on acoustic vibration at t $\simeq$ 6 min yields a marked drop of the %CO_2 while turning it off gives rise to an increase of the %CO_2. Note, however, that in this latter case the CO_2 breakthrough curve keeps well below the curve obtained for the ordinary test in spite that the sound had been turned off. This indicates that the acoustic vibration applied during the first minutes of carbonation preconditioned the material behavior likely by irreversibly disrupting particle aggregates and destabilizing channels. On the other hand, **Fig. 96**b shows that application of sound when %CO_2 = 10% (t=50 min) does not affect CO_2 capture. At the slow carbonation stage, CO_2 sorption is no longer controlled mainly by the gas-solid contact efficiency but by the diffusion of CO_2 through the carbonate layer on the particles' surface. Thus, it is explainable that turning on sound when carbonation has reached the diffusion controlled stage does not yield a remarkable effect.

Tab. 29 Experimental results of the Ca-looping tests.

Sound Parameters	t_5, min	t_{10}, min
Ordinary	6	47
140dB-100Hz	16	51
140dB-130Hz	18	51
140dB-160Hz	18	49
150dB-100Hz	29	52

III.7.3.1   Effect of Sound on Repeated Carbonation/Calcination Cycles

Gas pressure drop curves, obtained both in ordinary and sound assisted conditions, for the material after being subjected to the second calcination step are plotted in **Fig. 97**a (the curves obtained for the fresh CaO are also reported for comparison). As indicated by the large fluctuations of $\Delta P/\Delta P_0$, the level of fluidization heterogeneity exhibited by the cycled CaO has further increased as compared to the fresh CaO.
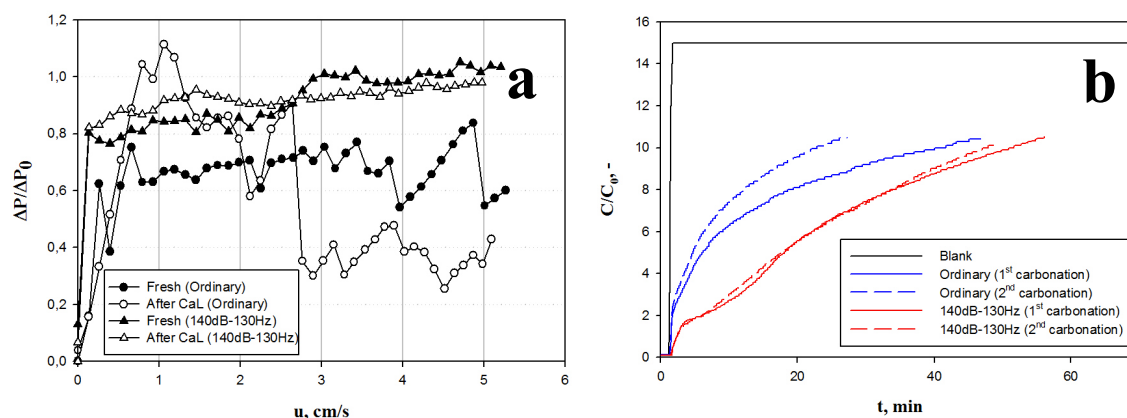
Fig. 97 a) Fluidization curves for fresh CaO and for CaO subjected to one calcination/carbonation cycle in ordinary and sound assisted conditions. b) CO₂ breakthrough curves obtained during the carbonation phases of two calcination/carbonation cycles carried out successively in ordinary and sound assisted conditions.

Note also that the particle size distribution (**Fig. 98**) of cycled CaO is shifted to smaller particle sizes due to its loss of mechanical strength, which makes the material more cohesive after one carbonation/calcination cycle. Nevertheless, application of acoustic vibrations on the cycled material serves to recover the material fluidizability.

Gas pressure drops curves for the fresh and cycled materials subjected to acoustic vibrations are similar (**Fig. 97**a), which leads us to expect that acoustic vibrations would serve not only to enhance the fast CO_2 capture capacity but also to improve the material regenerability after being cycled.
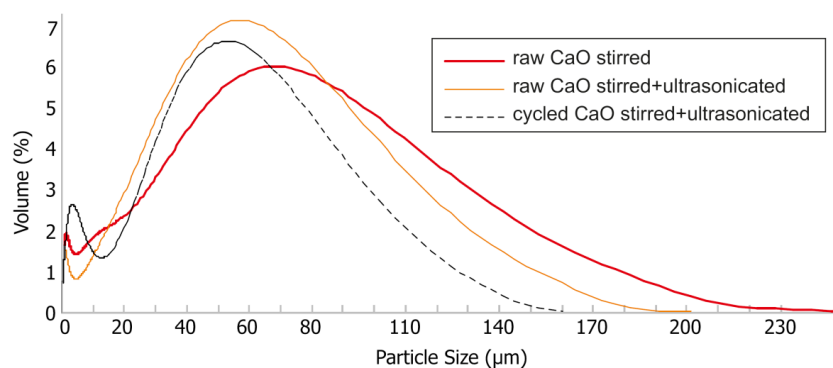
Fig. 98 Particle size distribution of CaO samples before and after one carbonation/calcination cycle.

This is confirmed by the CO_2 breakthrough curves obtained for 2 calcination/carbonation cycles performed successively. As can be observed in **Fig. 97**b, while the fast capture capacity of the material has decreased in the second cycle carried out in the absence of sound, application of acoustic vibrations yields a similar CO_2 breakthrough curve for the second carbonation, i.e. the fast capture capacity of the first cycle is maintained in the second cycle. It is worth noting that the application of the sound is effective only during the first stage of carbonation because regardless the sintering process within the pores (which is a thermal phenomenon not depending on the quality of gas-solid contact) the application of the sound avoids the phenomenon of sintering between particles (i.e. agglomeration) taking places during ordinary fluidization tests, thus consequently avoiding the collapse of the gas-solid contact efficiency, which is one of the key parameters ruling the fast carbonation stage.

In summary, these results, even though concerning a preliminary study, suggest that application of acoustic vibrations would be a highly effective method to enhance the efficiency of the Ca-looping technology for CO_2 capture.

IV CONCLUSIONS AND FUTURE PERSPECTIVES

The present PhD thesis has been focused on the study of a CO_2 capture process by temperature swing adsorption on fine porous materials in a sound-assisted fluidized bed reactor. In particular, the proposed reactor configuration should be capable to fully exploit the potential and properties of the sorbent by maximizing the contact between the CO_2 molecules and the adsorbent particles and to better control the temperature of the process.

To this aim the following steps have been followed:

- Design and setup of a laboratory-scale sound assisted fluidized bed reactor to perform an experimental campaign;
- Selection and chemico-physical and fluid-dynamic characterization of CO_2 adsorbent materials;
- Realization of adsorption tests to firstly assess the capability of sound assisted fluidization to promote the adsorption of CO_2 on fine powders and then to in-depth examine the main operating variables influencing the CO_2 adsorption process and compare the adsorption performances of all the selected sorbents;
- Choice and study of possible regeneration strategies and investigation of the main operating variables affecting the desorption process;
- Realization of cyclic adsorption/desorption tests, with assessment of the stability of the sorbents to cycles.

Design and setup of a suitable fluidized bed reactor

As a first step of the thesis, an experimental plant at a laboratory scale, which allows the contact between the sorbent material and a CO_2/N_2 mixture, has been designed and set up in order to perform adsorption/desorption tests. It consists of a Pyrex column, equipped with a system for the generation of the acoustic fields introduced inside the column through a sound wave guide located at the top of the freeboard. For the regeneration tests the reactor is externally heated by an ad-hoc designed heating jacket, i.e. provided with a window to allow

the fluidization quality to be visually assessed. The experimental apparatus is equipped with an analysis system for the continuous monitoring of the CO_2 concentration.

Selection of adsorbent materials

Commercial adsorbent materials, two activated carbons and HZSM-5 and 13 zeolites with different chemico-physical properties, were chosen, to firstly verify the capability of the sound assisted fluidization in actually promoting the CO_2 adsorption on fine powders, whereas a more specific adsorbent material was selected, to apply the sound assisted fluidization technology also to cutting-edge materials (metal organic framework HKUST-1). All the sorbents have been characterized by a chemico-physical and fluid-dynamic point of view.

Adsorption tests

The experimental results of the adsorption tests show that the application of the sound can improve the fluidization quality (by maximizing the gas-solid contact) as well as the adsorption efficiency of all the selected adsorbent materials in terms of remarkably higher breakthrough time, adsorption capacity, fraction of bed utilized until breakthrough and adsorption rate.

A systematic experimental campaign has been carried out at ambient temperature and pressure in order to highlight the effect of the main operating variables influencing the adsorption process:

- Sound parameters: the influence of SPL (120-140dB) and frequency (20-300Hz) on the adsorption efficiency reproduces that observed on the fluidization quality, thus confirming a tight link between the adsorption efficiency and the fluid-dynamics of the system. In particular, increasing SPLs yields a better adsorption performance, whereas, sound frequency has a not monotone effect on the fluidization quality and adsorption efficiency.
- CO_2 partial pressure: the CO_2 capture capacity increases with CO_2 partial pressure (0.05-0.15atm), coherently with the partial pressure being the thermodynamic driving force of the adsorption process.
- Fluidization velocity (0.1-4.5cm/s): the dependence of the breakthrough time on the contact time is linear for the tests performed in ordinary conditions, whereas, it is not monotone for the sound assisted tests.

At the end of the experimental campaign, all the investigated adsorbent materials have been compared and their different adsorption behaviours explained on the basis of their textural properties. HKUST-1 is by far the adsorbent characterized by the highest CO_2 adsorption

capacity, whereas, as regards the kinetics, it is slower than both the zeolites and activated Sigma Aldrich. In particular, it emerges that neither the BET surface area nor the total pore volume can account for their different adsorption performances. Indeed, under the investigated operating conditions the adsorption process is mainly affected by a specific microporosity (micropores falling in the range 8.3-12Å).

Regeneration tests

Desorption tests have been performed on the materials characterized by the best adsorption performances, the MOF (HKUST-1) and one of the activated carbons.

In particular, since HKUST-1 presents problems of thermal stability, thus constituting an upper limit for the desorption temperature to be used in a TSA process, an extra-situ regeneration strategy (150°C under a vacuum of 50mbar) has been developed to study the stability of HKUST-1 to cyclic adsorption/desorption operations. Ten adsorption/desorption cycles have been performed showing that HKUST-1 is very stable and keeps its adsorption performances over 10 adsorption/desorption cycles.

As regards AC Norit, which does not show significant limits on the choice of the desorption temperature, regeneration tests have been performed to recover the CO_2 from the spent sorbent by means of TSA in the sound assisted experimental apparatus. The standard regeneration strategy consists in an isothermal purge (N_2 is fluxed through the fluidization columns after the reactor has been heated to the desired desorption temperature).

CO_2 recovery and purity have opposing trends, so, it is always necessary to find the most convenient compromise between the two of them. In particular, due to the shape of desorbing profiles, a higher desorption time is expected to give a more effective regeneration, namely a higher CO_2 recovery, but it leads to a lower CO_2 mean concentration in the desorbing flow.

The results obtained show that the application of the sound makes it possible, from one hand, to remarkably increase the desorption rate (shorter desorption time needed to obtain the same CO_2 recovery) and, on the other, to significantly enrich the recovered CO_2 stream.

Similarly to the adsorption phase, the effect of the main operating variables affecting the regeneration efficiency has been evaluated:

- Desorption temperature (25-150°C): For each desorption temperature (even at ambient temperature) the activated carbon can always been completely regenerated (recovery=100%), thus confirming that the CO_2 molecules are only weakly bonded on its surface. Increasing desorption temperatures yield, from one hand, a faster desorption process due to faster adsorption kinetics, and, from the other, more concentrated CO_2 streams. Desorption temperatures higher than 70°C are always not

139

favorable, because, for all the investigated N_2 purge flow rates, the desorbing gas flow is more diluted than the gas stream treated during the adsorption step.

- N_2 purge flow rate (45.2-90.4Nl h^{-1}): the desorption rate is also positively affected by N_2 purge flow rate. Indeed, the time needed to obtain a desired CO_2 recovery monotonically decreases with increasing N_2 purge flow rate. On the contrary, it is noteworthy that the N_2 purge flow rate has influence neither on the maximum CO_2 concentration, which is mainly due to the desorption temperature, nor on the mean CO_2 concentration, which is mainly due to the total volume of CO_2 fluxed during the desorption test.

Aiming to the enrichment of the recovered CO_2 stream with respect to the standard desorption procedure, the heating and purge regeneration strategy has been tested, consisting in desorbing part of the CO_2 by the sole thermal effect, thus eliminating the unavoidable dilution effect caused by purge, and the remainder reducing the CO_2 partial pressure. The results obtained show that heating is very effective since 80% of the captured CO_2 can be can be recovered with a 100% purity at a bland desorption temperature of 130°C. Obviously, the CO_2 purity decreases immediately with the introduction of the purge gas, whereas the CO_2 recovery is accordingly increased. It is worth noting that for each desorption temperature the heating and purge strategy always makes it possible to enrich the stream of CO_2 recovered with respect to the standard purge strategy, the CO_2 recovery level being the same. In particular starting from temperatures of 100°C, it is always possible to obtain 100%vol. CO_2 purity with recovery levels higher than 50%. Obviously, the maximum recovery still corresponding to a pure CO_2 stream increases with desorption temperatures.

Cyclic adsorption/desorption tests

The possibility to use AC Norit in cyclic operation has been assessed. The results show that AC Norit can be completely regenerated due to the establishment of relatively weak interactions between CO_2 molecules and the sorbent surface active sites. Therefore, it is very stable, indeed it keeps its adsorption performances over 16 adsorption/desorption cycle.

Considerations about the energy cost and scale-up of the proposed technology for CO_2 capture by temperature swing adsorption have also been reported.

A parallel research activity has been carried out at the Department of Electronics and Electromagnetism - Faculty of Physics - University of Seville in order to further assess the capability of the sound in promoting the capture of CO_2. In particular, a lab-scale experimental study on the carbonation/decarbonation of a fluidized bed of CaO particles at Ca-looping conditions as affected by the application of a high-intensity acoustic field has also

been carried out. The results obtained demonstrate that both carbonation and decarbonation are remarkably enhanced for sound intensity levels above 140dB and frequencies of about 100Hz. The application of the sound yields a strong agitation of the bed and improves the gas-solid contact efficiency. On the other hand, an intense convection of gas flow (acoustic streaming) is generated on the surface of larger particles unmovable by the sound wave, which promotes the heat/mass transfer at the gas–solid boundary in this case. Either of these mechanisms, whose relative importance will depend on the average particle size and sound frequency, contribute to increase the carbonation and decarbonation rates of CaO fluidized beds in the Ca-looping technology.

With reference to the CO_2 capture by temperature swing adsorption, future perspectives for this PhD thesis could be the following:

- The effect of temperature on the capture process could be investigated. A flue gas stream may be available over a range of temperatures (120-220°C) depending on the design and process operation of the power generation system. Even though cooling to lower temperatures is possible, it represents additional cost and cooling water consumption. Therefore, there is a desire to treat the flue gas stream without cooling. So adsorption tests at higher temperatures could be performed. Considering the strong thermodynamic influence of temperature on adsorption capacity, a large impact on adsorption performance can be expected. It can be anticipated that also the regeneration step will be affected, since higher desorption temperatures will be required with respect to a capture step realized at ambient temperature.

- The effect of a change of purge gas could be assessed. Steam could be used, instead of N_2 as purge gas, for the regeneration of adsorbents, thus solving the problems of dilution effect typical of common TSA operations, since CO_2 could be very easily recovered by water condensation.

- The composition of a real flue gas could be more accurately simulated by adding some of the typical pollutants (SOx, NOx, HCl). This is most likely expected to affect the adsorption process due to competition phenomena of these pollutants with the CO_2 molecules.

V NOMENCLATURE

b	affinity coefficient between the adsorbent and adsorbed phases in the Langmuir equation
C	CO_2 concentration in the outlet stream
C_0	inlet CO_2 concentration
C_m	CO_2 mean concentration in the desorbing flow
f	sound frequency
H	actual bed height
H_0	initial bed height in condition of fixed bed
H/H_0	dimensionless bed expansion
n_{ads}	moles of CO_2 adsorbed per unit mass of adsorbent
$n_{CO_2}^s$	the moles of CO_2 adsorbed until saturation
ΔP	actual pressure drop across the bed
ΔP_0	pressure drop equal to buoyant weight of particles per unit area of bed
$\Delta P / \Delta P_0$	dimensionless pressure drop across the bed
P_{CO_2}	CO_2 partial pressure
$Q_{CO_2}^{IN}$	CO_2 inlet flow rate
$Q_{CO_2}^{OUT}$	CO_2 outlet flow rate
$Q_{N_2}^p$	N_2 purge flow rate
R	CO_2 recovery
r_{CO_2}	the rate of CO_2 concentration increase
SPL	Sound intensity
t_{10}	the time it takes for CO_2 outlet concentration to reach the 10% of the inlet concentration

t_5	the time it takes for CO_2 outlet concentration to reach the 5% of the inlet concentration
t_{95}	the time it takes for CO_2 to reach the 95% of the inlet concentration
t_{95}-t_b	time difference indication of the adsorption rate
t_b	breakthrough time or break point
t_c	contact time
t_d	desorption time
T_{des}	desorption temperature
u	superficial gas velocity
$V_d^{CO_2}$	total volume of CO_2 desorbed
$V_d^{N_2}$	N_2 purge gas volume
W	the fraction of bed utilized at breakpoint

VI REFERENCES

1. Song, C. (2006). Global challenges and strategies for control, conversion and utilization of CO_2 for sustainable development involving energy, catalysis, adsorption and chemical processing. Catalysis Today, 115(1-4), 2-32.

2. Boot-Handford, ME, Abanades, JC, Anthony, EJ Blunt, MJ, Brandani, F Dowell, Fernández, JR, Ferrari, MC, Gross, R, Hallett, JP, Haszeldine, RS, Heptonstall, P, Lyngfelt, A, Makuch, Z, Mangano, E, Porter, RTJ, Pourkashanian, M, Rochelle, GT, Shah, N, Yaoa, JG and Fennell, PS, (2014). Carbon capture and storage update, Energy Environ. Sci., 7, 130-189

3. Kenarsari, S.D., Yang, D., Jiang, G., Zhang, S., Wang, J., Russell, A.G., Weif, Q. and Fan, M., (2013) Review of recent advances in carbon dioxide separation and capture. RSC Adv., 3, 22739-22773.

4. IPCC, 2001c: Climate Change 2001: Mitigation. A Contribution of Working Group III to the Third Assessment Report of the Intergovernmental Panel on Climate Change [Metz, B., O. Davidson, R. Swart, and J. Pan (eds.)]. Cambridge University Press, Cambridge, United Kingdom and New York, NY, USA, 752 pp.

5. Yang, H., Xu, Z., Fan, M., Gupta, R., Slimane, R. B., Bland, A. E., & Wright, I. (2008). Progress in carbon dioxide separation and capture: a review. *Journal of environmental sciences*, *20*(1), 14-27.

6. D.M. Etheridge, L.P. Steele, R.L. Langenfelds, R.J. Francey, J.-M. Barnola, V.I. Morgan, Historical CO_2 record from the Law Dome DE08, DE08-2, and DSS ice cores (atmospheric CO_2 concentrations, Antarctic ice cores). in: Trends: A Compendium of Data on Global Change, on line at the Carbon Dioxide Information Analysis Center, http://cdiac.esd.ornl.gov/, June 1998.

7. Yamasaki A, (2003). An overview of CO_2 mitigation options for global warming – Emphasizing CO_2 sequestration options. Journal of Chemical Engineering of Japan, 36(4): 361–375.

8. Damen, K., Troost, M., Faaij, A., & Turkenburg, W. (2006). A comparison of electricity and hydrogen production systems with CO_2 capture and storage. Part A: Review and selection of promising conversion and capture technologies. Progress in Energy and Combustion Science, 32(2), 215-246.

9. Stewart, C. (2005). A study of methods of carbon dioxide capture and sequestration - the sustainability of a photosynthetic bioreactor approach. Energy Conversion and Management, 46(3), 403-420.

10. IPCC, 2001a: Climate Change 2001: The Scientific Basis. A Contribution of Working Group I to the Third Assessment Report of the Intergovernmental Panel on Climate Change [Houghton, J.T., Y. Ding, D.J. Griggs, M. Noguer, P.J. van der Linden, X. Dai, K. Maskell, and C.A. Johnson (eds.)]. Cambridge University Press, Cambridge, United Kingdom and New York, NY, USA, 881 pp.

11. C.D.Keeling, T.P. Whorf, Atmospheric CO_2 records from sites in the SiO air sampling network, in: Trends: A Compendium of Data on Global Change. Carbon Dioxide Information Analysis Center, Oak Ridge National Laboratory, U. S. Department of Energy, Oak Ridge, TN, USA, 2005.

12. Spigarelli, B. P., & Kawatra, S. K. (2013). Opportunities and challenges in carbon dioxide capture. Journal of CO_2 Utilization, 1, 69–87.

13. Tock, L., & Maréchal, F. (2014). Process design optimization strategy to develop energy and cost correlations of CO_2 capture processes. Computers & Chemical Engineering, 61, 51–58.

14. Mac Dowell, N., & Shah, N. (2013). Identification of the cost-optimal degree of CO_2 capture: An optimisation study using dynamic process models. International Journal of Greenhouse Gas Control, 13, 44-58.

15. Steeneveldt, R., Berger, B., & Torp, T. (2006). CO_2 Capture and Storage Closing the Knowing–Doing Gap. Chemical Engineering Research and Design, 84(9), 739-763.

16. Watson, J., Kern, F., & Markusson, N. (2014). Resolving or managing uncertainties for carbon capture and storage: Lessons from historical analogues. Technological Forecasting and Social Change, 81, 192-204.

17. Lotz, M., & Brent, A.C. (2008). A review of carbon dioxide capture and sequestration and the Kyoto Protocol's clean development mechanism and prospects for Southern Africa. Journal Of Energy In Southern Africa, 19(1), 13-24.

18. Martínez, I., Romano, M. C., Fernández, J. R., Chiesa, P., Murillo, R., & Abanades, J. C. (2014). Process design of a hydrogen production plant from natural gas with CO_2 capture based on a novel Ca/Cu chemical loop. Applied Energy, 114, 192-208.

19. IEA GHG, 2000a, Leading options for the capture of CO_2 emissions at power stations, Report Ph3/14. IEA Greenhouse Gas R&D Programme, Cheltenham, UK.

20. Figueroa, J.D., 2006. Carbon dioxide capture and sequestration potential and issues in the United States. APPA New Generation Meeting, Washington, DC.

21. Eckhause, J., & Herold, J. (2013). Using real options to determine optimal funding strategies for CO_2 capture, transport and storage projects in the European Union. Energy Policy, Article in Press, doi:10.1016/j.enpol.2013.11.030

22. Kanniche, M., Gros-Bonnivard, R., Jaud, P., Valle-Marcos, J., Amann, J.-M., & Bouallou, C. (2010). Pre-combustion, post-combustion and oxy-combustion in thermal power plant for CO_2 capture. Applied Thermal Engineering, 30(1), 53-62.

23. Damen, K., Troost, M., Faaij, A., & Turkenburg, W. (2006). A comparison of electricity and hydrogen production systems with CO_2 capture and storage. Part A: Review and selection of promising conversion and capture technologies. Progress in Energy and Combustion Science, 32(2), 215-246.

24. Ghoniem, A. F. (2011). Needs, resources and climate change: Clean and efficient conversion technologies. Progress in Energy and Combustion Science, 37(1), 15-51.

25. Wall, T., Stanger, R., & Liu, Y. (2013). Gas cleaning challenges for coal-fired oxy-fuel technology with carbon capture and storage. Fuel, 108, 85–90.

26. Mayer, F., Bidwe, A. R., Schopf, A., Taheri, K., Zieba, M., & Scheffknecht, G. (2014). Comparison of a new micaceous iron oxide and ilmenite as oxygen carrier for Chemical looping combustion with respect to syngas conversion. Applied Energy, 113, 1863–1868.

27. Lyngfelt, A. (2014). Chemical-looping combustion of solid fuels – Status of development. Applied Energy, 113, 1869–1873.

28. J. Merel, M. Clausse, F. Meunier, Experimental investigation on CO_2 post- combustion capture by indirect thermal swing adsorption using 13X and 5A zeolites, Ind. Eng. Chem. Res. 47 (2008) 209–215.

29. Thiruvenkatachari, R., Su, S., An, H., & Yu, X. X. (2009). Post combustion CO_2 capture by carbon fibre monolithic adsorbents. Progress in Energy and Combustion Science, 35(5), 438-455.

30. Figueroa, J. D., Fout, T., Plasynski, S., McIlvried, H., & Srivastava, R. D. (2008). Advances in CO_2 capture technology—The U.S. Department of Energy's Carbon Sequestration Program. International Journal of Greenhouse Gas Control, 2(1), 9-20.

31. Audus, H. (1997). Greenehouse gas mitigation technology: an overview of the CO_2 capture and sequestration studies and further activities of the IEA greenhouse gas R&D programme, Energy 22, 217–221.

32. Wang, M., Lawal, A., Stephenson, P., Sidders, J., & Ramshaw, C. (2010). Post-combustion CO_2 Capture with Chemical Absorption: A State-of-the-art Review. Chemical Engineering Research and Design, (May), 1-16.

33. Von Harbou, I., Imle, M., & Hasse, H. (2014). Modeling and simulation of reactive absorption of CO2 with MEA: Results for four different packings on two different scales. Chemical Engineering Science, 105, 179–190.

34. Von Harbou, I., Hoch, S., Mangalapally, H. P., Notz, R., Sieder, G., Garcia, H., Hasse, H. (2014). Removal of carbon dioxide from flue gases with aqueous MEA solution containing ethanol. Chemical Engineering and Processing: Process Intensification, 75, 81–89.

35. Mac Dowell, N., Samsatli, N. J., & Shah, N. (2013). Dynamic modelling and analysis of an amine-based post-combustion CO2 capture absorption column. International Journal of Greenhouse Gas Control, 12, 247–258.

36. Jayarathna, S. a., Lie, B., & Melaaen, M. C. (2013). Dynamic modelling of the absorber of a post-combustion CO2 capture plant: Modelling and simulations. Computers & Chemical Engineering, 53, 178–189.

37. Karla M, Wrightb RF, Berglena TF, Denbya B. Worst case scenario study to assess the environmental impact of amine emissions from a CO2 capture plant. Int J Greenhouse Gas Con 2011;5:439–47.

38. Zhao G, Aziz B, Hedin N. Carbon dioxide adsorption on mesoporous silica surfaces containing amine-like motifs. Appl Energy 2010;87:2907–13.

39. Pitts JN, Grosjean D, Vanmcauwenberghe K, Schmidt JP, Fitz DR. Photooxidation of aliphatic amines under simulated atmospheric conditions: formation of nitrosamines, nitramines, amides, and photochemical oxidant. Environ Sci Technol 1978;12:946.

40. Reh BD, DeBord DG, Butler MA, Reid TM, Mueller C, Fajen JM. O6- methylguanine DNA adducts associated with occupational nitrosamine exposure. Carcinogenesis 2000;21:29–33.

41. Zeng, Q., Zuo, Y.-bo, Fan, C.-gang, & Chen, C.-sheng. (2009). CO_2-tolerant oxygen separation membranes targeting CO_2 capture application. Journal of Membrane Science, 335(1-2), 140-144.

42. Yeo, Z. Y., Chew, T. L., Zhu, P. W., Mohamed, A. R., & Chai, S.P. (2013). Synthesis and performance of microporous inorganic membranes for CO_2 separation: a review. Journal of Porous Materials, 20(6), 1457–1475.

43. Olajire, A. a. (2010). CO_2 capture and separation technologies for end-of-pipe applications – A review. Energy, 35(6), 2610-2628.

44. Olajire, A. a. (2013). A review of mineral carbonation technology in sequestration of CO2. Journal of Petroleum Science and Engineering, 109, 364–392.

45. Mayoral, M. C., Andrés, J. M., & Gimeno, M. P. (2013). Optimization of mineral carbonation process for CO_2 sequestration by lime-rich coal ashes. Fuel, 106, 448–454.

46. Pacheco, F. G., Voga, G. P., de Lima, G. M., & Belchior, J. C. (2013). Optimization of a lime-based sorbent for carbonation at low temperature enhanced by water vapor. Fuel, 106, 827–836.

47. Pirngruber, G. D., Guillou, F., Gomez, a., & Clausse, M. (2013). A theoretical analysis of the energy consumption of post-combustion CO_2 capture processes by temperature swing adsorption using solid sorbents. International Journal of Greenhouse Gas Control, 14, 74–83.

48. D.M. Ruthven, Principles of Adsorption and Adsorption Processes, Wiley-Interscience, New York, 1984.

49. Sing, K. S. W., Everett, D. H., Haul, R. A. W., Moscou, L., Pierotti, R. A., Rouquérol, J., & Siemieniewska, T. (1985). INTERNATIONAL UNION OF PURE COMMISSION ON COLLOID AND SURFACE CHEMISTRY INCLUDING CATALYSIS * REPORTING PHYSISORPTION DATA FOR GAS / SOLID SYSTEMS with Special Reference to the Determination of Surface Area and Porosity. Pure & Applied Chemistry, 57(4), 603–619.

50. Brunauer, S., Emmett, P. H., & Teller, E. (1936). Gases in Multimolecular Layers. Journal of the American Chemical Society, 407(1), 309–319.

51. R.T. Yang, Gas Separation by Adsorption Processes, Imperial College Press, Boston, 1997

52. Scholl, S. (1993). Adsorption and desorption kinetics in activated carbon. Gas Separation & Purification, 7(4), 207-212.

53. Sayari, A., Belmabkhout, Y., & Serna-guerrero, R. (2011). Flue gas treatment via CO_2 adsorption. Chemical Engineering Journal, 1-15.

54. Ho, M.T., Allinson, G.W., Wiley, D.E. (2008). Reducing the cost of CO_2 capture from flue gases using pressure swing adsorption, Ind. Eng. Chem. Res. 47 4883–4890.

55. Sjostrom, A., Krutka, H. (2010). Evaluation of solid sorbents as a retrofit technology for CO_2 capture, Fuel 89 1298–1306

56. D. Aaron, C. Tsouris, Separation of CO_2 from flue gas: a review, Sep. Sci. Technol. 40 (2005) 321–348.

57. D'Alessandro, D. M., Smit, B., & Long, J. R. (2010). Carbon dioxide capture: prospects for new materials. Angewandte Chemie (International ed. in English), 49(35), 6058-82.

58. C.J. Major, B.J. Sollami, K. Kammermeyer, Carbon dioxide removal from air by adsorbents, Ind. Eng. Chem. Process Des. Dev. 4 (1965) 327–333

59. D. Lozano-Castello, D. Cazorla-Amoros, A. Linares-Solano, Powdered activated carbons and activated carbon fibers for methane storage: a comparative study, Energy Fuels 16 (2002) 1321–1328.

60. C.G. Coe, Structural effects on the adsorptive properties of molecular sieves for air separation, in: T.J. Pinnavaia, M.F. Thorpe (Eds.), Access in Nanoporous Materials, Plenum Press, New York, 1995, pp. 213–229.

61. S. Hayashi, M. Kawai, T. Kaneko, Dynamics of high purity oxygen PSA, Gas Sep. Purif. 10 (1996) 19–23.

62. V.S. Filipe, C.A. Lopes, A.M. Grande, J.M. Ribeiro, E. Loureiro, V. Oikonomopoulos, A.E. Nikolakis, Rodrigues, Adsorption of H_2, CO_2, CH_4, CO, N_2 and H_2O in activated carbon and zeolite for hydrogen production, Sep. Sci. Technol. 44 (2009) 1045–1073.

63. F. Dreisbach, R. Staudt, J.U. Keller, High pressure adsorption data of methane, nitrogen, carbon dioxide and their ternary mixture on activated carbon, Adsorption 5 (2005) 215–227.

64. Y. Kurniwan, S.K. Bathia, V. Rudolph, Simulation of binary mixture adsorption of methane and CO_2 at supercritical conditions in carbons, AIChE J. 52 (2006) 957–967.

65. S. Himeno, T. Komatsu, S. Fujita, High-pressure adsorption equilibria of methane and carbon dioxide on several activated carbons, J. Chem. Eng. Data 50 (2005) 369–376.

66. D.D. Do, K.A. Wang, New model for the description of adsorption kinetics in heterogeneous activated carbon, Carbon 36 (1998) 1539–1554.

67. F. Dreisbach, R. Staudt, J.U. Keller, Experimental investigation of the kinetics of adsorption of pure gases and binary gas mixtures on activated carbon, in: F. Meunier (Ed.), Proceedings of Fundamental of Adsorption 6, Elsevier, Amsterdam, 1998, pp. 1219–1224.

68. Y. Belmabkhout, R. Serna-Guerrero, A. Sayari, Adsorption of CO_2 from dry gases on MCM-41 silica at ambient temperature and high pressure. 1: pure CO_2 adsorption, Chem. Eng. Sci. 64 (2009) 3721–3728.

69. Ch. Baerlocher, L.B. McCusker, D.H. Olson, Atlas of Zeolite Structure TypesEDN 6th revised ed., Elsevier, Amsterdam, 2007.

70. R.V. Siriwardane, M.S. Shen, E.P. Fisher, J.A. Poston, Adsorption of CO_2 on molecular sieves and activated carbon, Energy Fuels 15 (2001) 279–284.

71. A. Goj, D.S. Sholl, E.D. Akten, D.J. Kohen, Atomistic simulations of CO_2 and N_2 adsorption in silica zeolites: the impact of pore size and shape, Phys. Chem. B 106 (2002) 8367–8375.

72. P.J.E. Harlick, F.H. Tezel, An experimental adsorbent screening study for CO_2 removal from N_2,Micropor. Mesopor. Mater. 76 (2004) 71–79.

73. C. Lu, H. Bai, B. Wu, F. Su, J.F. Hwang, Comparative study of CO_2 capture by carbon nanotubes, activated carbon, and zeolites, Energy Fuels 22 (2008) 3050–3056.

74. N. Konduru, P. Lindner, N.M. Assaf-Annid, Curbing the greenhouse effect by carbon dioxide adsorption with zeolite 13X, AIChE J. 53 (2007) 3137–3143.

75. J. Zhang, P.A. Webley, P. Xiao, Effect of process paramaters on power requirements of vacuum swing adsorption technology for CO_2 capture from flue gas, Energy Convers. Manage. 49 (2008) 346–356.

76. G. Li, P. Xiao, P.A. Webley, J. Zhang, R. Singh, M. Marshal, Capture of CO_2 from high humidity flue gas by vacuum swing adsorption with 13X, Adsorption 14 (2008) 415–422.

77. J. Zhang, P.A. Webley, Cycle development and design for CO_2 capture from flue gas by vacuum swing adsorption, Environ. Sci. Technol. 42 (2008) 563–569.

78. R.M. Barrer, R.M. Gibbons, Zeolitic carbon dioxide: energetics and equilibrium in relation to exchangeable cations in faujasite, J. Chem. Soc., Faraday Trans. 61 (1965) 948–961.

79. K.S. Walton, M.B. Abney, M.D. LeVan, CO_2 adsorption in Y and X zeolites modified by alkali metal cation exchange, Micropor. Mesopor. Mater. 91 (2006) 78–84.

80. G. Maurin, P.L. Llewellyn, R.G. Bell, Adsorption mechanism of carbon dioxide in Faujasites: Grand Canonical Monte Carlo simulations and microcalorimetry measurements, J. Phys. Chem. B 109 (2005) 16084–16091.

81. G.D. Pirngruber, P. Raybaud, Y. Belmabkhout, J. Cejka, A. Zukal, The role of extraframework cations in the adsorption of CO_2 on faujasite Y, Phys. Chem. Chem. Phys. 12 (2010) 13534–13546.

82. S. Choi, J.H. Drese, C.W. Jones, Adsorbent materials for carbon dioxide capture from large anthropogenic point sources, ChemSusChem 2 (2009) 796–854.

83. F. Brandani, D. Ruthven, The effect of water on the adsorption of CO_2 and C_3H_8 on Type X zeolites, Ind. Eng. Chem. Res. 43 (2004) 8339–8344.

84. Petit, C., Burress, J., & Bandosz, T. J. (2010). The synthesis and characterization of copper-based metal – organic framework/graphite oxide composites. Carbon, 49(2), 563–572.

85. James SL Metal–organic frameworks. Chem Soc Rev 2003;32:276–88.

86. O. M. Yaghi, M. O'Keeffe, M. W. Ockwing, M. Chae, M. Eddaoudi, J. Kim, Reticular synthesis and the design of new materials, Nature 423 (2003) 705–714.

87. G. Ferey, Hybrid porous solids: past, present, future, Chem.Soc. Rev. 37 (2008) 191–214.

88. Liu, J., Thallapally, P. K., Mcgrail, B. P., Brown, D. R., & Liu, J. (2012). Chem Soc Rev Progress in adsorption-based CO_2 capture by metal – organic frameworks, 2308–2322.

89. Eddaoudi, M., Kim, J., Rosi, N., Vodak, D., Wachter, J., O'Keeffe, M., & Yaghi, O. M. (2002). Systematic design of pore size and functionality in isoreticular MOFs and their application in methane storage. Science (New York, N.Y.), 295(5554), 469–72.

90. O'Keeffe, M. (2009). Design of MOFs and intellectual content in reticular chemistry: a personal view. Chemical Society reviews, 38(5), 1215–1217.

91. S. Kitagawa and R. Matsuda. Chemistry of coordination space of porous coordination polymers. Coord. Chem. Rev., 2007, 251, 2490–2509.

92. Férey, G. (2008). Hybrid porous solids: past, present, future. Chemical Society reviews, 37(1), 191–214.

93. M. P. Suh, Y. E. Cheon and E. Y. Lee. Syntheses and functions of porous metallosupramolecular networks Coord. Chem. Rev., 2008, 252, 1007–1026.

94. Wang, Z., & Cohen, S. M. (2009). Postsynthetic modification of metal-organic frameworks. Chemical Society reviews, 38(5), 1315–1329.

95. H. L. Li, M. Eddaoudi, M. O'Keeffe and O. M. Yaghi (1999). Design and synthesis of an exceptionally stable and highly. Nature, 402(November), 276–279.

96. Rowsell, J. L. C., Spencer, E. C., Eckert, J., Howard, J. a K., & Yaghi, O. M. (2005). Gas adsorption sites in a large-pore metal-organic framework. Science (New York, N.Y.), 309(5739), 1350–1354.

97. Rosi, N. L., Eckert, J., Eddaoudi, M., Vodak, D. T., Kim, J., O'Keeffe, M., & Yaghi, O. M. (2003). Hydrogen storage in microporous metal-organic frameworks. Science (New York, N.Y.), 300(5622), 1127–1129.

98. Mueller, U., Schubert, M., Teich, F., Puetter, H., Schierle-Arndt, K., & Pastré, J. (2006). Metal–organic frameworks—prospective industrial applications. Journal of Materials Chemistry, 16(7), 626-636.

99. A.R. Millward, O.M. Yaghi, Metal-organic frameworks with exceptionally high capacity for storage of carbon dioxide at room temperature, J. Am. Chem. Soc. 127 (2005) 17998–17999.

100. P.L. Llewellyn, S. Bourrelly, C. Serre, A. Vimont, M. Daturi, L. Hamon, G. De Weireld, J.S. Chang, D.Y. Hong, Y.K. Hwang, S.H. Jhung, G. Ferey, High uptakes of CO_2 and CH_4 in mesoporous metal-organic frameworks MIL-100 and MIL-101, Langmuir 24 (2008) 7245–7754.

101. Q. Yang, C. Zhong, J.F. Chen., Computational study of CO_2 storage in metal-organic frameworks, J. Phys. Chem. C 112 (2008) 1562–1569.

102. V. Finsy, L. Ma, L. Alaert, D.E. De Vos, C.V. Baron, J.F.M. Denayer, Separation of CO_2 mixtures with the MIL-53 (Al) metal-organic framework, Micropor. Mesopor. Mater. 120 (2009) 221–227.

103. D. Britt, H. Furukawa, H.B. Wang, T.G. Glover, O.M. Yaghi, Highly efficient separation of carbon dioxide by metal-organic framework replete with open metal sites, PNAS 106 (2009) 20637–20640.

104. R. Banerjee, A. Phan, P. Wang, C. Knobler, H. Furukawa, M. O'Keeffe, O.M. Yaghi, High throughput synthesis of zeolitic imidazolate frameworks and application to CO_2 capture, Science 319 (2008) 939–943.

105. R. Banerjee, H. Furukawa, D. Britt, C. Kobler, M. O'Keeffe, O.M. Yaghi, Control of pore size and functionality in isoreticular zeolitic imidazolate frameworks and their carbon dioxide selective capture properties, J. Am. Chem. Soc. 131 (2009) 3875–3877.

106. B. Wang, A. Cote, H. Furukawa, M. O'Keeffe, O.M. Yaghi, Colossal cages in zeolitic imidazolate framework as selective carbon dioxide reservoirs, Nature 453 (2008) 207–211.

107. S.R. Caskey, A.G. Wong-Foy, A.J. Matzger, Dramatic tuning of carbon dioxide uptake via metal substitution in a coordination polymer with cylindrical pores, J. Am. Chem. Soc. 130 (2008) 10870–10871.

108. A.O. Yazaydin, R.Q. Snurr, T.H. Park, K. Koh, J. Liu, M.D. LeVan, A.I. Benin, P. Jakubczak, M. Lanuza, D.B. Galloway, J.J. Low, R.R. Willis, Screening of metal-organic frameworks for carbon dioxide capture from flue gas using a combined experimental and modeling approach, J.Am.Chem.Soc.131(2009) 18198–18199.

109.   Y.S. Bae, O.K. Farha, A.M. Spokoyny, C.A. Mirkin, S. Punatahnam, J.T. Hupp, Q.R. Snurr, Carborane-based metal-organic frameworks as highly selective sorbents for CO_2 over methane, Chem. Commun. (2008) 4135–4137.

110.   L. Bastin, P.S. Barcia, E.J. Hurtado, J.A.C. Silva, A.E. Rodrigues, B. Chen, A Microporous metal-organic framework for separation of CO_2/N_2 and CO_2/CH_4 by fixed-bed adsorption, J. Phys. Chem. C 112 (2008) 1575–1581.

111.   B. Liu, B. Smit, Comparative Molecular simulation study of CO_2/N_2 and CH_4/N_2 separation in zeolites and metal-organic frameworks, Langmuir 25 (2008) 5918–5926.

112.   A.I. Skoulidas, D.S. Sholl, Self-diffusion and transport of light gases in metal-organic framework materials assessed using molecular dynamics simulations, J. Phys. Chem. B 109 (2005) 15760–15768.

113.   Babarao, R., & Jiang, J. (2008). Diffusion and separation of CO_2 and CH_4 in silicalite, C168 schwarzite, and IRMOF-1: a comparative study from molecular dynamics simulation. Langmuir : the ACS journal of surfaces and colloids, 24(10), 5474–5484.

114.   Yang, Q., Zhong, C., & Chen, J.-F. (2008). Computational Study of CO_2 Storage in Metal-Organic Frameworks. Journal of Physical Chemistry C, 112(5), 1562–1569.

115.   Zhao, Z., Li, Z., & Lin, Y. S. (2009). Adsorption and Diffusion of Carbon Dioxide on Metal−Organic Framework (MOF-5). Industrial & Engineering Chemistry Research, 48(22), 10015–10020.

116.   F. Salles, H. Jobic, G. Maurin, M. M. Koza, P. L. Liewellyn, T.Devic, C. Serre andG. Ferey, Experimental evidence supported by simulations of the hydrogen super-mobility in metal-organic frameworks materials. Phys.Rev.Lett., 2008, 100, 245901.

117.   J. Liu, Y. Wang, A. I. Benin, P. Jakubczak, R. R. Willis and M. D. LeVan, CO_2/H_2O adsorption equilibrium and rates on metal-organic frameworks: HKUST-1 and Ni/DOBDC. Langmuir, 2010, 26, 14301–14307.

118.   Thiruvenkatachari, R., Su, S., Yu, X. X., & Bae, J.-S. (2013). Application of carbon fibre composites to CO_2 capture from flue gas. International Journal of Greenhouse Gas Control, 13, 191–200.

119.   Kikkinides, E.S., Yang, R.T., Cho, S.H., 1993. Concentration and recovery of carbon dioxide from flue gas by pressure swing adsorption. Industrial and Engineering Chemistry Research 32, 2714–2720.

120.   Dutcher, B., Adidharma, H., Radosz, M., 2011. Carbon filter process for flue-gas carbon capture on carbonaceous sorbents: steam-aided vacuum swing adsorption option. Industrial and Engineering Chemistry Research 50, 9696–9703.

121.   Xiao, P., Zhang, J., Webley, P., Li, G., Singh, R., Todd, R., 2008. Capture of CO2 from flue gas streams with zeolite 13X by vacuum-pressure swing adsorption. Adsorption 14, 575–582.

122.   Plaza, M.G., García, S., Rubiera, F., Pis, J.J., Pevida, C., 2010. Post-combustion CO2 cap- ture with a commercial activated carbon: comparison of different regeneration strategies. Chemical Engineering Journal 163, 41–47.

123.   Yu, C.-H. (2012). A Review of CO2 Capture by Absorption and Adsorption. Aerosol and Air Quality Research, 745–769.

124.   Wang, X., Liu, L.-H., Ramström, O., & Yan, M. (2009). Engineering nanomaterial surfaces for biomedical applications. Experimental biology and medicine (Maywood, N.J.), 234(10), 1128-39.

125.   Keramati, M., & Ghoreyshi, A. A. (2014). Improving CO_2 adsorption onto activated carbon through functionalization by chitosan and triethylenetetramine. Physica E: Low-dimensional Systems and Nanostructures, 57, 161–168.

126.   Dawson, R., Cooper, A. I., & Adams, D. J. (2013). Chemical functionalization strategies for carbon dioxide capture in microporous organic polymers. Polymer International, 62(3), 345–352.

127.   Sjostrom, S., Krutka, H., Starns, T., & Campbell, T. (2011). Pilot test results of post-combustion CO_2 capture using solid sorbents. Energy Procedia, 4, 1584–1592.

128.   Yang, W.C., & Hoffman, J. (2009). Exploratory Design Study on Reactor Configurations for Carbon Dioxide Capture from Conventional Power Plants Employing Regenerable Solid Sorbents. Industrial & Engineering Chemistry Research, 48(1), 341–351.

129.   Zhu, C., Yu, Q., Dave, R.N., Pfeffer, R. (2005). Gas fluidization characteristics of nanoparticles agglomerates, AIChE J. 51 426–439.

130.   Wang, Y., Gu, G., Fei, W., Wu, J. (2002). Fluidization and agglomerate structure of SiO_2 nanoparticles, Powder Technol. 124 152–159.

131.   Ammendola, P., Chirone, R., & Raganati, F. (2011). Effect of mixture composition, nanoparticle density and sound intensity on mixing quality of nanopowders. Chemical Engineering and Processing: Process Intensification, 50(8), 885-891.

132.   Wang, X., Rahman, R.F., Rhodes, M.J. (2007) Nanoparticle fluidization and Geldart's classification, Chem. Eng. Sci. 62 3455–3461.

133.   Ammendola, P., Chirone, R., & Raganati, F. (2011). Fluidization of binary mixtures of nanoparticles under the effect of acoustic fields. Advanced Powder Technology, 22(2), 174-183.

134.   Chui SSY, Lo SMF, Charmant JPH, Orpen AG, Williams ID. A Chemically functionalizable nanoporous material [Cu_3 $(TMA)_2$ $(H_2O)_3$]n. Science 1999; 283:1148–50.

135.   Prestipino C, Regli L, Vitillo JG, Bonino F, Damin A, Lamberti C, et al. Local structure of framework Cu(II) in HKUST-1 metallorganic framework: spectroscopic characterization upon activation and interaction with adsorbates. Chem Mater 2006; 18 (5):1337–46.

136.   Chirone, R.; Massimilla, L.; Russo, S. (1993) Bubble-free fluidization of a cohesive powder in an acoustic field. Chem. Eng. Sci., 48 (1), 41- 52.

137.   Tlili, N., Grévillot, G., Vallières, C. (2009). Carbon dioxide capture and recovery by means of TSA and/or VSA. International Journal of Greenhouse Gas Control, 3 (5), 519-527.

138.   A. Wahby, J. Silvestre-Albero, A. Sepúlveda-Escribano, F. Rodríguez-Reinoso. (2012) CO_2 adsorption on carbon molecular sieves, Micropor. Mesopor. Mat. 164 280–287.

139.   D.P. Vargas, L. Giraldo, J. Silvestre-Albero, J.C. Moreno-Piraján. (2010) CO_2 adsorption on binderless activated carbon monoliths, Adsorption 17 497–504.

140.   Sevilla, M., Parra, J. B., Fuertes, A. B. (2013). Assessment of the role of micropore size and N-doping in CO_2 capture by porous carbons. ACS Applied Materials & Interfaces, 5 (13), 6360–8.

141. Liu, Y., Wilcox, J. (2012). Molecular simulation of CO_2 adsorption in micro- and mesoporous carbons with surface heterogeneity. International Journal of Coal Geology, 104, 83–95.

142. Lee, S.-Y., Park, S.J. (2014). Carbon dioxide adsorption performance of ultramicroporous carbon derived from poly(vinylidene fluoride). Journal of Analytical and Applied Pyrolysis, 106, 147–151.

143. Grande CA, Ribeiro RPPL, Rodrigues E. (2009) CO_2 Capture from NGCC power stations using electric swing adsorption. Energy Fuel 11, 2797–803.

144. Ruiz E, Sánchez JM, Maroño M, Otero J. CO2 capture from PCC power plants using solid sorbents: bench scale study on synthetic gas. Fuel 2012.

145. Galindo P, Schäffer A, Brechtel K, Unterberger S, Scheffknecht G. (2012) Experimental research on the performance of CO_2-loaded solutions of MEA and DEA at regeneration conditions. Fuel 101, 2–8.

146. Valverde, J. M. (2013). Acoustic streaming in gas-fluidized beds of small particles. Soft Matter, 9(37), 8792.

147. Ward D, Abhayapala TD. (2001) Reproduction of a plane-wave sound field using an array of loudspeakers. Speech Audio Process IEEE Trans 9, 697–707.

148. Ahrens J, Spors S. (2010) Sound field reproduction using planar and linear arrays of loudspeakers. Audio Speech, Lang Process IEEE Trans 18, 2038–50

149. G. Grasa , R. Murillo, M. Alonso, J.C. Abanades. (2009) Application of the random pore model to the carbonation cyclic reaction, AIChE 55 1246-1255.

150. J. Blamey, E. J. Anthony, J. Wang and P. S. Fennell, The calcium looping cycle for large-scale CO2 capture, Prog. Energy Combust. Sci., 2010, 36, 260–279.

151. S. V. Komarov, Advanced Topics in Mass Transfer, ch. Application of Airborne Sound Waves for Mass Transfer Enhancement, pp. 61-86. InTech, 2011.

152. Arias, B., Abanades, J. C., & Grasa, G. (2010). An Analysis of the Effect of Carbonation Conditions on CaO Deactivation Curves. Chemical Engineering Journal, (2011) 167, 255-261

153. Grasa, G., & Abanades, J. C. (2006). CO_2 Capture Capacity of CaO in Long Series of Carbonation/Calcination Cycles. Industrial & Engineering Chemistry Research, 45(26), 8846-8851.

154. Abanades, J. C., Anthony, E. J., Lu, D. Y., Salvador, C., & Alvarez, D. (2004). Capture of CO2 from combustion gases in a fluidized bed of CaO. AIChE Journal, 50(7), 1614–1622.